Thermodynamic Properties of Organometallic Dihydrogen Complexes for Hydrogen Storage Applications

Thesis by

David Gregory Abrecht

In Partial Fulfillment of the Requirements

for the Degree of

Doctor of Philosophy

California Institute of Technology

Pasadena, California

2013

(Defended December 4, 2012)

This work is dedicated to my family...

Steel is shaped by the hammer and anvil, but it is the care and patience of the smith that make the shape meaningful.

Acknowledgements

There are many people without whom this document would not exist. First and foremost, I would like to acknowledge my advisor, Brent Fultz, for both his efforts in helping to see this work to completion and for his willingness to take a risk on me, a student from another discipline with an idea that he wanted to follow. Without his support and guidance, this project would neither have gotten off of the ground nor would it have survived the crises of direction, funding, and drive that inevitably plague all research projects.

Similarly, I would like to thank all of the current and former members of the Fultz laboratory who have served as mentors, friends, brainstorming collaborators, and sympathetic ears: Channing Ahn, Hongjin Tan, Justin Purewal, Mike Winterrose, Jorge Munoz, Sally Tracy, Tian Lan, Nick Stadie, Max Murialdo, Hillary Smith, Lisa Mauger, Jiao Lin, Dennis Kim, Elsa Callini, Delphine Borivent, and Brandon Keith. The support of this exceptional group of people has been instrumental not only for the training and advice they offered freely but in also helping me maintain the necessary work-life balance to be productive and healthy.

I am extremely grateful to the Resnick Sustainability Institute and its staff for their financial, ideological, and personal support of both this project and sustainability science students overall. This group of extraordinary people were not only willing to support student projects in burgeoning fields during difficult and increasingly risk averse economic times, but have done so with the understanding that, in order to produce experienced researchers, you must allow fresh researchers experience. In particular I wish to recognize the sacrifice and long hours put forward by the Institute staff, Harry Atwater, Neil Fromer, Valerie Otten, and Heidi Rusina, to build the Institute into an environment where new ideas can flourish and scientists can be trained and can work effectively toward the solution to some of our world's toughest challenges.

I would like to thank my collaborators Joseph Reiter, Jason Zan, and Phil Wilson at the Jet Propulsion Laboratory for providing access to instruments and for lending their engineering and systems expertise. These men taught me not only what world-class science and engineering looks like, but what otherworldly science and engineering has to look like to be successful, and my work has been and will be only the better for it.

Thanks goes to Theo Agapie and the Agapie research group for training and assistance with the chemistry aspects of this work: Madalyn Radlauer, Davide Lionetti, Sibo Lin, Jacob Kanady, Dave Herbert, Guy Eduoard, Justin Henthorn, Kyle Horak, Sandy Suseno, Paul Kelley, Emily Tsui, Josh Wiensch, Steven Chao, Christine Cheng, Nadia Lara, and Eva Nichols.

Finally, I would like to thank the instrument and support staff at Caltech, without whom nothing at all would ever get done. In particular, I would like to thank Sonjong Hwang at Caltech's Solid-State NMR Facility, David VanderVelde at Caltech's Liquid NMR Facility, Larry Henling at Caltech's Small Molecule Crystallography Facility, and Carol Garland at Caltech's TEM Facility for training and support during my time here. I am grateful to Mike Vondrus, Mike Roy, Steve Olson, and Rick Gerhart in the Instrument Shops for their help on design, construction and repair of instrumentation. Special thanks go to Avalon Johnson at Caltech's Center for Advanced Computing Research for her assistance with the computational chemistry included in this work, and for management of the computational clusters and software.

Abstract

Hydrogen gas has been lauded as a clean fuel technology for its direct combustion to water vapor and its potential for production from renewable fuel sources. However, as a lightweight gas the low volumetric density of hydrogen makes it inappropriate for use in most fuel applications. Hydrogen storage technologies that promote the compression of the gas to useable volumes are a critical component to further development of a hydrogen fuel-based economy.

A number of solid-state storage systems based on metal and complex hydrides, chemical hydrides, and high-surface-area materials have been developed for use as storage media for hydrogen fuel. However, these technologies, which are separated broadly into absorption and adsorption complexes, display typical binding enthalpies too high or too low for practical applications, respectively. In recent years, new complexes designated as Kubas materials containing unsaturated metal centers and high surface areas have been produced and show binding energies intermediate to absorption and adsorption complexes while maintaining beneficial kinetics and binding capacities, demonstrating great promise as hydrogen storage candidates. This behavior has been attributed to the Kubas bond, which binds H_2 chemically as a molecule to an unsaturated metal center based on the Dewar-Chatt-Duncanson molecular binding model. However, the bulk absorption mechanism and thermodynamic behaviors for these interactions remain unknown. Kubas materials have historically been evaluated as physisorption materials for hydrogen storage applications; however, the recent display of absorption plateaus and exact stoichiometric values in isotherm measurements has led to uncertainty in the use of the physisorption model to explain the bulk interaction mechanism, which is necessary to accurately assess thermodynamic properties.

The bulk thermodynamic mechanism of hydrogen binding in dihydrogen complexes, which display "pure" Kubas bonds, is also poorly understood in the solid state. Identifying the mechanism of Kubas bonding can lead to improved thermodynamic characterization of both dihydrogen complexes and new generation hydrogen storage materials. To address this issue, the solid-state complex $[Mn(CO)dppe_2][BArF^{24}]$ was synthesized and the thermodynamic behavior and properties of the hydrogen absorption reaction to form the dihydrogen complex $[Mn(\eta^2\text{-}H_2)dppe_2][BArF^{24}]$ were measured over the temperature range 313K–373K and pressure range 0–600 torr using the Sieverts method. The absorption behavior was accurately described by Langmuir isotherms, and enthalpy and entropy values of ΔH° = -52.2 kJ/mol and ΔS° = -99.6 J/mol-K for the absorption reaction were obtained from the Langmuir equilibrium constant. The observed binding strength was similar to metal hydrides and other organometallic complexes, despite rapid kinetics suggesting a site-binding mechanism similar to physisorption materials. Electronic structure calculations using the LANL2DZ-ECP basis set were performed for hydrogen absorption over the organometallic fragments $[M(CO)dppe_2]^+$ (M = Mn, Tc, Re). Langmuir isotherms derived from calculation for absorption onto the manganese fragment successfully simulated both the pressure-composition behavior and thermodynamic properties obtained from experiment. Results from calculations for the substitution of the metal center reproduced qualitative binding strength trends of 5d > 3d > 4d previously reported for the group 6 metals.

Solid-state complexes $[FeHdppe_2][NTf_2]$ and $[FeH(\eta^2\text{-}H_2)dppe_2][NTf_2]$ were also synthesized and measured by x-ray diffraction and Mössbauer spectroscopy to determine the thermal decomposition pathway. Simulations at the B3LYP/TZV level of theory and experimental Mössbauer spectra confirmed the direct thermal decomposition from singlet state $[FeH(\eta^2\text{-}H_2)dppe_2][NTf_2]$ to triplet state $[FeHdppe_2][NTf_2]$ under vacuum conditions at 398K. Sieverts analysis showed samples to have extremely rapid H_2 uptake rates and significantly slower decomposition rates, with an Arrhenius activation energy of E_a = 32.3 kJ/mol for hydrogen release. Evaluation of the partial quadrupole splitting values from Mössbauer spectroscopy revealed a value of $Q(H_2)$ = -0.245 mm/s, similar to the values obtained by Morris and Schlaf for similar complexes and significantly different from values obtained for hydrides, indicating an underutilized mechanism for identification of dihydrogen ligands.

Langmuir simulations of hydrogen absorption onto the singlet-state complexes $[\mathrm{MHdppe}_2]^+$ (M = Fe, Ru, Os) revealed the same 5d > 3d > 4d trend and similar enthalpies to those observed for the group 7 complexes. Singlet-state thermodynamic values from simulation were consistent with experimental observations for Ru and Os, and ruthenium complexes were found to have thermodynamic properties within appropriate ranges for hydrogen storage applications. Simulated thermodynamic values for Fe complexes were found to significantly underestimate experimental behavior, demonstrating the importance of the magnetic spin state of the molecule to hydrogen binding properties.

Contents

Acknowledgements **iv**

Abstract **vi**

1 Introduction to Hydrogen Storage Technologies **1**

1.1 Background 2

1.2 Evaluation of Thermodynamic Properties 3

1.3 Properties of Absorption Materials 6

1.3.1 Absorption Thermodynamics 7

1.3.2 State-of-the-Art: Absorption Materials 11

1.4 Properties of Physisorption Materials 18

1.4.1 Physisorption Thermodynamics 20

1.4.2 State-of-the-Art: Physisorption materials 24

1.5 Kubas Binding 28

2 Review of Dihydrogen Complexes **29**

2.1 General Properties, Structure, and Bonding 29

2.2 Synthesis and Characterization 32

2.2.1 Synthetic Routes 33

2.2.2 Dihydride/Dihydrogen Identification 35

2.3 Binding Strength and Hydrogenation Thermodynamics 37

3 Studies of $[M(\eta^2\text{-}H_2)(CO)dppe_2]^+$ (M = Mn, Tc, Re) Complexes 41

3.1 Experimental 41

3.1.1 H_2 Absorption Measurements 44

3.1.2 Computations 45

3.2 Results and Discussion 47

3.2.1 Experimental Results 47

3.2.2 Computational Results 52

3.3 Conclusions 57

4 Studies of $[MH(\eta^2\text{-}H_2)dppe_2]^+$ (M = Fe, Ru, Os) Complexes 59

4.1 Experimental 60

4.1.1 X-Ray Diffraction 62

4.1.2 Mössbauer Spectroscopy 62

4.1.3 Computation 62

4.1.4 Kinetic Isotherms 64

4.2 Results and Discussion 65

4.2.1 Experimental Results 65

4.2.2 Computational Results 69

4.2.2.1 Mössbauer Simulations 69

4.2.2.2 Isotherm Simulations 71

4.2.3 Conclusions 74

5 Conclusions 76

5.1 Summary of the Current Work 76

5.2 Considerations for Future Studies 77

5.2.1 Known Dihydrogen Complexes for Hydrogen Storage 78

5.2.2 Computational Discovery of New Complexes 79

5.2.3 Engineering Considerations 80

5.3 Concluding Remarks 81

Appendix: GAMESS Input Files **82**

5.3.1 Geometry Optimization 83

5.3.2 Vibrational Analysis 122

5.3.3 Total Energy Calculation 153

Bibliography **185**

List of Figures

1.1 Sieverts Apparatus Schematic 5

1.2 General Thermodynamic System for Sieverts Measurements 8

1.3 Fugacity Coefficient of Hydrogen at Relevant Temperatures and Pressures 10

1.4 Idealized Pressure-Composition Isotherm and van't Hoff Plot for Absorption Processes 12

1.5 Wetting Behavior of $LiBH_4$ on MgH_2 18

1.6 Chahine's Rule for Physisorption Materials 19

1.7 Gibbs' Dividing Surface in Liquid-Vapor and Gas-Adsorbate Systems 23

1.8 Absolute vs. Excess Adsorption Isotherms 24

2.1 Octahedral Coordination and Side-On Bonding in $[FeH(\eta^2\text{-}H_2)dppe_2]^+$ 30

2.2 Bonding Model for Orbitals During Transition Metal-Dihydrogen Binding 31

2.3 Coupling Constant J_{HD} in Substituted Dihydrogen Complexes 36

3.1 Structure of the $[Mn(\eta^2\text{-}H_2)(CO)dppe_2]^+$ Cation 46

3.2 Absorption Isotherms for H_2 onto $[Mn(CO)dppe_2][BArF^{24}]$ 48

3.3 Initial Rate Kinetics for H_2 Absorption onto $[Mn(CO)dppe_2][BArF^{24}]$ 49

3.4 Van't Hoff Plot for H_2 Absorption onto $[Mn(CO)dppe_2]^+$ 52

3.5 Simulated Isotherms for H_2 Absorption onto $[Mn(CO)dppe_2]^+$ 54

4.1 Thermal Decomposition Kinetics of $[FeH(\eta^2\text{-}H_2)dppe_2][NTf_2]$ 66

4.2 X-Ray Diffraction Structure of $[FeH(\eta^2\text{-}H_2)dppe_2][NTf_2]$ 67

4.3 Mössbauer Spectra of $[FeH(\eta^2\text{-}H_2)dppe_2][NTf_2]$ and $[FeHdppe_2][NTf_2]$ 69

4.4 Simulated Isotherms for Hydrogen Absorption over $[RuHdppe_2]^+$ up to 5 Bar Pressure 74

List of Tables

3.1 Langmuir Equilibrium Constants for H_2 Absorption onto $[Mn(CO)dppe_2]^+$ 51

3.2 Simulated Thermodynamic Values for H_2 Absorption onto $[M(CO)dppe_2]^+$ (M = Mn, Tc, Re) 55

4.1 Mössbauer Parameters for $[FeH(\eta^2\text{-}H_2)dppe_2]^+$ and $[FeHdppe_2]^+$ 68

4.2 Simulated Thermodynamic Values for H_2 Absorption onto $[MHdppe_2]^+$ (M = Fe, Ru, Os) 73

Chapter 1

Introduction to Hydrogen Storage Technologies

With high gravimetric energy density, clean combustion, and renewable production capability, hydrogen gas shows great potential as a sustainable alternative to fossil fuels for energy production. This potential has led to a worldwide development effort for hydrogen technology to power industrial, residential and transportation infrastructure—a concept known as the hydrogen economy.[1] Mitigation of fossil fuel usage for transportation applications has dominated research efforts, with development of fuel cell-based powertrains for light-duty vehicles as the primary focus.[2] A number of unique technological challenges are inherent to these systems, including the efficient, safe storage of sufficient volumes of hydrogen gas to provide a fuel cell vehicle with comparable range to modern gasoline vehicles. Improvement of the volumetric energy density of the fuel storage system remains one of the largest hurdles to commercial implementation of fuel cell vehicles, and significant research efforts have been employed over the last decade to overcome this challenge.

Solid-state storage materials are currently the primary focus of research into storage of hydrogen gas for fuel systems.[3] In these materials, hydrogen gas is reversibly bound through chemical or physical interactions, increasing the volumetric energy density of the fuel, and correspondingly the fuel tank capacity, while maintaining safe operating temperatures and pressures. Multiple classes of solid-state storage materials have been identified based on the properties of their interaction with hydrogen, with numerous potential materials in each class, and research activities have been primarily focused on identification of new storage materials and optimization of the identified systems for energy efficiency. These efforts have led to significant advancements in the kinetics, thermodynamics, and capacity of solid hydrogen storage systems, but so far have not been able to meet the stringent requirements for commercial systems[1, 2, 4]

Continuing need for commercial hydrogen storage systems and concern that current materials have met intrinsic limits have provided motivation for parallel investigations into new classes of materials that exhibit unique binding motifs with hydrogen gas.[5] This chapter reviews the thermodynamic requirements of vehicular hydrogen storage systems and the current solid-state hydrogen-storage technologies. The advantages and limitations of each class of materials is discussed, and the motivation for investigations into an alternative class of storage materials exhibiting Kubas binding, where a dihydrogen molecule is bound to an organometallic complex as a ligand, is presented.

1.1 Background

Solid-state hydrogen-storage materials are broadly divided into two classes: absorption materials and physisorption materials.[1] These class distinctions are based on the location of the hydrogen-solid interaction; in absorption materials, hydrogen atoms dissociate at the solid surface and are subsequently bound within the bulk of the solid material, whereas in physisorption materials molecular hydrogen binds to the material surfaces. These class distinctions also roughly divide storage materials by binding strength, although some overlap can exist between their ranges. Absorption materials are characterized by strong chemical bonds between hydrogen atoms and atoms of the substrate. Physisorption materials bind hydrogen through weak van der Waals interactions, and hydrogen molecules maintain their molecular bond. Each of these broad classes is divided into several subclasses of materials, representing hundreds of potential storage materials with a wide range of properties.

Approaching the development and evaluation of these materials requires a practical method for screening promising candidates from the hundreds of potential materials available. Recent hydrogen storage research has focused on vehicular applications, directed by the US Department of Energy's Fuel Cell Technologies Program that, in 2005, introduced a research plan and series of engineering criteria to implement commercialization of fuel storage and delivery systems in hydrogen-fueled vehicles.[4] These criteria cover a wide range of economic, engineering, and material design specifications but mostly fall outside of the scope of basic research. However, several criteria have historically been used to direct basic hydrogen storage research,[2] and a review of the role of these criteria in choosing materials for study is necessary to understand the current state-of-the-art in the field.

Five of the criteria established by the US Department of Energy are commonly implemented in basic materials research: gravimetric energy density, volumetric energy density, cycling life, operating pressure and temperature, and filling kinetics. Gravimetric energy density and volumetric energy density depend upon the material structure and chemical makeup. Cycling life, operating conditions, and filling kinetics depend upon reactions within the material and the energy transfer between the solid and hydrogen gas during absorption. Procedures for evaluating these properties vary according to the binding mechanism, with different techniques for absorption materials and physisorption materials to accommodate the differences in the physical interactions within these materials.

The USDOE target ranges[4] for hydrogen delivery conditions to a fuel cell are 3–100 bar and 233K–358K. These values directly correlate to the thermodynamic properties of the reaction between the solid storage medium and the hydrogen atmosphere, and the evaluation of the standard enthalpy, ΔH°, and standard entropy, ΔS°, of hydrogen absorption is the primary goal of research into hydrogen storage materials.

1.2 Evaluation of Thermodynamic Properties

Experimental evaluation of thermodynamic data for hydrogen storage materials is commonly performed through the collection of isothermal absorption profiles using a Sieverts apparatus.[6,7] A schematic of a Sieverts apparatus appears in Figure 1.1. The instrument consists of a series of rigid calibrated volumes attached to a hydrogen source and a calibrated reaction chamber containing the material under investigation. During a measurement, hydrogen gas is introduced into an evacuated calibrated volume and allowed to equilibrate while pressure and temperature are recorded, and a value for the number of moles of hydrogen in the volume is obtained using the appropriate equation of state. The calibrated volume is then opened to the evacuated reaction chamber, and hydrogen is allowed to react with the storage material. The pressure and temperature are again recorded, and the change in moles between the original measurement and the measurement after exposure to the storage material is recorded as the number of moles absorbed by the sample, giving a single pressure-temperature-composition (P-T-x) data point.

Single point isotherms are commonly reported,[8–10] particularly for materials that do not have strong reversibility or when simultaneous evaluation of thermodynamics and analysis of the kinetics is desired. While thermodynamic information may be extracted from these isotherms, for many materials it is difficult to differentiate between solubility of H_2 in the material and reactive absorption from them, and the incorrect treatment of the physical process can sometimes be used. More complete iterative isotherms are comprised of multiple single point isotherm P-T-x data points, created by serial exposures of the material to new hydrogen pressures. Kinetic information is sacrificed to produce these isotherms, but a more complete expression of the absorption properties and thermodynamics is obtained. Thermodynamic information is obtained from the comparison of isotherms at multiple temperatures, using appropriate equations for the expected absorption mechanism.[11–13]

Thermogravimetric analysis and differential scanning calorimetry, respectively, are also used for evaluating the gravimetric capacity and thermodynamic properties of hydrogen storage materials.[14,15] The temperature of the hydrogen storage material is raised at a constant rate under a flow of inert gas, and the mass of the sample and heat flow required to maintain the rate of increase relative to a standard are recorded. Loss of mass during the experiment, identifiable as H_2 gas by mass spectroscopy, indicates the desorption capacity of the material. Changes in the heat flux necessary to maintain the temperature ramp indicate the onset of the chemical reaction, and integration of the heat flux curves provides the enthalpy of the interaction. These techniques are accurate, rapid, relatively easy to perform, and require very little sample material. However, a hydrogenated material that is stable at room temperature is required, and the techniques do not allow measurements at multiple pressures. As such, these methods are inappropriate for certain types of absorption materials and for all currently known physisorption materials.

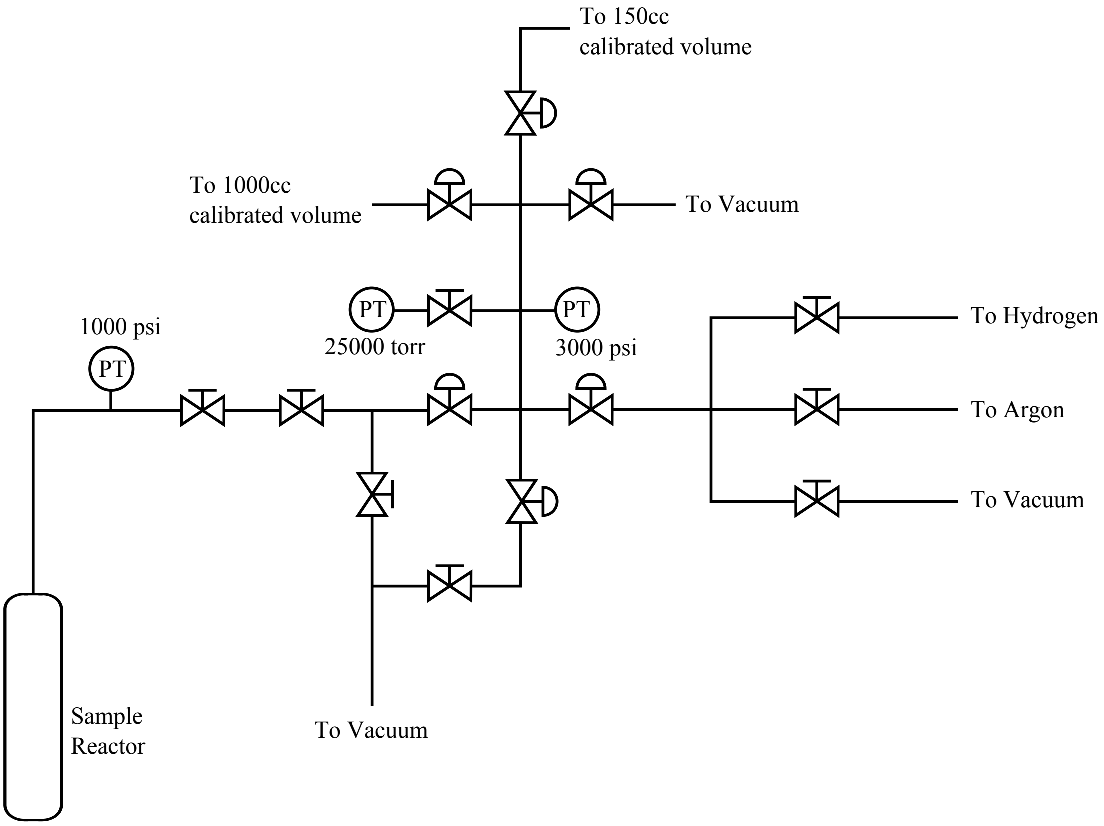

Figure 1.1: Schematic diagram of a Sieverts apparatus. Calibrated volumes are filled from a hydrogen source through a valved manifold (also calibrated) and exposed to the temperature controlled reactor for absorption measurements. Multiple calibrated volumes are used to match the expected pressure drop from absorption in the reactor. Argon expansion is used to calibrate the volumes of the reactor. Pressure and temperature measurements are obtained on the reactor and on each of the available volumes.

Electronic structure calculations are used to estimate the thermodynamic binding properties in hydrogen storage materials, most commonly with storage materials that exhibit hydrogen dissociation or chemical reaction.[16,17] Density functional theory (DFT) calculations simulate the geometry and electronic energy of each component of the absorption reaction. The energies are then summed to produce a reaction energy that approximates the standard enthalpy of the reaction. This powerful technique is useful for screening potential candidates and, more broadly, mixtures of potential candidates that fall within the desired thermodynamic range.

Analysis of the data to obtain thermodynamic information is dependent on the expected interaction mechanism. Properties of absorption materials and physisorption materials, calculation methods for their thermodynamic parameters and state-of-the-art materials for each group are reviewed below.

1.3 Properties of Absorption Materials

Absorption hydrogen storage materials undergo a chemical reaction with hydrogen gas, causing dissociation of the gas molecule at the material surface and migration of atomic hydrogen within the material structure.[3] The atomic hydrogen may then occupy interstitial sites in the crystalline solid material, as in transition metal hydrides, or form new chemical bonds between the hydrogen atoms and the atoms of the substrate. Generally, this process can be described by the chemical equation:

$$\mathrm{S} + \mathrm{nH_2} \rightleftharpoons \mathrm{SH_{2n}} \tag{1.1}$$

This category of materials includes alkali and alkaline earth metal hydrides (e.g., LiH, NaH, MgH_2, CaH_2), transition metal hydrides (e.g., $PdH_{0.6}$, $LaNi_5H_6$), alanes (e.g., AlH_3, $NaAlH_4$), boranes (e.g., $LiBH_4$, $NaBH_4$, NH_3BH_3), solid hydrocarbons, and amines and imines (e.g., $LiNH_2$, Li_2NH). These materials are primarily characterized by high gravimetric and volumetric energy densities, high binding enthalpies, slow solid-state kinetics, and moderate to poor cycling behavior.[2, 1]

Gravimetric energy density is the easiest of these properties to evaluate and is used extensively in screening potential absorption materials.[17] Except for transition metal hydrides, hydrogen binds to these materials in fixed stoichiometric ratios and the theoretical gravimetric energy density is directly obtainable from the chemical formula of the hydrogenated material. For example, in the absorption equation

$$\mathrm{2Li} + \mathrm{H_2} \longrightarrow \mathrm{2LiH}$$

the gravimetric energy density of LiH is obtained as the product of the standard lower heating value of hydrogen gas, 120 kJ/gram H_2, and the weight ratio of hydrogen in lithium hydride as obtained from the molecular weights, 0.1268 grams H/gram LiH (MW(H) = 1.0079, MW(LiH) =

7.9489). Because the lower heating value is a standard, gravimetric energy density is often reported as the weight ratio or weight percentage of hydrogen in the material. However, for transition metal hydrides the gravimetric capacity does not necessarily follow stoichiometric rules and must be obtained experimentally, although rules of thumb based on the crystal structure exist.[18] The USDOE target equivalent of 4.5–7.5%wt storage has mostly limited examination of new absorption hydrogen storage materials to those comprised of elements from the first three rows of the periodic table. These limitations allow for lightweight and compact storage materials, but often at the expense of thermodynamic or kinetic efficiency.

Volumetric energy density for absorption materials is determined from the unit cell volume of the crystalline hydrogenated product. This information is also easily obtainable and tabulated from x-ray diffraction (XRD) measurements[19] or DFT geometry optimizations,[20] and is used as an additional screening parameter along with weight percentage. For most absorption materials, volumetric energy density far exceeds the targets set by the USDOE. Because of this, weight percentage of hydrogen is favored in reports.

1.3.1 Absorption Thermodynamics

Thermodynamic properties of absorption hydrogen storage materials are typically evaluated through the ideal gas absorption van't Hoff equation[1]

$$\ln\left(\frac{P}{P_0}\right) = \frac{\Delta H^\circ_{rxn}}{RT} - \frac{\Delta S^\circ_{rxn}}{R} \tag{1.2}$$

where P and T are the pressure and temperature of the system, P_0 is the standard or reference pressure of the system (typically 1 atm or 1 bar), R is the universal gas constant, and ΔH° and ΔS° are the enthalpy and entropy of the absorption reaction at standard pressure and temperature. This relationship is developed from the equivalence of free energy between the products and reactants in Equation 1.1 during chemical equilibrium. Given the equivalent thermodynamic system of the Sieverts reactor, schematically illustrated in Figure 1.2, the equilibrium condition between the gas

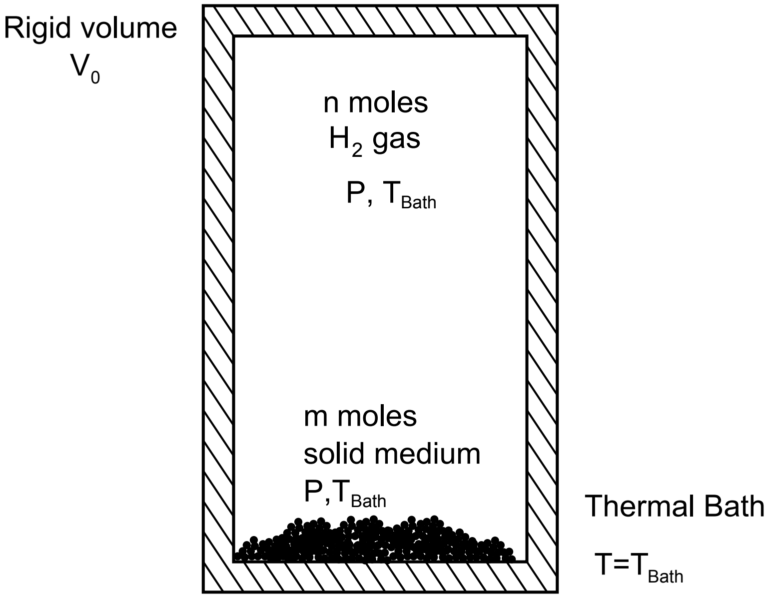

Figure 1.2: Schematic of the general thermodynamic system for hydrogen storage measurements

phase and the condensed phases can be expressed mathematically as

$$G_{solid} - G_{gas} = 0 \tag{1.3a}$$

$$\partial G_{solid} - \partial G_{gas} = 0 \tag{1.3b}$$

where G_{solid} and G_{gas} represent the total molar Gibbs free energy of the solid and gas phases, respectively. This definition of equilibrium for absorption systems is universal and independent of the absorption mechanism. For absorption systems, Equation 1.3a is expanded with respect to the absorption portion of Equation 1.1, giving

$$G_{\mathrm{SH_{2n}}} - G_{\mathrm{S}} - nG_{\mathrm{H_2}} = 0$$

where $G_{\mathrm{SH_{2n}}}$, $G_{\mathrm{H_2}}$ and G_{S} are the molar Gibbs free energy reaction components. To apply the equation to isotherms, the temperature is assumed to be fixed and the standard molar Gibbs free energy is defined at the fixed temperature and a standard pressure, P°. Separating the Gibbs free energies into standard and non-standard components gives

$$\left(G^\circ_{\mathrm{SH_{2n}}} - G^\circ_{\mathrm{S}} - nG^\circ_{\mathrm{H_2}}\right) + \int\limits_{P_0}^{P} \left[\left(\frac{dG_{\mathrm{SH_{2n}}}}{dP}\right)_T - \left(\frac{dG_{\mathrm{S}}}{dP}\right)_T - n\left(\frac{dG_{\mathrm{H_2}}}{dP}\right)_T\right] dP = 0$$

where G° is the standard molar Gibbs free energy, T, P are the isothermal temperature and pressure of the system, and P_0 is the standard pressure of the system. This equation completely describes the equilibrium condition for absorption in absorption materials for any conditions. However, to obtain the van't Hoff equation given in Equation 1.2, a few assumptions regarding the absorption conditions must be made.

Solid phases in the reaction are generally assumed to be incompressible, such that their free energy has no dependence on the system pressure. This assumption takes advantage of the large values of the bulk modulus for hard condensed matter to simplify the integral and eliminate the terms containing the solids. For hydrides, complex hydrides, ammonia borane, and other small molecule, densely packing absorption material, this assumption will be valid across a wide range of pressures and can safely be made within the 0–100 bar pressure range specified in the USDOE criteria. However, for materials consisting of polymers and other soft condensed matter this assumption may not hold. With this assumption, the equation becomes

$$\Delta G^\circ_{\mathrm{rxn}} = \int\limits_{P_0}^{P} \left(\frac{dG_{\mathrm{H_2}}}{dP}\right)_T dP$$

$$n\Delta G^\circ_{\mathrm{rxn}} = G^\circ_{\mathrm{SH_{2n}}} - G^\circ_{\mathrm{S}} - nG^\circ_{\mathrm{H_2}}$$

with $\Delta G^\circ_{\mathrm{rxn}}$ defining the change in the standard molar Gibbs free energy of the absorption reaction, normalized to the moles of hydrogen gas. The constant temperature derivative of the molar Gibbs free energy of a single component gas with respect to pressure is the thermodynamic molar volume:

$$\Delta G^\circ_{\mathrm{rxn}} = \int\limits_{P_0}^{P} V_{\mathrm{H_2}} dP$$

which can be related to the system temperature and pressure through an appropriate equation of state. The second assumption applies the ideal gas equation of state to evaluate the molar volume

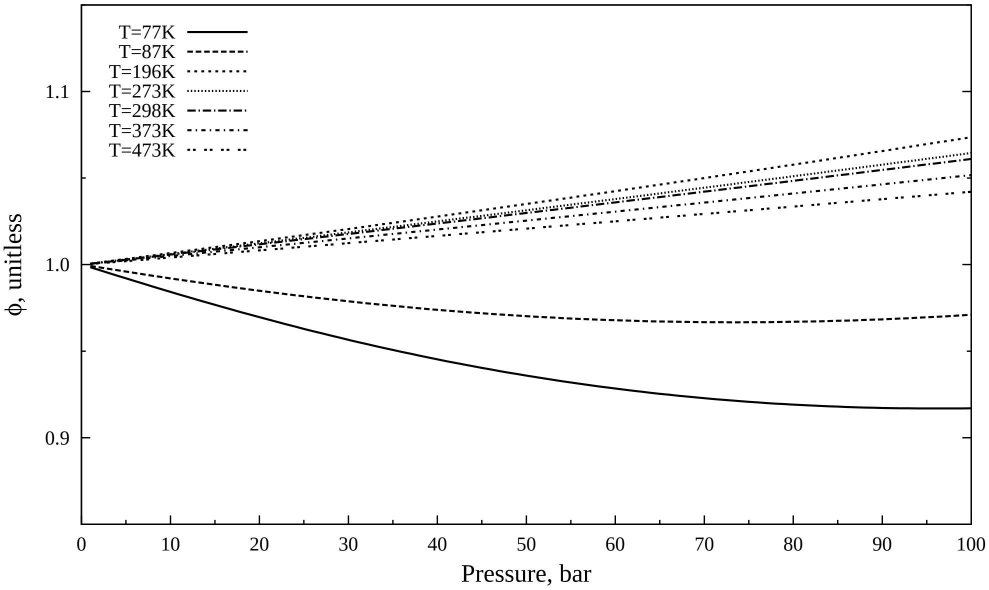

Figure 1.3: Fugacity coefficient of hydrogen at relevant temperatures and pressures

and obtain expressions based on temperature and pressure. Substituting the ideal gas equation in for the molar volume gives

$$\Delta G^\circ_{\mathrm{rxn}} = \int_{P_0}^{P} \frac{RT}{P} dP$$

$$\Delta G^\circ_{\mathrm{rxn}} = RT \ln \left(\frac{P}{P_0} \right)$$

Rearranging and separating the Gibbs free energy into enthalpy and entropy components gives the van't Hoff equation, Equation 1.2, for hydrogen absorption. The derivation above and Equation 1.2 are considered from the perspective of absorption; the signs on the enthalpy and entropy terms are reversed for desorption reactions.

The correct application of this equation to hydrogen storage systems requires hydrogen to be within the range of ideal gas behavior. The deviation of hydrogen from ideal gas behavior can be estimated by calculation of the fugacity coefficient for hydrogen at various temperatures and pressures:

$$\phi = \exp\left\{\frac{G_{\mathrm{H}_2}(T,P) - G^{\mathrm{IG}}_{\mathrm{H}_2}(T,P)}{RT}\right\} = \exp\left\{\frac{1}{RT}\int_0^P \left(V_{\mathrm{H}_2} - \frac{RT}{P}\right)\partial P\right\}$$

where the superscript IG denotes the equivalent ideal gas properties. A value of one for ϕ denotes that the gas behaves as an ideal gas, and deviations from a value of one represent non-idealities. These values are derived from direct measurements of the hydrogen equation of state, and have been compiled for a range of pressures and temperatures by the National Institutes of Science and Technology (NIST).[21] A graph of hydrogen gas fugacity coefficients at temperatures and pressures relevant for hydrogen storage appears in Figure 1.3. For pressures below 100 bar, the fugacity coefficient for hydrogen is a weak function of pressure and is a weak function of temperature above 196K, which has been shown in the past to be sufficient for use of the van't Hoff equation in evaluating absorption hydrogen storage materials to meet the USDOE requirements. For basic research involving higher pressures or lower temperatures, however, the values may deviate significantly, and Equation 1.2 would be inappropriate to describe the absorption system.

The pressures and temperatures used in the van't Hoff equation are the values that correspond to chemical equilibrium between the gas and solid phases. Experimentally, these values must be obtained from pressure-composition isotherms. For absorption processes, this equilibrium is easily determined; isotherms for absorption processes demonstrate a flat plateau, illustrated schematically in Figure 1.4, which corresponds to the equilibrium conditions of the reaction where the change of the Gibbs free energy is zero as the reactants are converted to products.[1] The flat shape of the plateau is characteristic of a reaction-dominated process, indicating independence of the Gibbs free energy of absorption on the composition of the phases.

1.3.2 State-of-the-Art: Absorption Materials

Although no absorption materials have been commercially developed, several material types are under active investigation and are considered state-of-the-art materials for hydrogen absorption. Each material type exhibits several benefits and drawbacks for use with commercial systems. A brief overview of each material type is given below.

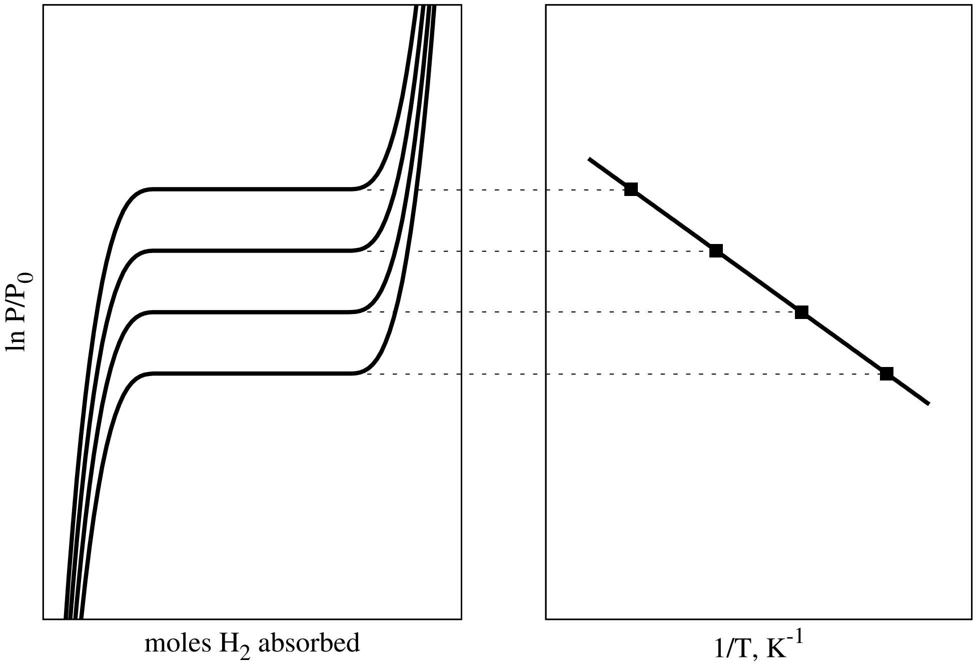

Figure 1.4: Idealized pressure-composition isotherm (left) and van't Hoff plot (right) for absorption processes, demonstrating the expected curve-shapes for absorption dominant processes and translation to thermodynamic quantities.

Borohydrides—Borohydrides are complex hydride materials which primarily store hydrogen in the form of the tetrahydridoboride anion,[22,23] $[BH_4]^-$. Typically used as mild reducing agents in chemical applications, these materials are lightweight, earth-abundant, and are available on industrial production scales. The complexes primarily under development for hydrogen storage applications are $LiBH_4$, $NaBH_4$, $Mg(BH_4)_2$ and $Ca(BH_4)_2$, with $LiBH_4$ dominating the literature because of its high weight percentage of hydrogen. $NaBH_4$ has received less attention in recent years because its primary mechanism for release of hydrogen is through hydrolysis of the borohydride anion, an irreversible process.[24]

Borohydrides suffer from a number of drawbacks that limit their applications as hydrogen storage materials. Thermodynamically, the absorption enthalpy of borohydrides is relatively strong, ranging from 67 kJ/mol for $LiBH_4$[25] to 53 kJ/mol for $CaBH_4$.[26] Materials within this range of enthalpies require extremely high temperatures for hydrogen cycling; often temperatures greater than 550K are required to observe hydrogen release. Such high temperatures also promote side reactions and the release of unfavorable product gases, primarily diborane[27] (B_2H_6), which can foul fuel cell catalysts and surfaces and remove reversible capacity from the material.

Borohydrides also suffer from poor solid-state diffusion kinetics and a complex decomposition chain, which leads to multiple side reactions and the formation of highly stable side and end products, notably metal borides and materials containing the $[B_{12}H_{12}]^{2-}$ anion.[28] Both of these features lead to poor reversibility of the desorption reaction and effective prevention of true cycling behavior. Recent research efforts have aimed at control of the size of borohydride crystallite sizes and confinement of crystallites to nanocavities,[29] as well as using catalytic additives,[30] in the hopes of limiting diffusion and promoting reversible hydrogen release at lower temperatures.

Alane/Alanates—Both the neutral alane,[31] AlH_3, and alanate salts comprised of the tetrahydridoaluminate anion,[11] $[AlH_4]^+$, have been consistent candidates for hydrogen storage materials since the discovery that titanium and organotitanium catalyzes the release and reabsorption of hydrogen from sodium alanate. Neutral AlH_3 is thermodynamically unstable to hydrogen decomposition at room temperature, with an absorption enthalpy of only -14.85 kJ/mol H_2, which corresponds to an equilibrium pressure of 5×10^5 bar at room temperature.[32] Alane is kinetically stabilized in the solid state, only decomposing at approximately 440K in a single step to give hydrogen and aluminum powder. Once decomposed, the resulting aluminum powder is highly resistant to reabsorption of hydrogen to regenerate alane. *In situ*, alane is thus considered a single-use material that must be removed and regenerated through chemical means. Ongoing research into alane as a hydrogen storage material focuses on safely controlling the release kinetics of hydrogen from the material, and methods to efficiently regenerate the hydrogenated material from spent aluminum powder.[33]

Alanate salts, particularly $NaAlH_4$ and $LiAlH_4$, have been more widely reviewed for hydrogen storage applications. Both materials decompose by a two-step pathway, typified by the equations

$$3NaAlH_4 \rightleftharpoons Na_3AlH_6 + 2Al + 3H_2$$

$$Na_3AlH_6 \rightleftharpoons 3NaH + Al + 3/2H_2$$

For the sodium analog, both reactions have been shown to be reversible when titanium is present, with mild enthalpies of 37 kJ/mol and 47 kJ/mol, respectively.[34] However, because aluminum must be mobile within the phases for the decomposition to occur, the kinetics of desorption are slow. Titanium doping and the introduction of other impurities have been shown to improve the kinetics to reasonable levels in sodium alanate, making it one of the few complex hydrides to demonstrate reversible kinetics near room temperature. However, a combined reversible weight percentage of only 5.6 wt% for $NaAlH_4$ has prompted studies into the lithium analog, which decomposes through the same mechanism. $LiAlH_4$ was found to be considerably less stable, with initiation of desorption at 453K and extremely high absorption pressures, making reversible hydrogen storage extremely difficult.[35]

$NaAlH_4$ continues to be explored as a potential vehicle fuel system material, and current research on the material is concerned with engineering properties the material.[36,37] Investigations into $LiAlH_4$ and other alanates are primarily concerned with increasing the stability of the compound and reversibility of the desorption.[38,39]

Amides/Imides—Lithium nitride/lithium amide has been one of the more promising materials systems for hydrogen storage since it was first investigated by Chen, et al.[40] Absorption of hydrogen over lithium nitride has been shown to occur in a two-step, reversible process:

$$\mathrm{Li_3N + H_2 \rightleftharpoons Li_2NH + LiH}$$

$$\mathrm{Li_2NH + H_2 \rightleftharpoons LiNH_2 + LiH}$$

These two reactions give absorption of 5.5 wt% and 6.5 wt%, respectively, exhibiting comparable absorption capacity to $NaAlH_4$ with fast absorption kinetics. However, the first step was found to be irreversible, and the reversible absorption enthalpy of -66.1 kJ/mol for the imide requires temperatures greater than 673K, preventing practical use of this system. Experimental investigations of the system have also found significant quantities of ammonia[14] can be released, through the self-decomposition reaction of lithium amide:

$$\mathrm{2LiNH_2 \longrightarrow Li_2NH + NH_3}$$

This ammonia release is severely detrimental to the performance of the material in fuel systems; ammonia serves to poison fuel cell catalysts and drastically reduces the lifetime of a fuel system. Ammonia release can be prevented by the presence of LiH throughout the structure to absorb the molecule to form $LiNH_2$ and H_2. However, this kinetic effect makes the mixing of starting materials and prevention of chemical segregation crucial to the performance of the material, and unfortunately any efforts to maintain these properties cannot be expected to be maintained upon cycling.

Other amide systems, based on the lithium nitride system, are being investigated for improvement of the thermodynamic behavior and reduction of ammonia release. The $Mg(NH_2)_2$ + LiH mixture has received attention as a replacement in recent years, showing promise both in gravimetric capacity and thermodynamic properties.[41] This is a form of chemical destabilization, discussed in more detail below.

Ammonia Borane and Amidoboranes—Ammonia borane (NH_3BH_3), at 19.6 wt% hydrogen, has received a great deal of attention as a potential hydrogen storage material. Unlike most absorption storage materials, ammonia borane is air stable and release of hydrogen occurs primarily from the molten state just past the melting temperature of 377K.[42] Hydrogen release is also exothermic and self-promoting, with an overall decomposition enthalpy of -21.7 kJ/mol.

The release of hydrogen occurs through a complex polymerization decomposition, with three steps relevant for hydrogen storage:

$$\mathrm{nNH_3BH_3} \longrightarrow \mathrm{[NH_2BH_2]_n + nH_2}$$

$$\mathrm{[NH_2BH_2]_n} \longrightarrow \mathrm{[NHBH]_n + nH_2}$$

$$\mathrm{[NH_2BH_2]_n} \longrightarrow \mathrm{nN_3B_3H_6 + nH_2}$$

These reactions create observable pressures between approximately 380K and 473K. After formation of polyaminoborane ($[NH_2BH_2]_n$), the formation of polyiminoborane ($[NHBH]_n$) is exothermic, spontaneous and favorable at lower temperatures. This reaction path is desirable; borazine ($N_3B_3H_6$) formed through the last reaction pathway is a volatile liquid that can be released into the fuel lines, removing storage capacity from the fuel tanks and potentially fouling fuel cell catalysts. However, because the kinetics of hydrogen release are slow at lower temperatures, a compromise between borazine production and release rate often can be made to mitigate the formation of detrimental products.

Initialization of the decomposition is slow, and the decomposition is not directly reversible. Catalytic systems are under development for both improving the release rate and facilitating regeneration of the final product. Iridium organometallic complexes have been shown to be extremely effective at improving the decomposition rate, but are impractical for scale-up.[43] Less expensive options based on 3d transition metals are under investigation to replace iridium complexes and other precious metals in such systems.[44]

The mechanism for removal of the polymeric end products from fuel systems and efficient chemical regeneration of ammonia borane remain the most significant engineering and scientific challenges associated with its use. A number of catalytic regeneration cycles have been proposed, including the use of organotin catalytic cycles[45, 46] and regeneration in pressurized, liquefied ammonia with hydrazine.[47] These methods have serious safety and economic hurdles to overcome before being commercially realizable, and ongoing research seeks to improve the engineering properties of these regeneration techniques, as well as further improving the efficiency of regeneration processes and increasing control of kinetic rates of release and gaseous product trapping and recovery.

Destabilized Materials Mixtures—One of the common features of absorption storage materials that limits their applications in fuel systems is the high enthalpy of absorption. This feature forces the use of impractically high temperatures to activate hydrogen release from the solid. From Equation 1.2, reduction of the binding enthalpy leads to exponential increases in the available pressure at a given temperature, and making small improvements in the overall system thermodynamics worth pursuing. Some recent work has centered on the use of complex hydride and simple metal hydride mixtures, designed to increase the stability of the desorption products at the sacrifice of some capacity. A prototypical example of this effect is the mixture of $LiBH_4$ and MgH_2.[25] Individually, these materials release hydrogen through the reactions

$$\mathrm{LiBH_4} \longrightarrow \mathrm{LiH} + \mathrm{B} + 3/2\mathrm{H_2}$$

$$\mathrm{MgH_2} \longrightarrow \mathrm{Mg} + \mathrm{H_2}$$

However, as a mixture of 2:1 $LiBH_4$:MgH_2, dehydrogenation occurs via the overall reaction

$$\mathrm{LiBH_4} + \frac{1}{2}\mathrm{MgH_2} \longrightarrow \frac{1}{2}\mathrm{MgB_2} + \mathrm{LiH} + 2\mathrm{H_2}$$

The mixture, at 11.54 wt% usable capacity, represents a ∼2% reduction in the absorption capacity from $LiBH_4$ alone. However, formation of the more stable MgB_2 species reduces the dehydrogenation enthalpy to 40.5 kJ/mol from 67 kJ/mol for $LiBH_4$ alone and 75 kJ/mol for MgH_2 alone. This reduction leads to a decrease in the 1 bar equilibrium temperature from greater than 673K for $LiBH_4$ to 498K, representing a significant improvement in the operating properties of the storage material. Millions of such combinations of absorption hydrogen storage materials have been identified from available crystal structures, and DFT calculations have been used to screen these combinations for the highest potential for meeting the USDOE requirements.[16, 17] Combinations identified by the theoretical studies are currently undergoing experimental investigations.[48, 49, 41]

The use of mixtures can lead to reductions in the kinetic rate of absorption and desorption, which can offset the benefits in operating temperature obtained through lower thermodynamics by kinetic stabilization of the hydrogenated products. Solid-state diffusion limitations of larger elements like boron or magnesium can easily dominate the kinetic behavior at lower temperatures and limit the release rate. A balance between the benefits of the thermodynamic destabilization and the kinetic stabilization must therefore be found for the efficient use of destabilized mixtures. Unfortunately, this information is unavailable from current DFT simulations, and must be evaluated experimentally.

Evaluation and improvement of kinetic properties is difficult in experimental mixtures, and additional, non-chemical complications can arise. For example, in the $LiBH_4$ + $1/2MgH_2$ system above, as shown in Figure 1.5, the $LiBH_4$ melt was found to have poor surface adhesion to MgH_2, which belies an unfavorable interaction energy between the two materials that disfavors mixing and increases the diffusional barriers. This physical property prevents the formation of classic composites

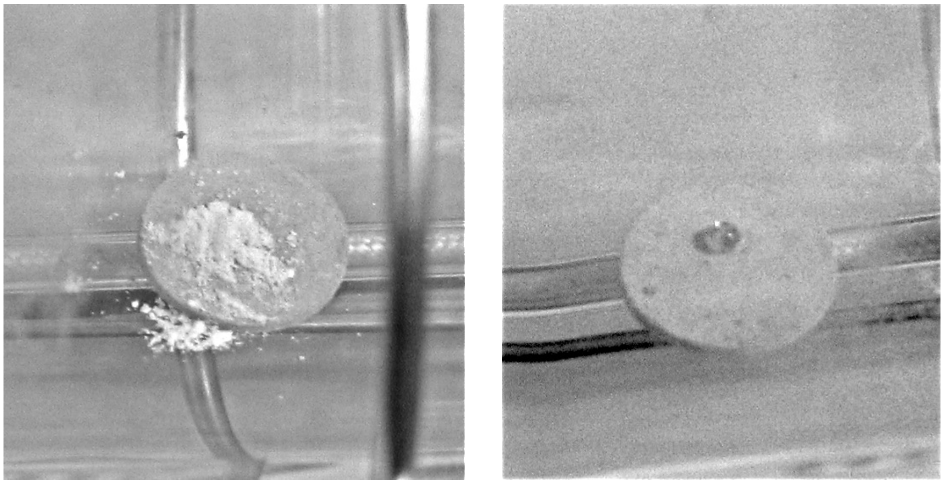

(a) (b)

Figure 1.5: $LiBH_4$ on a compacted disk of MgH_2, under an argon atmosphere. a) Powdered $LiBH_4$ (white) at room temperature. b) The same system at 573K, after melting of the $LiBH_4$. Molten $LiBH_4$ forms a large contact angle with the MgH_2 surface, indicating a poor wetting interaction.

from the suspension of MgH_2 in molten $LiBH_4$, and impedes efforts at nanoconfinement and other techniques. Mitigation of such effects is a large area of research in destabilized systems.

1.4 Properties of Physisorption Materials

Physisorption storage materials bind hydrogen to the material surface through van der Waals forces.[1] These binding forces, produced by polarization of the interacting molecules through mutual repulsion of their electron clouds and random fluctuations in electron density, occur at any interface between hydrogen gas and a solid material. The bonds formed between hydrogen and the solid in these materials are typically made over long distances and are correspondingly weak and non-chemical in nature, which gives characteristically low binding enthalpies and poor storage capacity at room temperatures. However, these materials are characterized by rapid kinetics, low cost, and long cycle lifetimes. Solids designed to act as physisorption storage materials are treated to maximize the available surface area for these interactions, and thus the amount of hydrogen capable of being stored on the surface.

Evaluation of the USDOE parameters in physisorption materials is similar to the methods for absorption materials. Gravimetric energy density is again the most straightforward of the criteria to

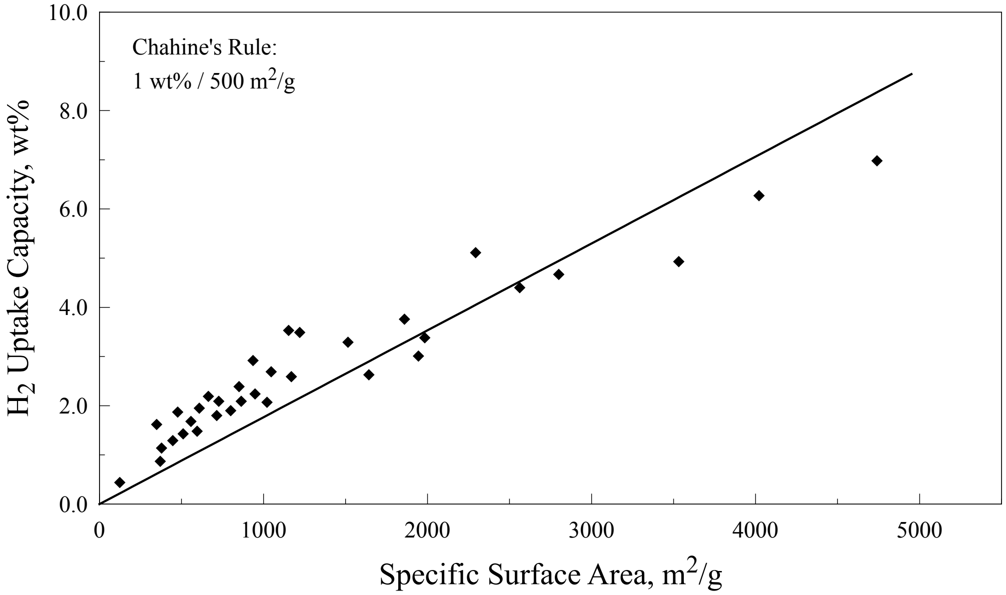

Figure 1.6: Plot of specific surface area vs. gravimetric capacity at saturation for hydrogen absorption over adsorbent materials, demonstrating Chahine's rule of approximately 1 wt% increase in adsorption capacity for every 500 m^2/g increase in specific surface area. Data obtained from Hirscher and Panella, 2007.[50]

determine from the material properties. The ultimate gravimetric storage capacity of physisorption materials with similar chemical composition has been shown to be directly proportional to the specific surface area of the material.[50] This correlation, known as "Chahine's rule", is shown graphically for various carbon-based materials in Figure 1.6. This allows rapid estimation of the gravimetric capacity from BET or other surface-area tests.

Because gravimetric capacities are typically lower for physisorption materials than for absorption materials, physisorption material chemical compositions are primarily carbon, boron and boron nitride. Limiting the basic chemical composition to these two materials minimizes the density of the material, allowing for the highest gravimetric ratio of the surface hydrogen to the bulk material. Physisorption materials can also incorporate small quantities of other elements to improve specific properties; this technique is primarily used to modify the absorption enthalpy. These additional elements include transition metals,[51] intercalated alkali metals or alkaline earth metals,[52] and fluorine adatoms.[53] Heavier atoms are only added in small amounts, however, to avoid reducing the gravimetric capacity too much.

Volumetric capacity in physisorption materials is difficult to estimate or measure. Because hydrogen is only adsorbed onto the surface and not absorbed into the bulk, no true volumetric energy density can be defined for the material. Instead, the volumetric capacity is typically assigned as the improvement in the number of moles stored in a given tank volume when the adsorbent material is added, with appropriate adjustments for the volume displaced by the adsorbent itself.[3] Based on this metric, the volumetric capacity is not an independent quantity, being dependent on both the temperature and pressure of the measurement, and on the gravimetric capacity of the material. Because the volumetric capacity must be derived from measurements, is tank specific, and is not a true physical quantity, it is a less meaningful description of the properties of physisorption materials, and is rarely reported in the literature.

Diffusional barriers are largely absent from physisorption materials, and the weak inherent binding to the surface reduces activation barriers for hydrogen release. Side reactions and modifications of the solid surface during the adsorption process are also largely absent, because no true chemical bonds with the surface are formed. These properties translate into rapid kinetics for hydrogen adsorption and release and high cycling lifetimes, typically far in excess of the USDOE targets. Because of this, kinetic rate measurements are often not performed for hydrogen absorption measurements in basic research. However, these values become important in engineering applications when coupled with heat management requirements. The rapid absorption of gas onto the surface can lead to high thermal fluxes or rapid temperature increases. Both of these properties may be detrimental to the operation of an adsorption system.

1.4.1 Physisorption Thermodynamics

Derivation of the surface thermodynamics for physisorption processes also begin with equivalence of the free energies of gaseous and bound hydrogen, given in Equation 1.3a and Equation 1.3b. However, unlike absorption materials the hydrogen molecule does not lose its identity, and no chemical reaction occurs. Instead, the hydrogen molecule exists in both solid and gaseous states with differing potentials, with the solid-state potential modified by interaction with the substrate. This process parallels phase transition models. Taking this approach, Equation 1.3a and 1.3b may be used directly to arrive at pressure and temperature dependence of the system. For phase equilibrium of a single species, Equation 1.3b can be rewritten as

$$\mathrm{V_{gas}\partial P - S_{gas}\partial T = V_{solid}\partial P - S_{solid}\partial T}$$

Where gas and solid subscripts describe hydrogen within those phases. Also, using the definition G = H - TS in Equation 1.3a, the entropy can be related to the enthalpy

$$\mathrm{H_{gas} - TS_{gas} = H_{solid} - TS_{solid}}$$

Combining these two equations yields the Clapeyron equation:

$$\left(\frac{\partial \mathrm{P}}{\partial \mathrm{T}}\right) = \frac{\mathrm{S_{gas} - S_{solid}}}{\mathrm{V_{gas} - V_{solid}}} = \frac{\Delta \mathrm{H_{des}}}{\mathrm{T}\Delta \mathrm{V}} \tag{1.4}$$

where $\Delta\mathrm{H_{des}} = \mathrm{H_{gas} - H_{solid}}$ is the desorption enthalpy, analogous to the heat of vaporization in liquid-vapor equilibrium, and $\Delta\mathrm{V} = \mathrm{V_{gas} - V_{solid}}$ and P is the saturation pressure corresponding to equilibrium. The Clapeyron equation exactly describes the thermodynamic system. However, it is difficult to work with, and the specific volume of hydrogen at the surface of the substrate is difficult to define. As with absorption materials and the van't Hoff equation, assumptions are made to simplify the use of the Clapeyron equation to a more usable form.

While the volume of the adsorbed hydrogen cannot be directly assessed, the specific volume of hydrogen on the solid surface is assumed similar to the specific volume of solid hydrogen, and small relative to the specific volume of the gas. This assumption holds for pressures of less than 100 bar and temperatures greater than 77K.[21] At higher pressures and lower temperatures, hydrogen gas density becomes an appreciable percentage of the solid-state density, and validation of this assumption is required. Applying this assumption to the Clapeyron equation gives

$$\left(\frac{\partial \mathrm{P}}{\partial \mathrm{T}}\right) = \frac{\Delta \mathrm{H}_{\mathrm{des}}}{\mathrm{TV}_{\mathrm{gas}}}$$

To eliminate the volume of the gas and reduce the equation to a function of temperature and pressure only, and equation of state for hydrogen can be used, and typically the ideal gas equation is used. Applying the ideal gas equation yields the Clausius-Clapeyron equation, which is typically used in the literature to evaluate the enthalpy of physisorption storage materials[54, 55]

$$\left(\frac{\partial \ln(\mathrm{P})}{\partial \mathrm{T}}\right) = \frac{\Delta \mathrm{H}_{\mathrm{des}}}{\mathrm{RT}^2}$$

The Clausius-Clapeyron equation is subject to the same restrictions for the assumption of ideal gas behavior as the van't Hoff equation, discussed earlier. These assumptions hold well for the pressures specified in the USDOE targets. Higher pressure systems may need a fugacity correction to retain accuracy in non-ideal systems. Typically, ΔH_{des} is a weak function of temperature but a relatively strong function of surface coverage. Because of this values of ΔH_{des} are defined along isosteres, or constant values of surface coverage and are often defined in the literature as isosteric heat.[56]

An additional complication to the thermodynamic discussions arises in physisorption processes.[57] The Clausius-Clapeyron equation is based on a liquid-vapor equilibrium model, in which the liquid and vapor are separate phases occupying their own distinct volumes. In the gas-adsorbate system, however, these boundaries are less distinct, and molecules from the vapor phase may penetrate or otherwise be included within the volume associated with the adsorbate phase due to the normal compression of the gas, as illustrated in Figure 1.7. This behavior leads to two descriptions of the adsorption: absolute adsorption, which treats the volumes as separate layers and includes some gas phase molecules within the adsorbate layer, and excess adsorption, which excludes these gas molecules from the adsorbate layer. The molar balance between absolute and excess quantities can be defined as

$$n_{\mathrm{excess}} = n_{abs} - \rho V_{\mathrm{Gibbs}}$$

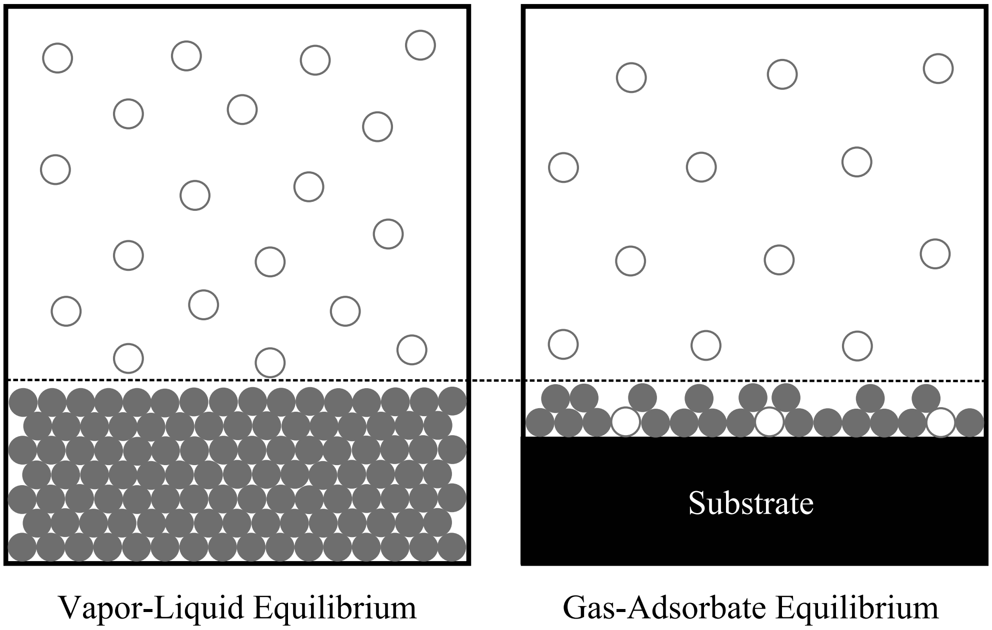

Figure 1.7: Schematic diagram of the relationship between liquid-vapor equilibrium and gas-adsorbate equilibrium. The dashed line represents the Gibbs dividing line for both phases, with spheres below the line representing the absolute condensed phase. The liquid-vapor system has a well-defined interface, while the gas-adsorbate does not. Spheres in white below the line in the gas-adsorbate system are considered part of the gas phase density and are excluded from the excess adsorption calculation.

where ρ is the density of the gas phase, and V_{Gibbs} is the volume of the adsorbate on the material surface defined by a second boundary layer called the Gibbs dividing surface. The location of this surface is defined somewhat arbitrarily as the endpoint of the extension of the potential well from the material surface. Defining the location of the Gibbs defining surface from experiment is currently beyond available imaging technologies, and the surface location is also likely a function of system conditions.

The separation of measurements into absolute and excess isotherms also result from these definitions. Idealized versions of these isotherms, based on the Langmuir adsorption isotherm, appear in Figure 1.8. Experimental measurements can only yield excess isotherms, as these represent the pressure drop from expected values. Absolute isotherms are only available from theoretical calculations, requiring a definition of the Gibbs dividing surface. Excess isosteric heats are typically reported for physisorption materials for both theoretical and experimental studies, to maintain consistency

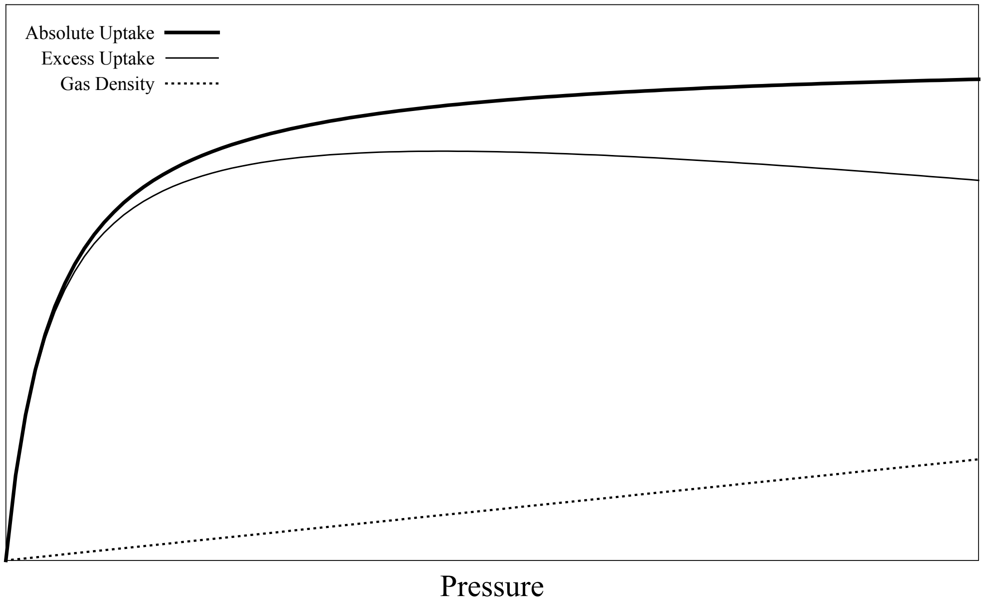

Figure 1.8: Idealized adsorption curves showing the relationship between absolute adsorption, excess adsorption, and gas density and typical lineshapes for the three types. Curves are based on the Langmuir isotherm and the ideal gas equation of state.

within measurements. These values typically lie between 5 kJ/mol and 20 kJ/mol, representing the relatively weak binding in these materials.[58]

1.4.2 State-of-the-Art: Physisorption materials

As with absorption materials, no physisorption materials have yet been developed for commercial vehicular hydrogen storage materials. A number of state-of-the-art material types exist for physisorption materials which have the potential to fill this role. These types are reviewed briefly below.

Activated and Templated Carbons—The largest class of adsorbent materials for hydrogen storage, carbon-based materials are lightweight, easily produced and commercially available. Research into carbonaceous sorbent materials has focused on improving techniques for producing high specific surface areas, and thus improving overall adsorption capacity for hydrogen.[58, 55]

Carbon sorbent materials are produced by pyrolysis of organic molecules at high temperatures in reduced oxygen environments. Organic molecules used for this process can be either natural or artificial in origin, and research into the benefits to the properties of the final carbon material resulting from various starting materials, particularly polymers such as polyether ether ketone[59] (PEEK), is ongoing.

For most carbon materials, the resulting pyrolyzed material is then "activated" to produce the high surface areas for adsorption. Several processes for performing this operation exist, and many proprietary methods are claimed by commercial producers. Two common laboratory techniques for activation are steam explosion, which rapidly flashes superheated water introduced into the carbon structure to physically rend the structure, and carbon dioxide maceration, which used high temperature reaction of the carbon surface with CO_2 to produce gaseous CO, causing chemical erosion of the surface. These processes are capable of producing carbon materials with surface areas up to $\sim$3000 m^2/g, but consume a large portion of the starting material in the process. These high surface-area materials, such as AX-21 and MSC-30, are used commonly as a standard for comparison of new physisorption materials.[60, 61]

Recently, efforts to increase the surface area of carbon materials beyond activated carbons and to control the microporosity have led to templated carbon materials. These materials contain carbon in regular nanostructures that provide very high surface areas, and still largely obey Chahine's rule. Investigations into carbon nanotubes and nanotube bundles quickly led to more advanced regular nanostructured materials[63, 65, 64] and carbon aerogels.[66] The latest materials in this area are based on zeolite frameworks.[60, 62] Pyrolysis of polymers within the channels of a zeolite leads to a carbon negative of the zeolite, which can be extracted by dissolving the zeolite material in hydrofluoric acid. This produces a high surface area carbon with very uniform micropores and low skeletal density, and has shown similar uptake to the high surface area MSC-30 with an improved adsorption profile.

Unfortunately, the limits to surface area modification are being approached for pure carbon materials. Research efforts in this area relative to hydrogen storage have been increasingly directed toward engineering applications and reduction of the cost associated with producing these materials. Carbon nanoscaffolds and aerogels are also used frequently to improve the kinetics of absorption materials, and the interactions of the scaffold with these materials is under investigation.[67–69]

Metal Decorated, Doped, and Intercalated Carbons—The low adsorption enthalpies for hydrogen in carbon-based physisorption materials have led to continuous efforts to dope or otherwise transform these materials without adding significant weight to the structure. The most common technique used is to incorporate a small fraction of adatoms or inclusions, which have strong bulk interactions with hydrogen gas, into the material's structure. These dopants may then increase the overall interaction potential of the material.

Initial doping strategies used platinum or palladium nanocluster incorporations onto carbon structures, to produce a material similar to supported-metal catalysts.[51, 71] Because of the high cost of precious metals, later studies have focused on the use of 3d transition metals, particularly titanium,[70] to produce similar effects. The metallic clusters in these materials were unfortunately found to act independently in most cases, with the metal clusters maintaining their own surface coverage of chemisorbed hydrogen atoms at stronger energies than the remaining carbon structure. Several groups have reported *spillover* in such materials, where dissociated hydrogen is transferred from metallic clusters to the carbon structure, providing higher surface area coverage of strongly bound hydrogen atoms.[72, 73] These interactions have been observed at high temperature for platinum and ruthenium catalysts on carbon supporting structures through neutron spectroscopy,[74] and enhanced adsorption capacity at room temperature has been demonstrated. However, these enhancements appear to be a minor effect, and spillover processes are unlikely to produce increases in adsorption enthalpies that are significant for storage applications.

Additional techniques involve direct doping of the carbon structure, rather than surface modifications. Boron and nitrogen doping of the graphitic layers have both shown to increase the adsorption capacity of activated carbons.[75–77] However, whether the increase is due primarily to modification of the surface potential or to increased accessible surface area due to bowing of graphitic layers remains unknown. Intercalation of alkali metals into graphitic structures have also been used, and shown to both modify the interlayer spacing in the structure and increase the hydrogen adsorption enthalpy.[52] These materials, however, are difficult to produce and tend to produce alkali metal hydrides after a few cycles.

Relatively few studies continue to examine these methods for improving the binding enthalpy in hydrogen storage applications, but continue to be relevant for chemical catalysis applications. Studies are largely directed at examination of metal substitutions and reduction of metal size and increase in metal dispersion to reduce the amount of metal loading necessary to produce desired effects.

Metal-Organic Frameworks—Metal organic frameworks (MOFs) have received a large amount of attention in physisorptive hydrogen storage research, both for the very high specific surface areas available in these materials and for large variability in the possible frameworks.[78] These crystalline materials, composed of metal atoms linked together with organic molecules in a three-dimensional framework, contain uniform pores and structures which allow for greater control over the adsorption capacity and enthalpy. MOFs have consistently shown meaningful adsorption capacities at room temperature, making them promising candidates for further development.[79–81]

Hundreds of MOFs have been identified, with varying pore sizes and chemical makeup, and these variations are being actively pursued for gas adsorption applications. Overall, trends in hydrogen binding show an increase in hydrogen adsorption capacity with smaller pore sizes or higher specific surface area, in accordance with Chahine's rule. Incorporation of mid-row transition metals and alkaline earth metals at the metal site have also been shown to increase binding enthalpies, increasing hydrogen storage at high temperatures.[82] Examination of various chemistries and binding motifs are still ongoing. Besides basic materials work, research into improvements in the scale-up and large scale production of MOFs are needed before these materials can be implemented outside of the laboratory.

1.5 Kubas Binding[1]

Recently, a new classification of hydrogen storage materials has been identified: Kubas materials. These materials, first identified in early work on MOFs[80, 83, 84] (MOFs) and Prussian blue analog[13] physisorption materials, showed enhancement in the isosteric heat of adsorption by approximately 2 kJ/mol H_2 over similar materials if unsaturated metal centers were included in the framework. These materials appeared to take advantage of a new binding motif, designated as Kubas binding, which binds a dihydrogen molecule chemically to the unsaturated metal center, in an arrested dissociative absorption. This interaction provides thermodynamics in the ideal range between the ranges of standard physisorption and absorption materials, with the rapid kinetics associated with physisorption materials and long cycle lives. Materials designed to exploit this effect in hydrogen storage materials have shown enhancement of physisorption enthalpies by up to 35 kJ/mol.[85] Moreover, these properties are believed to be tunable, with alterations to the ligands attached to the metal center providing modifications to the binding enthalpy.

Because Kubas binding was initially discovered in MOFs and other physisorption materials during hydrogen storage measurements, the interaction has consistently been treated as physisorption. However, recent experimental studies[86] have also demonstrated unusual behaviors arising in Kubas materials, such as activation energies and plateaus within the isotherms and widely varying adsorption enthalpies, that are not typically associated with physisorption processes. Because an understanding of the mechanism is important to proper calculation of the thermodynamic properties, these oddities have prompted further investigation into the mechanism of these interactions to enable a detailed understanding of these materials and enable rational design.

Mechanistic studies of Kubas binding require materials that exhibit this binding type almost exclusively. The original complexes exhibiting this behavior, the dihydrogen complexes first reported[87] by Gregory Kubas, provide such a model. In the next chapter, the properties of dihydrogen complexes and the complexes useful for thermodynamic studies in the solid state are reviewed.

---

[1] Parts of this section have been reproduced with permission from *Evaluation of the Thermodynamic Properties of H_2 Binding in Solid State Dihydrogen Complexes $[M(\eta^2\text{-}H_2)(CO)dppe_2][BArF^{24}]$ (M = Mn, Tc, Re): An Experimental and First Principles Study* by David G. Abrecht and Brent Fultz. Copyright 2012 American Chemical Society.

Chapter 2

Review of Dihydrogen Complexes

The unexpected discovery of the first dihydrogen complex, $W(\eta^2\text{-}H_2)(CO)_3(PCy_3)_2$, has led to the subsequent reports of hundreds of complexes containing the dihydrogen ligand, including the reclassification of many previously reported as polyhydrides.[88] These complexes demonstrate the full range of molecular bond breaking in the hydrogen molecule to form a metal dihydride. Furthermore, the degree of bond breaking in the ligated dihydrogen molecule has been shown to be a function of the degree and type of electron donation from other ligands attached to the metal center.[89, 93] This property has led to considerable interest in dihydrogen complex research, both for furthering the basic understanding of metal-hydrogen interactions and H-H bond breaking, and for applications in catalysis, biochemistry, and hydrogen storage and production.

In this chapter, the properties and synthesis of dihydrogen complexes are reviewed, and their applications as model compounds for Kubas binding to further basic understanding and rational design of Kubas materials for hydrogen storage applications are discussed. Complexes and properties relevant to hydrogen storage are the primary focus of this review; no attempt is made to cover the extremely rich expanse of dihydrogen complex chemistry, which includes such diverse topics as protein activity and extreme low temperature chemistry.

2.1 General Properties, Structure, and Bonding

Dihydrogen complexes cover an extremely diverse range of properties and chemistries, and while the majority share common properties, there are few rules of thumb associated with these complexes that

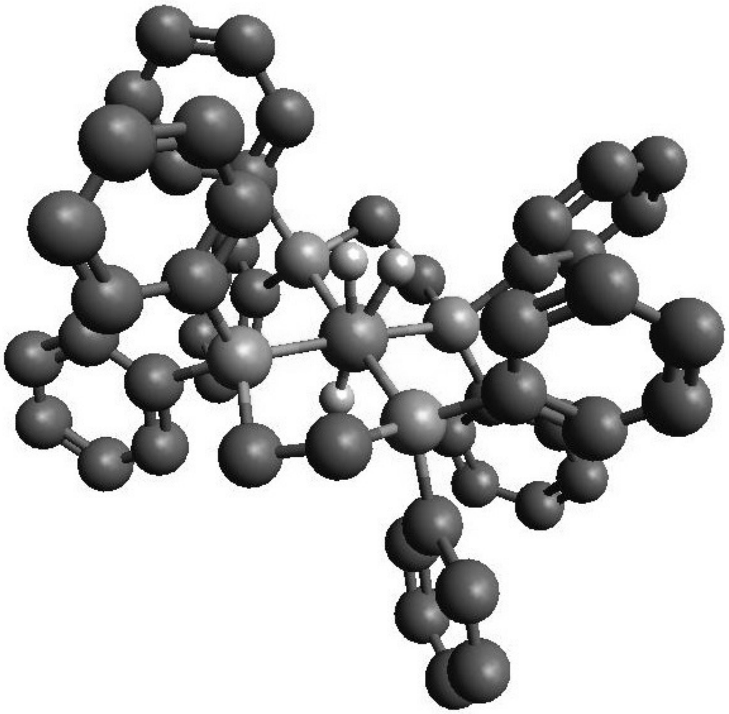

Figure 2.1: Ball-and-stick model[91] of the organometallic dihydrogen fragment [FeH(η^2-H$_2$)dppe$_2$]$^+$, showing octahedral configuration of the central iron atom and side-on coordination of the hydrogen molecule to the metal center. Alkyl and aryl hydrogens have been removed for clarity.

do not have demonstrated exceptions.[88] Organometallic dihydrogen complexes normally contain one dihydrogen molecule bound chemically to a transition metal center, although occasionally two dihydrogen ligands may be present. Most known dihydrogen complexes are octahedrally coordinated,[90] and all known dihydrogen complexes contain hydrogen bound in a side-on (η^2) configuration, as shown in Figure 2.1. These configurations preferentially position the molecular orbitals of both the hydrogen molecule and the organometallic molecule for bonding interactions. Dihydrogen binds as a neutral, or L-type, ligand and does not change the formal oxidation state of the metal center or charge on the molecule.[87] However, dissociation of the dihydrogen molecule at the complex forms a dihydride, which increases the oxidation state of the metal by two. Instability of the corresponding dihydride oxidation state may be a factor in stability of the dihydrogen complex, as in iron (II) dihydrogen complexes like [FeH(H$_2$)dppe$_2$][BF$_4$].[96]

Bonding theory for dihydrogen complexes was developed relatively quickly after their discovery.[92] The binding mechanism for dihydrogen complex formation has been described primarily through analogy to the Dewar-Chatt-Duncanson model for π complexes, which introduces the concept of *backdonation* of electron density. In this model, the π electrons associated with an olefinic double bond are partially donated to an empty d-shell of a metal center, forming a coordination complex in a similar fashion to the lone pair donation in classic Werner complexes. Backdonation from the metal center to the π^* orbital of the olefin, which becomes a bonding orbital with respect to the complex, prevents complete rupture of the π bond and stabilizes the complex.

Dihydrogen complexes follow a similar model, donating electron density from bonding electrons in the σ orbital of the hydrogen molecule to an empty d-shell of the metal, while electron density from filled d-shells of the metal center is backdonated to the σ^* orbital of the hydrogen molecule to stabilize the three-center bond and redistribute charge. Molecules exhibiting this binding have been designated σ-complexes.[92] Unlike π complexes, donation from the absorbed molecule in σ complexes occurs through donation of the main bonding electrons, and can lead to complete bond rupture and dissociation if donation from the absorbed molecule or backdonation from the metal center becomes too strong. This balance allows direct control over bond breaking and formation of dihydrides in dihydrogen complexes, such that the entire reaction coordinate can be represented.[88]

Lability of the dihydrogen molecule has been directly related to the degree of bond dissociation in H_2 complexes.[113, 114] Additional backdonation to the σ^* orbital causes elongation of the H-H bond towards bond breaking, which has been linked to reduced lability of the dihydrogen complex and more hydridic character. Increased backdonation results from higher electron density at the metal center, and is a factor of both the identity and valency of the central metal atom and donation from the accompanying ligands, particularly the ligand *trans* to the H_2 binding site. This effect has been cataloged computationally by Li and Ziegler[89] in the $Mo(CO)_x(PR_3)_{5-x}(H_2)$ system, where substitution of strongly π accepting carbonyl groups by weakly π accepting phosphines leads to increasing dissociation of the H-H bond.

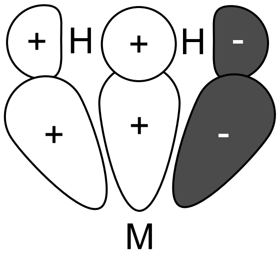

Figure 2.2: Bonding model for orbitals during transition metal-dihydrogen binding.

A strong σ donor *trans* to the dihydrogen complex, such as hydride, also reduces H-H bond elongation and increases dihydrogen character by forcing electron density to remain within the σ orbital of the hydrogen molecule, despite increased electron density at the metal center. This effect allows dihydrogen ligands to be present despite highly electrophilic metal centers.

Reduced electron density at the metal center leads to decreased backdonation to the hydrogen molecule. This effect leads to a reduction in bond stability in π accepting ligands like N_2 and instability of the complex. However, the reduced backdonation in electron-poor dihydrogen complexes is often compensated by increased σ donation from the H_2 molecule. Li and Ziegler found a decrease in the energetic contribution to the molecule from backdonation from -21.2 kcal/mol in $Mo(CO)(PH_3)(H_2)$ to -11.9 kcal/mol in $Mo(CO)_5(H_2)$, representing an increased instability with less backdonation, but a corresponding and near equivalent energetic stabilization from σ donation from the H_2 molecule, leading to nearly equivalent decomposition energies for the entire series.[89] This allows the hydrogen ligand to bind effectively to relatively electron-poor metals, and allows stabilization of dihydrogen complexes by reducing the total electron density available in the molecule. For this reason, cationic dihydrogen complexes are more stable, and make up the majority of reported dihydrogen complexes. The same effect may be produced by using electron-poor metals (i.e., early transition metals) and by using metals with poor backdonation ability.

2.2 Synthesis and Characterization

Synthesis and characterization of dihydrogen complexes described in the chemical literature are primarily concerned with the solution state. Since the metal centers are isolated within a large coordination sphere created by the ligands in both solution and solid states, crystal fields and intermolecular interactions are not expected to cause major deviations in the binding behavior for small molecules at the central site, and in many cases the properties can be translated directly. However, ligand rearrangements and other kinetic processes are often considerably slower in the solid state, and reaction mechanisms that take advantage of a dynamic equilibrium between geometric arrangements may be inaccessible when considering these complexes for hydrogen storage materials.

Most dihydrogen complexes are air-sensitive, and must be prepared under an inert atmosphere. Inert gases such as argon or helium must be used when formation of the N_2 adduct is undesirable. Excess moisture should also be avoided, although certain dihydrogen complexes are entropically stabilized against substitution of the H_2 ligand by H_2O at room temperature.[88]

2.2.1 Synthetic Routes

Stable dihydrogen complexes are primarily formed through one of four synthetic routes:[87, 94–97] direct hydrogenation of an unsaturated precursor, hydrogen displacement of a neutral or charged ligand, and protonation of a hydride complex:

$$\mathrm{L_nM + H_2 \rightleftharpoons L_nM(H_2)}$$

$$\mathrm{L_nML' + H_2 \rightleftharpoons L_nM(H_2) + L'}$$

$$\mathrm{L_nMX + H_2 \rightleftharpoons [L_nM(H_2)]^+ + X^-}$$

$$\mathrm{L_nMH + HX \rightleftharpoons [L_nM(H_2)]^+ + X^-}$$

The first equation, representing direct hydrogenation of an unsaturated precursor, is the most relevant for hydrogen storage and is the expected reaction during cycling in solid-state fuel storage applications. However, this reaction is one of the most difficult for initial production of the complexes, due to solution formation of complexes and the general instability of unsaturated organometallic clusters towards addition of solvent or other small molecules. As a result, this synthetic mechanism is reported for only a small portion of dihydrogen complexes.

Unsaturated precursors capable of absorbing hydrogen directly in solution are stabilized by the presence of agostic interactions, where C-H bonds from pendant groups on attached ligands weakly occupy the open coordination site, entropically stabilizing the complex towards addition of a molecule.[98, 99, 88] For example, in $W(CO)_3(PCy_3)_2$ or $[Mn(CO)dppe_2][BArF^{24}]$ cyclohexyl and phenyl groups located on the phosphines, respectively, have been shown through crystallographic methods to preferentially arrange to coordinate the *ortho* proton to the open site.[99, 100] While H_2 has been shown to actively displace the agostic interaction in $W(CO)_3(PCy_3)_2$, $[Mn(CO)dppe_2][BArF^{24}]$

in the agostic configuration has been shown to be inactive to hydrogen absorption in the solid state despite ready absorption of hydrogen in solution, and similar steric effects have been shown to inhibit dihydrogen binding in the solid state.[86] Separate evaluations of direct hydrogenation of complexes containing agostic interactions are therefore needed for solid-state applications.

Displacement of small molecule ligands, such as H_2O or N_2, also produces H_2 complexes amenable to hydrogen storage applications.[94, 95] Dihydrogen complexes commonly have corresponding dinitrogen complexes[101, 100, 107, 97, 102] due to the similarity in π acceptor ability of the H_2 and N_2 ligands, and the weak σ donation ability of N_2 relative to H_2 favors dihydrogen coordination in many complexes, allowing easy displacement. This method provides effective protection of the binding site during synthesis, and the small, gaseous N_2 molecule can be removed from the coordination site in the solid state more easily than agostic interactions arising from bulky ligands. N_2 release from initial charging would be benign to fuel cell catalysts and other catalytic converters in the system, and removal of the protective N_2 adduct can correspondingly be performed after the fuel tank is charged.

Displacement of a charged ligand is typically not desirable for hydrogen storage applications because of the weight of the persistant anion; however, methods exist to reduce the complex *in situ* to separate the ionic pair. Direct displacement of a charged ligand is difficult without a precipitating cation such as sodium to drive the reaction,[103, 104] although examples exist: chlorine is displaced by H_2 without an intermediate in $Re(CN\text{-}t\text{-}Bu)_3(PCy_3)Cl$ in dichloromethane.[105] Formation of a neutral complex is possible if a hydride is used as a reducing agent:

$$L_nMX_m + mH^- + H_2 \longrightarrow L_nM(H_2)H_m + mX^-$$

This method has successfully been used to produce several dihydrogen complexes,[117, 106] and NaH, $NaBH_4$, or $LiAlH_4$ may be used as hydride sources. NaH is ideal chemically for these reactions, although poor solubility in organic solvents often prevents its direct use. Use of borohydrides and alanates may produce side products because of the strong reductive power of $LiAlH_4$ and the coordination potential of borohydride.

Protonation of a hydride complex has received a great deal of attention as a synthetic route because of both the higher stability of cationic dihydrogen complexes and the relevance of these processes to modeling the behavior of hydrogenase enzymes.[88] However, because a large, poorly coordinating anion, such as BPh_4,[96] remains, these methods are less favorable for hydrogen storage applications except to produce model complexes to test properties of Kubas binding. Direct acidification of a hydride by the strong acid of a poorly coordinating anion in an organic solvent, producing a dihydrogen salt that is poorly soluble in the organic solvent, allows clean production and purification of the complexes and is used for nearly all dihydrogen complex production because of the simplicity of the synthetic method.

2.2.2 Dihydride/Dihydrogen Identification

Characterization of dihydrogen complexes is often difficult, as belied by their late discovery. Spectroscopy remains the most definitive method for determining the existence of a dihydrogen ligand.[88] The existence of the H-H bond produces isotope-dependent vibrational and rotational modes in the organometallic complex that are not present in hydrides, and uniquely identify the dihydrogen molecule.[108] These modes produce significant, observable shifts in IR and Raman spectroscopy band energies between H_2 and D_2 isotopes, on the order of hundreds of wavenumbers. Additionally, substitution of H_2 by HD leads to unique mode energies lying between H_2 and D_2 rather than a splitting of the two homoisotope bands.

Of the six normal modes for the dihydrogen molecule, only the symmetric stretching mode and H-H stretch produce strong bands in IR and Raman spectroscopy, and H-H stretching modes in the 2080–3200 cm^{-1} range often overlap with the C-H stretching modes of other attached ligands.[88, 109] Observation of the weak mode bands can be facilitated by the use of inelastic neutron scattering (INS) techniques with perdeuteration of the remaining ligands to isolate the H-H modes.[110, 111] This technique, although extremely powerful for determination of the vibrational modes in dihydrogen ligands, is used less frequently because of the expense associated with the measurement.

The existence of a dihydrogen ligand may also be inferred from crystallographic characterization

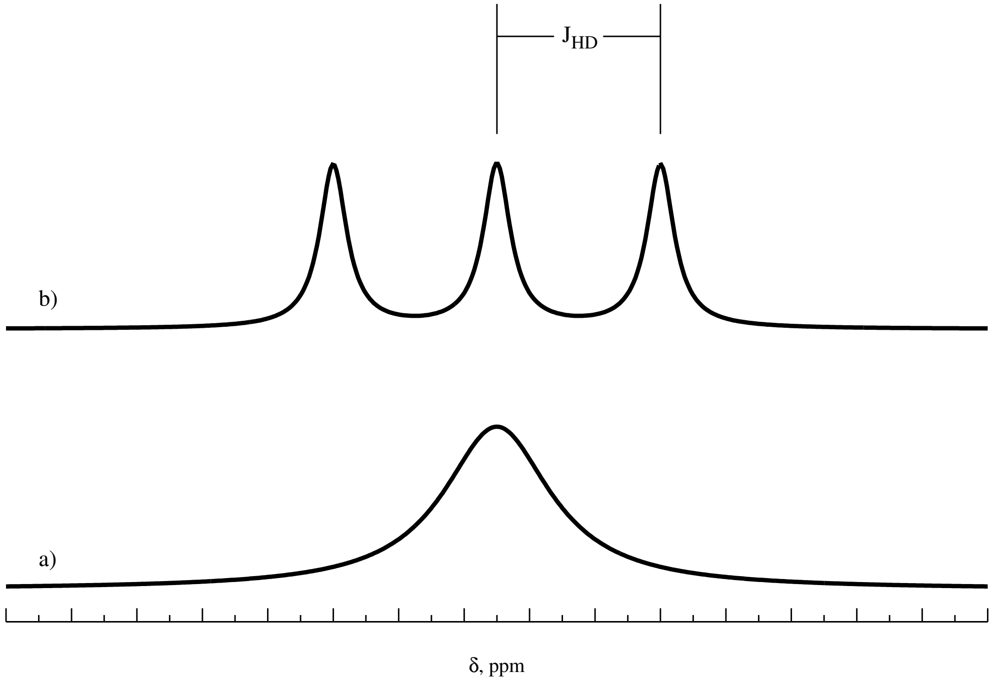

Figure 2.3: Idealized NMR spectra peaks for a) H_2 complex, showing broadened signal and b) HD substitution, showing 1:1:1 triplet splitting of the peaks and sharpened signal. J_{HD}, the coupling constant for the spin-spin coupling of the hydrogen and deuterium atoms is measured as shown and is proportional to the H-D bond distance, and is absent in the absence of a bond. HD and H_2 signals may share the same chemical shift, or the HD signal may be shifted by a small amount due to isotope effects on the bonding properties.

techniques. X-ray and neutron diffraction studies used to characterize the bond lengths and angles of the molecule to provide insight into the bonding orbitals and electronic character can simultaneously provide separation distances between hydrogen atoms. Distances of less than 1.3 Å between hydrogen atom positions indicate potential dihydrogen complexes, and distances greater than 1.3 Å are unlikely to retain any dihydrogen character.[88, 112, 113] However, these techniques cannot be used to confirm the existence of a bond between the hydrogen atoms, and spectroscopic methods are needed for confirmation. Interatomic distances determined from crystallographic techniques are also used to determine the existence of agostic complexes in unsaturated complexes used for direct hydrogenation formation of dihydrogen complexes.[99]

NMR spectroscopy is used extensively for identification of dihydrogen complexes.[96, 115, 97, 88, 90, 113] Substitution of the H_2 molecule with HD produces a 1:1:1 triplet splitting pattern at the chemical shift corresponding to the dihydrogen complex in ^{1}H NMR spectra, as shown in Figure 2.3. This splitting occurs due to spin-spin coupling between the atoms along the residual H-D bond, and is absent if insufficient electron density remains between the two molecules. This technique provides rapid, inexpensive evidence for the presence of an H_2 ligand in both solid and solution states, and is included in the majority of literature reports for dihydrogen complexes. Correlations have also been established between the H-H distance and the dipole-dipole relaxation time (T_1) in solution NMR,[116, 117] but temperature dependence and interference from adjacent ligands makes this technique less favorable.[118]

Some compound-specific techniques for identification of dihydrogen complexes have also been reported. Morris and Schlaf[119] reported unique Mössbauer isomer shifts and quadrupole splittings for dihydrogen complexes with iron centers, and unique partial quadrupole splittings for the dihydrogen ligand relative to hydride ligands. King et al. report[100] carbonyl shifts for complexes containing carbonyl *trans* to the dihydrogen complex similar to those for dinitrogen or dicarbonyl complexes, due to π acceptor ability of the dihydrogen ligand that is absent in hydride ligands. These techniques can provide strong support for the presence of a dihydrogen complex, but are limited to specific chemistries.

2.3 Binding Strength and Hydrogenation Thermodynamics[1]

The binding strength of the H_2 molecule in dihydrogen complexes is typically evaluated from the stretching of the H-H bond when bound to the metal center. This property is a measure of the electron density removed from the bonding σ orbital of the hydrogen molecule and donated to the anti-bonding σ^* orbital by the metal center, representing the degree of bond breaking within the H_2 molecule and the strength of the electronic interaction. H-H distances less than ~1.0 Å, representing the "true" dihydrogen complexes, are considered weakly bound and easily removed from the dihydrogen complex. Bond distances of greater than ~1.0 Å, representing complexes with

---

[1] Parts of this section have been reproduced with permission from *Evaluation of the Thermodynamic Properties of H_2 Binding in Solid State Dihydrogen Complexes $[M(\eta^2\text{-}H_2)(CO)dppe_2][BArF^{24}]$ (M = Mn, Tc, Re): An Experimental and First Principles Study* by David G. Abrecht and Brent Fultz. Copyright 2012 American Chemical Society.

more dihydride character, are considered more tightly bound and less likely to reversibly absorb the dihydrogen complex.[112, 113]

X-ray diffraction and neutron diffraction provide the only truly definitive method for determining H-H bond distance. However, x-ray scattering from the low mass hydrogen atom relative to large metal atoms is often weak and indeterminate, and neutron diffraction experiments are expensive and difficult to perform. Estimates of the H-H bond separation are available from NMR spectroscopy measurements, and are the most commonly reported method of approximating the binding strength. Maltby[121] and Luther[122] independently developed relationships correlating the H-H bonding distance from x-ray and neutron diffraction measurements to the solid-state NMR coupling constant, J_{HD}, of isotopomeric HD complexes. The relationship given by Maltby is:

$$d_{\mathrm{HH}} = 1.42 - 0.0167 J_{\mathrm{HD}}$$

where d_{HH} is the H-H bond distance, in angstroms, and J_{HD} is given in hertz. The equation given by Luther is the same as the equation above, with values within experimental error of those found by Maltby. These relationships have also been shown to hold approximately in solution NMR studies, despite the potential for interference from solvent molecules and increased molecular motion. Because of the ease and clarity of solution state NMR spectra relative to solid-state NMR spectra or organometallic crystallographic methods, this method has come to dominate the literature for estimates of binding strength.

While the interatomic distances can provide relative measures of the dihydrogen binding strength in similar families of complexes, these values only provide approximations to the binding strength and are not universally applicable as measures of thermodynamic properties. The dihydrogen molecule often exists in equilibrium with its corresponding dihydride, with a low energy barrier separating the two states. Removal of dihydrogen may be possible through the transient formation of a weak dihydrogen complex, as seen in $\mathrm{W(CO)_3(P(^{i}\text{-}Pr)_3)_2(H_2)}$, despite the complete dissociation of the H_2 molecule to form the dihydride.[120] The existence of additional hydrides ligated to the metal surface can also add entropic stabilization to the complex through intramolecular site exchange, stabilizing weaker complexes.[96] Varying ratios of σ and π donation ability created by the metal-ligand pairs lead to poor correlation between the observed lability of the dihydrogen ligand and the H-H distance for molecules with widely disparate chemistries. Additionally, the bond distance provides no measure of the stability of the dehydrogenated complex; rearrangement of the molecular geometry after dehydrogenation can strongly affect the thermodynamic properties of hydrogen absorption and release, and consequently the equilibrium pressure and temperature.[88]

Thermodynamic information on dihydrogen complexes has largely been focused on the heterolytic cleavage of the dihydrogen molecule and the protonation ability of the complexes,[96] in order to obtain greater information on the activity of hydrogenases.[88] These interactions are unfortunately detrimental to direct hydrogenation hydrogen storage applications, as they represent a potentially irreversible side reaction to form stable hydride complexes, and thermodynamic values presented in these studies do not typically include the unsaturated complex for assistance in evaluating direct hydrogenations. The available thermodynamic data on direct hydrogenations to form dihydrogen complexes remains scarce. Calorimetric studies have reported solution-state binding enthalpies of $\Delta H°$= -41.8 and -46.9 kJ/mol for the complexes $W(CO)_3(PCy_3)_2$ and $W(CO)_3(P\text{-i-}Pr_3)_2$ in toluene, respectively.[123, 124] A similar study in THF, attempting to develop relationships between the group 6 metals in the complexes $M(CO)(PCy_3)_2$ (M=Cr, Mo, W), found $\Delta H°$ between -27.2 kJ/mol and -41.8 kJ/mol, and entropy values $\Delta S°$ between -100 and -110 J/mol-K.[95] Solid-state measurements are limited and show deviations from solution behavior, with one study giving $\Delta H° =$ -13.22 kJ/mol and $\Delta S° =$ -9.62 J/mol-K for hydrogen absorption over the complex[125] $[Ir(cod)(PPh_3)_2]SbF_6$, representing a significant reduction in binding strength and an unexpected increase in the entropy of the bound state. While most of the data are consistent with values obtained from hydrogen storage materials, the current measurements represent a wide range of metals and ligands providing different chemical properties that, apart from the systematic study performed by Gonzalez, et al. for the group 6 complexes, do not provide chemical trends to aid in the design of new materials.

Difficulties in obtaining systematic thermodynamic data for dihydrogen complexes arise from their inherent stability, with the equilibrium pressures of most known materials falling outside of acceptable ranges for traditional chemistry techniques. New techniques for measuring the thermodynamic properties of dihydrogen complexes, especially at elevated pressures, are necessary to evaluate their potential as hydrogen storage materials. In the next chapters, the mechanism of pressurized hydrogenation to form dihydrogen complexes in the solid state is examined, and techniques for establishing the thermodynamic properties of these materials are established.

Chapter 3

Studies of $[\mathrm{M}(\eta^2-\mathrm{H}_2)(\mathrm{CO})\mathrm{dppe}_2]^+$ (M = Mn, Tc, Re) Complexes[1]

As discussed in the previous chapter, technical difficulties have largely prevented direct quantification of thermodynamic properties for dihydrogen binding in organometallic complexes. To help resolve these difficulties and enable the generation of systematic thermodynamic data relevant to the hydrogen storage community, we have used the Sieverts method to obtain experimental isotherm measurements on the interaction of hydrogen gas with the dihydrogen complex $[\mathrm{Mn(CO)dppe_2}][\mathrm{BArF^{24}}]$ (dppe = 1,2-bis(diphenylphosphino)ethane, $\mathrm{BArF^{24}}$ = tetrakis-(3,5-trifluoromethyl)phenylborate). In addition, we report electronic structure calculations on the hydrogenation of the fragments $[\mathrm{M(CO)dppe_2}]^+$ (M = Mn, Tc, Re) to examine trends in the binding energy within the group 7 metals. We interpret our results in terms of the solid-state binding mechanism for hydrogen in these materials, and show a relatively rapid and facile means to quantitatively evaluate thermodynamic properties and establish chemical trends that are useful for materials design.

3.1 Experimental

Unless otherwise stated, all reactions were performed under a dinitrogen atmosphere using either a controlled atmosphere glovebox or Schlenk line techniques. Manganese pentacarbonyl bromide, magnesium metal and sodium tetrafluoroborate were purchased from Alfa-Aesar and used without

---

[1] This chapter has been reproduced with permission from *Evaluation of the Thermodynamic Properties of H_2 Binding in Solid State Dihydrogen Complexes $[M(\eta^2\text{-}H_2)(CO)dppe_2][BArF^{24}]$ (M = Mn, Tc, Re): An Experimental and First Principles Study* by David G. Abrecht and Brent Fultz. Copyright 2012 American Chemical Society.

further purification. 1,2-bis(diphenylphosphino)ethane was purchased from Strem Chemicals and used without further purification. 3,5-bis(trifluoromethyl)bromobenzene was purchased from Sigma-Aldrich and was degassed using three freeze-pump-thaw cycles and dried over activated alumina before use. Research-grade gases were purchased from Matheson and used directly. All solvents were dried and deoxygenated by purging with dry dinitrogen gas for 15 minutes before passing through packed columns of activated alumina and activated copper. Mass spectroscopy of off-gassing products was performed using a Stanford Research Systems RGA-200 residual gas analyzer with observable pressure ranges from 10^{-8} to 10^{-5} torr. After synthesis, materials were stored under dry argon in an atmosphere-controlled glovebox until used for sorption measurements.

Solution-state NMR spectra were recorded on a Varian 300 MHz instrument with ^{1}H shifts reported relative to the residual solvent peak, and ^{31}P peaks reported relative to 85% H_3PO_4. Deuterated NMR solvents were purchased from Cambridge Isotopes Laboratories. Deuterated dichloromethane was vacuum distilled from a sodium/benzophenone solution before use. Deuterated acetone was vacuum distilled twice from $CaSO_4$ and stored over 4A molecular sieves before use.

Preparation of Na[BArF^{24}]—This procedure was a modification of one in the literature.[131] 3,5-bis(trifluoromethyl)bromobenzene (5 mL, 8.55 grams, 2.918 mmol) was added to a suspension of anhydrous $NaBF_4$ (0.8173 grams, 7.446 mmol) and magnesium metal (5.028 grams, 206.87 mmol, excess) in 150 mL of diethyl ether under a nitrogen atmosphere, causing the solution to turn olive green. The suspension was stirred for 24 hours, producing an orange solution with white precipitate. The solution was exposed to air and quenched with 20 mL of saturated aqueous sodium carbonate solution, followed by filtration over a coarse frit to remove precipitated salt. The ether layer was removed, and the aqueous layer was washed with 50 mL of fresh ether. The ether layers were combined, dried over sodium sulfate and filtered. The solvent was removed *in vacuo* and the resulting residue was dissolved in benzene and distilled in a Dean-Stark apparatus under nitrogen for three hours to remove residual water. The benzene was then removed *in vacuo*, and the residue was washed with dichloromethane and filtered to produce the product as an off-white powder. ^{1}H NMR (300 MHz) in d_6-acetone: δ 7.67 (s, 4H); 7.79 (t, 8H).

Preparation of *fac*-MnBr(CO)$_3$dppe—This procedure was a modification of one in the literature.[132] A solution of the phosphine ligand 1,2-bis(diphenylphosphino)ethane (dppe, 3.5326 grams, 8.866 mmol) in 100 mL benzene was added to crystalline Mn(CO)$_5$Br (1.2180 grams, 4.430 mmol) in a 250 mL quartz round-bottom flask and allowed to stir for one hour, causing Mn(CO)$_5$Br to slowly dissolve and release CO gas to produce a yellow solution containing both the remaining free ligand and the product. The compound was observed by NMR in CD$_2$Cl$_2$ but not isolated. ^{1}H NMR (300 MHz) in CD$_2$Cl$_2$: δ 2.80 (m, 4H); 3.16 (m, 4H); 7.41(m, 20H). ^{31}P NMR (300 MHz) in CD$_2$Cl$_2$: δ 69.6 (s).

Preparation of *trans*-MnBr(CO)dppe$_2$—This procedure was a modification of one in the literature.[132] The solution of *fac*-MnBr(CO)$_3$dppe and free ligand in benzene from the previous synthesis was irradiated with UV light for 2 hours under an evacuated headspace and strong stirring in a 250 mL fused quartz round-bottom flask, causing the precipitation of 0.8 grams of red-orange solid that adhered to the flask walls and blocked further irradiation. The solvent was removed *in vacuo*, and the resulting residue was washed with fresh benzene and filtered to obtain the product as an orange powder. The filtrate was collected and the procedure was repeated until no additional precipitate was formed. Total yield 3.365 grams (3.506 mmol, 79.1%) on manganese. ^{1}H NMR (300 MHz) in CD$_2$Cl$_2$: δ 2.52 (m, 4H); 2.80 (m, 4H); 7.04 (t, 16H); 7.10 (m, 8H); 7.22 (quart., 8H), 7.32 (m, 8H). ^{31}P NMR (300 MHz) in CD$_2$Cl$_2$: δ 72.1.

Preparation of [Mn(CO)dppe$_2$][BArF^{24}]—This procedure was a modification of one in the literature.[115] Solid Na[BArF^{24}] (3.059 grams, 3.452 mmol) was mixed with solid *trans*-MnBr(CO)dppe$_2$ (3.266 grams, 3.403 mmol) in a 100 mL round-bottom flask and 50 mL of dichloromethane was added to the solid mixture, immediately forming an emerald green solution that was stirred for one hour. After one hour the solution was filtered over celite to remove excess insoluble Na[BArF^{24}] and bromide salts. The filtrate was collected and the solvent removed *in vacuo*, causing a color change from emerald green to aquamarine blue. The residue was redissolved in toluene, producing a green solution, and filtered to remove any remaining bromide salts. The filtrate was collected and the solvent removed *in vacuo*, producing a blue-green powder containing mixed adducts and toluene within the structure, as described by King et. al.[115] Removal of adducts and toluene was performed under high vacuum conditions at 373K until no additional toluene was observable by residual gas mass spectroscopy, producing the five-coordinate product in 90% purity. ^{1}H NMR (300 MHz) in CD_2Cl_2 under argon atmosphere: δ 2.78 (s, 8H); 6.20 (s, broad, 8H); 6.95–7.40 (m, 32H); 7.56 (s, 4H); 7.73 (s, 8H). ^{31}P NMR (300 MHz) in CD_2Cl_2 under argon atmosphere: δ 82.47 (s, broad).

Reaction of [Mn(CO)dppe$_2$][BArF^{24}] with H_2 for NMR spectroscopy - Confirmation of the dihydrogen absorption ability of [Mn(CO)dppe$_2$][BArF^{24}] was performed by solution NMR. CD_2Cl_2 was vacuum transferred into a J. Young tube containing solid [Mn(CO)dppe$_2$][BArF^{24}], forming a deep blue solution. One atmosphere of hydrogen gas was introduced into the tube, and upon shaking the solution rapidly turned yellow. ^{1}H NMR (300MHz) in CD_2Cl_2: δ -7.22 (s, broad, 1.5H); 2.24 (s, 4H); 2.52 (s, 4H); 6.88-7.44 (m, broad, 40H); 7.56 (s, 4H); 7.73 (s, 8H). ^{31}P NMR (300MHz) in CD_2Cl_2: δ 85.2 (s, broad).

3.1.1 H_2 Absorption Measurements

Iterative isotherm and kinetic rate measurements were performed on 2.9 grams of degassed [Mn(CO)dppe$_2$] [BArF^{24}] using a custom-built Sieverts apparatus, described in detail previously.[133] Samples were loaded into a 14 mL stainless steel reactor under an argon atmosphere and sealed before transfer to the instrument. Swagelok VCR copper filter gaskets with 2 μm stainless steel filters were used to confine the powdered sample to the reactor during measurements. After transferring the reactor to the assembly, samples were allowed to pump down overnight to 3.1x10^{-7} torr at the pump inlet before measurements were performed. Pressure on the reactor and manifold during isotherm measurements was measured using an MKS model 120AA-25000RBJ capacitance transducer with a resolution of 0.25 torr in the range of interest. Higher pressures during kinetic measurements were recorded using an MKS model 870B33PCD2GC1 capacitance transducer with a 0-3000 psi range. The time resolution of the instrument was 1500 ms during kinetic measurements.

Manifold and reactor volumes were calibrated prior to absorption measurements through iterative expansion from a calibrated volume with argon gas. Isotherms and kinetic rate measurements were recorded by expanding an equilibrated amount of hydrogen gas from the manifold into the reactor, and the quantity of hydrogen absorbed was determined by ideal gas mole balance between the two volumes after equilibration. This procedure was repeated until no additional hydrogen uptake was observed. After completion of the measurement, the reactor and manifold were evacuated to 10^{-7} torr before heating to the next temperature.

3.1.2 Computations

Electronic structure calculations were performed for the singlet state of the cationic fragments $[M(\eta^2\text{-}H_2)(CO)dppe_2]^+$ and $[M(CO)dppe_2]^+$ (M = Mn, Tc, Re), and the hydrogen molecule using the GAMESS-US software package.[134] Geometry optimizations for the organometallic fragments were performed using fully spin-restricted (RHF) density functional theory calculations, with the B3LYP exchange-correlation functional[135, 136] and the LANL2DZ basis set.[137–140] An additional *p* polarization shell for light atoms and *d* polarization shell for heavier atoms was added to augment the basis set. Effective core potentials[138–140] representing the core 10 electrons for manganese and phosphorous atoms, the core 28 electrons for technetium and the core 60 electrons for rhenium were used. SCF convergence was set to 5.0 x 10^{-6} for all calculations. Geometry optimizations were performed to a tolerance of 10^{-4} au.

The initial structure for $[M(\eta^2\text{-}H_2)(CO)dppe_2]^+$ was taken from structural data reported previously for the manganese compounds by King, et al.[100] Two structures representing both an "open" geometry, in which the hydrogen molecule was removed from the H_2 adduct geometry, and the rearranged "agostic" geometry reported by King et al., in which ortho hydrogens from phenyl groups on the ligands form long-range bonds with the open coordination site, were used for $[M(CO)dppe_2]^+$. Differences between the relaxed structures obtained from calculations and the reported experimental geometries for the manganese complexes were unremarkable, beyond a contraction of all bond lengths within the structure attributable to thermal effects. The H-H bond in each dihydrogen complex was found to align parallel to the phosphorus-metal-phosphorus axis, as shown by the relaxed structure for $[Mn(CO)(\eta^2\text{-}H_2)dppe_2]^+$ appearing in 3.1.

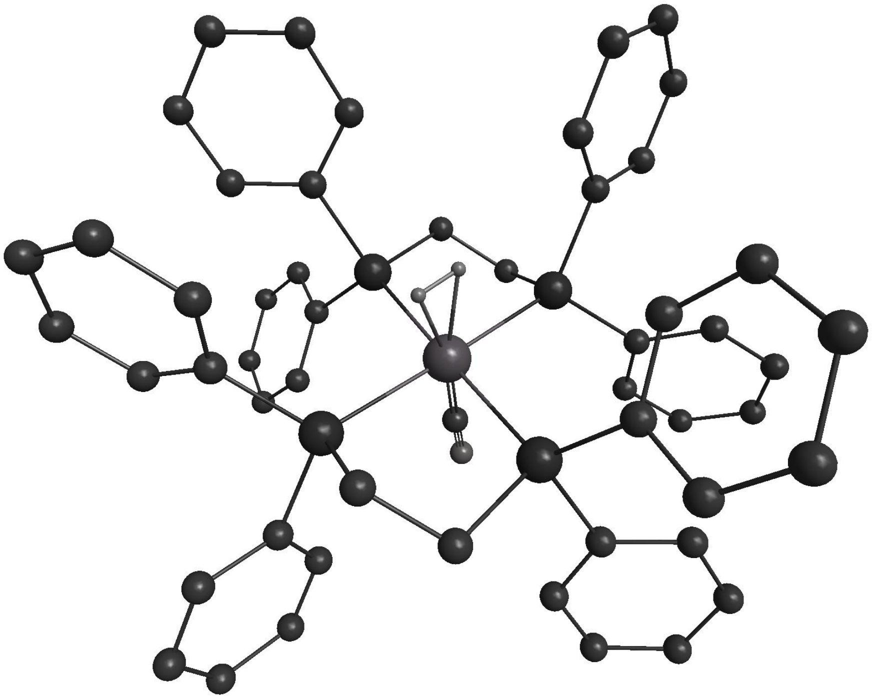

Figure 3.1: Relaxed structure of the $[Mn(\eta^2\text{-}H_2)(CO)dppe_2]^+$ cation, showing the hydrogen molecule aligned along the P-Mn-P axis. Alkyl and aryl hydrogens have been removed for clarity.

Ab-initio ground state electronic energies were calculated using the spin-component scaled Møller-Plesset second-order perturbation[141] (SCS-MP2) scheme with the LANL2DZ-ECP basis set from the optimized geometries found from DFT calculations, which has been shown by Tomàs et al. to lead to accurate calculations for dihydrogen complexes.[114,142] To obtain thermal corrections to the energy and normal mode frequencies, the Hessian matrix for each fragment was calculated at the B3LYP/LANL2DZ-ECP level of theory using seminumerical methods, with contributions from positive and negative displacements of 0.01 Bohr. Vibrational analysis in the rigid rotor approximation was performed to obtain partition functions and normal modes of the fragments, q_{tot}, at 1 atm pressure. A scaling factor of 0.96 was used for the vibrational analysis to correct known errors in the LANL2DZ basis set, consistent with common practice.[143]

The chemical potential of hydrogen gas was calculated from the partition function for the hydrogen molecule obtained from GAMESS, through the relationship:

$$\mu_{\text{gas}}(T, P) = -kT \ln\left(q_{\text{tot}}(T, P^{\circ})\right) + \ln\left(\frac{P}{P^{\circ}}\right) \tag{3.1}$$

where k is Boltzmann's constant, T is the temperature in Kelvin, P is the pressure of the system, and P° is the standard pressure of the system, taken to be 1 atm. Rotational degeneracy for the hydrogen molecule is included in the calculated partition function from the GAMESS software.

The corrected energy, E, for each fragment was obtained as the sum of the ground-state energy, ϵ_0, and the thermal correction to the energy obtained from vibrational analysis, $\epsilon_{\text{corr}}(T)$, which contains contributions from translational, vibrational, and rotational motions of the molecule. The binding energy of the hydrogen molecule to the organometallic site was calculated from the corrected energies as:

$$\Delta E(T) = E_{\text{M}-\text{H}_2}(T) - E_{\text{H}_2}(T) - E_{\text{M}}(T) \tag{3.2}$$

where the subscripts M-H_2, H_2, and M represent the organometallic adduct fragment, hydrogen gas, and the bare organometallic fragment, respectively.

3.2 Results and Discussion

3.2.1 Experimental Results

Absorption isotherms were measured for H_2 onto [Mn(CO)dppe$_2$][BArF^{24}] at temperatures of 313K, 333K, 343K, 353K, 363K, and 373K, and are shown in 3.2. Reversible absorption capacity for all temperatures was approximately 0.35 H_2 molecules per manganese center. No irreversible absorption was observed. This capacity value was consistent throughout measurements at all temperatures, and was stable after multiple absorption/desorption cycles performed during the course of isotherm and kinetic measurements. These properties are consistent with previous reports for solid-state

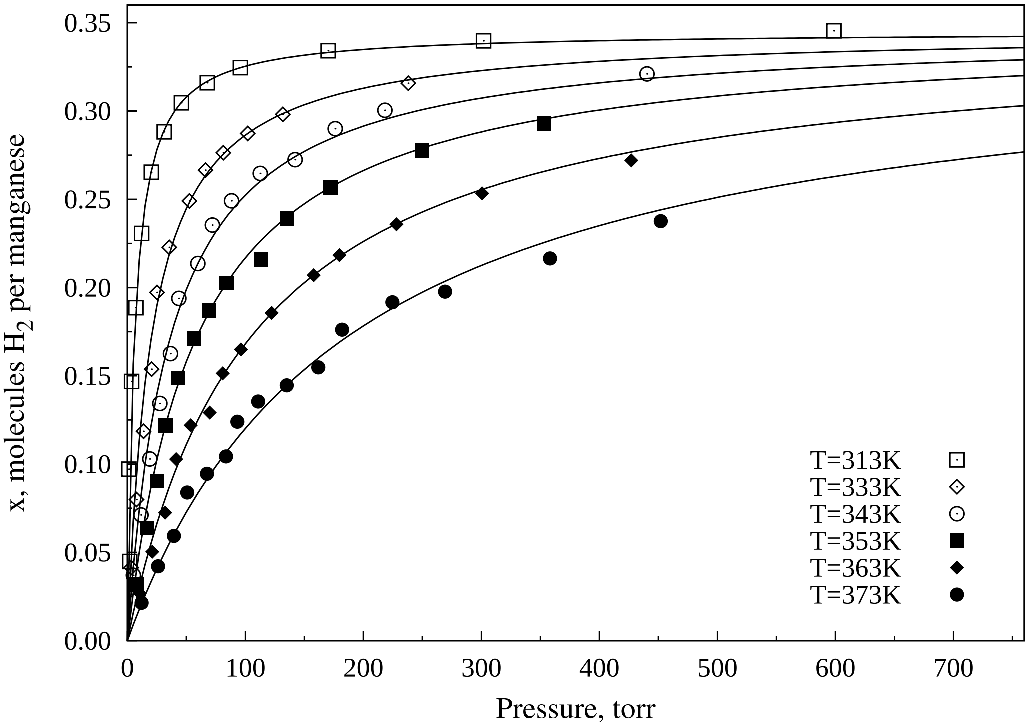

Figure 3.2: Absorption isotherms for hydrogen gas onto [Mn(CO)dppe$_2$][BArF^{24}]. Solid lines are Langmuir isotherm fits to the data.

dihydrogen materials.[125]

Initial rate kinetics measurements were performed at 298K and 318K to determine the dependence of the absorption rate on pressure and quantity absorbed. The results for 318K appear in 3.3. The rate of change of the pressure was determined to be linearly dependent on the pressure and the remaining capacity, such that:

$$\frac{\partial P}{\partial t} = -kP(1-\theta)$$

where θ is the fraction of the reversible absorption capacity absorbed, and k is the rate constant. Rate constants for 298K and 318K were 0.3090 s^{-1} and 0.3116 s^{-1}, respectively. The Arrhenius activation energy obtained from these values is E_a = 330 J/mol, indicating a very low activation barrier to absorption.

The isotherms presented in 3.2 do not demonstrate a maximum like with physisorptive materials,

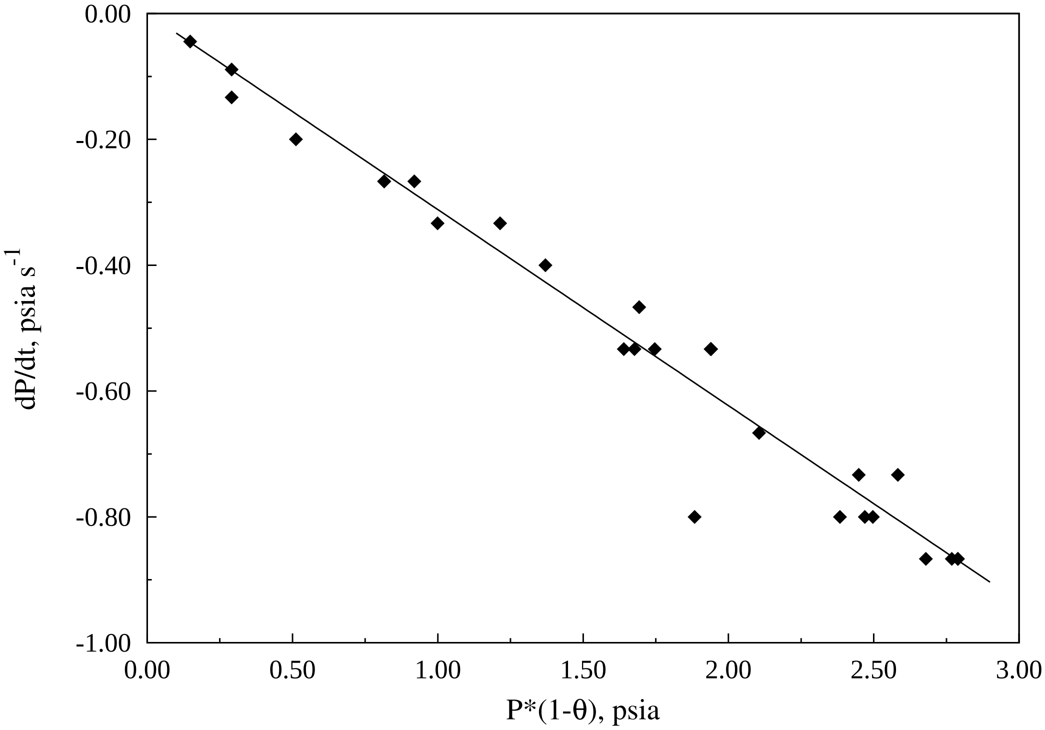

Figure 3.3: Initial rate measurements for hydrogen absorption onto [Mn(CO)dppe$_2$][BArF^{24}] at 318K. Absorption kinetics were found to be linearly dependent on pressure and capacity. Linear regression gives a rate constant of k = 0.3661, $R^2 = 0.9545$.

but rather achieve a stable plateau at 0.35 H_2 molecules per manganese. This behavior is particularly evident in the isotherm at 313K. The existence of the stable plateau in the experimental isotherms is consistent with total absorption[144] and indicates that hydrogen absorbs into the bulk material instead of adsorbing onto the surface. However, the absorption rate is comparable to physisorption materials, despite no additional processing used to increase the surface area of the solid or the exposure of manganese centers to the gas. This rapid absorption is likely due to the loose packing of the bulky organic ligands in the solid, which allows the small hydrogen molecule to diffuse rapidly through the structure.[100]

The rapid kinetics and high reversibility observed in the absorption process suggest a site-binding mechanism for the binding interaction of H_2 with solid [Mn(CO)dppe$_2$][BArF^{24}] that is similar to physisorptive materials. In organometallic dihydrogen complexes, the binding orientation of the ligands is considered fixed by the atomic orbitals of the metal center, producing distinct binding sites for each ligand at the metal center. The isolation of the metal centers by the organic constituents ensures both non-interacting sites and chemical uniformity, suggesting the binding interaction at each site is isoenergetic. With this interpretation of the coordination site, we investigated the binding behavior by fitting the experimental isotherms to the Langmuir model. The Langmuir isotherm model assumes an established equilibrium between a mobile phase of guest molecules and fixed sites capable of binding a single molecule, with homogeneous, non-interacting, and isoenergetic interactions, representing an appropriate description of the organometallic coordination site if the behavior is similar to other site-binding mechanisms.

For the assumed ideal gas reaction:

$$[M(CO)dppe_2][BArF^{24}] + H_2 \rightleftharpoons [M(\eta^2\text{-}H_2)(CO)dppe_2][BArF^{24}] \tag{3.3}$$

in which a single hydrogen molecule binds to the open coordination site on the metal, represented by *M*, the Langmuir isotherm is given by:

$$\frac{n}{N} = \frac{\alpha P}{1 + \alpha P}\ , \qquad \alpha = \frac{K_{\mathrm{eq}}}{RT} \tag{3.4}$$

where n is the number of bound hydrogen molecules, N is the total number of active binding sites, P is the pressure of the gas in atmospheres, R is the universal gas constant, T is the system temperature in Kelvin, and K_{eq} is the equilibrium constant for Equation 3.3.

Langmuir fits to the experimental data are shown as the solid lines in 3.2. The fit for 313K was obtained by varying both the total number of active binding sites, *N*, and α as fitting parameters. A value of 0.344 H_2 per manganese center was found for N at 313K, and was held constant for the fits at all other temperatures. The values for K_{eq} derived from the fitted values for α and the R^2 values of the fits appear in 3.1. As can be seen from the figure and the R^2 values, the Langmuir model very accurately describes hydrogen absorption by the manganese complex, indicating that the open coordination sites within $[\mathrm{Mn(CO)dppe_2}][\mathrm{BArF}^{24}]$ interact with hydrogen gas through a site-binding mechanism.

The standard enthalpy and entropy of the absorption interaction are readily obtained from the values of the equilibrium constant in Equation 3.4 through the general form of the van't Hoff equation:

$$\ln K_{eq} = -\frac{\Delta H^\circ}{RT} + \frac{\Delta S^\circ}{R} \tag{3.5}$$

where ΔS° and ΔH° are the entropy and enthalpy of the absorption reaction, as defined by Equation 3.3, at standard conditions of one atmosphere pressure and 298K. A van't Hoff plot of the equilibrium constants from the Langmuir fits appears in 3.4. Linear regression gives values of ΔH° = -52.2 kJ/mol and ΔS° = -99.6 J/mol-K for hydrogen absorption over [Mn(CO)dppe$_2$][BArF^{24}]. This enthalpy is similar to experimental values found by Gonzalez and Hoff[95] for hydrogen binding to the group 6 complexes M(CO)$_3$(PCy$_3$)$_2$ (M = Cr, Mo, W) by solution calorimetry, and represents an interaction of comparable strength to chemisorption seen in the formation of metal hydrides. In addition, a significant increase in the absorption entropy from the standard[145] -131 J/mol-K typical for hydrogen storage materials is observed. The higher enthalpy and entropy values allow [Mn(CO)dppe$_2$][BArF^{24}] to bind hydrogen effectively near room temperature while exhibiting the rapid absorption kinetics and long cycle life characteristic of physisorption materials, a combination of properties that are highly favorable for hydrogen storage applications.

The kinetic absorption behavior is consistent with observations made by Gonzalez, et al.[123] that the kinetics of absorption and dissociation of H_2 with W(CO)$_3$(PCy$_3$)$_2$ in solution were several times faster than oxidative (dissociative) addition, which also supports the site-binding model. The

Table 3.1: Equilibrium constants and R^2 values from experimental Langmuir fits and simulated Langmuir isotherms for H_2 absorption onto [Mn(CO)dppe$_2$]$^+$

Temperature	$K_{eq,exp}$, atm^{-1}	$K_{eq,sim}$, atm^{-1}	R^2_{exp}	R^2_{sim}
313K	3241.74	3117.22	0.9702	0.9692
333K	1013.12	926.34	0.9882	0.9902
343K	581.82	528.31	0.9919	0.9892
353K	371.65	309.63	0.9937	0.9766
363K	214.78	186.08	0.9962	0.9800
373K	124.19	114.37	0.9914	0.9808

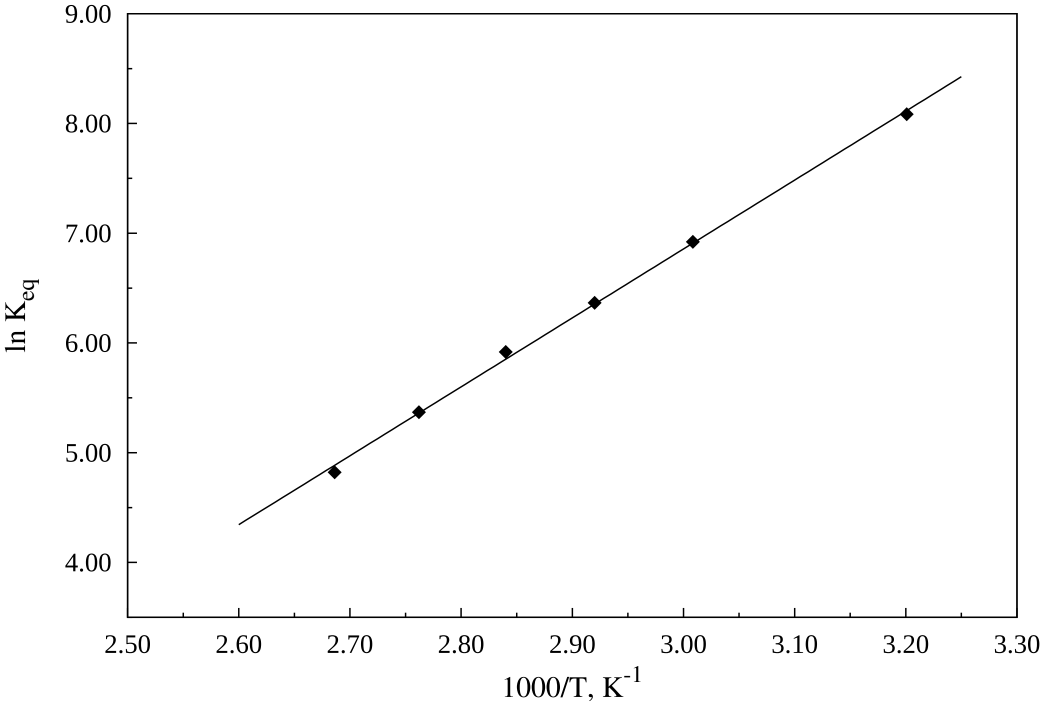

Figure 3.4: Van't Hoff plot of the equilibrium constants derived from the Langmuir model. Linear regression gives $\ln K_{eq}$ = 6280.6/T - 11.986, R^2 = 0.9985, giving thermodynamic properties ΔH° = -52.2 kJ/mol and ΔS° = -99.6 J/mol-K.

solution results also imply that the site-binding mechanism is not limited to the solid state. Qualitative assessments of affinities based on competitive ligand binding would thus require control of the local hydrogen concentration, particularly in solution state measurements where the concentration of dissolved hydrogen depends on the solvent used. This additional aspect needs to be considered before using such assessments to disqualify materials as potential candidates.

3.2.2 Computational Results

The physics of the Langmuir model are well defined at the molecular scale and calculation of the isotherms from simulated binding energies is straightforward, allowing for direct comparison between experimental and computational results to establish the accuracy of computational methods. From statistical mechanics, the fractional coverage of absorbed molecules at the binding sites in the Langmuir model is:

$$\frac{\langle n \rangle}{N} = -\left(\frac{\partial W}{\partial \mu}\right)_{\beta} = \frac{q_s e^{\beta(\mu_{gas} - \Delta E)}}{1 + q_s e^{\beta(\mu_{gas} - \Delta E)}} \tag{3.6}$$

where $\beta = (kT)^{-1}$, W is the grand potential of the bound system, $\langle n \rangle$ represents the ensemble average number of absorbed molecules, and $q_s e^{\beta(\mu_{gas} - \Delta E)}$ is the partition function of the molecular species at the binding site. The pressure dependence of the fractional occupancy is expressed through the chemical potential of the gas, as shown in Equation 3.1. The values of $\epsilon_{\mathrm{corr}}(T)$ obtained from GAMESS contain the contributions to the partition function from the normal modes of hydrogen at the binding site. However, because symmetry is calculated based on the entire organometallic fragment, the output from GAMESS does not treat rotational symmetry of the hydrogen molecule appropriately, and the variable q_s in Equation 3.6 is used as a correction term to account for degeneracy in the rotational mode.

Carbonyl stretch frequencies obtained from the vibrational analysis were found to be 1824.32, 1820.56, and 1849.69 cm^{-1} for the open configuration of $[\mathrm{Mn(CO)dppe_2}]^+$, the agostic configuration, and $[\mathrm{Mn(CO)}(\eta^2\text{-}\mathrm{H_2})\mathrm{dppe_2}]^+$, respectively, in good agreement with the literature values.[100, 115] The standard Gibbs free energy for the transformation from the open configuration to the agostic configuration was also calculated from the vibrational analysis, and was found to be ΔG° = -39.6 kJ/mol, similar to values found for other agostic interactions.[123]

Six primary normal modes for dihydrogen motion at the binding site were defined as the modes having the largest magnitude eigenvectors on the dihydrogen molecule as obtained from the output of vibrational analysis on each adduct fragment. For the manganese complex, these modes correlated well with literature values obtained from inelastic neutron scattering.[100] In all three cases only the rotational mode, with frequencies of 196.79 cm^{-1}, 269.2 cm^{-1}, and 556.7 cm^{-1} for Mn, Tc, and Re, respectively, was found to be significantly populated at the temperatures of interest. The symmetry of the rotational mode was determined from analysis of the components of the eigenvector associated with the atoms of the hydrogen molecule, and the mode was defined as symmetric if the x, y, and z components were opposite in sign and had differences in their magnitude of less than 0.1 millidyne/angstrom. Within this definition, dihydrogen rotational modes in the manganese and

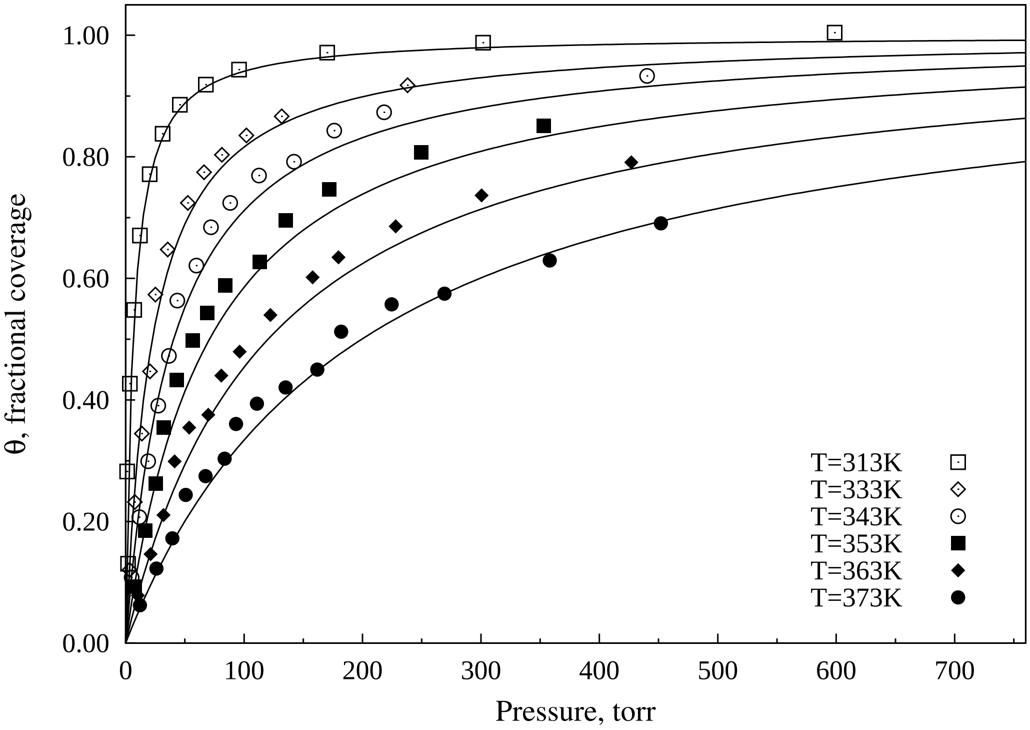

Figure 3.5: Comparison of simulated isotherms for H_2 absorption onto $[Mn(CO)dppe_2]^+$ (solid black lines) to experimental data for $[Mn(CO)dppe_2][BArF^{24}]$.

technetium adducts were found to be symmetric, while rotation in the rhenium adduct was asymmetric with respect to the center of mass of the hydrogen molecule. To correct for the degeneracy of the symmetric modes in the manganese and technetium adducts, q_s was defined such that:

$$\frac{1}{q_s} = \frac{1}{2}\left(\frac{e^{-\frac{\Theta_v}{2T}}}{1 - e^{-\frac{\Theta_v}{T}}}\right) \tag{3.7}$$

where $\Theta_v = h\nu/k$ is the characteristic mode temperature obtained from the rotational mode frequency, ν. This correction removes half of the mode contribution from the total partition function, accounting for the reduction in states due to symmetric rotation. For rhenium, a value of $q_s = 1$ was used, since no degeneracy exists in the asymmetric rotation mode.

Simulated equilibrium constants and standard binding energies for absorption onto both the open and agostic configurations appear in 3.1 and 3.2, and simulated isotherms for the manganese fragment in the open geometry appear as solid lines against the experimental data in 3.5. Simulated isotherms

Table 3.2: Calculated energies, enthalpies, and entropies of the H_2 absorption reaction at 1 atm, 298K and rotational entropy of the bound states at 298K and 373K. Energy and enthalpy values are given in kJ/mol, and entropy values are given in J/mol-K.

Compound		ΔE°	ΔH°	ΔS°	S_{rot}(298K)	S_{rot}(373K)
$[Mn(CO)dppe_2]^+$						
	open	-43.0	-53.5	-103.8	3.20	5.04
	agostic	-1.5	-11.5	-103.9		
$[Tc(CO)dppe_2]^+$						
	open	-38.1	-49.3	-103.5	0.86	2.60
	agostic	-8.51	-18.7	-103.0		
$[Re(CO)dppe_2]^+$						
	open	-50.6	-57.5	-97.4	2.17	3.39
	agostic	-20.4	-27.1	-96.7		

for the open geometry are nearly identical to fits for the experimental data, indicating that the open geometry sites are the active sites for the absorption reaction. The simulated enthalpy and entropy values, calculated from Equations 3.4, 3.5, and 3.6 are ΔH° = -53.5 kJ/mol and ΔS° = -103.8 J/mol-K, demonstrating that both pressure-composition behavior and thermodynamic properties can be accurately simulated through electronic structure calculations using the B3LYP/LANL2DZ level of theory for geometry optimization and vibrational analysis, and the MP2/LANL2DZ level of theory for the electronic energy used to obtain the binding energy.

Calculations for absorption onto the agostic geometry validate the observation by King et al.[100] that direct hydrogenation of the agostic manganese complex in the solid state fails under one atmosphere of hydrogen pressure. Evaluation of Equation 3.6 for the agostic complex at one atmosphere hydrogen pressure and 313K gives a fractional coverage of 1.443 x 10^{-5}, indicating that molecules in the agostic configuration do not contribute to hydrogen binding in the experimental results. The experimental result of 0.344 for the fraction of active manganese centers evidently represents the fraction of the total manganese centers in the open configuration. This number was maintained throughout all temperatures studied, indicating that no exchange between the agostic and open configurations occurs in the solid, despite the favorable value of the free energy for the agostic complex found from calculation. Solution NMR results reported by King, et al. for the same compound[115] in CH_2Cl_2 found a similar 37% of the manganese centers were active for N_2 absorption at room temperature. It is likely that the precipitation of the N_2 adduct and subsequent release of the

N_2 molecule produce the open configuration in the solid state necessary for H_2 absorption. Once precipitated, the thermal stability of the active site fraction suggests that kinetic stabilization in the solid state prevents exchange between the two configurations. This stabilization would prevent hydrogen absorption over agostic complexes in the solid state even if favorable thermodynamics were predicted, due to the inability of the ligand to leave the binding site.

With the accuracy of the calculation method established, standard energies, enthalpies, and entropies were obtained from calculation for hydrogen absorption over $[Tc(CO)dppe_2]^+$ and $[Re(CO)dppe_2]^+$. These values appear in 3.2. The resulting binding enthalpies for the open configuration are similar in strength to findings for other dihydrogen complexes. The trends in the binding enthalpies and entropies in the group 7 metals from these simulations are in good agreement with the solution calorimetry results for group 6 metals reported by Gonzalez and Hoff,[95] with the enthalpy increasing as 5d > 3d > 4d. Quantitatively, the energetic difference between 3d and 4d metals matches with the value found for the group 6 metals, despite the differences in group, molecular charge, and chemical environment. A slightly lower energetic difference of 4 kJ/mol between manganese and rhenium complexes was found relative to the reported 11 kJ/mol difference between chromium and molybdenum complexes. The good quantitative agreement implies a consistent trend in the thermodynamic values within the transition metals. Unfortunately, no direct cause for this relationship was evident from the calculations. The relationships are expected to rely upon the relative σ- and π- donation ability at the metal center, a complex property dependent upon the metal-ligand interactions and geometry.[113] Although several studies have examined the governing principles behind these properties, their exact nature remains uncertain.[146–148]

The individual contribution of excited rotational modes to the site entropy can be calculated from Equation 3.7 through the expression:

$$S_{rot} = k\left(\ln q_s + T\frac{\partial \ln q_s}{\partial T}\right) \tag{3.8}$$

Values for the rotational entropy of the bound state at 298K and 373K for each of the complexes appear in 3.2. Since only the bound state is considered, the value is equivalent for both the open and agostic configurations. The softer rotational mode in the manganese adduct leads to increased entropic contributions at all temperatures, and an increased dependence on temperature relative to the other two complexes. The near equivalence of the standard entropies of technetium and manganese, despite a much lower contribution from rotation of the hydrogen molecule in technetium, is due to increased contributions from other modes within the organometallic complex. The asymmetry of the rotation in the rhenium complex leads to higher contributions to the entropy than in the technetium adduct, despite the high stiffness in the mode. The much stiffer, asymmetric rotational mode in the rhenium complex, along with the higher binding enthalpy, suggest that the H_2 molecule may have undergone oxidative addition and dissociated to form the dihydride complex. However, because both hydrogen atoms remain bound to the same metal center, the assumptions of the Langmuir isotherm are not violated. Effects from this transition are modeled in the Langmuir isotherm as a contribution to the site binding energy. This allows the absorption enthalpy to be modeled accurately by the Langmuir isotherm in cases of oxidative addition, but does not allow determination of whether the compound is a dihydrogen complex or a dihydride.

3.3 Conclusions

We report experimental and computational results on the properties of dihydrogen complexes, and interpretations with the Langmuir isotherm model. Langmuir fits for the absorption of hydrogen onto $[\mathrm{Mn(CO)dppe_2}][\mathrm{BArF^{24}}]$ to form the dihydrogen complex $[\mathrm{Mn}(\eta^2\text{-}\mathrm{H_2})\mathrm{(CO)dppe_2}][\mathrm{BArF^{24}}]$ were found to accurately describe the experimental pressure-composition behavior, giving an enthalpy and entropy for the binding interaction of ΔH° = -52.2 kJ/mol and ΔS° = -99.6 J/mol-K, in general agreement with previous observations of model Kubas complexes. While the complexes within this study do not meet gravimetric or volumetric capacity expectations for vehicular hydrogen storage, they exhibit a unique binding motif capable of storing hydrogen at desirable temperatures and pressures with kinetics rivaling physisorption materials. The combination of these properties holds strong promise for the development of lower weight organometallic storage materials for applications.

Computationally derived isotherms using a mixed calculation scheme of B3LYP/LANL2DZ-

ECP for geometry optimization and vibrational analysis and MP2/LANL2DZ-ECP for total energy were also found to accurately describe the experimental behavior of the manganese complex and have provided additional insight into the configuration of the active binding site and the individual contributions from configurational and rotational entropy to the binding properties. Calculations for substitution of the metal center with other group 7 metals found similar trends in the thermodynamic properties to experimental reports for group 6 metals, with increasing binding enthalpy such that 5d > 3d > 4d, suggesting an overall trend in properties for transition metals moving down the periodic table.

Chapter 4

Studies of $[MH(\eta^2\text{-}H_2)dppe_2]^+$ (M = Fe, Ru, Os) Complexes

In the previous chapter, the Langmuir isotherm model was found to accurately describe the experimental behavior for hydrogen absorption onto the complex $[Mn(CO)dppe_2][BArF^{24}]$ to form the dihydrogen complex $[Mn(\eta^2\text{-}H_2)(CO)dppe_2][BArF^{24}]$. Electronic structure simulations of hydrogen absorption over the fragment $[Mn(CO)dppe_2]^+$ were also successful in quantitatively reproducing the experimental behavior and thermodynamic properties, and simulations were used to extend the analysis to the other group 7 metal fragments $[Tc(CO)dppe_2]^+$ and $[Re(CO)dppe_2]^+$ to develop trends for the hydrogen absorption behavior within the periodic table. In this chapter, the analysis is extended to describe hydrogen binding to the isoelectronic organometallic fragments $[MHdppe_2]^+$ (M = Fe, Ru, Os) to form the dihydrogen complexes $[MH(\eta^2\text{-}H_2)dppe_2]^+$.

The group 8 complexes containing the cationic fragment $[MH(\eta^2\text{-}H_2)dppe_2]^+$ (M = Fe, Ru, Os) are among the most well-studied dihydrogen compounds available in the literature. The crystal structures for all three dihydrogen complexes have been determined by x-ray diffraction[149–152] and found to be isostructural, and neutron diffraction experiments have been performed for the iron and ruthenium complexes to determine dihydrogen positions.[149, 150] Extensive NMR work has been performed[96] to examine the dynamics of dihydrogen exchange, heterolytic cleavage, and intramolecular exchange of the hydride and dihydrogen within all three dihydrogen complexes. Multiple spectroscopic studies have been performed to characterize the iron complex, including Mössbauer spectroscopy[119] and analysis of the vibrational modes through inelastic neutron scattering.[110]

Thermodynamic properties of the dihydrogen interaction with the metal center remain undetermined, largely because of the high stability of the dihydrogen products and strong reactivity of the five-coordinate species in the iron and osmium compounds that prevent characterization. While Mössbauer, UV-vis and IR spectroscopy have been reported for the directly synthesized five-coordinate iron complex[107] and H_2/D_2 exchange has been shown to occur through a stable intermediate,[96] the thermal decomposition products of the iron and osmium species have not been directly identified and have only been assigned through the analogous $[RuHdppe_2]^+$ cation, which is stable at room temperature. No characterization studies are available for $[OsHdppe_2]^+$ or $[RuHdppe_2]^+$ complexes, despite the stability of the ruthenium species.

Identification of the complexes involved in reversible hydrogen absorption is the first step required for accurate thermodynamic simulations. Mössbauer spectroscopy, in particular, provides a probe of the valence and spin state of the central iron atom in iron complexes, as well as a measure of the charge transfer between the metal center and attached ligands. The availability of this information and the atomic selectivity of the technique makes Mössbauer spectroscopy uniquely suited for investigating group 8 dihydrogen complexes, and for determining mechanisms in Kubas binding. Evidence for the identification of the thermal decomposition product of $[FeH(\eta^2\text{-}H_2)dppe_2][NTf_2]$ (NTf_2 = bis(trifluoromethlysulfonyl)imide) through Mossbauer spectroscopy and other techniques is presented below, and simulated thermodynamic parameters are reported for the hydrogen binding interaction in the group 8 fragments $[MH(\eta^2\text{-}H_2)dppe_2]^+$ (M = Fe, Ru, Os).

4.1 Experimental

Unless otherwise stated, all reactions were performed under a dinitrogen atmosphere using either a controlled atmosphere glovebox or Schlenk line techniques. 1,2-bis(diphenylphosphino)ethane was purchased from Strem Chemicals and used without further purification. Crystalline bis(trifluoromethanesulfonyl)imide was purchased from Acros Organics and used without further purification. Research-grade gases were purchased from Matheson and used directly. All solvents were dried and deoxygenated by purging with dry dinitrogen gas for 15 minutes before passing through packed columns of activated alumina and activated copper. After synthesis, materials were stored under dry argon in an atmosphere-controlled glovebox until their use in testing.

Solution-state NMR spectra were recorded on a Varian 300 MHz instrument with ^1H shifts reported relative to the residual solvent peak, and ^{31}P peaks reported relative to 85% H_3PO_4. Deuterated NMR solvents were purchased from Cambridge Isotopes Laboratories. Deuterated benzene was purified by vacuum distillation from a sodium/benzophenone solution before use. Deuterated bromobenzene was dried over CaH_2 and vacuum distilled before use.

Preparation of *cis*-FeH$_2$dppe$_2$—This procedure was a modification of existing literature procedures.[96,153] Anhydrous $FeCl_2$ (319.8 mg, 2.523 mmol) was suspended in 2 mL THF. A solution of 1,2-bis(diphenylphosphino)ethane (2.0052 g, 5.033 mmol) in 6 mL THF was added and the suspension was stirred until a milky white precipitate formed. $NaBH_4$ (220.0 mg, 5.680 mmol) in 8 mL of dry ethanol was then added, producing strong outgassing and causing all components to immediately dissolve to form a dark red solution. The solution was stirred for 3 hours during which outgassing continued and a yellow powder precipitated. The remaining solution was decanted from the precipitate, and the precipitate was dissolved in benzene and filtered over celite to remove salt impurities. Removal of the solvent *in vacuo* produced the product as a fine yellow powder. Yield 1.8533 g (73.5% on iron). ^1H NMR spectra was broad, indicating a fluxional molecule. ^1H NMR (300 MHz) in C_6D_6: δ -12.76 (quad., 2H); 1.80 (s, 4H); 2.14 (s, 2H); 2.40 (s, 2H); 6.44 (s, 4H); 6.58–7.12 (m, 20H); 7.14–7.80 (m, 12H); 8.67 (s, 4H). ^{31}P NMR (300 MHz) in C_6D_6: δ 91.5 (s); 103.3 (s).

Preparation of [FeH(η^2-H$_2$)dppe$_2$][NTf$_2$]—This procedure was a modification of an existing literature procedure.[96] Bis(trifluoromethylsulfonyl)imide (327.8 mg, 1.166 mmol) in 5mL diethyl ether was added to a solution of *cis*-FeH$_2$dppe$_2$ (1.015 g, 1.188 mmol) in 12 mL diethyl ether and allowed to stir for one hour, forming a light green precipitate. The precipitate was filtered over a medium frit and washed twice with diethyl ether. Removal of residual diethyl ether *in vacuo* produced the product as a light green powder. Yield 1.098 mg (81.8% on iron). Some N_2 adduct was included in the product. ^1H NMR (300 MHz) in C_6D_5Br: δ -12.61 (s, broad, 1H); -7.76 (s, broad, 2H); 2.13 (s, 8H); 7.16–7.51 (m, 40H). ^{31}P NMR (300 MHz) in C_6D_5Br: δ 92.0 (s).

Thermal decomposition of [FeH(η^2-H$_2$)dppe$_2$][NTf$_2$]—[FeH(η^2-H$_2$)dppe$_2$][NTf$_2$] was placed under vacuum and heated at 125° for 12 hours, producing an extremely reactive blue-green powder. This powder was found to react with all available solvents, preventing direct characterization by NMR.

4.1.1 X-Ray Diffraction

Diffraction quality crystals of [FeH(η^2-H$_2$)dppe$_2$][NTf$_2$] were grown by layering diethyl ether over a saturated solution of the complex in benzene. The resulting yellow needles were mounted on glass fiber with Paratone oil and spectrum were recorded over 12 hours with a Bruker KAPPA APEXII x-ray diffractometer under flowing nitrogen at 298K using Mo Kα radiation.

4.1.2 Mössbauer Spectroscopy

Isotopically enriched [^{57}FeH(η^2-H$_2$)dppe$_2$][NTf$_2$] and its thermal decomposition products were made according to the procedures above. ^{57}Fe metal was purchased from Isoflex USA. ^{57}FeCl$_2$ was made by reacting shavings of ^{57}Fe (0.13 mg, 0.228 mmol) metal with excess concentrated hydrochloric acid (1.0 mL, 12M) in 5 mL methanol. The resulting yellow solution was reduced and dried at 160° under vacuum for 8 hours to produce the anhydrous starting material.

Samples were loaded into a custom-built, O-ring sealed PTFE sample cell under an argon atmosphere. Sealed samples were stable for up to 24 hours in air at room temperature. Spectra were recorded over six hours in the transmission configuration using a gas scintillation detector and source radiation from the decay of ^{57}Co in a rhodium matrix. Isomer shifts were referenced to bcc iron.

4.1.3 Computation

Electronic structure calculations were performed for the singlet state of the cationic fragments [MH(η^2-H$_2$)dppe$_2$]$^+$ and [MHdppe$_2$]$^+$ (M = Fe, Ru, Os), and the hydrogen molecule using the GAMESS-US software package.[134] Geometry optimizations for the organometallic fragments were performed using fully spin-restricted (RHF) density functional theory calculations, with the B3LYP exchange-correlation functional[135, 136] and the LANL2DZ basis set.[137–140] An additional p polarization shell for light atoms and d polarization shell for heavier atoms were added to augment the basis set. Starting structures for optimizations were taken from XRD experiments reported previously for $[FeH(\eta^2\text{-}H_2)dppe_2][BF_4]$[152] and on calculated singlet structures[107] for $[FeHdppe_2]^+$. Effective core potentials[138–140] representing the core 10 electrons for iron and phosphorus atoms, the core 28 electrons for ruthenium and the core 60 electrons for osmium were used. SCF convergence was set to $5.0 \text{ x } 10^{-6}$ for all calculations. Geometry optimizations were performed to a tolerance of 10^{-4} au.

Ab initio ground state electronic energies were calculated using the spin-component scaled Møller-Plesset second order perturbation[141] (SCS-MP2) scheme with the LANL2DZ-ECP basis set from the optimized geometries found from DFT calculations. Thermal corrections to the energy and normal mode frequencies were obtained from vibrational analysis of the Hessian matrix for each fragment calculated using the B3LYP/LANL2DZ-ECP level of theory with seminumerical methods, with contributions from positive and negative displacements of 0.01 Bohr. Partition functions of the fragments, q_{tot} at 1 atm pressure were also obtained from vibrational analysis. A scaling factor of 0.96 was in calculated the thermodynamic properties and normal mode frequencies to correct known errors in the LANL2DZ basis set, consistent with common practice.[143] Symmetry of the rotational modes was determined by analysis of the components of the mode eigenvector associated with the two hydrogen atoms, and the mode was considered symmetric if the x, y, and z components of the force constants for each atom were of opposite sign and deviated in value by less than 0.1 millidyne/angstrom.

The chemical potential of hydrogen gas was calculated from the partition function for the hydrogen molecule, through the relationship:

$$\mu_{\text{gas}}(T,P) = -kT \ln\left(q_{\text{tot}}(T,P^\circ)\right) + \ln\left(\frac{P}{P^\circ}\right) \tag{4.1}$$

where k is Boltzmann's constant, T is the temperature in Kelvin, P is the pressure of the system, and P° is the standard pressure of the system, taken to be 1 atm. Rotational degeneracy for the hydrogen molecule is included in the calculated partition function from the GAMESS software.

The energy for each fragment, E, was obtained as the sum of the ground-state energy, ϵ_0, and the thermal correction obtained from vibrational analysis, $\epsilon_{\mathrm{corr}}(T)$, which contains contributions from the electronic, translational, vibrational, and rotational motions of the molecule. The binding energy of the hydrogen molecule to the organometallic site, ΔE, was calculated as:

$$\Delta E(T) = E_{\mathrm{M\text{-}H_2}}(T) - E_{\mathrm{H_2}}(T) - E_{\mathrm{M}}(T) \tag{4.2}$$

where the subscripts M-H_2, H_2, and M represent the organometallic adduct fragment, hydrogen gas, and the bare organometallic fragment, respectively.

To obtain the Mössbauer parameters for the iron fragments, fully *ab initio* geometry optimizations and total energy calculations were performed using the TZVP level of theory for $[\mathrm{FeH}(\eta^2\text{-H}_2)\mathrm{dppe}_2]^+$ and $[\mathrm{FeHdppe}_2]^+$, with p and d polarization shells as described above. Calculations were also performed on the nitroprusside anion, $[\mathrm{Fe(NO)CN}_5]^{2-}$, to be used as a reference state for isomer shifts. Isomer shift and electric quadrupole splitting values were obtained from the electronic charge density and electric field gradient at the iron nucleus according to the method described by Blaha.[154] Isomer shifts were converted from the nitroprusside scale to the bcc iron scale by subtracting 0.257 mm/s.

4.1.4 Kinetic Isotherms

Kinetic isotherms were recorded for the thermal release of the H_2 ligand from $[\mathrm{FeH}(\eta^2\text{-H}_2)\mathrm{dppe}_2][\mathrm{NTf}_2]$ using a custom-built Sieverts apparatus. Solid $[\mathrm{FeH}(\eta^2\text{-H}_2)\mathrm{dppe}_2][\mathrm{NTf}_2]$ (257 mg) was loaded into a 14mL stainless steel reactor under an argon atmosphere and sealed before transfer to the instrument. Swagelok VCR copper filter gaskets with 2 μm stainless steel filters were used to prevent loss of the powdered sample from the reactor during measurements. After transferring the reactor to the assembly, samples were allowed to pump down overnight to $3.1\mathrm{x}10^{-7}$ torr at the pump inlet before measurements were performed.

The rate of hydrogen release was measured by placing the sample under vacuum conditions for nominally one hour at the desired temperature, followed by expansion of hydrogen gas from a calibrated volume into the reactor. Residual gas mass spectroscopy was performed during the evacuation of the reactor to identify the decomposition products. Ideal gas mole balance was used to determine the quantity reabsorbed after exposure of the degassed sample to 0.5 atm hydrogen gas. Time and pressure resolution of the instrument were 500 ms and 5 torr, respectively.

4.2 Results and Discussion

4.2.1 Experimental Results

Thermodynamic isotherms such as those measured for the isoelectronic manganese complexes could not be obtained for [FeH(η^2-H_2)dppe$_2$][NTf$_2$] in reasonable timescales. Equilibrium pressures from the samples were below detectable levels for all temperatures measured, and reabsorption of hydrogen under 0.5 atmospheres occurred faster than the time resolution of the instrument, preventing quantification of the absorption properties. Alternatively, kinetic rates of desorption were measured between 350K and 410K, and the results appear in Figure 4.1. An Arrhenius fit to the kinetic data gave an activation energy of $E_A = 32.3$ kJ/mol for the release process, representing a significantly higher release barrier than expected from the previous manganese studies but lower than reported kinetics of dihydrogen release rates for $W(CO)_3(PCy_3)_2$ in solution,[155] suggesting a wide range of kinetic behavior for dihydrogen complexes. During the course of kinetic testing, the complex underwent multiple absorption/desorption cycles without observed decomposition in the capacity, and residual gas mass spectroscopy confirmed that hydrogen gas was the only volatile decomposition product produced. Irreversible decomposition occurred at 420K, producing a black solid mixture of multiple decomposition products and hydrogen gas.

Single crystals of [FeH(η^2-H_2)dppe$_2$][NTf$_2$] were grown to confirm the structure of the complex and assess any effects of the anion on the structure. The structure refined from the x-ray diffraction pattern appears in Figure 4.2. As shown, the organometallic cation retains the same conformation as in structures reported[152, 149] for [FeH(η^2-H_2)dppe$_2$][BF$_4$] and [FeH(η^2-H_2)dppe$_2$][BPh$_4$]. The bistri-

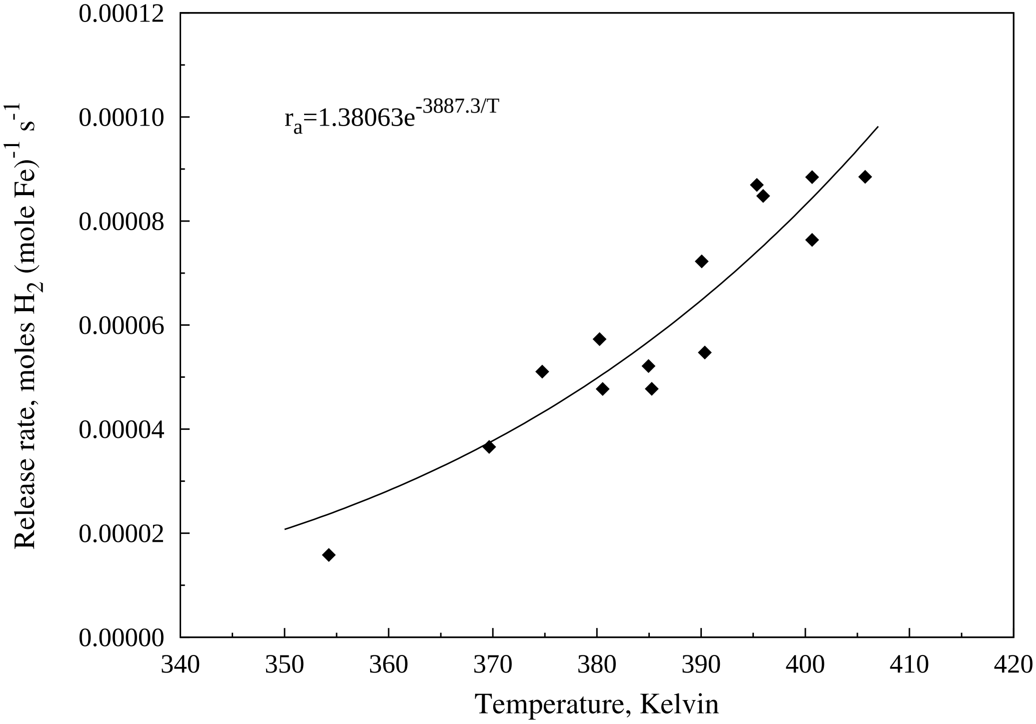

Figure 4.1: Kinetic measurements for hydrogen release from the reversible thermal decomposition of [FeH(η^2-H_2)dppe$_2$][NTf$_2$]. The sample was desorbed at the temperature shown from a state of full coverage for nominally one hour before exposure to hydrogen gas. The rate of release was calculated as the amount of gas reabsorbed divided by the time under vacuum. All data points were acquired on the same sample. Arrhenius fit gives $E_A = 32.3$ kJ/mol, $R^2 = 0.8659$.

flimide anion is highly disordered and positioned directly over the hydrogen coordination sites on the iron, but remains outside of the first coordination sphere. During reversible hydrogen release from the solid state, kinetic barriers to structural rearrangement are expected to prevent recombination of the cation-anion pair and produce the organometallic species [FeHdppe$_2$][NTf$_2$], as has been shown in the analogous ruthenium species.[96] However, the strong disorder associated with the bistriflimide anion, which is typically used for ionic liquid formulations, may lead to a lower activation barrier and a lower recombination temperature in the solid state than would be expected for a comparably sized anion, which may be the cause of the observed irreversible transition at 420K.

Thermal decomposition by direct heating of the [FeH(η^2-H_2)dppe$_2$][NTf$_2$] crystals under vacuum was attempted by the methods described in the procedures. This process produced blue needles of the same shape as the original crystals, with no degradation of the crystal quality observable by

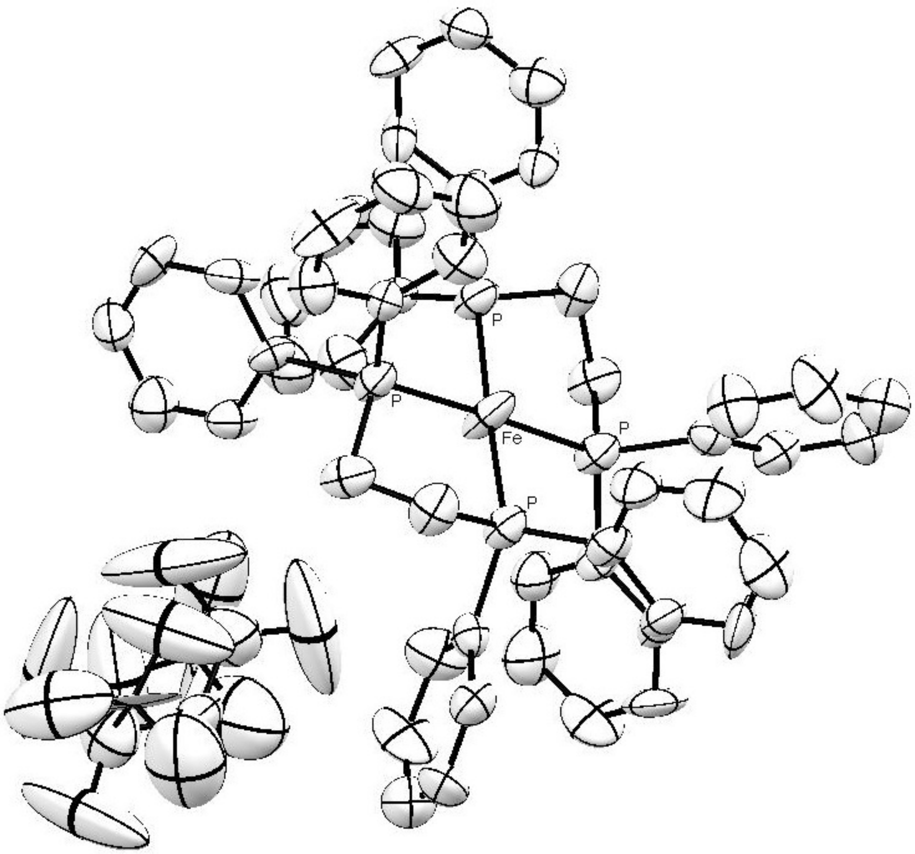

Figure 4.2: ORTEP structural drawing of $[FeH(\eta^2\text{-}H_2)dppe_2][NTf_2]$ obtained from single crystal x-ray diffraction measurements at 298K. Ellipsoids represent 50% probability. Hydrogen atom positions were not resolvable. An additional benzene molecule co-crystallized within the structure has been removed for clarity.

optical microscopy. The new crystals were stable under an argon atmosphere for several hours but were highly reactive to trace air and moisture, changing color to form red crystals within a flame-sealed capillary over 24 hours through reaction with residual contaminants. As a result of this extraordinary reactivity, x-ray diffraction patterns could not be obtained and the structure of the decomposition product could not be determined.

Mössbauer spectra were obtained from samples of thermally decomposed $[^{57}FeH(\eta^2\text{-}H_2)dppe_2][NTf_2]$ before and after reabsorption of hydrogen to help identify the cycling products. These spectra appear in Figure 4.3 and the values for the isomer shifts and electric quadrupole splittings, along with the literature values for the directly synthesized $[FeH(\eta^2\text{-}H_2)dppe_2][BF_4]$ and $[FeHdppe_2][BPh_4]$, appear in Table 4.1. Despite the harsh conditions used, only partial decomposition of the dihy-

Table 4.1: Isomer shift and electric quadrupole splitting values of iron complexes obtained from Mössbauer spectroscopy. For EQS values, a sign designation is absent if the sign was not directly determined by the measurement.

Complex	IS, mm/s	EQS, mm/s
$[FeH(\eta^2\text{-}H_2)dppe_2][NTf_2]$	+0.0532	0.5695
$[FeH(\eta^2\text{-}H_2)dppe_2][BF_4]$, lit.[119]	-0.097	-0.56
$[FeH(\eta^2\text{-}H_2)dppe_2]^+$, sim.	+0.3411	-0.7774
$[FeHdppe_2][NTf_2]$	+0.1552	1.5104
$[FeHdppe_2][BPh_4]$, lit.[107]	+0.2274	1.5178
$[FeHdppe_2]^+$, singlet, sim.	-0.3693	-0.3961
$[FeHdppe_2]^+$, triplet, sim.	-0.2726	+1.3383
$[Fe(NO)CN_5]^{2-}$, lit.[160]	reference	+1.726
$[Fe(NO)CN_5]^{2-}$, sim.	reference	+1.5620

drogen complex was observed. Electric quadrupole splitting (EQS) values for the major peaks in the thermally decomposed and reabsorbed samples correspond well to literature values for the five-coordinate species and the H_2 adduct, respectively. The spectra for the partially decomposed sample contains the spectra for $[FeHdppe_2][NTf_2]$ and $[FeH(\eta^2\text{-}H_2)dppe_2][NTf_2]$ as the active species, suggesting either a direct transition between the two species or that intermediates produced during the decomposition are unstable. The small, broad peak visible at ∼2 mm/s in both spectra indicates the presence of unreacted $^{57}FeCl_2$.

EQS values describe perturbations of the electric field around the metal center due to variations in the chemical environment arising from the attached ligands, specifically asymmetric perturbations, and are less sensitive to changes in the cation-anion pairing. The similarity of the EQS values to the literature values thus provides strong evidence for the presence of the $[FeHdppe_2]^+$ cation in the decomposed sample. The large EQS value for this complex is characteristic of nonbonding electrons in a high-spin d^6 configuration, which corresponds to the paramagnetism of the $[FeHdppe_2]^+$ cation found through magnetic susceptibility measurements performed by Franke, et al.[107] However, while isomer shift values for the study complexes deviate from the literature values, they remain within the range associated with low-spin Fe^{II} complexes, suggesting that the typical reduction in the s-electron density in high spin states is compensated for by donation from the attached ligands.

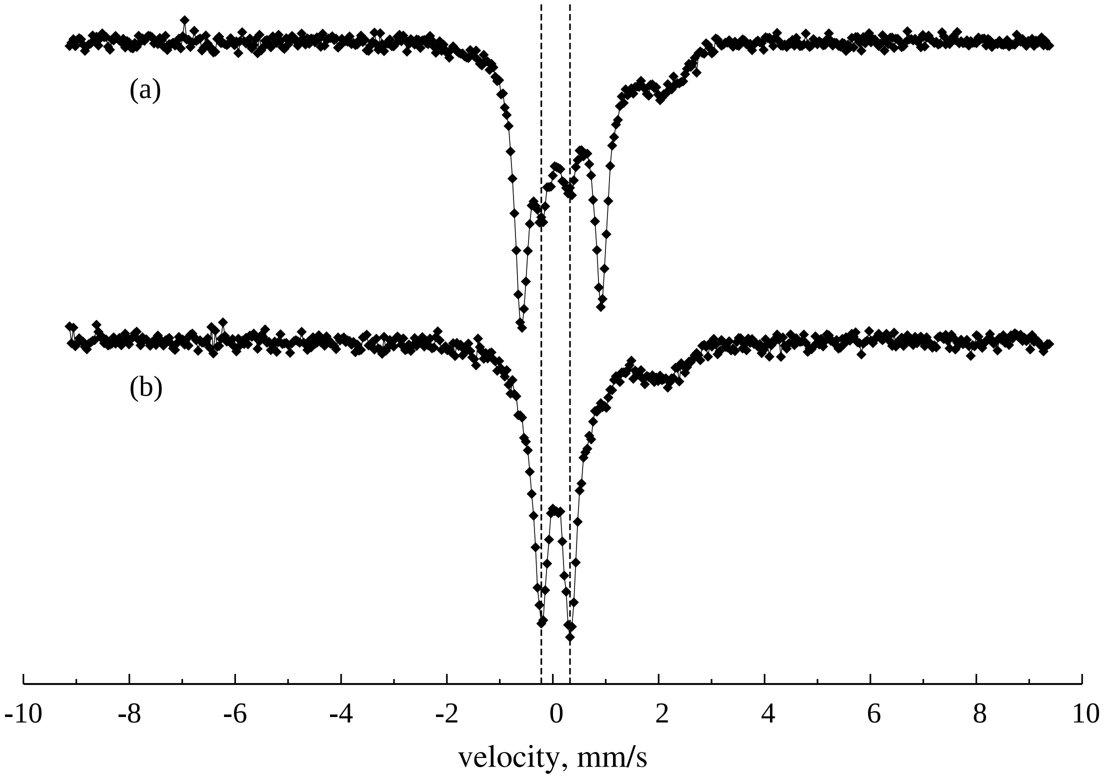

Figure 4.3: Mössbauer spectra for a) thermally decomposed [FeH(η^2-H_2)dppe$_2$][NTf$_2$] and b) thermally decomposed [FeH(η^2-H_2)dppe$_2$][NTf$_2$]. Thermally decomposed spectrum shows partial decomposition to the five-coordinate [FeHdppe$_2$][NTf$_2$] species. Dashed lines correspond to the peak positions for the dihydrogen species. Both spectra also contain a small, broad doublet between 0.5 and 2.0 mm/s, corresponding to unreacted ^{57}FeCl$_2$.[156]

4.2.2 Computational Results

4.2.2.1 Mössbauer Simulations

With the crystal structure for [FeHdppe$_2$]$^+$ complexes unavailable from experiments, computational methods must be used to help identify the structure and electronic character of the molecule. Computational studies to determine the ground-state structure of [FeHdppe$_2$]$^+$ have previously been performed by Franke, et al.,[107] and the singlet and triplet states of the molecule fragment were reported to be nearly isoenergetic, with the singlet state slightly more favorable. These states were also reported to have very different molecular geometries, which are expected to have a strong impact on the EQS values obtained through Mössbauer spectroscopy. Therefore, comparison between simulated Mössbauer parameters for the singlet and triplet states and experimental values can be used to determine which of the spin states is preferred at room temperature.

Simulations of the Mössbauer EQS values were performed, and the results appear in Table 4.1. Geometries of the singlet and triplet five-coordinate states were similar to those found by Franke, et al. The principal component of the electric field gradient was found to be oriented primarily along the iron-hydride axis in each of the simulations, with a slight skew in the triplet-state five-coordinate complex towards the empty coordination state, which no longer aligns with the hydride in the skewed geometry. The expected differentiation in the EQS values between the singlet state and triplet state was observed, and the value for the triplet state was found to be consistent with experimental Mössbauer studies. Simulations of the EQS values for singlet $[\mathrm{FeH}(\eta^2\text{-}\mathrm{H}_2)\mathrm{dppe}_2]^+$ and the nitroprusside anion were also performed, and found to have similar deviations from their experimental values, within the expected range of error for simulations of Mössbauer properties.[154] These results provide strong evidence for predominance of the triplet-state configuration of $[\mathrm{FeHdppe}_2]^+$ at room temperature, and for the direct conversion from the triplet five-coordinate species to the singlet hydrogen adduct.

The simulations used to calculate EQS values allow for determination of the sign of the principal component of the electric field gradient, and correspondingly the sign of the EQS. These signs are presented with their values in Table 4.1. With identification of the sign, the method of partial quadrupole splittings presented by Bancroft,[157] can be used to determine the individual contribution of the H_2 ligand to the EQS from the experimental value. The expression for the EQS based on partial quadrupole splittings (Q) is

$$EQS = \sum_i Q(L_\mathrm{i})(3\cos^2\theta_\mathrm{i} - 1) \tag{4.3}$$

where $Q(L_\mathrm{i})$ is the partial quadrupole splitting of ligand i, and θ_i is the angle the ligand-metal bond makes with the principal component axis of the electric field gradient. Assuming perfect octahedral geometry and the principle axis aligned along the H-Fe-H_2 axis, the expression for the EQS becomes

$$EQS = 2\ Q(\mathrm{H}^-) + 2\ Q(\mathrm{H}_2) - 4\ Q(\mathrm{dppe}/2) \tag{4.4}$$

Using the values of $Q(\mathrm{H}^-) = -1.04$ mm/s and $Q(\mathrm{dppe}/2) = -0.50$ mm/s, this expression leads to a value of $Q(\mathrm{H}_2) = -0.245$ mm/s, which correlates well with the value of -0.22 mm/s presented by Morris and Schlaf for $[\mathrm{FeH}(\eta^2\text{-}\mathrm{H}_2)\mathrm{dppe}_2][\mathrm{BF}_4]$.[119] The low Q value of dihydrogen as a ligand, compared to the large value of the hydride ligand, should be universally obtainable for $\mathrm{Fe}^{mathrmII}$ complexes because of the additive nature of the partial quadrupole splitting model. This distinct feature of dihydrogen as a ligand may be useful in identifying dihydrogen complexes and Kubas binding in Mössbauer active materials, as well as defining the onset of dihydrogen-dihydride transitions.

4.2.2.2 Isotherm Simulations

The importance of the magnetic transition in the iron complexes can be inferred from calculations of the singlet-state species, and, based on general trends in the periodic table, the analogous ruthenium and osmium complexes are expected only to exist in the singlet states. In this context, we have performed calculations to simulate the Langmuir absorption behavior onto the singlet-state complexes $[\mathrm{MHdppe}_2]^+$ (M = Fe, Ru, Os), similar to the calculations performed for the group 7 complexes in the previous chapter.

An additional complication to the simulations not present in the group 7 complexes arises from the hydride ligand *trans* to the coordination site. Bautista et al.[96] found through NMR experiments that the dihydrogen and hydride ligands can rapidly exchange positions at room temperature in the iron and osmium complexes through the formation of the transient trihydride $[\mathrm{MH}_3\mathrm{dppe}_2]^+$. In the solid state, where the orientation of the molecule with respect to the rest of the solid is fixed, this intramolecular conversion produces "up" and "down" bound states that introduce additional entropy, and an adjustment of the Langmuir model is necessary to account for this effect. Because the unbound states are unable to alter their configuration, this inversion only affects the entropy of the bound states. The partition function describing this behavior can be formulated by assigning an orientation to the hydrogen molecules, such that "up" or "down" molecules bind to the open site with equivalent binding energies. This convention produces a new system partition function, expressed as:

$$\Xi = \sum_{n_\uparrow}^{N} \sum_{n_\downarrow}^{N-n_\uparrow} \frac{N!}{n_\uparrow! n_\downarrow! \left(N - n_\uparrow - n_\downarrow\right)!} \mathrm{e}^{-\beta \Delta E (n_\downarrow + n_\uparrow)} \mathrm{e}^{\beta \mu_{\mathrm{gas}} (n_\downarrow + n_\uparrow)} \tag{4.5}$$

where the subscript arrows denote the orientation of the binding molecule, with the total number of bound dihydrogen molecules $n = n_\downarrow + n_\uparrow$. From this partition function, a new Langmuir isotherm was derived, giving:

$$\frac{\langle n \rangle}{N} = \frac{2q_{\mathrm{s}} \mathrm{e}^{\beta(\mu_{\mathrm{gas}} - \Delta E)}}{1 + 2q_{\mathrm{s}} \mathrm{e}^{\beta(\mu_{\mathrm{gas}} - \Delta E)}} \tag{4.6}$$

Equation 4.6 was used for iron and osmium simulations. In the same study, Bautista et al. found that inversion did not occur significantly in the analogous ruthenium complex, and 3.6 was used for ruthenium simulations. Analysis of the rotational mode eigenvector components indicated that the rotation of the H_2 molecule about its center of mass was asymmetric for each complex, and a value of q_{s}=1 was used for all simulations.

As with the group 7 complexes, the vibrational analysis revealed that occupied normal modes of the hydrogen molecule in the group 8 H_2 adducts were dominated by the rotational modes, with frequencies of 385.7, 385.5, and 202.1 cm^{-1} for Fe, Ru, and Os species, respectively. The rotational mode at 385.7 cm^{-1} for the iron complex was previously assigned by Eckert et al.[110] as a translation mode based on the presence of additional peaks at 225 and 255 cm^{-1} in the vibration spectra from inelastic neutron scattering experiments. These lower energy peaks were also reproduced by the GAMESS simulations at 237.6 and 254.3 cm^{-1}, and were found to be associated with strong translation modes of the iron center towards the hydride which couple to both the hydride and the dihydrogen atoms. The broad peak at 400 cm^{-1} in the neutron scattering experiment thus likely corresponds to the primary rotational mode of the dihydrogen molecule.

The standard enthalpy and entropy obtained from the K_{eq} values of the simulated Langmuir isotherms appear in Table 4.2. As with the group 6 complexes reported by Gonzalez and Hoff[123] and the group 7 complexes reported in the previous chapter, the binding enthalpy in the singlet-state group 8 complexes increases as 5d > 3d > 4d. Interestingly, the difference between the

Table 4.2: Calculated energies, enthalpies, and entropies of the H_2 absorption reaction at 1 atm, 298K and rotational entropy of the bound states at 298K and 373K. Energy and enthalpy values are given in kJ/mol, and entropy values are given in J/mol-K.

Compound	ΔE°	ΔH°	ΔS°	S_{rot}(298K)	S_{rot}(373K)
$[FeH(\eta^2\text{-}H_2)dppe_2]^+$	-41.2	-48.0	-91.4	4.19	5.74
$[RuH(\eta^2\text{-}H_2)dppe_2]^+$	-33.9	-41.4	-98.5	4.19	5.74
$[OsH(\eta^2\text{-}H_2)dppe_2]^+$	-76.3	-80.6	-82.9	8.76	10.59

enthalpies and entropies of the osmium species and the other group 8 complexes is much higher than the corresponding differences in the group 6 and 7 complexes. This result suggests stronger backdonation from the osmium center and stabilization of the trihydride species, which is consistent with reported NMR studies in solution that indicate the trihydride is present.[96]

Simulated thermodynamic values and isotherms for the osmium and ruthenium complexes correlate well with experimental observations.[96] $[OsH(\eta^2\text{-}H_2)dppe_2]^+$ was found to be extremely stable to loss of the dihydrogen ligand at all temperatures, with greater than 97% coverage down to 0.25 torr at 373K. This behavior is consistent with observations of exchange kinetics in the complex, which indicate that $[OsH(\eta^2\text{-}H_2)dppe_2][BF_4]$ is highly stable to exchange of the H_2 ligand with N_2, D_2, or CH_3CN in the solid state or in solution. Simulated isotherms for absorption over the ruthenium complex appear in Figure 4.4. As shown in the figure, the ruthenium complex has only ∼80% coverage at room temperature and significant overpressure is required to maintain the dihydrogen complex, consistent with experimental reports. At higher temperatures the stability of the dihydrogen complex is reduced, with only ∼40% coverage at 373K and 5 bar. This behavior is ideal for hydrogen storage applications, which require cycles with materials showing room temperature stability but strong release of the absorbed gas upon mild heating.

The absorption enthalpy for the singlet iron fragment $[FeHdppe_2]^+$ is lower than that of the manganese fragment $[Mn(CO)dppe_2]^+$ reported in the previous chapter, which significantly underestimates the binding strength in the iron complex relative to our experimental observations and reported behavior in the solid state. This deviation demonstrates the importance of the magnetic spin state to the binding behavior in these materials, despite previous reports of the nearly isoenergetic nature of the singlet and triplet states for the iron complex. Such spin state transitions

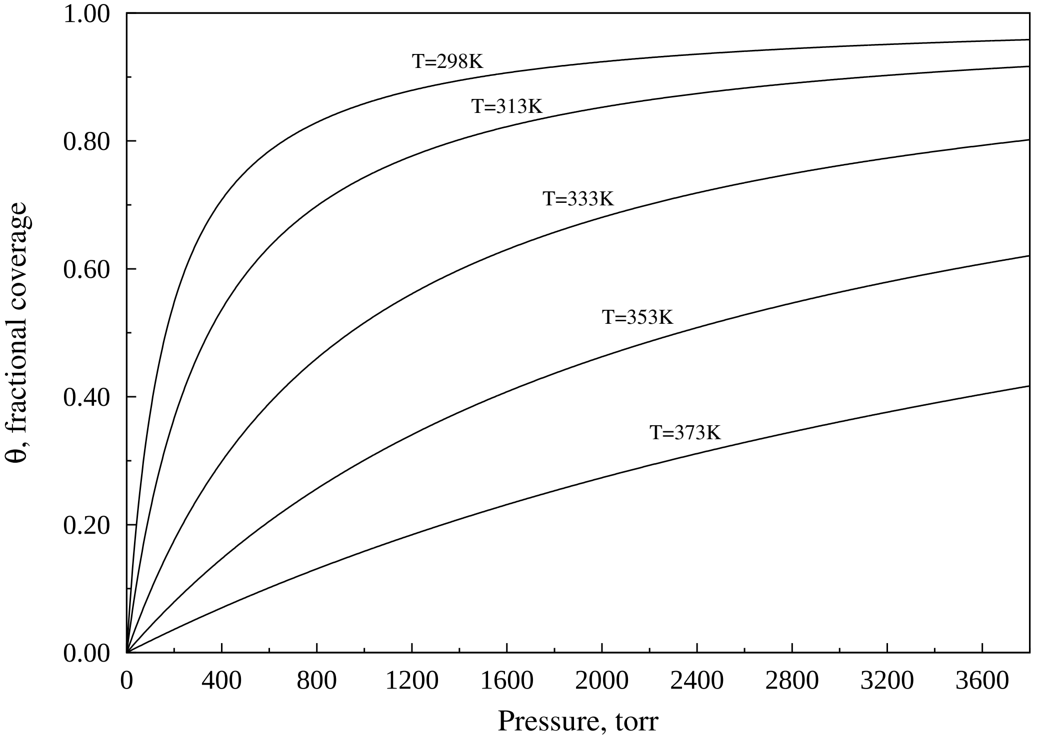

Figure 4.4: Simulated isotherms for hydrogen absorption over $[RuHdppe_2]^+$ up to 5 bar pressure

may be responsible for other complications known to exist selectively in iron dihydrogen complexes. For instance, Bianchini et al.[158, 159] found that during the catalysis of alkyne hydrogenation, the tetraphosphine complex $[(PP_3)FeH(H_2)][BPh_4]$ preferentially removes a phosphine arm before releasing the dihydrogen ligand, while the ruthenium analog $[(PP_3)RuH(H_2)][BPh_4]$ first releases the dihydrogen molecule for the same catalytic process. If present in the tetraphosphine complexes, the loss of hydrogen to form a high-energy triplet state may be less favorable than the removal of a phosphine arm to form a singlet state, and this effect would not be present in the analogous ruthenium complex. The potential for such magnetic transitions should be assessed carefully when evaluating these materials for both chemical and hydrogen storage applications.

4.2.3 Conclusions

Mössbauer parameters for the thermal cycling products of $[FeH(\eta^2\text{-}H_2)dppe_2][NTf_2]$ have been determined experimentally and through electronic structure simulations using the GAMESS software.

From these parameters, the triplet spin state of the dehydrogenated product [FeHdppe$_2$][NTf$_2$] was found to be the predominant dehydrogenation product at room temperature, with the absorption reaction accompanied by a triplet→singlet magnetic transition that greatly affects the thermodynamic stability of the hydrogen adduct. A partial quadrupole splitting value of -0.245 mm/s was identified for the dihydrogen ligand in these complexes, which differs significantly from the value of -1.04 mm/s for hydride ligands and may be used to help distinguish Kubas binding from hydride formation in hydrogen storage materials.

A modification of the Langmuir isotherm model used to describe the behavior of group 7 dihydrogen complexes was applied to absorption of hydrogen onto the singlet-state complexes [MHdppe$_2$]$^+$ (M = Fe, Ru, Os). This model accurately described the reported behavior for the ruthenium and osmium complexes and illustrated the magnitude of the spin-state transition on the absorption behavior in the iron complex, which showed singlet-state enthalpy values similar to the manganese complex reported in the previous chapter despite experimental evidence for much stronger binding. Singlet-state absorption enthalpies demonstrated the familiar trend of increase as 5d $>$ 3d $>$ 4d, indicating a consistent trend within transition metals exhibiting the same spin state. However, the magnitude of the differences between the metal centers were significantly different, particularly in osmium complexes. Simulated isotherms for the ruthenium complex was found to have near ideal behavior for hydrogen absorption applications, showing great promise for the development of future organometallic hydrogen storage.

Chapter 5

Conclusions

5.1 Summary of the Current Work

In the preceding chapters, new methods and techniques based on the Sieverts technique used for the evaluation of hydrogen storage materials have been successfully employed to evaluate the thermodynamic properties of hydrogen binding in dihydrogen complexes. These *enabling technologies* provide methods for evaluation of the thermodynamic properties of these hydrogenation reactions that have, to date, proven elusive by traditional chemical methods because of the stability of known dihydrogen complexes and the instability of the dehydrogenated products. These methods may prove invaluable not only to the assessment and design of future hydrogen storage materials, but also to organometallic chemistry fields for the study of complexes that are sensitive to solvent addition or are only moderately stable at room temperature and require higher pressures to form.

Mössbauer spectroscopy has also been confirmed as a viable technique for distinguishing between dihydrogen and dihydride complexes, and for determining the identity of dehydrogenation products when solvent sensitivity is an issue.[107] This underutilized spectroscopic technique may prove useful in future chemical evaluations of dihydrogen complexes, given that the majority of known dihydrogen complexes have iron, ruthenium, osmium, or rhenium metal centers,[88, 90] all of which are Mössbauer active atoms.

The Langmuir isotherm and computational studies using B3LYP/LANL2DZ-ECP DFT theory for geometry optimization and vibrational analysis of complexes, combined with MP2-SCS/LANL2DZ-

ECP theory calculations for the total molecular energy, have been shown to be effective tools for producing highly accurate estimates of the equilibrium absorption behavior for dihydrogen complexes. Previous efforts using only ideal gas behavior van't Hoff equations have found difficulty in reproducing such behaviors, due to the difficulty in estimating entropic contributions to the thermal behavior.[16, 17, 20] The Langmuir isotherm, both in classical and statistical formulations, provides methods to avoid these difficulties and directly determine the thermodynamic properties from the equilibrium constant, providing more accurate determination of the enthalpy and entropy.

Enthalpy values obtained for the complexes in these studies were shown to be surprisingly high relative to estimates in the hydrogen storage literature,[5] and in all cases were comparable to tightly bound metal and complex hydride materials. However, significantly reduced entropy from the values expected[16, 17] for formation of hydrides allows near room temperature cycling for these complexes. This unique behavior, combined with rapid kinetics observed in many dihydrogen complexes, holds significant promise for dihydrogen complexes and other Kubas materials for hydrogen storage applications.

The source of the reduced absorption entropy of ∼30 J/mol-K for all of the studied complexes relative to expectation has not been fully established. The rotational mode of the dihydrogen molecule in the complex was the only mode found to be significantly populated in dihydrogen complexes that would be absent in the corresponding hydride complexes, and accounted for up to ∼11 J/mol-K of the entropy change. The remaining contributions to the entropy change remain unknown but may be electronic in nature, associated with the spread of electronic charge throughout the large ligand framework. Investigations of the additional sources of entropy provide grounds for future study.

5.2 Considerations for Future Studies

P-T-x behavior relevant for hydrogen storage has been found for hydrogenation of $[\mathrm{Mn(CO)dppe_2}]^+$ and $[\mathrm{RuHdppe_2}]^+$ cationic complexes. Although these complexes were only originally intended as models for evaluation of the Kubas mechanisms because of their weight and bulk, the surprising discovery of extremely rapid absorption kinetics in these materials provides renewed enthusiasm for the use of dihydrogen complexes as hydrogen storage materials.

In the following sections, some considerations are presented for the further exploration of dihydrogen complexes for hydrogen storage applications.

5.2.1 Known Dihydrogen Complexes for Hydrogen Storage

The majority of materials exhibiting Kubas binding are high surface area or porous materials, such as MOFs or decorated carbons, designed to incorporate unsaturated metal centers as well as a high surface area for physisorption. However, as discussed previously, while such schemes have been shown to increase binding enthalpies in physisorption materials, it is unclear whether this is due to a greater binding potential throughout the entire material or whether the metal centers act independently of the physisorption sites, binding hydrogen with a higher enthalpy at the metal while weak binding interactions still predominate at the majority of the sites. If the latter, these schemes may not produce the desired binding properties until metal centers account for significant weight in the complex, which defeats the intention of the technique.

The bulk absorption properties found for hydrogen in $[\mathrm{Mn(CO)dppe_2}]^+$ have the advantage of producing equivalent binding sites for each hydrogen absorbed, leading to uniform and easily characterized absorption and desorption behavior. Development of higher weight dihydrogen complexes for hydrogen storage is therefore a viable method to provide additional control of operating properties. However, dihydrogen complexes containing significant percentages of removable hydrogen are rare.[88] Most complexes contain less than 1 wt % hydrogen; the complex $\mathrm{CpMn(H_2)(CO)_2}$, a half-sandwich complex, has the highest reportable weight percent of dihydrogen for isolable dihydrogen complexes at 1.1 wt%.

Reports of dihydrogen complexes as potential hydrogen storage materials are further complicated by poor communication of fuel system requirements. Many complexes, such as $\mathrm{Cr(CO)_5(H_2)}$, are reported as potential hydrogen storage materials but require extreme low temperatures to form and are unlikely to have stable unsaturated dehydrogenation products, which can cause potential release of carbon monoxide in fuel systems. Others, such as $[Ru(H_2O)_5(H_2)]^+$ and $[Os(NH_3)_5(H_2)]^+$, exist only as solvated ions, which require a large portion of the weight of the storage material to be solvent. Additionally, complexes such as $Ru(H)_2(H_2)_2(PCp_3)_2$ are reported for potential hydrogen storage applications. Up to 10 H_2 molecules may be reversibly extracted from this complex for a total of 1.7 wt% hydrogen release, but only through a substitution reaction with ethylene.[161] Only two H_2 molecules are labile through thermal decomposition, which reduces the usable percentage of hydrogen to 0.69 wt%.[162]

Significant material discovery efforts will be needed if dihydrogen complexes are to meet the USDOE gravimetric capacity requirements. However, it should be noted that these requirements are specific for vehicular and mobile systems. Stationary applications, such as fuel storage systems at refilling stations or electrical generation plants, may have more relaxed requirements for gravimetric capacity and could make use of currently known dihydrogen complexes. The relevant specification in these applications is the compression capability, designated by the volumetric storage capacity. This metric is poorly reported for dihydrogen complexes.

5.2.2 Computational Discovery of New Complexes

Unfortunately, dihydrogen complexes suitable for hydrogen storage applications are unlikely to be discovered in the chemical literature. The requirement of 3–100 bar hydrogen delivery pressure set by the USDOE[4] for working fuel systems requires dihydrogen complexes that are *unstable* under ambient pressure and near room temperature conditions. Performance of the spectroscopic measurements necessary to identify dihydrogen complexes under pressurized conditions is extremely difficult, and limited to the work of a few specialized research groups. Few dihydrogen complexes have been synthesized under greater than one atmosphere of hydrogen pressure, although some, such as $[RuH(H_2)dppe_2]^+$ have reported instabilities at room temperature[96] unless a hydrogen atmosphere is maintained. Unstable complexes may be formed at lower pressures and detected by solution NMR if lower temperatures are used; however, lower temperatures increase competition for the binding site by solvent, reducing the likelihood of observation of pure species and subsequent reporting. Additionally, such complexes may not be discovered simply through reluctance to explore the lower temperature parameter space; complexes that are unreactive to hydrogen at room temperature are less likely to be tested at lower temperatures because of generally slower kinetics and difficulties in experimental procedure.

The computational techniques presented in this paper not only provide methods for evaluating equilibrium behavior in known complexes, but also an opportunity for discovery and screening of new materials for hydrogen storage applications. Lightweight complexes that otherwise have not been observed to absorb hydrogen at room temperature but are otherwise of interest for their hydride character, such as Ni(dmpe)$_2$, can be evaluated for direct hydrogenation and use as hydrogen storage opportunities. Trends have been developed for the relationship between the identity of the *trans* ligand and the H-H bond distance;[168] additional studies using the Langmuir isotherm can now be included to evaluate the full reaction coordinate. Complexes of the M(dmpe)$_2$ structure are known for 3d transition metals from Cr to Ni,[164–167] and appropriate calculations can provide trends across the periodic table. Extension of such studies can also provide additional chemical trends to guide materials design.

5.2.3 Engineering Considerations

One of the promising potential benefits for dihydrogen complexes as hydrogen storage materials is the availability of the raw materials. Complexes in this study with relevant hydrogen storage properties were composed of earth-abundant 3d transition metals and organic molecules. This provides a significant advantage for these materials in energy applications over lithium-based or rare-earth derived storage materials, which are available in recoverable quantities in only a few locations and could face significant shortages if relied upon for energy infrastructure replacement. At the moment, phosphine complexes such as dppe are produced in small quantities and are quite expensive. However, organophosphorus compounds are produced in large quantities for pesticide and fire retardant applications, and the potential for large scale production is available for countries with developed chemical industries.

Because of the high enthalpies and rapid kinetics observed for the complexes in this study and on the basis of similar enthalpy values found in previous studies, heat management is expected to be a critical component for operation of a dihydrogen complex hydrogen storage system. As mostly organic complexes and salts, dihydrogen complexes are expected to be thermal insulators and poor conductors of heat in the solid state, which can lead to rapid localized heating upon absorption, producing decomposition and potentially damaging fuel systems. Future studies for use of dihydrogen complexes as hydrogen storage materials should include evaluation of heat transfer properties in these materials and identification of proper heat management technologies.

5.3 Concluding Remarks

The use of hydrogen for fuel applications has been a prominent goal of energy technology research for its potential for renewable production and clean combustion. Fuel storage is one of several critical components to the development of hydrogen energy infrastructure and, while research efforts have produced drastic improvements in the performance of storage materials, significant materials discovery and engineering development are still required before hydrogen can become a consistent part of the US energy profile.

The efforts presented in this work have been directed at developing methods and techniques for evaluating new storage materials. Application of these techniques, and further evaluation of dihydrogen complexes as storage materials, can lead not only to new materials but to the capability to rationally design dihydrogen complexes for specific hydrogen applications and rapidly improve energy storage systems toward inclusion in the national energy infrastructure.

Appendix: GAMESS Input Files

In this section, the GAMESS input files used to calculate thermodynamic properties and Mössbauer parameters for the 3d organometallic clusters and the H_2 molecule are reprinted. Files for the 3d transition metal organometallic fragments are representative of files for 4d and 5d fragments. The effective core potentials and LANL2DZ basis set are those defined for the "LANL2DZ ECP" basis set in the EMSL Basis Set Exchange database mhosted by Pacific Northwest National Laboratory[169, 170]

Because of their length, automatically generated molecular eigenvector printouts have been excluded from some of the files below. These values are generated after a completed run, and are used for improving performance on subsequent runs or restarts.

5.3.1 Geometry Optimization

```
! H2 molecule geometry optimization and vibrational analysis
 $CONTRL SCFTYP=RHF RUNTYP=OPTIMIZE EXETYP=RUN DFTTYP=B3LYP
    MAXIT=30 $END
 $SYSTEM MEMDDI=0 MWORDS=50 PARALL=.TRUE. $END
 $BASIS GBASIS=LANL2DZ EXTFIL=.T. NDFUNC=1 NPFUNC=1 $END
 $GUESS GUESS=HUCKEL $END
 $SCF DIRSCF=.TRUE. CONV=1.0e-7 $END
 $STATPT OPTTOL=0.0000001 TRMIN=0.01 NSTEP=100 HSSEND=.T. $END
 $FORCE METHOD=SEMINUM NVIB=2 VIBSIZ=0.01 SCLFAC=0.96 VIBANL=.TRUE.
   TEMP(1)=295 TEMP(2)=298 TEMP(3)=300 TEMP(4)=313 TEMP(5)=333
   TEMP(6)=343 TEMP(7)=353 TEMP(8)=363 TEMP(9)=373
 $END
 $DATA
H2 molecule
C1
H     1.0    -0.02189     0.00000     0.00000
H     1.0     0.72189     0.00000     0.00000
 $END
```

```
!   Input file for GAMESS - [Mn(CO)dppe2]+ geom. opt.
 $CONTRL SCFTYP=RHF RUNTYP=OPTIMIZE EXETYP=RUN DFTTYP=B3LYP
    MAXIT=100 ICHARG=1 ECP=READ $END
 $SYSTEM MEMDDI=0 MWORDS=300 PARALL=.TRUE. $END
 $BASIS GBASIS=LANL2DZ EXTFIL=.T. NDFUNC=1 NPFUNC=1 $END
 $GUESS GUESS=MOREAD NORB=204 $END
 $SCF DIRSCF=.TRUE. CONV=5.0e-6 $END
 $STATPT OPTTOL=0.0001 NSTEP=100 TRMIN=0.01 $END
 $DATA
Mn(CO)dppe2
C1
Mn    25.0     7.67008     8.28046    -0.21132
P    15.0     6.82809    10.48811     0.40010
P    15.0    10.06459     8.71101     0.34001
C     6.0     7.79196    12.04727    -0.03090
C     6.0     8.41215    12.82113     0.97456
C     6.0     9.12716    13.98499     0.63619
C     6.0     9.23721    14.38322    -0.70971
C     6.0     8.63746    13.60362    -1.71663
C     6.0     7.92188    12.43929    -1.38223
C     6.0     6.10959    10.87473     2.10781
C     6.0     5.49090    12.12274     2.35226
C     6.0     4.91432    12.40192     3.60388
C     6.0     4.94926    11.43686     4.63110
C     6.0     5.55991    10.19105     4.39570
C     6.0     6.13327     9.91252     3.13868
C     6.0    11.07368     9.82148    -0.80511
C     6.0    11.55828    11.07234    -0.36890
C     6.0    12.30455    11.88731    -1.24034
C     6.0    12.57049    11.46497    -2.55567
C     6.0    12.07386    10.22453    -3.00068
C     6.0    11.32339     9.41041    -2.13349
C     6.0    10.63577     9.24256     2.06158
C     6.0    12.00782     9.22436     2.40702
C     6.0    12.42099     9.58568     3.70144
C     6.0    11.47033     9.97577     4.66753
C     6.0    10.10641    10.00906     4.32674
C     6.0     9.69565     9.64348     3.02909
C     6.0     5.25128    10.64162    -0.66231
C     6.0    10.96897     7.03049     0.17398
H     1.0     8.33046    12.53592     2.02002
H     1.0     9.58941    14.57841     1.42145
H     1.0     9.78134    15.28786    -0.97007
H     1.0     8.72562    13.89542    -2.76002
H     1.0     7.48231    11.85019    -2.18217
H     1.0     5.46694    12.88327     1.57525
H     1.0     4.44339    13.36630     3.77712
H     1.0     4.50770    11.65571     5.60011
H     1.0     5.59048     9.44016     5.18185
H     1.0     6.59693     8.94168     2.97505
H     1.0    11.36802    11.41498     0.64379
H     1.0    12.67562    12.84704    -0.88906
H     1.0    13.15238    12.09304    -3.22578
H     1.0    12.26465     9.89324    -4.01840
H     1.0    10.93921     8.46489    -2.50774
H     1.0    12.75969     8.94998     1.67027
H     1.0    13.47787     9.56669     3.95459
H     1.0    11.79230    10.25368     5.66818
H     1.0     9.36538    10.31820     5.05981
H     1.0     8.64286     9.68103     2.77689
```

```
H      1.0     4.75163    11.59040    -0.43599
H      1.0     5.55059    10.65836    -1.71560
H      1.0    11.29153     6.91198    -0.86582
H      1.0    11.86538     7.04421     0.80134
P     15.0     8.47111     5.95830    -0.51579
P     15.0     5.26265     7.78020    -0.52788
O      8.0     7.93872     9.30652    -2.96195
C      6.0     7.48214     4.46650     0.08401
C      6.0     6.82874     3.61342    -0.83270
C      6.0     6.11130     2.49310    -0.37448
C      6.0     6.02815     2.21806     1.00387
C      6.0     6.65748     3.07828     1.92346
C      6.0     7.37805     4.19713     1.46654
C      6.0     9.22559     5.32067    -2.13502
C      6.0     9.80386     4.02919    -2.16757
C      6.0    10.42320     3.55238    -3.33593
C      6.0    10.47239     4.35878    -4.49152
C      6.0     9.89754     5.64150    -4.46655
C      6.0     9.28041     6.12254    -3.29409
C      6.0     4.31683     6.68925     0.69969
C      6.0     3.84956     5.41090     0.32779
C      6.0     3.15366     4.61027     1.25248
C      6.0     2.92345     5.06957     2.56232
C      6.0     3.39811     6.33933     2.94378
C      6.0     4.09141     7.14233     2.01937
C      6.0     4.64766     7.14540    -2.19622
C      6.0     3.26451     7.15139    -2.49435
C      6.0     2.80264     6.69775    -3.74213
C      6.0     3.71690     6.22734    -4.70719
C      6.0     5.09182     6.20873    -4.41204
C      6.0     5.55321     6.66677    -3.16214
C      6.0     7.85001     8.86482    -1.85190
C      6.0    10.03155     5.88650     0.58752
C      6.0     4.32384     9.45135    -0.36984
H      1.0     6.89343     3.80041    -1.90135
H      1.0     5.62634     1.83620    -1.09275
H      1.0     5.48293     1.34601     1.35628
H      1.0     6.59121     2.88014     2.99033
H      1.0     7.86006     4.84199     2.19845
H      1.0     9.75984     3.38513    -1.29242
H      1.0    10.86157     2.55759    -3.34557
H      1.0    10.95080     3.98985    -5.39535
H      1.0     9.92570     6.27187    -5.35204
H      1.0     8.85336     7.11771    -3.30762
H      1.0     4.01117     5.03670    -0.67837
H      1.0     2.79386     3.63098     0.94632
H      1.0     2.37992     4.45134     3.27256
H      1.0     3.22392     6.70756     3.95225
H      1.0     4.43227     8.12299     2.33709
H      1.0     2.54094     7.48804    -1.75511
H      1.0     1.73741     6.70845    -3.95889
H      1.0     3.35947     5.88077    -5.67375
H      1.0     5.80487     5.84664    -5.14857
H      1.0     6.61586     6.65060    -2.95164
H      1.0    10.51292     4.91053     0.46239
H      1.0     9.73468     5.98446     1.63887
H      1.0     3.91885     9.51865     0.64537
H      1.0     3.47971     9.44409    -1.06554
 $END
 $ECP
```

```
 MN-ECP GEN     10     2
 3      ----- d potential     -----
   -10.0000000        1    357.3914469
   -60.2990287        2     64.6477389
   -10.4217834        2     16.0960833
 5      ----- s-d potential     -----
     3.0000000        0    107.4127215
    16.2591819        1    111.4958973
   276.9373928        2     46.5568346
   241.3174342        2      8.3688135
  -146.4635329        2      7.7237489
 5      ----- p-d potential     -----
     5.0000000        0     80.0415103
     5.7589756        1    105.6043646
   285.2918654        2     40.8300466
   143.4222647        2      8.0098457
   -88.7031851        2      7.3390928
 P-ECP GEN     10     2
 5      ----- d   potential     -----
   -10.0000000        1    462.1211423
   -79.4864658        2     93.6863701
   -28.3668251        2     21.2349094
    -9.8577589        2      6.3388415
    -1.0163783        2      2.0620684
 5      ----- s-d potential     -----
     3.0000000        0     78.0831823
    12.9104154        1     58.9576810
   150.0250298        2     36.0571255
    71.7083146        2     11.2464453
    23.0397012        2      2.6757561
 6      ----- p-d potential     -----
     5.0000000        0     75.1617880
     6.3446507        1     57.4544041
   198.5585104        2     47.9481748
   111.1470820        2     18.4588360
    40.3944144        2      5.9414190
     6.4483233        2      1.8487507
P-ECP
C-ECP NONE
C-ECP NONE
C-ECP NONE
C-ECP NONE
C-ECP NONE
C-ECP NONE
C-ECP NONE
C-ECP NONE
C-ECP NONE
C-ECP NONE
C-ECP NONE
C-ECP NONE
C-ECP NONE
C-ECP NONE
C-ECP NONE
C-ECP NONE
C-ECP NONE
C-ECP NONE
C-ECP NONE
C-ECP NONE
C-ECP NONE
C-ECP NONE
```

```
C-ECP NONE
C-ECP NONE
C-ECP NONE
C-ECP NONE
H-ECP NONE
H-ECP NONE
H-ECP NONE
H-ECP NONE
H-ECP NONE
H-ECP NONE
H-ECP NONE
H-ECP NONE
H-ECP NONE
H-ECP NONE
H-ECP NONE
H-ECP NONE
H-ECP NONE
H-ECP NONE
H-ECP NONE
H-ECP NONE
H-ECP NONE
H-ECP NONE
H-ECP NONE
H-ECP NONE
H-ECP NONE
H-ECP NONE
H-ECP NONE
H-ECP NONE
P-ECP
P-ECP
O-ECP NONE
C-ECP NONE
C-ECP NONE
C-ECP NONE
C-ECP NONE
C-ECP NONE
C-ECP NONE
C-ECP NONE
C-ECP NONE
C-ECP NONE
C-ECP NONE
C-ECP NONE
C-ECP NONE
C-ECP NONE
C-ECP NONE
C-ECP NONE
C-ECP NONE
C-ECP NONE
C-ECP NONE
C-ECP NONE
C-ECP NONE
C-ECP NONE
C-ECP NONE
C-ECP NONE
C-ECP NONE
C-ECP NONE
C-ECP NONE
C-ECP NONE
H-ECP NONE
H-ECP NONE
```

```
H-ECP NONE
H-ECP NONE
H-ECP NONE
H-ECP NONE
H-ECP NONE
H-ECP NONE
H-ECP NONE
H-ECP NONE
H-ECP NONE
H-ECP NONE
H-ECP NONE
H-ECP NONE
H-ECP NONE
H-ECP NONE
H-ECP NONE
H-ECP NONE
H-ECP NONE
H-ECP NONE
H-ECP NONE
H-ECP NONE
H-ECP NONE
H-ECP NONE
 $END
```

```
!   Input file for GAMESS - [Mn(CO)dppe2]+ agostic config geom opt
 $CONTRL SCFTYP=RHF RUNTYP=OPTIMIZE EXETYP=RUN DFTTYP=B3LYP
    MAXIT=100 ICHARG=1 ECP=READ $END
 $SYSTEM MEMDDI=0 MWORDS=300 PARALL=.TRUE. $END
 $BASIS GBASIS=LANL2DZ EXTFIL=.T. NDFUNC=1 NPFUNC=1 $END
 $GUESS GUESS=MOREAD NORB=204 $END
 $SCF DIRSCF=.TRUE. CONV=5.0e-6 $END
 $STATPT OPTTOL=0.0001 NSTEP=100 TRMIN=0.01 $END
 $FORCE METHOD=SEMINUM NVIB=1 VIBSIZ=0.010000 SCLFAC=0.960000 $END
 $DATA
Mn(CO)dppe2
C1
Mn    25.0     6.02112     6.32333     5.71956
P    15.0     7.99457     5.19338     6.52813
P    15.0     3.98246     7.26267     4.83182
P    15.0     4.49051     5.29315     7.35026
P    15.0     7.48030     6.85712     3.79648
O     8.0     6.59743     8.76430     7.27125
C     6.0     8.48299     5.19195     8.34333
C     6.0     8.87444     6.40826     8.94757
C     6.0     9.21149     6.44684    10.31242
C     6.0     9.15495     5.27405    11.09026
C     6.0     8.76174     4.06149    10.49289
C     6.0     8.42687     4.01920     9.12630
C     6.0     8.28256     3.42634     5.93519
C     6.0     9.50161     2.75039     6.17259
C     6.0     9.71366     1.46342     5.64544
C     6.0     8.70969     0.83526     4.87945
C     6.0     7.49040     1.49831     4.64911
C     6.0     7.28163     2.78714     5.17507
C     6.0     3.04741     6.17369     3.61376
C     6.0     1.70384     6.43727     3.26201
C     6.0     1.00838     5.56048     2.41024
C     6.0     1.64977     4.41408     1.89619
C     6.0     2.99107     4.15395     2.23240
C     6.0     3.68446     5.03054     3.08884
C     6.0     3.82453     9.00867     4.14982
C     6.0     3.89969    10.10941     5.03364
C     6.0     3.79533    11.42345     4.54066
C     6.0     3.62412    11.65230     3.16148
C     6.0     3.55948    10.55866     2.27752
C     6.0     3.65955     9.24292     2.76787
C     6.0     4.51866     5.58776     9.21612
C     6.0     5.31307     6.60263     9.78481
C     6.0     5.24019     6.86737    11.16747
C     6.0     4.38134     6.11802    11.99114
```

C	6.0	3.58675	5.09926	11.42673
C	6.0	3.65035	4.83956	10.04726
C	6.0	4.35081	3.41381	7.20663
C	6.0	3.63155	2.82900	6.14027
C	6.0	3.57512	1.42932	5.99934
C	6.0	4.24380	0.59645	6.91634
C	6.0	4.97065	1.17411	7.97543
C	6.0	5.02705	2.57240	8.11824
C	6.0	7.03187	6.04341	2.14706
C	6.0	6.37874	6.79522	1.14461
C	6.0	5.99937	6.19099	-0.06792
C	6.0	6.26198	4.82624	-0.29473
C	6.0	6.90305	4.06888	0.70389
C	6.0	7.28019	4.67099	1.92029
C	6.0	7.94704	8.60614	3.26355
C	6.0	8.85239	8.77761	2.18859
C	6.0	9.25218	10.06514	1.79441
C	6.0	8.75292	11.19725	2.47136
C	6.0	7.85304	11.03032	3.53887
C	6.0	7.45023	9.73901	3.93560
C	6.0	6.36558	7.77004	6.64086
C	6.0	9.21639	6.12153	4.17538
C	6.0	9.46241	6.07963	5.69159
C	6.0	2.71044	5.89614	6.94329
C	6.0	2.76393	7.28994	6.30042
H	1.0	6.32756	3.27869	5.00447
H	1.0	4.72646	4.82517	3.32259
H	1.0	8.90974	7.32988	8.37139
H	1.0	9.51473	7.38822	10.76416
H	1.0	9.41336	5.30495	12.14576
H	1.0	8.71804	3.15148	11.08660
H	1.0	8.13949	3.07280	8.67591
H	1.0	10.28433	3.21901	6.76518
H	1.0	10.65629	0.95397	5.82886
H	1.0	8.87681	-0.15790	4.47031
H	1.0	6.70537	1.01863	4.06987
H	1.0	1.20013	7.32560	3.63753
H	1.0	-0.02467	5.77103	2.14513
H	1.0	1.11122	3.73836	1.23634
H	1.0	3.49898	3.28282	1.82607
H	1.0	4.04185	9.96142	6.10169
H	1.0	3.84532	12.26168	5.23148
H	1.0	3.54032	12.66776	2.78221
H	1.0	3.42968	10.72710	1.21121
H	1.0	3.59531	8.40859	2.07410
H	1.0	5.98202	7.19413	9.17157

```
H     1.0     5.85488     7.65640    11.59329
H     1.0     4.33104     6.32050    13.05830
H     1.0     2.92141     4.51190    12.05495
H     1.0     3.02759     4.05272     9.62757
H     1.0     3.10546     3.44443     5.41525
H     1.0     3.00168     0.99511     5.18376
H     1.0     4.19538    -0.48450     6.81138
H     1.0     5.49114     0.53923     8.68814
H     1.0     5.57885     3.00127     8.94998
H     1.0     6.18542     7.85407     1.29419
H     1.0     5.97689     4.36258    -1.23595
H     1.0     7.12080     3.01658     0.53580
H     1.0     7.77498     4.05773     2.66914
H     1.0     9.23713     7.91512     1.64806
H     1.0     9.94781    10.18445     0.96737
H     1.0     9.06268    12.19400     2.16680
H     1.0     7.46018    11.89750     4.06310
H     1.0     6.75353     9.63246     4.75830
H     1.0     9.27502     5.11360     3.75279
H     1.0     9.96685     6.74056     3.67455
H     1.0     9.53477     7.09030     6.10842
H     1.0    10.39076     5.54667     5.92510
H     1.0     2.22947     5.17927     6.27041
H     1.0     2.14009     5.91574     7.87708
H     1.0     3.11571     8.03899     7.01903
H     1.0     1.77373     7.60209     5.94948
H     1.0     5.50594     6.78530    -0.83315
 $END
 $ECP
 MN-ECP GEN     10     2
 3      ----- d potential     -----
   -10.0000000        1    357.3914469
   -60.2990287        2     64.6477389
   -10.4217834        2     16.0960833
 5      ----- s-d potential     -----
     3.0000000        0    107.4127215
    16.2591819        1    111.4958973
   276.9373928        2     46.5568346
   241.3174342        2      8.3688135
  -146.4635329        2      7.7237489
 5      ----- p-d potential     -----
     5.0000000        0     80.0415103
     5.7589756        1    105.6043646
   285.2918654        2     40.8300466
   143.4222647        2      8.0098457
   -88.7031851        2      7.3390928
```

```
 P-ECP GEN     10     2
 5      ----- d   potential     -----
   -10.0000000        1    462.1211423
   -79.4864658        2     93.6863701
   -28.3668251        2     21.2349094
    -9.8577589        2      6.3388415
    -1.0163783        2      2.0620684
 5      ----- s-d potential     -----
     3.0000000        0     78.0831823
    12.9104154        1     58.9576810
   150.0250298        2     36.0571255
    71.7083146        2     11.2464453
    23.0397012        2      2.6757561
 6      ----- p-d potential     -----
     5.0000000        0     75.1617880
     6.3446507        1     57.4544041
   198.5585104        2     47.9481748
   111.1470820        2     18.4588360
    40.3944144        2      5.9414190
     6.4483233        2      1.8487507
P-ECP
P-ECP
P-ECP
O-ECP NONE
C-ECP NONE
C-ECP NONE
C-ECP NONE
C-ECP NONE
C-ECP NONE
C-ECP NONE
C-ECP NONE
C-ECP NONE
C-ECP NONE
C-ECP NONE
C-ECP NONE
C-ECP NONE
C-ECP NONE
C-ECP NONE
C-ECP NONE
C-ECP NONE
C-ECP NONE
C-ECP NONE
C-ECP NONE
C-ECP NONE
C-ECP NONE
C-ECP NONE
C-ECP NONE
```

```
C-ECP NONE
C-ECP NONE
C-ECP NONE
C-ECP NONE
C-ECP NONE
C-ECP NONE
C-ECP NONE
C-ECP NONE
C-ECP NONE
C-ECP NONE
C-ECP NONE
C-ECP NONE
C-ECP NONE
C-ECP NONE
C-ECP NONE
C-ECP NONE
C-ECP NONE
C-ECP NONE
C-ECP NONE
C-ECP NONE
C-ECP NONE
C-ECP NONE
C-ECP NONE
C-ECP NONE
C-ECP NONE
C-ECP NONE
C-ECP NONE
C-ECP NONE
C-ECP NONE
C-ECP NONE
C-ECP NONE
H-ECP NONE
H-ECP NONE
H-ECP NONE
H-ECP NONE
H-ECP NONE
H-ECP NONE
H-ECP NONE
H-ECP NONE
H-ECP NONE
H-ECP NONE
H-ECP NONE
H-ECP NONE
H-ECP NONE
H-ECP NONE
H-ECP NONE
```

```
H-ECP NONE
H-ECP NONE
H-ECP NONE
H-ECP NONE
H-ECP NONE
H-ECP NONE
H-ECP NONE
H-ECP NONE
H-ECP NONE
H-ECP NONE
H-ECP NONE
H-ECP NONE
H-ECP NONE
H-ECP NONE
H-ECP NONE
H-ECP NONE
H-ECP NONE
H-ECP NONE
H-ECP NONE
H-ECP NONE
H-ECP NONE
H-ECP NONE
H-ECP NONE
H-ECP NONE
H-ECP NONE
H-ECP NONE
H-ECP NONE
H-ECP NONE
H-ECP NONE
H-ECP NONE
H-ECP NONE
H-ECP NONE
H-ECP NONE
 $END
```

```
!   Input file for GAMES - [Mn(H2)(CO)dppe2]+ geom. opt.
 $CONTRL SCFTYP=RHF RUNTYP=OPTIMIZE EXETYP=RUN DFTTYP=B3LYP
    MAXIT=100 ICHARG=1 ECP=READ $END
 $SYSTEM MEMDDI=0 MWORDS=300 PARALL=.TRUE. $END
 $BASIS GBASIS=LANL2DZ EXTFIL=.T. NDFUNC=1 NPFUNC=1 $END
 $GUESS GUESS=MOREAD NORB=205 $END
 $SCF DIRSCF=.TRUE. CONV=5.0e-6 $END
 $STATPT OPTTOL=0.0001 NSTEP=100 TRMIN=0.01 $END
 $DATA
Mn(CO)(H2)dppe2
C1
Mn    25.0     7.67576     8.22448    -0.12178
P    15.0     6.83327    10.45430     0.43250
P    15.0    10.06332     8.69409     0.36432
C     6.0     7.80841    11.99878    -0.03434
C     6.0     8.45608    12.76695     0.95860
C     6.0     9.17345    13.92493     0.60741
C     6.0     9.25855    14.32434    -0.74008
C     6.0     8.63101    13.55139    -1.73484
C     6.0     7.91235    12.39258    -1.38706
C     6.0     6.09251    10.94136     2.11397
C     6.0     5.47634    12.20832     2.25118
C     6.0     4.87178    12.58455     3.46316
C     6.0     4.87489    11.70153     4.56176
C     6.0     5.48965    10.44254     4.43703
C     6.0     6.09026    10.06608     3.21871
C     6.0    11.05943     9.82761    -0.77263
C     6.0    11.57839    11.05719    -0.31663
C     6.0    12.32206    11.87977    -1.18342
C     6.0    12.55208    11.48597    -2.51430
C     6.0    12.02028    10.26783    -2.97968
C     6.0    11.27317     9.44684    -2.11636
C     6.0    10.63915     9.21527     2.08928
C     6.0    12.00959     9.17201     2.43955
C     6.0    12.42759     9.53507     3.73206
C     6.0    11.48361     9.95427     4.69216
C     6.0    10.12188    10.01682     4.34568
C     6.0     9.70649     9.64896     3.05041
C     6.0     5.26353    10.57745    -0.64244
C     6.0    10.99919     7.03352     0.15058
H     1.0     8.39079    12.48325     2.00563
H     1.0     9.65802    14.51231     1.38382
H     1.0     9.80486    15.22481    -1.01030
H     1.0     8.69941    13.84463    -2.77927
H     1.0     7.44721    11.81145    -2.17792
H     1.0     5.47627    12.91125     1.42170
H     1.0     4.40391    13.56195     3.55023
H     1.0     4.40830    11.99312     5.49935
H     1.0     5.50344     9.75619     5.28014
H     1.0     6.55738     9.08720     3.15309
H     1.0    11.41741    11.37643     0.70846
```

H	1.0	12.71797	12.82370	-0.81628
H	1.0	13.13441	12.11831	-3.18028
H	1.0	12.18183	9.95912	-4.00935
H	1.0	10.86562	8.51719	-2.50528
H	1.0	12.75814	8.87547	1.70857
H	1.0	13.48394	9.49608	3.98693
H	1.0	11.80847	10.23204	5.69196
H	1.0	9.38644	10.35119	5.07314
H	1.0	8.65543	9.70975	2.79554
H	1.0	4.75679	11.52689	-0.43699
H	1.0	5.56434	10.57324	-1.69525
H	1.0	11.33104	6.96262	-0.89080
H	1.0	11.89191	7.04268	0.78312
P	15.0	8.51252	5.94342	-0.55946
P	15.0	5.28634	7.71747	-0.47996
O	8.0	7.91042	9.28841	-2.87927
C	6.0	7.52403	4.44506	0.02457
C	6.0	6.84994	3.61479	-0.89782
C	6.0	6.12215	2.49719	-0.44903
C	6.0	6.04972	2.20156	0.92542
C	6.0	6.70371	3.03677	1.85106
C	6.0	7.43317	4.15317	1.40334
C	6.0	9.23691	5.33699	-2.20521
C	6.0	9.80525	4.04218	-2.27099
C	6.0	10.40976	3.58571	-3.45495
C	6.0	10.45251	4.41438	-4.59443
C	6.0	9.88990	5.70156	-4.53581
C	6.0	9.28820	6.16268	-3.34745
C	6.0	4.32532	6.63288	0.73931
C	6.0	3.81456	5.37397	0.36070
C	6.0	3.10565	4.58525	1.28643
C	6.0	2.90380	5.03908	2.60250
C	6.0	3.42017	6.29120	2.99044
C	6.0	4.13024	7.07932	2.06630
C	6.0	4.67692	7.09808	-2.15707
C	6.0	3.29527	7.10753	-2.46372
C	6.0	2.84057	6.67412	-3.72131
C	6.0	3.76015	6.22126	-4.68990
C	6.0	5.13309	6.19755	-4.38644
C	6.0	5.58669	6.63519	-3.12661
C	6.0	7.83949	8.83336	-1.77737
C	6.0	10.09176	5.84875	0.51106
C	6.0	4.34498	9.38740	-0.32448
H	1.0	6.90340	3.81854	-1.96395
H	1.0	5.62083	1.85808	-1.17199
H	1.0	5.49445	1.33297	1.27060
H	1.0	6.64990	2.82093	2.91530
H	1.0	7.93091	4.77970	2.14076
H	1.0	9.76314	3.37867	-1.40993
H	1.0	10.84277	2.58953	-3.48889
H	1.0	10.91466	4.05856	-5.51190

```
H     1.0     9.91697     6.35089    -5.40770
H     1.0     8.86631     7.15988    -3.33668
H     1.0     3.95452     5.00502    -0.65048
H     1.0     2.71125     3.62125     0.97500
H     1.0     2.35119     4.43003     3.31331
H     1.0     3.26394     6.65692     4.00380
H     1.0     4.51032     8.04439     2.38974
H     1.0     2.56685     7.43323    -1.72437
H     1.0     1.77585     6.68619    -3.94281
H     1.0     3.40879     5.89325    -5.66516
H     1.0     5.85070     5.84673    -5.12382
H     1.0     6.64826     6.61640    -2.91213
H     1.0    10.59550     4.89419     0.32347
H     1.0     9.80766     5.87934     1.56945
H     1.0     3.95487     9.46316     0.69608
H     1.0     3.49044     9.37158    -1.00721
H     1.0     7.33615     8.01632     1.61587
H     1.0     7.62186     7.30652     1.41285
 $END
 $ECP
 MN-ECP GEN     10     2
 3      ----- d potential     -----
   -10.0000000        1    357.3914469
   -60.2990287        2     64.6477389
   -10.4217834        2     16.0960833
 5      ----- s-d potential     -----
     3.0000000        0    107.4127215
    16.2591819        1    111.4958973
   276.9373928        2     46.5568346
   241.3174342        2      8.3688135
  -146.4635329        2      7.7237489
 5      ----- p-d potential     -----
     5.0000000        0     80.0415103
     5.7589756        1    105.6043646
   285.2918654        2     40.8300466
   143.4222647        2      8.0098457
   -88.7031851        2      7.3390928
 P-ECP GEN     10     2
 5      ----- d   potential     -----
   -10.0000000        1    462.1211423
   -79.4864658        2     93.6863701
   -28.3668251        2     21.2349094
    -9.8577589        2      6.3388415
    -1.0163783        2      2.0620684
 5      ----- s-d potential     -----
     3.0000000        0     78.0831823
    12.9104154        1     58.9576810
   150.0250298        2     36.0571255
    71.7083146        2     11.2464453
    23.0397012        2      2.6757561
 6      ----- p-d potential     -----
```

```
     5.0000000        0     75.1617880
     6.3446507        1     57.4544041
   198.5585104        2     47.9481748
   111.1470820        2     18.4588360
    40.3944144        2      5.9414190
     6.4483233        2      1.8487507
P-ECP
C-ECP NONE
C-ECP NONE
C-ECP NONE
C-ECP NONE
C-ECP NONE
C-ECP NONE
C-ECP NONE
C-ECP NONE
C-ECP NONE
C-ECP NONE
C-ECP NONE
C-ECP NONE
C-ECP NONE
C-ECP NONE
C-ECP NONE
C-ECP NONE
C-ECP NONE
C-ECP NONE
C-ECP NONE
C-ECP NONE
C-ECP NONE
C-ECP NONE
C-ECP NONE
C-ECP NONE
C-ECP NONE
C-ECP NONE
H-ECP NONE
H-ECP NONE
H-ECP NONE
H-ECP NONE
H-ECP NONE
H-ECP NONE
H-ECP NONE
H-ECP NONE
H-ECP NONE
H-ECP NONE
H-ECP NONE
H-ECP NONE
H-ECP NONE
H-ECP NONE
H-ECP NONE
H-ECP NONE
H-ECP NONE
H-ECP NONE
```

```
H-ECP NONE
H-ECP NONE
H-ECP NONE
H-ECP NONE
H-ECP NONE
H-ECP NONE
P-ECP
P-ECP
O-ECP NONE
C-ECP NONE
C-ECP NONE
C-ECP NONE
C-ECP NONE
C-ECP NONE
C-ECP NONE
C-ECP NONE
C-ECP NONE
C-ECP NONE
C-ECP NONE
C-ECP NONE
C-ECP NONE
C-ECP NONE
C-ECP NONE
C-ECP NONE
C-ECP NONE
C-ECP NONE
C-ECP NONE
C-ECP NONE
C-ECP NONE
C-ECP NONE
C-ECP NONE
C-ECP NONE
C-ECP NONE
C-ECP NONE
C-ECP NONE
C-ECP NONE
H-ECP NONE
H-ECP NONE
H-ECP NONE
H-ECP NONE
H-ECP NONE
H-ECP NONE
H-ECP NONE
H-ECP NONE
H-ECP NONE
H-ECP NONE
H-ECP NONE
H-ECP NONE
H-ECP NONE
H-ECP NONE
H-ECP NONE
```

```
H-ECP NONE
H-ECP NONE
H-ECP NONE
H-ECP NONE
H-ECP NONE
H-ECP NONE
H-ECP NONE
H-ECP NONE
H-ECP NONE
H-ECP NONE
H-ECP NONE
 $END
```

```
!   Input file for GAMESS - [FeHdppe2]+ geom. opt.
 $CONTRL SCFTYP=RHF RUNTYP=OPTIMIZE EXETYP=RUN DFTTYP=B3LYP
    MAXIT=100 ICHARG=1 ECP=READ $END
 $SYSTEM MEMDDI=0 MWORDS=300 PARALL=.TRUE. $END
 $BASIS GBASIS=LANL2DZ EXTFIL=.T. NDFUNC=1 NPFUNC=1 $END
 $GUESS GUESS=MOREAD NORB=198 $END
 $SCF DIRSCF=.TRUE. CONV=5.0e-6 $END
 $STATPT OPTTOL=0.0001 NSTEP=100 TRMIN=0.01 $END
 $DATA
[FeHdppe2]+
C1
Fe    26.0     7.16521     8.36314     2.15572
P    15.0     7.62895    10.03782     3.76560
P    15.0     6.73905     6.62594     3.75760
P    15.0     7.47440    10.13252     0.56510
P    15.0     6.89845     6.63125     0.54769
C     6.0     7.56086    11.76845     1.55707
C     6.0     6.92868     4.97390     1.50238
H     1.0     8.01203    12.54180     0.92683
H     1.0     6.54239     4.18075     0.85384
H     1.0     6.54442    12.08823     1.81159
H     1.0     7.96806     4.73333     1.74935
C     6.0     8.87556     9.78389     5.15218
C     6.0     5.41725     6.85727     5.08241
C     6.0    10.24635     9.68521     4.82440
C     6.0     4.05109     6.84532     4.71978
H     1.0    10.57620     9.75338     3.78998
H     1.0     3.74906     6.65677     3.69130
C     6.0     6.10947    10.48488    -0.68852
C     6.0     8.20622     6.33517    -0.77452
C     6.0     9.07218    10.26638    -0.42468
C     6.0     5.25280     6.46287    -0.35540
C     6.0     8.48082     9.66816     6.50191
C     6.0     5.76633     7.10696     6.42756
H     1.0     7.43232     9.74964     6.77515
H     1.0     6.80992     7.11507     6.72949
C     6.0     6.24235    10.10100    -2.04064
C     6.0     7.96580     6.61920    -2.13545
H     1.0     7.16717     9.65166    -2.39212
H     1.0     6.99676     6.99282    -2.45560
C     6.0     5.17778    12.65773     5.94655
C     6.0     9.02191     4.08267     6.17628
H     1.0     5.30897    13.52212     6.59285
H     1.0     8.83140     3.26551     6.86778
C     6.0     6.30482    12.00377     5.41784
C     6.0     7.94341     4.74408     5.56292
H     1.0     7.29825    12.36787     5.67089
H     1.0     6.92768     4.42784     5.79135
C     6.0     3.84875    11.29503    -1.16985
C     6.0    10.47307     5.61362    -1.34967
H     1.0     2.92926    11.76542    -0.82884
H     1.0    11.43781     5.21853    -1.03987
C     6.0    10.81052     9.38231     7.17848
C     6.0     3.40723     7.30431     7.02868
H     1.0    11.55403     9.23522     7.95801
H     1.0     2.63618     7.46705     7.77776
C     6.0     4.85019    10.41595     4.28121
C     6.0     9.50304     6.20696     4.39302
H     1.0     4.71199     9.53439     3.65885
H     1.0     9.68449     7.02630     3.70506
```

```
C     6.0     8.38303    11.52375     2.82982
C     6.0     6.08536     5.11924     2.77657
H     1.0     8.37464    12.40154     3.48438
H     1.0     6.15070     4.22758     3.40868
H     1.0     9.42489    11.28960     2.58637
H     1.0     5.03096     5.28349     2.52756
C     6.0     9.26004    11.32882    -1.33972
C     6.0     4.98927     5.36766    -1.21038
H     1.0     8.45936    12.04003    -1.53156
H     1.0     5.76040     4.62611    -1.40866
C     6.0    11.20798     9.49133     5.83185
C     6.0     3.05259     7.06412     5.68711
H     1.0    12.26075     9.42813     5.56702
H     1.0     2.00515     7.03933     5.39585
C     6.0     3.99042    10.91632    -2.51884
C     6.0    10.22639     5.89306    -2.70803
H     1.0     3.18088    11.08832    -3.22363
H     1.0    10.99926     5.71666    -3.45200
C     6.0     4.89905    11.07530    -0.25903
C     6.0     9.47197     5.83951    -0.38810
H     1.0     4.76142    11.37469     0.77795
H     1.0     9.69015     5.62986     0.65668
C     6.0     9.44489     9.46813     7.50885
C     6.0     4.76668     7.32573     7.39410
H     1.0     9.13051     9.38667     8.54661
H     1.0     5.04974     7.50676     8.42839
C     6.0     3.88173    12.19353     5.64057
C     6.0    10.34601     4.47718     5.89486
H     1.0     3.01106    12.69982     6.05018
H     1.0    11.17944     3.95990     6.36378
C     6.0     5.18989    10.31756    -2.94933
C     6.0     8.97182     6.39933    -3.09601
H     1.0     5.30877    10.02381    -3.98960
H     1.0     8.77330     6.61720    -4.14274
C     6.0     3.72004    11.07009     4.80900
C     6.0    10.58281     5.54151     5.00619
H     1.0     2.72397    10.69931     4.57955
H     1.0    11.60100     5.85806     4.79286
C     6.0    10.12184     9.35562    -0.19477
C     6.0     4.23881     7.41561    -0.12682
H     1.0     9.97983     8.53957     0.50611
H     1.0     4.43076     8.27751     0.50777
C     6.0     6.14970    10.87682     4.57795
C     6.0     8.17851     5.81248     4.66559
C     6.0    11.34805     9.50225    -0.87228
C     6.0     2.97774     7.27883    -0.73908
H     1.0    12.14955     8.78970    -0.69340
H     1.0     2.20728     8.02522    -0.56262
C     6.0    10.48377    11.47124    -2.01697
C     6.0     3.73130     5.23098    -1.82345
H     1.0    10.61943    12.28814    -2.72160
H     1.0     3.54005     4.38712    -2.48176
C     6.0    11.53312    10.55857    -1.78222
C     6.0     2.72102     6.18613    -1.58739
H     1.0    12.48032    10.67188    -2.30395
H     1.0     1.74937     6.08011    -2.06368
H     1.0     8.62481     8.03061     2.14143
 $END
 $ECP
 FE-ECP GEN     10     2
```

```
 3      ----- d potential     -----
   -10.0000000        1    392.6149787
   -63.2667518        2     71.1756979
   -10.9613338        2     17.7320281
 5      ----- s-d potential     -----
     3.0000000        0    126.0571895
    18.1729137        1    138.1264251
   339.1231164        2     54.2098858
   317.1068012        2      9.2837966
  -207.3421649        2      8.6289082
 5      ----- p-d potential     -----
     5.0000000        0     83.1759490
     5.9535930        1    106.0559938
   294.2665527        2     42.8284937
   154.4244635        2      8.7701805
   -95.3164249        2      8.0397818
 P-ECP GEN     10     2
 5      ----- d   potential     -----
   -10.0000000        1    462.1211423
   -79.4864658        2     93.6863701
   -28.3668251        2     21.2349094
    -9.8577589        2      6.3388415
    -1.0163783        2      2.0620684
 5      ----- s-d potential     -----
     3.0000000        0     78.0831823
    12.9104154        1     58.9576810
   150.0250298        2     36.0571255
    71.7083146        2     11.2464453
    23.0397012        2      2.6757561
 6      ----- p-d potential     -----
     5.0000000        0     75.1617880
     6.3446507        1     57.4544041
   198.5585104        2     47.9481748
   111.1470820        2     18.4588360
    40.3944144        2      5.9414190
     6.4483233        2      1.8487507
P-ECP
P-ECP
P-ECP
C-ECP NONE
C-ECP NONE
H-ECP NONE
H-ECP NONE
H-ECP NONE
H-ECP NONE
C-ECP NONE
C-ECP NONE
C-ECP NONE
C-ECP NONE
H-ECP NONE
H-ECP NONE
C-ECP NONE
C-ECP NONE
C-ECP NONE
C-ECP NONE
C-ECP NONE
C-ECP NONE
H-ECP NONE
H-ECP NONE
C-ECP NONE
```

```
C-ECP NONE
H-ECP NONE
H-ECP NONE
C-ECP NONE
C-ECP NONE
H-ECP NONE
H-ECP NONE
C-ECP NONE
C-ECP NONE
H-ECP NONE
H-ECP NONE
C-ECP NONE
C-ECP NONE
H-ECP NONE
H-ECP NONE
C-ECP NONE
C-ECP NONE
H-ECP NONE
H-ECP NONE
C-ECP NONE
C-ECP NONE
H-ECP NONE
H-ECP NONE
C-ECP NONE
C-ECP NONE
H-ECP NONE
H-ECP NONE
H-ECP NONE
H-ECP NONE
C-ECP NONE
C-ECP NONE
H-ECP NONE
H-ECP NONE
C-ECP NONE
C-ECP NONE
H-ECP NONE
H-ECP NONE
C-ECP NONE
C-ECP NONE
H-ECP NONE
H-ECP NONE
C-ECP NONE
C-ECP NONE
H-ECP NONE
H-ECP NONE
C-ECP NONE
C-ECP NONE
H-ECP NONE
H-ECP NONE
C-ECP NONE
C-ECP NONE
H-ECP NONE
H-ECP NONE
C-ECP NONE
C-ECP NONE
H-ECP NONE
H-ECP NONE
C-ECP NONE
C-ECP NONE
H-ECP NONE
```

```
H-ECP NONE
C-ECP NONE
C-ECP NONE
H-ECP NONE
H-ECP NONE
C-ECP NONE
C-ECP NONE
C-ECP NONE
C-ECP NONE
H-ECP NONE
H-ECP NONE
C-ECP NONE
C-ECP NONE
H-ECP NONE
H-ECP NONE
C-ECP NONE
C-ECP NONE
H-ECP NONE
H-ECP NONE
H-ECP NONE
 $END
```

```
! Input file for GAMESS - [FeH(H2)dppe2]+ geom. opt.
 $CONTRL SCFTYP=RHF RUNTYP=OPTIMIZE EXETYP=RUN DFTTYP=B3LYP
    MAXIT=100 ICHARG=1 ECP=READ $END
 $SYSTEM MEMDDI=0 MWORDS=300 PARALL=.TRUE. $END
 $BASIS GBASIS=LANL2DZ EXTFIL=.T. NDFUNC=1 NPFUNC=1 $END
 $GUESS GUESS=MOREAD NORB=199 $END
 $SCF DIRSCF=.TRUE. CONV=5.0e-6 $END
 $STATPT OPTTOL=0.0001 NSTEP=100 TRMIN=0.01 $END
 $FORCE METHOD=SEMINUM NVIB=2 VIBSIZ=0.010000 SCLFAC=0.960000 $END
 $DATA
[FeH(H2)dppe2]+
C1
Fe    26.0     7.00802     8.38472     2.15354
P    15.0     7.52923    10.04519     3.77844
P    15.0     6.69778     6.65550     3.75359
P    15.0     7.37082    10.12452     0.56724
P    15.0     6.85618     6.63321     0.54180
C     6.0     7.44452    11.75690     1.55924
C     6.0     6.85432     4.98849     1.52097
H     1.0     7.87829    12.53931     0.92800
H     1.0     6.46268     4.19328     0.87956
H     1.0     6.42767    12.06234     1.83035
H     1.0     7.88812     4.73670     1.77945
C     6.0     8.82132     9.73748     5.11427
C     6.0     5.42090     6.89963     5.11801
C     6.0    10.18025     9.61886     4.74820
C     6.0     4.05064     6.96100     4.77631
H     1.0    10.48247     9.69894     3.70639
H     1.0     3.72720     6.81637     3.74709
C     6.0     6.03471    10.47528    -0.71551
C     6.0     8.24055     6.34199    -0.70400
C     6.0     8.99092    10.26793    -0.38520
C     6.0     5.28208     6.39046    -0.48681
C     6.0     8.46078     9.60326     6.47200
C     6.0     5.80017     7.09655     6.46331
H     1.0     7.42205     9.69871     6.77595
H     1.0     6.84741     7.05152     6.74888
C     6.0     6.20475    10.12434    -2.07214
C     6.0     8.06623     6.62123    -2.07594
H     1.0     7.14635     9.70334    -2.41441
H     1.0     7.11168     6.98810    -2.44388
C     6.0     5.44500    12.83880     6.11639
C     6.0     9.04434     4.07329     6.06610
H     1.0     5.70271    13.70406     6.72226
H     1.0     8.87101     3.25401     6.75955
C     6.0     6.46332    12.09362     5.49662
C     6.0     7.95082     4.75856     5.50840
H     1.0     7.49877    12.39147     5.64669
H     1.0     6.94157     4.46028     5.78406
C     6.0     3.76459    11.24064    -1.22568
C     6.0    10.53437     5.62589    -1.16490
H     1.0     2.82665    11.67936    -0.89337
H     1.0    11.48354     5.23319    -0.80765
C     6.0    10.80053     9.26052     7.08112
C     6.0     3.46197     7.39622     7.10377
H     1.0    11.56108     9.08255     7.83729
H     1.0     2.71071     7.58400     7.86678
C     6.0     4.79820    10.59348     4.55897
C     6.0     9.47967     6.19095     4.26380
H     1.0     4.52436     9.71379     3.98642
```

```
H     1.0     9.64376     7.00923     3.57009
C     6.0     8.29003    11.50942     2.81611
C     6.0     6.00662     5.15867     2.78938
H     1.0     8.30973    12.39234     3.46230
H     1.0     6.05417     4.26854     3.42541
H     1.0     9.32233    11.25651     2.55171
H     1.0     4.95592     5.34508     2.53983
C     6.0     9.19300    11.33734    -1.28976
C     6.0     5.13007     5.22590    -1.27751
H     1.0     8.39288    12.04548    -1.49485
H     1.0     5.94237     4.50711    -1.36072
C     6.0    11.16424     9.38906     5.72654
C     6.0     3.07723     7.20371     5.76253
H     1.0    12.20830     9.31079     5.43301
H     1.0     2.02616     7.23926     5.48607
C     6.0     3.94232    10.89194    -2.57897
C     6.0    10.35336     5.89933    -2.53493
H     1.0     3.14185    11.05668    -3.29582
H     1.0    11.16228     5.72307    -3.23952
C     6.0     4.80279    11.02968    -0.29954
C     6.0     9.48743     5.85391    -0.25381
H     1.0     4.63963    11.30619     0.74028
H     1.0     9.65449     5.65059     0.80151
C     6.0     9.44623     9.36531     7.44909
C     6.0     4.82527     7.34085     7.44943
H     1.0     9.15676     9.26840     8.49278
H     1.0     5.13046     7.48492     8.48310
C     6.0     4.09454    12.46801     5.95228
C     6.0    10.36093     4.44326     5.72278
H     1.0     3.30648    13.04828     6.42579
H     1.0    11.20605     3.91050     6.15206
C     6.0     5.16479    10.33324    -2.99741
C     6.0     9.11825     6.40142    -2.98542
H     1.0     5.31138    10.06452    -4.04078
H     1.0     8.97077     6.61807    -4.04077
C     6.0     3.77554    11.33934     5.17694
C     6.0    10.57467     5.50355     4.82347
H     1.0     2.73887    11.03557     5.05366
H     1.0    11.58759     5.79747     4.55857
C     6.0    10.04258     9.36499    -0.13733
C     6.0     4.22106     7.31554    -0.43151
H     1.0     9.89154     8.54420     0.55574
H     1.0     4.31974     8.23634     0.13367
C     6.0     6.14967    10.96575     4.70026
C     6.0     8.16252     5.82371     4.60111
C     6.0    11.28207     9.52300    -0.78798
C     6.0     3.02187     7.07754    -1.13156
H     1.0    12.08475     8.81557    -0.59433
H     1.0     2.21695     7.80660    -1.07907
C     6.0    10.43076    11.49435    -1.93739
C     6.0     3.93495     4.98671    -1.97765
H     1.0    10.57776    12.32025    -2.62898
H     1.0     3.83385     4.08610    -2.57829
C     6.0    11.48031    10.58622    -1.68705
C     6.0     2.87208     5.90984    -1.90043
H     1.0    12.43830    10.70990    -2.18640
H     1.0     1.94590     5.72324    -2.43848
H     1.0     8.49462     8.10185     2.14830
H     1.0     5.33362     8.46313     1.83334
H     1.0     5.42077     8.90963     2.49640
```

```
 $END
 $ECP
 FE-ECP GEN     10     2
 3      ----- d potential     -----
   -10.0000000        1    392.6149787
   -63.2667518        2     71.1756979
   -10.9613338        2     17.7320281
 5      ----- s-d potential     -----
     3.0000000        0    126.0571895
    18.1729137        1    138.1264251
   339.1231164        2     54.2098858
   317.1068012        2      9.2837966
  -207.3421649        2      8.6289082
 5      ----- p-d potential     -----
     5.0000000        0     83.1759490
     5.9535930        1    106.0559938
   294.2665527        2     42.8284937
   154.4244635        2      8.7701805
   -95.3164249        2      8.0397818
 P-ECP GEN     10     2
 5      ----- d   potential     -----
   -10.0000000        1    462.1211423
   -79.4864658        2     93.6863701
   -28.3668251        2     21.2349094
    -9.8577589        2      6.3388415
    -1.0163783        2      2.0620684
 5      ----- s-d potential     -----
     3.0000000        0     78.0831823
    12.9104154        1     58.9576810
   150.0250298        2     36.0571255
    71.7083146        2     11.2464453
    23.0397012        2      2.6757561
 6      ----- p-d potential     -----
     5.0000000        0     75.1617880
     6.3446507        1     57.4544041
   198.5585104        2     47.9481748
   111.1470820        2     18.4588360
    40.3944144        2      5.9414190
     6.4483233        2      1.8487507
P-ECP
P-ECP
P-ECP
C-ECP NONE
C-ECP NONE
H-ECP NONE
H-ECP NONE
H-ECP NONE
H-ECP NONE
C-ECP NONE
C-ECP NONE
C-ECP NONE
C-ECP NONE
H-ECP NONE
H-ECP NONE
C-ECP NONE
C-ECP NONE
C-ECP NONE
C-ECP NONE
C-ECP NONE
C-ECP NONE
```

```
H-ECP NONE
H-ECP NONE
C-ECP NONE
C-ECP NONE
H-ECP NONE
H-ECP NONE
C-ECP NONE
C-ECP NONE
H-ECP NONE
H-ECP NONE
C-ECP NONE
C-ECP NONE
H-ECP NONE
H-ECP NONE
C-ECP NONE
C-ECP NONE
H-ECP NONE
H-ECP NONE
C-ECP NONE
C-ECP NONE
H-ECP NONE
H-ECP NONE
C-ECP NONE
C-ECP NONE
H-ECP NONE
H-ECP NONE
C-ECP NONE
C-ECP NONE
H-ECP NONE
H-ECP NONE
H-ECP NONE
H-ECP NONE
C-ECP NONE
C-ECP NONE
H-ECP NONE
H-ECP NONE
C-ECP NONE
C-ECP NONE
H-ECP NONE
H-ECP NONE
C-ECP NONE
C-ECP NONE
H-ECP NONE
H-ECP NONE
C-ECP NONE
C-ECP NONE
H-ECP NONE
H-ECP NONE
C-ECP NONE
C-ECP NONE
H-ECP NONE
H-ECP NONE
C-ECP NONE
C-ECP NONE
H-ECP NONE
H-ECP NONE
C-ECP NONE
C-ECP NONE
H-ECP NONE
H-ECP NONE
```

```
C-ECP NONE
C-ECP NONE
H-ECP NONE
H-ECP NONE
C-ECP NONE
C-ECP NONE
H-ECP NONE
H-ECP NONE
C-ECP NONE
C-ECP NONE
C-ECP NONE
C-ECP NONE
H-ECP NONE
H-ECP NONE
C-ECP NONE
C-ECP NONE
H-ECP NONE
H-ECP NONE
C-ECP NONE
C-ECP NONE
H-ECP NONE
H-ECP NONE
H-ECP NONE
H-ECP NONE
H-ECP NONE
 $END
```

```
!   Input file for GAMESS - [Fe(NO)(CN)5]2- geom opt
 $CONTRL SCFTYP=RHF RUNTYP=OPTIMIZE EXETYP=RUN
    MAXIT=100 ICHARG=-2 MULT=1 $END
 $SYSTEM MEMDDI=0 MWORDS=150 PARALL=.TRUE. $END
 $BASIS GBASIS=TZV NDFUNC=1 NPFUNC=1 $END
 $GUESS GUESS=HUCKEL $END
 $SCF DIRSCF=.TRUE. CONV=5.0e-6 DAMP=.T. $END
 $STATPT OPTTOL=0.0001 NSTEP=100 TRMIN=0.01 $END
 $ELDENS IEDEN=1 WHERE=NUCLEI $END
 $ELFLDG IEFLD=2 WHERE=NUCLEI $END
 $ELPOT IEPOT=1 WHERE=NUCLEI $END
 $DATA
Nitroprusside ion
C1
Fe    26.0     1.00328    -0.01316     0.07755
C     6.0     1.00322     0.73734     1.90348
C     6.0     1.00337     1.85061    -0.54892
C     6.0    -0.96674     0.10855     0.03647
C     6.0     1.00333    -0.51946    -1.83045
N     7.0     1.00323    -1.56123     0.59897
C     6.0     2.97330     0.10841     0.03665
O     8.0     1.00321    -2.64721     0.96494
N     7.0    -2.12905     0.09704     0.04043
N     7.0     1.00328    -0.90045    -2.92858
N     7.0     4.13559     0.09721     0.04030
N     7.0     1.00342     1.09715     3.00873
N     7.0     1.00333     2.95140    -0.91868
 $END
```

```
!   Input file for GAMESS - [FeHdppe2]+ sing geom opt TZV
 $CONTRL SCFTYP=RHF RUNTYP=OPTIMIZE EXETYP=RUN MAXIT=200
    ICHARG=1 QMTTOL=1e-5 $END
 $SYSTEM MEMDDI=0 MWORDS=300 PARALL=.TRUE. $END
 $BASIS GBASIS=TZV NDFUNC=1 NPFUNC=1 $END
 $GUESS GUESS=MOREAD NORB=223 $END
 $SCF DIRSCF=.TRUE. DAMP=.T. $END
 $STATPT OPTTOL=0.0001 NSTEP=100 TRMIN=0.01 $END
 $ELDENS IEDEN=1 WHERE=NUCLEI $END
 $ELFLDG IEFLD=2 WHERE=NUCLEI $END
 $ELPOT IEPOT=1 WHERE=NUCLEI $END
 $DATA
[FeHdppe2]+
C1
Fe    26.0     7.40615     8.30950     2.15412
P    15.0     7.70477    10.24504     3.85524
P    15.0     6.72702     6.36014     3.83679
P    15.0     7.55588    10.36726     0.47140
P    15.0     6.91908     6.40631     0.45073
C     6.0     7.60132    11.86121     1.57944
C     6.0     7.03690     4.87626     1.49794
H     1.0     7.98820    12.71078     1.03319
H     1.0     6.77270     4.00455     0.91459
H     1.0     6.59496    12.11035     1.88663
H     1.0     8.06715     4.75491     1.80538
C     6.0     8.90466    10.00115     5.22835
C     6.0     5.37402     6.59697     5.06958
C     6.0    10.25380     9.82132     4.93594
C     6.0     4.03616     6.54880     4.69142
H     1.0    10.59756     9.83558     3.91990
H     1.0     3.75619     6.30483     3.68478
C     6.0     6.19191    10.71089    -0.72434
C     6.0     8.14772     6.13254    -0.89114
C     6.0     9.10112    10.55553    -0.50527
C     6.0     5.26879     6.21996    -0.34075
C     6.0     8.49243     9.93349     6.55300
C     6.0     5.68012     6.92941     6.38525
H     1.0     7.45870    10.06201     6.80679
H     1.0     6.70255     6.97566     6.70605
C     6.0     6.30346    10.30679    -2.05063
C     6.0     7.83931     6.38446    -2.22181
H     1.0     7.21275     9.86116    -2.40411
H     1.0     6.85468     6.70590    -2.49912
C     6.0     5.26481    12.95132     5.78367
C     6.0     8.84829     3.78111     6.22962
H     1.0     5.37295    13.88826     6.29628
H     1.0     8.63900     2.92417     6.84122
C     6.0     6.37739    12.31636     5.27246
C     6.0     7.82186     4.42059     5.56893
H     1.0     7.34182    12.76856     5.40532
H     1.0     6.81909     4.05439     5.68443
```

```
C     6.0     3.94669    11.46242    -1.18910
C     6.0    10.38758     5.54647    -1.55642
H     1.0     3.03653    11.91868    -0.84824
H     1.0    11.37525     5.21937    -1.29166
C     6.0    10.74995     9.54928     7.26584
C     6.0     3.34885     7.12698     6.91537
H     1.0    11.46181     9.38136     8.05145
H     1.0     2.57025     7.32101     7.62827
C     6.0     4.99640    10.53465     4.47375
C     6.0     9.38071     5.99656     4.65506
H     1.0     4.87621     9.58665     3.98511
H     1.0     9.59249     6.84665     4.03897
C     6.0     8.46777    11.58029     2.81361
C     6.0     6.12633     4.99409     2.72679
H     1.0     8.59713    12.48189     3.39716
H     1.0     6.10438     4.05960     3.27095
H     1.0     9.45320    11.24919     2.51331
H     1.0     5.11290     5.20600     2.41350
C     6.0     9.30853    11.67638    -1.31071
C     6.0     4.90683     5.06616    -1.03586
H     1.0     8.54494    12.42520    -1.40680
H     1.0     5.61279     4.26794    -1.16555
C     6.0    11.16937     9.60615     5.94792
C     6.0     3.03180     6.80723     5.60823
H     1.0    12.20788     9.48004     5.70668
H     1.0     2.00473     6.74992     5.30063
C     6.0     4.07420    11.06624    -2.50764
C     6.0    10.06762     5.79086    -2.88069
H     1.0     3.26389    11.21171    -3.19637
H     1.0    10.80514     5.65190    -3.64812
C     6.0     4.99490    11.28185    -0.30353
C     6.0     9.43873     5.72436    -0.56801
H     1.0     4.86240    11.59810     0.71323
H     1.0     9.71750     5.55472     0.45379
C     6.0     9.41028     9.70729     7.56465
C     6.0     4.67613     7.19012     7.29964
H     1.0     9.07629     9.66150     8.58387
H     1.0     4.93205     7.43495     8.31309
C     6.0     4.00889    12.37973     5.63731
C     6.0    10.15017     4.24666     6.10362
H     1.0     3.14414    12.87628     6.03490
H     1.0    10.94954     3.74635     6.61686
C     6.0     5.25436    10.48462    -2.93398
C     6.0     8.79452     6.21535    -3.20959
H     1.0     5.36296    10.17398    -3.95584
H     1.0     8.53891     6.40931    -4.23408
C     6.0     3.87531    11.17107     4.98566
C     6.0    10.41372     5.35024     5.32025
H     1.0     2.90868    10.71760     4.87813
H     1.0    11.41828     5.71515     5.22175
C     6.0    10.09937     9.59882    -0.41255
```

```
C     6.0     4.33643     7.23881    -0.21454
H     1.0     9.95801     8.73956     0.21088
H     1.0     4.59396     8.14740     0.29518
C     6.0     6.25706    11.09795     4.60458
C     6.0     8.07843     5.53708     4.77182
C     6.0    11.28865     9.75735    -1.11098
C     6.0     3.06666     7.11320    -0.75863
H     1.0    12.05420     9.00951    -1.03089
H     1.0     2.36026     7.91428    -0.65453
C     6.0    10.48892    11.83153    -2.00460
C     6.0     3.64585     4.93893    -1.57962
H     1.0    10.63674    12.69670    -2.62249
H     1.0     3.38193     4.04587    -2.11362
C     6.0    11.48382    10.86832    -1.90373
C     6.0     2.72095     5.96391    -1.43875
H     1.0    12.40375    10.99045    -2.44377
H     1.0     1.74018     5.86326    -1.86344
H     1.0     9.01216     7.98632     2.15653
 $END
```

```
!   Input file for GAMESS - [FeHdppe2]+ trip geom opt TZV
 $CONTRL SCFTYP=UHF RUNTYP=OPTIMIZE EXETYP=RUN MAXIT=200 ICHARG=1
    MULT=3 $END
 $SYSTEM MEMDDI=0 MWORDS=150 PARALL=.TRUE. $END
 $BASIS GBASIS=TZV NDFUNC=1 NPFUNC=1 $END
 $GUESS GUESS=HUCKEL $END
 $SCF DIRSCF=.TRUE. CONV=5e-6 DAMP=.T. $END
 $STATPT OPTTOL=0.0001 NSTEP=100 TRMIN=0.01 $END
 $DATA
[FeHdppe2]+
C1
Fe    26.0     7.61025     8.39110     2.20466
P    15.0     8.65176    10.09243     3.58641
P    15.0     5.85642     6.98590     3.47884
P    15.0     6.67404    10.29066     0.96975
P    15.0     7.79668     6.55855     0.65262
C     6.0     7.00150    11.83019     2.05855
C     6.0     6.98387     5.09043     1.56155
H     1.0     6.89920    12.73308     1.44533
H     1.0     6.78261     4.28970     0.83893
H     1.0     6.24536    11.86382     2.85130
H     1.0     7.75789     4.72804     2.24523
C     6.0    10.50260     9.96278     3.86133
C     6.0     4.03206     7.30346     3.85577
C     6.0     4.87450    10.45040     0.45925
C     6.0     9.52926     5.90761     0.31194
C     6.0     7.62639    10.76365    -0.59070
C     6.0     7.00584     6.52452    -1.06229
C     6.0     8.41500    11.75583     2.66839
C     6.0     5.69694     5.45873     2.33038
H     1.0     8.57527    12.58790     3.36284
H     1.0     5.35490     4.60279     2.92590
H     1.0     9.17431    11.81136     1.87868
H     1.0     4.88331     5.71257     1.64112
C     6.0     7.94005    10.48308     5.28853
C     6.0     6.47752     6.26773     5.10778
H     1.0     8.48135     7.35046     2.94094
C     6.0     3.41169     8.45518     3.32830
C     6.0     3.26562     6.39379     4.61907
C     6.0     2.04185     8.69556     3.55533
C     6.0     1.89758     6.63276     4.84437
C     6.0     1.28220     7.78471     4.31257
H     1.0     3.98449     9.16078     2.73262
H     1.0     1.57621     9.58544     3.13843
H     1.0     0.22496     7.96812     4.48896
H     1.0     1.31581     5.92626     5.43144
H     1.0     3.73243     5.51058     5.04898
C     6.0     4.32672     9.45466    -0.38173
C     6.0     4.05383    11.51338     0.89518
C     6.0     2.97906     9.52226    -0.77745
C     6.0     2.70142    11.57451     0.50400
```

C	6.0	2.16063	10.57984	-0.33217
H	1.0	4.94374	8.63181	-0.73501
H	1.0	2.57034	8.75283	-1.42744
H	1.0	1.11796	10.62941	-0.63628
H	1.0	2.07954	12.39929	0.84360
H	1.0	4.44864	12.30176	1.52963
C	6.0	7.05114	11.58078	-1.58785
C	6.0	8.96175	10.32843	-0.73742
C	6.0	7.80586	11.96151	-2.71351
C	6.0	9.71826	10.71550	-1.86016
C	6.0	9.14103	11.53328	-2.85100
H	1.0	6.01969	11.91264	-1.49970
H	1.0	7.35362	12.58948	-3.47737
H	1.0	9.72246	11.83049	-3.72035
H	1.0	10.74730	10.37877	-1.96114
H	1.0	9.41528	9.68255	0.01282
C	6.0	10.63805	6.48945	0.96029
C	6.0	9.72778	4.81276	-0.55944
C	6.0	11.93369	5.97991	0.74346
C	6.0	11.02110	4.30109	-0.76937
C	6.0	12.12727	4.88364	-0.11801
H	1.0	10.49275	7.32425	1.64107
H	1.0	12.78300	6.43692	1.24563
H	1.0	8.88501	4.36462	-1.08101
H	1.0	13.12640	4.48742	-0.28262
H	1.0	11.16451	3.45535	-1.43740
C	6.0	7.67070	7.16695	-2.13190
C	6.0	5.75949	5.90649	-1.30592
C	6.0	5.19207	5.92598	-2.59589
C	6.0	7.10516	7.18497	-3.41884
C	6.0	5.86197	6.56526	-3.65589
H	1.0	5.42662	6.57590	-4.65195
H	1.0	7.63357	7.67792	-4.23094
H	1.0	8.63574	7.64022	-1.97175
H	1.0	5.22185	5.39682	-0.51115
H	1.0	4.23723	5.43568	-2.77061
C	6.0	7.12143	5.01454	5.18763
C	6.0	6.31976	7.03038	6.28682
C	6.0	6.79094	6.54705	7.52023
C	6.0	7.59414	4.53034	6.42333
C	6.0	7.43185	5.29451	7.59356
H	1.0	7.26014	4.39857	4.30384
H	1.0	5.82289	7.99550	6.25340
H	1.0	6.65624	7.14562	8.41788
H	1.0	7.79422	4.91973	8.54765
H	1.0	8.08326	3.56023	6.46875
C	6.0	8.77424	10.72337	6.40084
C	6.0	8.21205	11.06255	7.64684
C	6.0	6.53796	10.57382	5.44164
C	6.0	5.97955	10.92983	6.68319
C	6.0	6.81589	11.17523	7.79022

```
H     1.0     6.38559    11.44524     8.75145
H     1.0     4.89968    11.00583     6.78672
H     1.0     8.86380    11.24064     8.49872
H     1.0     9.85359    10.64467     6.30722
H     1.0     5.87539    10.34946     4.60826
C     6.0    11.35945    11.07997     3.74514
C     6.0    11.04539     8.70768     4.21699
C     6.0    12.42575     8.57279     4.45675
C     6.0    12.74202    10.94024     3.97300
C     6.0    13.27757     9.68829     4.33195
H     1.0    14.34441     9.58381     4.51397
H     1.0    13.39339    11.80527     3.87706
H     1.0    12.83127     7.60424     4.73884
H     1.0    10.39187     7.84310     4.30450
H     1.0    10.96745    12.05908     3.48341
 $END
```

```
!   Input file for GAMESS - [FeH(H2)dppe2]+ geom opt TZV
 $CONTRL SCFTYP=RHF RUNTYP=OPTIMIZE EXETYP=RUN MAXIT=200
    ICHARG=1 QMTTOL=1e-5 $END
 $SYSTEM MEMDDI=0 MWORDS=300 PARALL=.TRUE. $END
 $BASIS GBASIS=TZV NDFUNC=1 NPFUNC=1 $END
 $GUESS GUESS=MOREAD NORB=224 $END
 $SCF DIRSCF=.TRUE. DAMP=.T. $END
 $STATPT OPTTOL=0.0001 NSTEP=100 TRMIN=0.01 $END
 $ELDENS IEDEN=1 WHERE=NUCLEI $END
 $ELFLDG IEFLD=2 WHERE=NUCLEI $END
 $ELPOT IEPOT=1 WHERE=NUCLEI $END
 $DATA
[FeH(H2)dppe2]+
C1
Fe    26.0     7.17513     8.35825     2.15545
P    15.0     7.63039    10.29775     3.87960
P    15.0     6.60684     6.39679     3.84226
P    15.0     7.42076    10.38563     0.46716
P    15.0     6.83509     6.38450     0.42940
C     6.0     7.45019    11.87701     1.57745
C     6.0     6.91722     4.88790     1.52969
H     1.0     7.79822    12.74045     1.02662
H     1.0     6.66864     3.99718     0.97039
H     1.0     6.44555    12.09653     1.91486
H     1.0     7.93809     4.77271     1.86709
C     6.0     8.93728     9.98947     5.14107
C     6.0     5.29442     6.61251     5.12176
C     6.0    10.25426     9.78016     4.74216
C     6.0     3.94457     6.55510     4.79075
H     1.0    10.51990     9.80669     3.70361
H     1.0     3.63208     6.31147     3.79364
C     6.0     6.09393    10.73865    -0.76703
C     6.0     8.19479     6.12010    -0.78562
C     6.0     8.99147    10.57226    -0.46852
C     6.0     5.29016     6.09155    -0.53491
C     6.0     8.62811     9.90670     6.49295
C     6.0     5.64350     6.93909     6.42859
H     1.0     7.62220    10.06262     6.82990
H     1.0     6.67639     6.99172     6.71337
C     6.0     6.23561    10.31827    -2.08581
C     6.0     7.99819     6.33141    -2.14446
H     1.0     7.14819     9.85667    -2.40938
H     1.0     7.03240     6.61353    -2.51508
C     6.0     5.54164    13.14764     6.01157
C     6.0     8.80051     3.77994     6.12747
H     1.0     5.73708    14.11409     6.43519
H     1.0     8.61048     2.91314     6.73142
C     6.0     6.54619    12.47425     5.34825
C     6.0     7.75368     4.43040     5.51069
H     1.0     7.51543    12.92914     5.28049
H     1.0     6.75494     4.06221     5.65218
```

```
C     6.0     3.87217    11.51467    -1.30157
C     6.0    10.50038     5.58801    -1.23956
H     1.0     2.95936    11.98678    -0.99074
H     1.0    11.46943     5.29539    -0.88182
C     6.0    10.92142     9.44592     7.02136
C     6.0     3.33078     7.11827     7.04004
H     1.0    11.68681     9.24330     7.74613
H     1.0     2.57627     7.30484     7.78016
C     6.0     5.05817    10.64942     4.93954
C     6.0     9.28311     6.02164     4.57477
H     1.0     4.85750     9.66742     4.55839
H     1.0     9.47408     6.88367     3.96896
C     6.0     8.36135    11.60690     2.78203
C     6.0     5.97868     5.04332     2.73345
H     1.0     8.53063    12.51710     3.33965
H     1.0     5.91093     4.11364     3.28239
H     1.0     9.32895    11.25888     2.44663
H     1.0     4.97967     5.28840     2.39536
C     6.0     9.22129    11.69153    -1.26998
C     6.0     5.02023     4.86049    -1.13345
H     1.0     8.46003    12.43952    -1.38968
H     1.0     5.73013     4.05846    -1.06964
C     6.0    11.23892     9.52071     5.67627
C     6.0     2.97054     6.80228     5.74320
H     1.0    12.25226     9.37481     5.35276
H     1.0     1.93381     6.74033     5.47091
C     6.0     4.02956    11.10069    -2.61133
C     6.0    10.29198     5.79416    -2.59220
H     1.0     3.23959    11.24729    -3.32294
H     1.0    11.09768     5.66140    -3.28891
C     6.0     4.89434    11.33142    -0.38603
C     6.0     9.46388     5.75951    -0.34204
H     1.0     4.74073    11.66519     0.62211
H     1.0     9.65771     5.62162     0.70368
C     6.0     9.61371     9.63333     7.42596
C     6.0     4.67041     7.18763     7.37870
H     1.0     9.35779     9.57636     8.46711
H     1.0     4.95987     7.42921     8.38383
C     6.0     4.28465    12.57452     6.13684
C     6.0    10.09796     4.24750     5.96813
H     1.0     3.50369    13.10058     6.65237
H     1.0    10.91290     3.73983     6.44854
C     6.0     5.21363    10.49974    -2.99933
C     6.0     9.04107     6.17217    -3.04089
H     1.0     5.34557    10.17550    -4.01419
H     1.0     8.87045     6.33681    -4.08806
C     6.0     4.04570    11.32372     5.60630
C     6.0    10.33644     5.36446     5.19570
H     1.0     3.08098    10.86517     5.71274
H     1.0    11.33733     5.73234     5.07303
C     6.0     9.98747     9.61656    -0.34584
```

```
C     6.0     4.36176     7.11218    -0.67700
H     1.0     9.82698     8.75758     0.27264
H     1.0     4.55402     8.08217    -0.26279
C     6.0     6.31613    11.21559     4.79259
C     6.0     7.98497     5.55998     4.72454
C     6.0    11.19666     9.77520    -1.00903
C     6.0     3.18293     6.91130    -1.38054
H     1.0    11.95938     9.02715    -0.90683
H     1.0     2.47991     7.71596    -1.48159
C     6.0    10.42132    11.84662    -1.92961
C     6.0     3.84996     4.65771    -1.83419
H     1.0    10.58542    12.71029    -2.54562
H     1.0     3.65983     3.70492    -2.29060
C     6.0    11.41421    10.88544    -1.79706
C     6.0     2.92438     5.68431    -1.95481
H     1.0    12.34956    11.00811    -2.30985
H     1.0     2.01408     5.52466    -2.50087
H     1.0     8.77710     8.04223     2.15755
H     1.0     5.08160     8.49069     1.91258
H     1.0     5.19078     9.03890     2.39595
 $END
```

5.3.2 Vibrational Analysis

```
!   Input file for GAMESS - [Mn(CO)dppe2]+ vib anal
 $CONTRL SCFTYP=RHF RUNTYP=HESSIAN EXETYP=RUN MAXIT=100
    ICHARG=1 ECP=READ DFTTYP=B3LYP
 $END
 $SYSTEM MEMDDI=0 MWORDS=300 PARALL=.TRUE. $END
 $BASIS GBASIS=LANL2DZ EXTFIL=.T. NDFUNC=1 NPFUNC=1 $END
 $GUESS GUESS=HUCKEL $END
 $SCF DIRSCF=.TRUE. CONV=5.0e-6 DAMP=.T. $END
 $FORCE METHOD=SEMINUM NVIB=2 SCLFAC=0.96 VIBANL=.TRUE.
   TEMP(1)=295 TEMP(2)=298 TEMP(3)=300 TEMP(4)=313
   TEMP(5)=333 TEMP(6)=343 TEMP(7)=353 TEMP(8)=363
   TEMP(9)=373
 $END
 $DATA
Mn(CO)dppe2
C1
Mn    25.0     7.63915     8.25871    -0.17076
P    15.0     6.80440    10.48348     0.40231
P    15.0    10.03343     8.68254     0.46829
C     6.0     7.80899    12.00670    -0.06697
C     6.0     8.41575    12.80365     0.92860
C     6.0     9.18881    13.92344     0.57182
C     6.0     9.37064    14.25496    -0.78388
C     6.0     8.77771    13.45677    -1.78008
C     6.0     8.00270    12.33682    -1.42714
C     6.0     6.09011    10.95594     2.08989
C     6.0     5.41715    12.19073     2.24304
C     6.0     4.85152    12.54799     3.47908
C     6.0     4.95272    11.67639     4.58227
C     6.0     5.62140    10.44598     4.43943
C     6.0     6.18261    10.08777     3.19684
C     6.0    10.99848     9.82003    -0.68696
C     6.0    11.57620    11.02012    -0.22346
C     6.0    12.24450    11.87684    -1.11772
C     6.0    12.33958    11.54598    -2.48175
C     6.0    11.76096    10.35003    -2.94897
C     6.0    11.09311     9.49230    -2.05749
C     6.0    10.64164     9.22840     2.17911
C     6.0    11.99512     9.04822     2.55223
C     6.0    12.45650     9.47932     3.80829
C     6.0    11.57490    10.10942     4.70993
C     6.0    10.23157    10.30581     4.34160
C     6.0     9.77060     9.86598     3.08386
C     6.0     5.22563    10.60882    -0.65777
C     6.0    10.92628     7.00022     0.27383
H     1.0     8.28047    12.56904     1.98092
H     1.0     9.64570    14.53016     1.34994
H     1.0     9.96799    15.12063    -1.05957
H     1.0     8.92200    13.69719    -2.83033
H     1.0     7.57290    11.72992    -2.21880
H     1.0     5.34222    12.88358     1.40787
```

H	1.0	4.33523	13.49950	3.57956
H	1.0	4.52123	11.95695	5.53969
H	1.0	5.71092	9.77276	5.28788
H	1.0	6.70066	9.13493	3.10543
H	1.0	11.51071	11.29539	0.82472
H	1.0	12.68419	12.79936	-0.74656
H	1.0	12.85050	12.21231	-3.17239
H	1.0	11.81724	10.08961	-4.00281
H	1.0	10.64476	8.58127	-2.44477
H	1.0	12.70675	8.59982	1.86342
H	1.0	13.49976	9.33314	4.07764
H	1.0	11.93331	10.44584	5.67969
H	1.0	9.54480	10.79879	5.02560
H	1.0	8.73462	10.03373	2.81571
H	1.0	4.71834	11.55759	-0.45158
H	1.0	5.51441	10.60044	-1.71413
H	1.0	11.25777	6.90672	-0.76625
H	1.0	11.81718	6.98247	0.90738
P	15.0	8.44675	5.93852	-0.48843
P	15.0	5.25408	7.75887	-0.54741
O	8.0	7.87916	9.25753	-2.93164
C	6.0	7.44457	4.42678	0.03607
C	6.0	6.84619	3.59186	-0.93305
C	6.0	6.10695	2.46108	-0.54091
C	6.0	5.94889	2.15606	0.82408
C	6.0	6.52941	2.99370	1.79527
C	6.0	7.26987	4.12484	1.40452
C	6.0	9.23256	5.34581	-2.11054
C	6.0	9.92018	4.10880	-2.13543
C	6.0	10.53720	3.65761	-3.31516
C	6.0	10.47460	4.43437	-4.49026
C	6.0	9.78854	5.66144	-4.47391
C	6.0	9.17572	6.11731	-3.28966
C	6.0	4.37805	6.60626	0.66776
C	6.0	3.75902	5.41269	0.24249
C	6.0	3.14358	4.55928	1.17719
C	6.0	3.14423	4.88402	2.54591
C	6.0	3.76927	6.07002	2.97799
C	6.0	4.38428	6.92451	2.04473
C	6.0	4.62751	7.15670	-2.22522
C	6.0	3.26925	7.31135	-2.58869
C	6.0	2.80543	6.85034	-3.83361
C	6.0	3.68904	6.21332	-4.72764
C	6.0	5.03906	6.04682	-4.36835
C	6.0	5.50333	6.51842	-3.12498
C	6.0	7.82093	8.83046	-1.81339
C	6.0	9.97754	5.85093	0.65043
C	6.0	4.31352	9.41607	-0.32056
H	1.0	6.96963	3.80229	-1.99186
H	1.0	5.66034	1.82250	-1.29933
H	1.0	5.38356	1.27781	1.12612

```
H     1.0     6.40590     2.77034     2.85201
H     1.0     7.70859     4.75473     2.17588
H     1.0     9.96301     3.48354    -1.24677
H     1.0    11.06700     2.70860    -3.31765
H     1.0    10.94763     4.08353    -5.40401
H     1.0     9.72549     6.26707    -5.37444
H     1.0     8.66213     7.06963    -3.30953
H     1.0     3.74910     5.14293    -0.80890
H     1.0     2.66763     3.64429     0.83320
H     1.0     2.66894     4.22232     3.26577
H     1.0     3.77553     6.33004     4.03384
H     1.0     4.84723     7.84247     2.39876
H     1.0     2.55812     7.76962    -1.90574
H     1.0     1.75890     6.97888    -4.09912
H     1.0     3.33012     5.85827    -5.69035
H     1.0     5.72990     5.55687    -5.05009
H     1.0     6.54792     6.39060    -2.86795
H     1.0    10.46594     4.87801     0.53073
H     1.0     9.65357     5.93540     1.69541
H     1.0     3.97098     9.47018     0.71924
H     1.0     3.42691     9.42236    -0.96062
 $END
 $ECP
 MN-ECP GEN     10     2
 3      ----- d potential     -----
   -10.0000000        1    357.3914469
   -60.2990287        2     64.6477389
   -10.4217834        2     16.0960833
 5      ----- s-d potential     -----
     3.0000000        0    107.4127215
    16.2591819        1    111.4958973
   276.9373928        2     46.5568346
   241.3174342        2      8.3688135
  -146.4635329        2      7.7237489
 5      ----- p-d potential     -----
     5.0000000        0     80.0415103
     5.7589756        1    105.6043646
   285.2918654        2     40.8300466
   143.4222647        2      8.0098457
   -88.7031851        2      7.3390928
 P-ECP GEN     10     2
 5      ----- d   potential     -----
   -10.0000000        1    462.1211423
   -79.4864658        2     93.6863701
   -28.3668251        2     21.2349094
    -9.8577589        2      6.3388415
    -1.0163783        2      2.0620684
 5      ----- s-d potential     -----
     3.0000000        0     78.0831823
    12.9104154        1     58.9576810
   150.0250298        2     36.0571255
```

```
    71.7083146        2     11.2464453
    23.0397012        2      2.6757561
 6      ----- p-d potential      -----
     5.0000000        0     75.1617880
     6.3446507        1     57.4544041
   198.5585104        2     47.9481748
   111.1470820        2     18.4588360
    40.3944144        2      5.9414190
     6.4483233        2      1.8487507
P-ECP
C-ECP NONE
C-ECP NONE
C-ECP NONE
C-ECP NONE
C-ECP NONE
C-ECP NONE
C-ECP NONE
C-ECP NONE
C-ECP NONE
C-ECP NONE
C-ECP NONE
C-ECP NONE
C-ECP NONE
C-ECP NONE
C-ECP NONE
C-ECP NONE
C-ECP NONE
C-ECP NONE
C-ECP NONE
C-ECP NONE
C-ECP NONE
C-ECP NONE
C-ECP NONE
C-ECP NONE
C-ECP NONE
C-ECP NONE
H-ECP NONE
H-ECP NONE
H-ECP NONE
H-ECP NONE
H-ECP NONE
H-ECP NONE
H-ECP NONE
H-ECP NONE
H-ECP NONE
H-ECP NONE
H-ECP NONE
H-ECP NONE
H-ECP NONE
H-ECP NONE
H-ECP NONE
```

```
H-ECP NONE
H-ECP NONE
H-ECP NONE
H-ECP NONE
H-ECP NONE
H-ECP NONE
H-ECP NONE
H-ECP NONE
H-ECP NONE
P-ECP
P-ECP
O-ECP NONE
C-ECP NONE
C-ECP NONE
C-ECP NONE
C-ECP NONE
C-ECP NONE
C-ECP NONE
C-ECP NONE
C-ECP NONE
C-ECP NONE
C-ECP NONE
C-ECP NONE
C-ECP NONE
C-ECP NONE
C-ECP NONE
C-ECP NONE
C-ECP NONE
C-ECP NONE
C-ECP NONE
C-ECP NONE
C-ECP NONE
C-ECP NONE
C-ECP NONE
C-ECP NONE
C-ECP NONE
C-ECP NONE
C-ECP NONE
C-ECP NONE
H-ECP NONE
H-ECP NONE
H-ECP NONE
H-ECP NONE
H-ECP NONE
H-ECP NONE
H-ECP NONE
H-ECP NONE
H-ECP NONE
H-ECP NONE
H-ECP NONE
H-ECP NONE
```

```
H-ECP NONE
H-ECP NONE
H-ECP NONE
H-ECP NONE
H-ECP NONE
H-ECP NONE
H-ECP NONE
H-ECP NONE
H-ECP NONE
H-ECP NONE
H-ECP NONE
H-ECP NONE
 $END
```

```
!   Input file for GAMESS - [Mn(CO)dppe2]+ agostic vib anal
 $CONTRL SCFTYP=RHF RUNTYP=HESSIAN EXETYP=RUN DFTTYP=B3LYP
    MAXIT=150 ICHARG=1 ECP=READ $END
 $SYSTEM MEMDDI=0 MWORDS=150 PARALL=.TRUE. $END
 $BASIS GBASIS=LANL2DZ EXTFIL=.T. NDFUNC=1 NPFUNC=1 $END
 $GUESS GUESS=HUCKEL $END
 $STATPT OPTTOL=0.0001 NSTEP=100 TRMIN=0.01 $END
 $SCF DIRSCF=.TRUE. CONV=5.0e-6 DAMP=.T. $END
 $FORCE METHOD=SEMINUM VIBSIZ=0.010000 SCLFAC=0.960000 NVIB=2
   TEMP(1)=295 TEMP(2)=298 TEMP(3)=300 TEMP(4)=313 TEMP(5)=333
   TEMP(6)=343 TEMP(7)=353 TEMP(8)=363 TEMP(9)=373
 $END
 $DATA
Mn(CO)dppe2
C1
Mn    25.0     6.01631     6.28789     5.69874
P    15.0     8.01900     5.20284     6.52822
P    15.0     3.96610     7.20457     4.77793
P    15.0     4.48275     5.24569     7.31666
P    15.0     7.47139     6.87365     3.80446
O     8.0     6.50326     8.73462     7.27172
C     6.0     8.53389     5.20945     8.33794
C     6.0     9.00099     6.40752     8.92414
C     6.0     9.37543     6.43610    10.27997
C     6.0     9.27948     5.27194    11.06670
C     6.0     8.80582     4.07888    10.48855
C     6.0     8.43392     4.04657     9.13158
C     6.0     8.34264     3.43273     5.96337
C     6.0     9.58723     2.80047     6.18972
C     6.0     9.82024     1.49998     5.70746
C     6.0     8.81222     0.81469     4.99763
C     6.0     7.56930     1.43584     4.77586
C     6.0     7.33970     2.73901     5.25608
C     6.0     2.99249     6.16247     3.54528
C     6.0     1.66144     6.49685     3.20369
C     6.0     0.92797     5.68514     2.32085
C     6.0     1.51791     4.53087     1.76519
C     6.0     2.84499     4.19831     2.09341
C     6.0     3.57801     5.01077     2.98091
C     6.0     3.81916     8.95877     4.11124
C     6.0     3.89696    10.05271     5.00273
C     6.0     3.79275    11.37035     4.51954
C     6.0     3.61866    11.60986     3.14263
C     6.0     3.55482    10.52295     2.25036
C     6.0     3.65609     9.20378     2.73071
C     6.0     4.52007     5.57842     9.17490
C     6.0     5.42793     6.49806     9.73422
C     6.0     5.38704     6.78678    11.11280
C     6.0     4.44166     6.15878    11.94216
C     6.0     3.53228     5.23369    11.38814
C     6.0     3.56928     4.94705    10.01299
```

```
C     6.0     4.33030     3.36433     7.21146
C     6.0     3.66755     2.76905     6.11397
C     6.0     3.58434     1.36811     6.00419
C     6.0     4.17197     0.54423     6.98315
C     6.0     4.84608     1.13205     8.07073
C     6.0     4.92731     2.53244     8.18395
C     6.0     7.02143     6.06276     2.15756
C     6.0     6.40426     6.81404     1.13291
C     6.0     6.01892     6.19540    -0.07088
C     6.0     6.23897     4.81825    -0.26487
C     6.0     6.84512     4.06198     0.75648
C     6.0     7.22938     4.67825     1.96293
C     6.0     7.92226     8.63690     3.30637
C     6.0     8.81777     8.84351     2.22933
C     6.0     9.21724    10.14346     1.87662
C     6.0     8.72974    11.25283     2.59805
C     6.0     7.84051    11.05097     3.66830
C     6.0     7.43674     9.74799     4.02229
C     6.0     6.30908     7.73755     6.63338
C     6.0     9.21457     6.14957     4.16804
C     6.0     9.46632     6.11495     5.68293
C     6.0     2.70409     5.83486     6.89141
C     6.0     2.75366     7.22978     6.25144
H     1.0     6.36785     3.19858     5.09725
H     1.0     4.61062     4.75280     3.20248
H     1.0     9.07261     7.32194     8.34007
H     1.0     9.74146     7.36221    10.71654
H     1.0     9.57188     5.29354    12.11354
H     1.0     8.72972     3.17573    11.08938
H     1.0     8.08682     3.11346     8.69559
H     1.0    10.36943     3.30844     6.74975
H     1.0    10.77993     1.02148     5.88672
H     1.0     8.99318    -0.19218     4.62961
H     1.0     6.78012     0.90984     4.24445
H     1.0     1.19642     7.39177     3.61161
H     1.0    -0.09402     5.95259     2.06415
H     1.0     0.95060     3.90565     1.08015
H     1.0     3.31301     3.32060     1.65463
H     1.0     4.04017     9.89639     6.06928
H     1.0     3.84447    12.20316     5.21669
H     1.0     3.53141    12.62798     2.77144
H     1.0     3.42257    10.69905     1.18550
H     1.0     3.58926     8.37519     2.03048
H     1.0     6.16425     6.99596     9.11667
H     1.0     6.09363     7.50022    11.52913
H     1.0     4.41078     6.38388    13.00547
H     1.0     2.79993     4.74016    12.02234
H     1.0     2.86652     4.22506     9.60229
H     1.0     3.20372     3.37906     5.34251
H     1.0     3.05441     0.92580     5.16375
H     1.0     4.10021    -0.53765     6.90361
```

```
H     1.0     5.30182     0.50358     8.83195
H     1.0     5.43330     2.96959     9.04025
H     1.0     6.24204     7.88106     1.25935
H     1.0     5.94926     4.34395    -1.19923
H     1.0     7.02827     2.99934     0.61460
H     1.0     7.69693     4.06703     2.73133
H     1.0     9.19586     7.99969     1.65568
H     1.0     9.90437    10.29019     1.04694
H     1.0     9.04023    12.25878     2.32640
H     1.0     7.45878    11.89978     4.22968
H     1.0     6.74937     9.61636     4.84839
H     1.0     9.27648     5.14134     3.74610
H     1.0     9.95751     6.77326     3.66171
H     1.0     9.51734     7.12918     6.09420
H     1.0    10.40675     5.60401     5.91655
H     1.0     2.23990     5.11369     6.21082
H     1.0     2.11949     5.84830     7.81634
H     1.0     3.10701     7.97732     6.97058
H     1.0     1.76213     7.54062     5.90377
H     1.0     5.55414     6.78851    -0.85473
 $END
 $ECP
 MN-ECP GEN     10     2
 3      ----- d potential     -----
   -10.0000000        1    357.3914469
   -60.2990287        2     64.6477389
   -10.4217834        2     16.0960833
 5      ----- s-d potential     -----
     3.0000000        0    107.4127215
    16.2591819        1    111.4958973
   276.9373928        2     46.5568346
   241.3174342        2      8.3688135
  -146.4635329        2      7.7237489
 5      ----- p-d potential     -----
     5.0000000        0     80.0415103
     5.7589756        1    105.6043646
   285.2918654        2     40.8300466
   143.4222647        2      8.0098457
   -88.7031851        2      7.3390928
 P-ECP GEN     10     2
 5      ----- d   potential     -----
   -10.0000000        1    462.1211423
   -79.4864658        2     93.6863701
   -28.3668251        2     21.2349094
    -9.8577589        2      6.3388415
    -1.0163783        2      2.0620684
 5      ----- s-d potential     -----
     3.0000000        0     78.0831823
    12.9104154        1     58.9576810
   150.0250298        2     36.0571255
    71.7083146        2     11.2464453
```

```
    23.0397012        2       2.6757561
 6      ----- p-d potential     -----
     5.0000000        0      75.1617880
     6.3446507        1      57.4544041
   198.5585104        2      47.9481748
   111.1470820        2      18.4588360
    40.3944144        2       5.9414190
     6.4483233        2       1.8487507
P-ECP
P-ECP
P-ECP
O-ECP NONE
C-ECP NONE
C-ECP NONE
C-ECP NONE
C-ECP NONE
C-ECP NONE
C-ECP NONE
C-ECP NONE
C-ECP NONE
C-ECP NONE
C-ECP NONE
C-ECP NONE
C-ECP NONE
C-ECP NONE
C-ECP NONE
C-ECP NONE
C-ECP NONE
C-ECP NONE
C-ECP NONE
C-ECP NONE
C-ECP NONE
C-ECP NONE
C-ECP NONE
C-ECP NONE
C-ECP NONE
C-ECP NONE
C-ECP NONE
C-ECP NONE
C-ECP NONE
C-ECP NONE
C-ECP NONE
C-ECP NONE
C-ECP NONE
C-ECP NONE
C-ECP NONE
C-ECP NONE
C-ECP NONE
C-ECP NONE
C-ECP NONE
C-ECP NONE
```

```
C-ECP NONE
C-ECP NONE
C-ECP NONE
C-ECP NONE
C-ECP NONE
C-ECP NONE
C-ECP NONE
C-ECP NONE
C-ECP NONE
C-ECP NONE
C-ECP NONE
C-ECP NONE
C-ECP NONE
C-ECP NONE
H-ECP NONE
H-ECP NONE
H-ECP NONE
H-ECP NONE
H-ECP NONE
H-ECP NONE
H-ECP NONE
H-ECP NONE
H-ECP NONE
H-ECP NONE
H-ECP NONE
H-ECP NONE
H-ECP NONE
H-ECP NONE
H-ECP NONE
H-ECP NONE
H-ECP NONE
H-ECP NONE
H-ECP NONE
H-ECP NONE
H-ECP NONE
H-ECP NONE
H-ECP NONE
H-ECP NONE
H-ECP NONE
H-ECP NONE
H-ECP NONE
H-ECP NONE
H-ECP NONE
H-ECP NONE
H-ECP NONE
H-ECP NONE
H-ECP NONE
H-ECP NONE
H-ECP NONE
H-ECP NONE
H-ECP NONE
```

```
H-ECP NONE
H-ECP NONE
H-ECP NONE
H-ECP NONE
H-ECP NONE
H-ECP NONE
H-ECP NONE
H-ECP NONE
H-ECP NONE
H-ECP NONE
H-ECP NONE
 $END
```

```
!   Input file for GAMESS - [Mn(H2)(CO)dppe2]+ vib anal
 $CONTRL SCFTYP=RHF RUNTYP=HESSIAN EXETYP=RUN DFTTYP=B3LYP
    MAXIT=150 ICHARG=1 ECP=READ $END
 $SYSTEM MEMDDI=0 MWORDS=300 PARALL=.TRUE. $END
 $BASIS GBASIS=LANL2DZ EXTFIL=.T. NDFUNC=1 NPFUNC=1 $END
 $GUESS GUESS=MOREAD NORB=205 $END
 $SCF DIRSCF=.TRUE. CONV=5.0e-6 DAMP=.T. $END
 $STATPT OPTTOL=0.0001 NSTEP=100 TRMIN=0.01 $END
 $FORCE METHOD=SEMINUM VIBSIZ=0.010000 SCLFAC=0.960000 NVIB=2
    TEMP(1)=295 TEMP(2)=298 TEMP(3)=300 TEMP(4)=313
    TEMP(5)=333 TEMP(6)=343 TEMP(7)=353 TEMP(8)=363
    TEMP(9)=373
 $END
 $DATA
Mn(CO)(H2)dppe2
C1
Mn    25.0     7.67730     8.22523    -0.12511
P    15.0     6.83663    10.45490     0.43054
P    15.0    10.06420     8.69477     0.35876
C     6.0     7.81434    12.00004    -0.02869
C     6.0     8.45704    12.76586     0.96929
C     6.0     9.17441    13.92583     0.62454
C     6.0     9.26547    14.32884    -0.72140
C     6.0     8.64309    13.55812    -1.72116
C     6.0     7.92416    12.39751    -1.37986
C     6.0     6.09032    10.93832     2.11054
C     6.0     5.47288    12.20460     2.24797
C     6.0     4.86593    12.57934     3.45919
C     6.0     4.86874    11.69562     4.55705
C     6.0     5.48313    10.43646     4.43179
C     6.0     6.08638    10.06183     3.21416
C     6.0    11.05912     9.83221    -0.77533
C     6.0    11.57075    11.06415    -0.31746
C     6.0    12.31376    11.89022    -1.18137
C     6.0    12.55061    11.49776    -2.51139
C     6.0    12.02709    10.27664    -2.97837
C     6.0    11.28000     9.45228    -2.11819
C     6.0    10.64005     9.21270     2.08456
C     6.0    12.01118     9.17540     2.43234
C     6.0    12.42944     9.53383     3.72608
C     6.0    11.48466     9.94225     4.68986
C     6.0    10.12176     9.99760     4.34669
C     6.0     9.70644     9.63487     3.04989
C     6.0     5.27107    10.58247    -0.65027
C     6.0    11.00144     7.03561     0.14125
H     1.0     8.38717    12.47921     2.01520
H     1.0     9.65371    14.51239     1.40474
H     1.0     9.81252    15.23021    -0.98688
H     1.0     8.71504    13.85471    -2.76449
H     1.0     7.46361    11.81775    -2.17443
H     1.0     5.47598    12.90947     1.42001
```

H	1.0	4.39684	13.55611	3.54631
H	1.0	4.40213	11.98683	5.49472
H	1.0	5.49316	9.74779	5.27324
H	1.0	6.55186	9.08220	3.14768
H	1.0	11.40396	11.38286	0.70696
H	1.0	12.70545	12.83506	-0.81250
H	1.0	13.13198	12.13301	-3.17519
H	1.0	12.19623	9.96741	-4.00694
H	1.0	10.87809	8.52094	-2.50886
H	1.0	12.76014	8.88775	1.69797
H	1.0	13.48610	9.49909	3.97945
H	1.0	11.80980	10.21800	5.69004
H	1.0	9.38515	10.32174	5.07802
H	1.0	8.65448	9.69031	2.79720
H	1.0	4.76541	11.53268	-0.44573
H	1.0	5.57637	10.57936	-1.70180
H	1.0	11.33035	6.96520	-0.90108
H	1.0	11.89587	7.04588	0.77144
P	15.0	8.51354	5.94307	-0.56221
P	15.0	5.28721	7.72144	-0.48258
O	8.0	7.91183	9.28937	-2.88259
C	6.0	7.52694	4.44538	0.02702
C	6.0	6.84736	3.61578	-0.89193
C	6.0	6.12196	2.49801	-0.43963
C	6.0	6.05710	2.20175	0.93507
C	6.0	6.71600	3.03656	1.85747
C	6.0	7.44372	4.15268	1.40612
C	6.0	9.23311	5.33421	-2.20904
C	6.0	9.79132	4.03508	-2.27776
C	6.0	10.39128	3.57597	-3.46305
C	6.0	10.44267	4.40832	-4.59982
C	6.0	9.88975	5.69953	-4.53872
C	6.0	9.29064	6.16188	-3.34951
C	6.0	4.32183	6.64454	0.74035
C	6.0	3.82768	5.37662	0.36970
C	6.0	3.11709	4.59018	1.29594
C	6.0	2.89676	5.05564	2.60493
C	6.0	3.39871	6.31543	2.98558
C	6.0	4.10931	7.10199	2.06062
C	6.0	4.67751	7.09314	-2.15619
C	6.0	3.29497	7.09395	-2.45847
C	6.0	2.83863	6.65365	-3.71305
C	6.0	3.75749	6.20138	-4.68230
C	6.0	5.13185	6.18857	-4.38438
C	6.0	5.58691	6.63306	-3.12738
C	6.0	7.84068	8.83405	-1.78076
C	6.0	10.09607	5.84994	0.50388
C	6.0	4.34801	9.39419	-0.33860
H	1.0	6.89503	3.81985	-1.95823
H	1.0	5.61639	1.85964	-1.16031
H	1.0	5.50375	1.33293	1.28270

```
H     1.0     6.66727     2.82057     2.92183
H     1.0     7.94590     4.77831     2.14128
H     1.0     9.74715     3.37165    -1.41727
H     1.0    10.81444     2.57527    -3.49980
H     1.0    10.90583     4.05296    -5.51695
H     1.0     9.92180     6.35052    -5.40907
H     1.0     8.87666     7.16245    -3.33638
H     1.0     3.98149     4.99862    -0.63624
H     1.0     2.73790     3.61779     0.99106
H     1.0     2.34048     4.44980     3.31603
H     1.0     3.23191     6.68812     3.99363
H     1.0     4.47629     8.07404     2.37833
H     1.0     2.56722     7.41701    -1.71719
H     1.0     1.77373     6.66052    -3.93190
H     1.0     3.40419     5.86442    -5.65381
H     1.0     5.84950     5.84186    -5.12391
H     1.0     6.64939     6.62192    -2.91673
H     1.0    10.60000     4.89586     0.31441
H     1.0     9.81518     5.88015     1.56315
H     1.0     3.94833     9.47299     0.67791
H     1.0     3.50022     9.37783    -1.02964
H     1.0     7.33331     8.01452     1.61113
H     1.0     7.62802     7.30800     1.41007
 $END
 $ECP
 MN-ECP GEN     10     2
 3      ----- d potential     -----
   -10.0000000        1    357.3914469
   -60.2990287        2     64.6477389
   -10.4217834        2     16.0960833
 5      ----- s-d potential     -----
     3.0000000        0    107.4127215
    16.2591819        1    111.4958973
   276.9373928        2     46.5568346
   241.3174342        2      8.3688135
  -146.4635329        2      7.7237489
 5      ----- p-d potential     -----
     5.0000000        0     80.0415103
     5.7589756        1    105.6043646
   285.2918654        2     40.8300466
   143.4222647        2      8.0098457
   -88.7031851        2      7.3390928
 P-ECP GEN     10     2
 5      ----- d   potential     -----
   -10.0000000        1    462.1211423
   -79.4864658        2     93.6863701
   -28.3668251        2     21.2349094
    -9.8577589        2      6.3388415
    -1.0163783        2      2.0620684
 5      ----- s-d potential     -----
     3.0000000        0     78.0831823
```

```
    12.9104154        1     58.9576810
   150.0250298        2     36.0571255
    71.7083146        2     11.2464453
    23.0397012        2      2.6757561
 6      ----- p-d potential     -----
     5.0000000        0     75.1617880
     6.3446507        1     57.4544041
   198.5585104        2     47.9481748
   111.1470820        2     18.4588360
    40.3944144        2      5.9414190
     6.4483233        2      1.8487507
P-ECP
C-ECP NONE
C-ECP NONE
C-ECP NONE
C-ECP NONE
C-ECP NONE
C-ECP NONE
C-ECP NONE
C-ECP NONE
C-ECP NONE
C-ECP NONE
C-ECP NONE
C-ECP NONE
C-ECP NONE
C-ECP NONE
C-ECP NONE
C-ECP NONE
C-ECP NONE
C-ECP NONE
C-ECP NONE
C-ECP NONE
C-ECP NONE
C-ECP NONE
C-ECP NONE
C-ECP NONE
C-ECP NONE
C-ECP NONE
H-ECP NONE
H-ECP NONE
H-ECP NONE
H-ECP NONE
H-ECP NONE
H-ECP NONE
H-ECP NONE
H-ECP NONE
H-ECP NONE
H-ECP NONE
H-ECP NONE
H-ECP NONE
H-ECP NONE
```

```
H-ECP NONE
H-ECP NONE
H-ECP NONE
H-ECP NONE
H-ECP NONE
H-ECP NONE
H-ECP NONE
H-ECP NONE
H-ECP NONE
H-ECP NONE
H-ECP NONE
P-ECP
P-ECP
O-ECP NONE
C-ECP NONE
C-ECP NONE
C-ECP NONE
C-ECP NONE
C-ECP NONE
C-ECP NONE
C-ECP NONE
C-ECP NONE
C-ECP NONE
C-ECP NONE
C-ECP NONE
C-ECP NONE
C-ECP NONE
C-ECP NONE
C-ECP NONE
C-ECP NONE
C-ECP NONE
C-ECP NONE
C-ECP NONE
C-ECP NONE
C-ECP NONE
C-ECP NONE
C-ECP NONE
C-ECP NONE
C-ECP NONE
C-ECP NONE
C-ECP NONE
H-ECP NONE
H-ECP NONE
H-ECP NONE
H-ECP NONE
H-ECP NONE
H-ECP NONE
H-ECP NONE
H-ECP NONE
H-ECP NONE
H-ECP NONE
```

```
H-ECP NONE
H-ECP NONE
H-ECP NONE
H-ECP NONE
H-ECP NONE
H-ECP NONE
H-ECP NONE
H-ECP NONE
H-ECP NONE
H-ECP NONE
H-ECP NONE
H-ECP NONE
H-ECP NONE
H-ECP NONE
H-ECP NONE
H-ECP NONE
 $END
```

```
!   Input file for GAMESS - [FeHdppe2]+ vib anal
 $CONTRL SCFTYP=RHF RUNTYP=HESSIAN EXETYP=RUN
    MAXIT=200 ICHARG=1 ECP=READ DFTTYP=B3LYP $END
 $SYSTEM MEMDDI=0 MWORDS=150 PARALL=.TRUE. $END
 $BASIS GBASIS=LANL2DZ EXTFIL=.T. NDFUNC=1 NPFUNC=1 $END
 $GUESS GUESS=MOREAD NORB=198 $END
 $SCF DIRSCF=.T. CONV=5.0e-6 DAMP=.T. $END
 $STATPT OPTTOL=0.0001 NSTEP=100 TRMIN=0.01 $END
 $FORCE METHOD=SEMINUM VIBSIZ=0.010000 SCLFAC=0.960000 NVIB=2
   TEMP(1)=295 TEMP(2)=298 TEMP(3)=300 TEMP(4)=313 TEMP(5)=333
   TEMP(6)=343 TEMP(7)=353 TEMP(8)=363 TEMP(9)=373
 $END
 $DATA
[FeHdppe2]+
C1
Fe    26.0     7.17168     8.36120     2.15485
P    15.0     7.63169    10.03577     3.76677
P    15.0     6.74479     6.62234     3.75390
P    15.0     7.48298    10.13150     0.56603
P    15.0     6.90199     6.63269     0.54478
C     6.0     7.56996    11.76737     1.55802
C     6.0     6.94193     4.97393     1.49593
H     1.0     8.02431    12.53977     0.92891
H     1.0     6.55830     4.18026     0.84642
H     1.0     6.55350    12.08928     1.80977
H     1.0     7.98298     4.73821     1.74047
C     6.0     8.87503     9.78535     5.15714
C     6.0     5.41708     6.85150     5.07310
C     6.0    10.24656     9.68658     4.83255
C     6.0     4.05199     6.83013     4.70696
H     1.0    10.57850     9.75114     3.79854
H     1.0     3.75373     6.63591     3.67845
C     6.0     6.11872    10.48553    -0.68796
C     6.0     8.19918     6.33903    -0.78829
C     6.0     9.08120    10.26428    -0.42313
C     6.0     5.24935     6.46508    -0.34510
C     6.0     8.47746     9.67266     6.50626
C     6.0     5.76109     7.10802     6.41823
H     1.0     7.42813     9.75344     6.77672
H     1.0     6.80403     7.12393     6.72258
C     6.0     6.25138    10.10097    -2.03994
C     6.0     7.94726     6.62073    -2.14757
H     1.0     7.17547     9.64986    -2.39116
H     1.0     6.97507     6.99227    -2.46041
C     6.0     5.17118    12.65483     5.93809
C     6.0     9.02087     4.08797     6.18725
H     1.0     5.29937    13.52104     6.58246
H     1.0     8.82847     3.26699     6.87367
C     6.0     6.30054    12.00311     5.41158
C     6.0     7.94429     4.74546     5.56673
H     1.0     7.29272    12.37253     5.66211
```

```
H     1.0     6.92823     4.42663     5.78957
C     6.0     3.85903    11.29830    -1.16995
C     6.0    10.46219     5.61962    -1.38116
H     1.0     2.93994    11.76946    -0.82924
H     1.0    11.42992     5.22616    -1.07879
C     6.0    10.80594     9.39066     7.18856
C     6.0     3.39954     7.29479     7.01234
H     1.0    11.54769     9.24560     7.97003
H     1.0     2.62587     7.45763     7.75855
C     6.0     4.85137    10.40700     4.27969
C     6.0     9.50658     6.21346     4.40679
H     1.0     4.71591     9.52263     3.66077
H     1.0     9.68999     7.03274     3.71935
C     6.0     8.38819    11.52183     2.83306
C     6.0     6.09952     5.11298     2.77129
H     1.0     8.37847    12.39948     3.48781
H     1.0     6.17048     4.22113     3.40250
H     1.0     9.43063    11.28733     2.59248
H     1.0     5.04403     5.27121     2.52325
C     6.0     9.27002    11.32606    -1.33870
C     6.0     4.97831     5.36924    -1.19685
H     1.0     8.46965    12.03736    -1.53158
H     1.0     5.74679     4.62617    -1.39961
C     6.0    11.20621     9.49627     5.84253
C     6.0     3.04974     7.04665     5.67098
H     1.0    12.25963     9.43363     5.58015
H     1.0     2.00325     7.01445     5.37700
C     6.0     4.00109    10.92016    -2.51903
C     6.0    10.20389     5.89668    -2.73773
H     1.0     3.19244    11.09448    -3.22437
H     1.0    10.97056     5.71956    -3.48792
C     6.0     4.90887    11.07736    -0.25892
C     6.0     9.46885     5.84593    -0.41173
H     1.0     4.77161    11.37866     0.77773
H     1.0     9.69639     5.63926     0.63164
C     6.0     9.43955     9.47623     7.51580
C     6.0     4.75773     7.32504     7.38124
H     1.0     9.12286     9.39704     8.55301
H     1.0     5.03713     7.51107     8.41558
C     6.0     3.87674    12.18593     5.63306
C     6.0    10.34552     4.48964     5.91799
H     1.0     3.00441    12.69072     6.04093
H     1.0    11.17749     3.97907     6.39706
C     6.0     5.19974    10.31968    -2.94915
C     6.0     8.94574     6.40127    -3.11601
H     1.0     5.31871    10.02645    -3.98949
H     1.0     8.73822     6.61769    -4.16124
C     6.0     3.71907    11.05922     4.80525
C     6.0    10.58435     5.55325     5.02905
H     1.0     2.72441    10.68411     4.57718
H     1.0    11.60286     5.87230     4.82122
```

```
C     6.0    10.13014     9.35278    -0.19282
C     6.0     4.23828     7.41951    -0.11071
H     1.0     9.98747     8.53741     0.50870
H     1.0     4.43571     8.28214     0.52127
C     6.0     6.14925    10.87354     4.57462
C     6.0     8.18175     5.81446     4.67070
C     6.0    11.35621     9.49749    -0.87106
C     6.0     2.97261     7.28335    -0.71356
H     1.0    12.15776     8.78546    -0.69024
H     1.0     2.20434     8.03091    -0.53269
C     6.0    10.49353    11.46672    -2.01671
C     6.0     3.71579     5.23318    -1.80054
H     1.0    10.63049    12.28419    -2.72031
H     1.0     3.51867     4.38856    -2.45612
C     6.0    11.54150    10.55227    -1.78279
C     6.0     2.70839     6.18974    -1.55842
H     1.0    12.48825    10.66358    -2.30587
H     1.0     1.73300     6.08410    -2.02704
H     1.0     8.63123     8.02756     2.14222
 $END
 $ECP
 FE-ECP GEN     10     2
 3      ----- d potential     -----
   -10.0000000        1    392.6149787
   -63.2667518        2     71.1756979
   -10.9613338        2     17.7320281
 5      ----- s-d potential     -----
     3.0000000        0    126.0571895
    18.1729137        1    138.1264251
   339.1231164        2     54.2098858
   317.1068012        2      9.2837966
  -207.3421649        2      8.6289082
 5      ----- p-d potential     -----
     5.0000000        0     83.1759490
     5.9535930        1    106.0559938
   294.2665527        2     42.8284937
   154.4244635        2      8.7701805
   -95.3164249        2      8.0397818
 P-ECP GEN     10     2
 5      ----- d   potential     -----
   -10.0000000        1    462.1211423
   -79.4864658        2     93.6863701
   -28.3668251        2     21.2349094
    -9.8577589        2      6.3388415
    -1.0163783        2      2.0620684
 5      ----- s-d potential     -----
     3.0000000        0     78.0831823
    12.9104154        1     58.9576810
   150.0250298        2     36.0571255
    71.7083146        2     11.2464453
    23.0397012        2      2.6757561
```

```
 6      ----- p-d potential     -----
     5.0000000        0     75.1617880
     6.3446507        1     57.4544041
   198.5585104        2     47.9481748
   111.1470820        2     18.4588360
    40.3944144        2      5.9414190
     6.4483233        2      1.8487507
P-ECP
P-ECP
P-ECP
C-ECP NONE
C-ECP NONE
H-ECP NONE
H-ECP NONE
H-ECP NONE
H-ECP NONE
C-ECP NONE
C-ECP NONE
C-ECP NONE
C-ECP NONE
H-ECP NONE
H-ECP NONE
C-ECP NONE
C-ECP NONE
C-ECP NONE
C-ECP NONE
C-ECP NONE
C-ECP NONE
H-ECP NONE
H-ECP NONE
C-ECP NONE
C-ECP NONE
H-ECP NONE
H-ECP NONE
C-ECP NONE
C-ECP NONE
H-ECP NONE
H-ECP NONE
C-ECP NONE
C-ECP NONE
H-ECP NONE
H-ECP NONE
C-ECP NONE
C-ECP NONE
H-ECP NONE
H-ECP NONE
C-ECP NONE
C-ECP NONE
H-ECP NONE
H-ECP NONE
C-ECP NONE
```

```
C-ECP NONE
H-ECP NONE
H-ECP NONE
C-ECP NONE
C-ECP NONE
H-ECP NONE
H-ECP NONE
H-ECP NONE
H-ECP NONE
C-ECP NONE
C-ECP NONE
H-ECP NONE
H-ECP NONE
C-ECP NONE
C-ECP NONE
H-ECP NONE
H-ECP NONE
C-ECP NONE
C-ECP NONE
H-ECP NONE
H-ECP NONE
C-ECP NONE
C-ECP NONE
H-ECP NONE
H-ECP NONE
C-ECP NONE
C-ECP NONE
H-ECP NONE
H-ECP NONE
C-ECP NONE
C-ECP NONE
H-ECP NONE
H-ECP NONE
C-ECP NONE
C-ECP NONE
H-ECP NONE
H-ECP NONE
C-ECP NONE
C-ECP NONE
H-ECP NONE
H-ECP NONE
C-ECP NONE
C-ECP NONE
H-ECP NONE
H-ECP NONE
C-ECP NONE
C-ECP NONE
C-ECP NONE
C-ECP NONE
H-ECP NONE
H-ECP NONE
```

```
C-ECP NONE
C-ECP NONE
H-ECP NONE
H-ECP NONE
C-ECP NONE
C-ECP NONE
H-ECP NONE
H-ECP NONE
H-ECP NONE
 $END
```

```
!   Input File for GAMESS - [FeH(H2)dppe2]+ vib anal
 $CONTRL SCFTYP=RHF RUNTYP=HESSIAN EXETYP=RUN DFTTYP=B3LYP
    MAXIT=200 ICHARG=1 ECP=READ $END
 $SYSTEM MEMDDI=0 MWORDS=150 PARALL=.TRUE. $END
 $BASIS GBASIS=LANL2DZ EXTFIL=.T. NDFUNC=1 NPFUNC=1 $END
 $GUESS GUESS=MOREAD NORB=199 $END
 $SCF DIRSCF=.TRUE. CONV=5.0e-6 DAMP=.T. $END
 $STATPT OPTTOL=0.0001 NSTEP=100 TRMIN=0.01 $END
 $FORCE METHOD=SEMINUM VIBSIZ=0.010000 SCLFAC=0.960000 NVIB=2
  TEMP(1)=295 TEMP(2)=298 TEMP(3)=300 TEMP(4)=313 TEMP(5)=333
  TEMP(6)=343 TEMP(7)=353 TEMP(8)=363 TEMP(9)=373
 $END
 $DATA
[FeH(H2)dppe2]+
C1
Fe    26.0     6.97167     8.39792     2.15327
P    15.0     7.54614    10.05383     3.76618
P    15.0     6.64272     6.67353     3.76011
P    15.0     7.35390    10.12366     0.54925
P    15.0     6.83222     6.64351     0.54574
C     6.0     7.43224    11.75571     1.53864
C     6.0     6.83850     5.00383     1.53105
H     1.0     7.85410    12.54044     0.90219
H     1.0     6.46173     4.20151     0.88973
H     1.0     6.41868    12.05642     1.82650
H     1.0     7.87203     4.76484     1.80209
C     6.0     8.86552     9.74790     5.07736
C     6.0     5.35766     6.88789     5.12295
C     6.0    10.22197     9.64709     4.69699
C     6.0     3.98417     6.88905     4.78906
H     1.0    10.51330     9.73493     3.65276
H     1.0     3.66063     6.72680     3.76263
C     6.0     6.02789    10.48040    -0.74263
C     6.0     8.23188     6.36007    -0.68614
C     6.0     8.97986    10.25492    -0.39300
C     6.0     5.27669     6.38382    -0.50292
C     6.0     8.52137     9.60631     6.43870
C     6.0     5.73567     7.10461     6.46570
H     1.0     7.48523     9.69195     6.75457
H     1.0     6.78546     7.10441     6.74542
C     6.0     6.19450    10.09710    -2.09106
C     6.0     8.06734     6.63618    -2.06000
H     1.0     7.12366     9.63826    -2.41801
H     1.0     7.11279     6.99409    -2.43652
C     6.0     5.51274    12.84594     6.14814
C     6.0     8.99841     4.11143     6.08724
H     1.0     5.77436    13.73602     6.71517
H     1.0     8.82745     3.29289     6.78220
C     6.0     6.51645    12.12801     5.47512
C     6.0     7.90265     4.78760     5.52282
H     1.0     7.54700    12.46793     5.55040
```

```
H      1.0     6.89431     4.48314     5.79481
C      6.0     3.78699    11.30822    -1.28366
C      6.0    10.53277     5.65456    -1.12847
H      1.0     2.86212    11.78432    -0.96654
H      1.0    11.48110     5.26708    -0.76337
C      6.0    10.87122     9.29365     7.02321
C      6.0     3.39033     7.29636     7.12061
H      1.0    11.64194     9.12619     7.77149
H      1.0     2.63583     7.44472     7.88914
C      6.0     4.85498    10.53670     4.68639
C      6.0     9.42735     6.22956     4.28478
H      1.0     4.58614     9.63399     4.14808
H      1.0     9.58976     7.04663     3.58961
C      6.0     8.29618    11.50808     2.78266
C      6.0     5.97585     5.16974     2.78957
H      1.0     8.33587    12.39529     3.42174
H      1.0     6.02400     4.28176     3.42847
H      1.0     9.32163    11.24704     2.50031
H      1.0     4.92672     5.34544     2.52624
C      6.0     9.18193    11.30107    -1.32399
C      6.0     5.14661     5.21233    -1.28699
H      1.0     8.37713    11.99435    -1.55903
H      1.0     5.96210     4.49457    -1.34482
C      6.0    11.21902     9.42856     5.66498
C      6.0     3.00660     7.08846     5.78138
H      1.0    12.26129     9.36715     5.36108
H      1.0     1.95332     7.07367     5.51133
C      6.0     3.96273    10.92987    -2.62907
C      6.0    10.36154     5.92608    -2.50007
H      1.0     3.17409    11.10953    -3.35540
H      1.0    11.17594     5.75047    -3.19852
C      6.0     4.81120    11.08016    -0.34577
C      6.0     9.47738     5.87812    -0.22596
H      1.0     4.64948    11.38176     0.68722
H      1.0     9.63741     5.67683     0.83076
C      6.0     9.51965     9.38033     7.40529
C      6.0     4.75694     7.30474     7.45769
H      1.0     9.24212     9.28092     8.45197
H      1.0     5.06197     7.46264     8.48937
C      6.0     4.17232    12.41216     6.09076
C      6.0    10.31409     4.49104     5.75115
H      1.0     3.39617    12.96740     6.61181
H      1.0    11.16096     3.96629     6.18674
C      6.0     5.16865    10.32265    -3.02777
C      6.0     9.12777     6.42196    -2.96087
H      1.0     5.31265    10.02769    -4.06438
H      1.0     8.98634     6.63413    -4.01795
C      6.0     3.84811    11.25267     5.36390
C      6.0    10.52446     5.55153     4.85142
H      1.0     2.82038    10.89992     5.32751
H      1.0    11.53631     5.85452     4.59285
```

```
C     6.0    10.03728     9.37060    -0.10588
C     6.0     4.21477     7.30932    -0.47990
H     1.0     9.88499     8.56838     0.60859
H     1.0     4.30044     8.23077     0.08649
C     6.0     6.19532    10.96957     4.72772
C     6.0     8.11122     5.85378     4.61600
C     6.0    11.28280     9.52277    -0.74613
C     6.0     3.03553     7.06456    -1.21190
H     1.0    12.08956     8.82824    -0.52513
H     1.0     2.22831     7.79238    -1.18859
C     6.0    10.42546    11.45141    -1.96198
C     6.0     3.97094     4.96619    -2.01620
H     1.0    10.57147    12.25709    -2.67729
H     1.0     3.88637     4.06064    -2.61205
C     6.0    11.48052    10.56130    -1.67400
C     6.0     2.90727     5.89058    -1.97580
H     1.0    12.44170    10.67766    -2.16891
H     1.0     1.99611     5.69889    -2.53717
H     1.0     8.44932     8.07448     2.15763
H     1.0     5.26921     8.36457     2.02598
H     1.0     5.42761     9.12683     2.24373
 $END
 $ECP
 FE-ECP GEN     10     2
 3      ----- d potential     -----
   -10.0000000        1    392.6149787
   -63.2667518        2     71.1756979
   -10.9613338        2     17.7320281
 5      ----- s-d potential     -----
     3.0000000        0    126.0571895
    18.1729137        1    138.1264251
   339.1231164        2     54.2098858
   317.1068012        2      9.2837966
  -207.3421649        2      8.6289082
 5      ----- p-d potential     -----
     5.0000000        0     83.1759490
     5.9535930        1    106.0559938
   294.2665527        2     42.8284937
   154.4244635        2      8.7701805
   -95.3164249        2      8.0397818
 P-ECP GEN     10     2
 5      ----- d   potential     -----
   -10.0000000        1    462.1211423
   -79.4864658        2     93.6863701
   -28.3668251        2     21.2349094
    -9.8577589        2      6.3388415
    -1.0163783        2      2.0620684
 5      ----- s-d potential     -----
     3.0000000        0     78.0831823
    12.9104154        1     58.9576810
   150.0250298        2     36.0571255
```

```
    71.7083146        2     11.2464453
    23.0397012        2      2.6757561
 6      ----- p-d potential     -----
     5.0000000        0     75.1617880
     6.3446507        1     57.4544041
   198.5585104        2     47.9481748
   111.1470820        2     18.4588360
    40.3944144        2      5.9414190
     6.4483233        2      1.8487507
P-ECP
P-ECP
P-ECP
C-ECP NONE
C-ECP NONE
H-ECP NONE
H-ECP NONE
H-ECP NONE
H-ECP NONE
C-ECP NONE
C-ECP NONE
C-ECP NONE
C-ECP NONE
H-ECP NONE
H-ECP NONE
C-ECP NONE
C-ECP NONE
C-ECP NONE
C-ECP NONE
C-ECP NONE
C-ECP NONE
H-ECP NONE
H-ECP NONE
C-ECP NONE
C-ECP NONE
H-ECP NONE
H-ECP NONE
C-ECP NONE
C-ECP NONE
H-ECP NONE
H-ECP NONE
C-ECP NONE
C-ECP NONE
H-ECP NONE
H-ECP NONE
C-ECP NONE
C-ECP NONE
H-ECP NONE
H-ECP NONE
C-ECP NONE
C-ECP NONE
H-ECP NONE
```

```
H-ECP NONE
C-ECP NONE
C-ECP NONE
H-ECP NONE
H-ECP NONE
C-ECP NONE
C-ECP NONE
H-ECP NONE
H-ECP NONE
H-ECP NONE
H-ECP NONE
C-ECP NONE
C-ECP NONE
H-ECP NONE
H-ECP NONE
C-ECP NONE
C-ECP NONE
H-ECP NONE
H-ECP NONE
C-ECP NONE
C-ECP NONE
H-ECP NONE
H-ECP NONE
C-ECP NONE
C-ECP NONE
H-ECP NONE
H-ECP NONE
C-ECP NONE
C-ECP NONE
H-ECP NONE
H-ECP NONE
C-ECP NONE
C-ECP NONE
H-ECP NONE
H-ECP NONE
C-ECP NONE
C-ECP NONE
H-ECP NONE
H-ECP NONE
C-ECP NONE
C-ECP NONE
H-ECP NONE
H-ECP NONE
C-ECP NONE
C-ECP NONE
H-ECP NONE
H-ECP NONE
C-ECP NONE
C-ECP NONE
C-ECP NONE
C-ECP NONE
```

```
H-ECP NONE
H-ECP NONE
C-ECP NONE
C-ECP NONE
H-ECP NONE
H-ECP NONE
C-ECP NONE
C-ECP NONE
H-ECP NONE
H-ECP NONE
H-ECP NONE
H-ECP NONE
H-ECP NONE
 $END
```

5.3.3 Total Energy Calculation

```
!   Input file for GAMESS - H2 molecule total energy
 $CONTRL SCFTYP=RHF RUNTYP=OPTIMIZE EXETYP=RUN MPLEVL=2
    MAXIT=30 $END
 $SYSTEM MEMDDI=12 MWORDS=50 PARALL=.TRUE. $END
 $BASIS GBASIS=LANL2DZ EXTFIL=.T. NDFUNC=1 NPFUNC=1 $END
 $GUESS GUESS=HUCKEL $END
 $SCF DIRSCF=.TRUE. CONV=1.0e-7 $END
 $STATPT OPTTOL=0.0000001 TRMIN=0.01 NSTEP=100 HSSEND=.T. $END
 $FORCE METHOD=SEMINUM NVIB=2 VIBSIZ=0.01 SCLFAC=0.96 VIBANL=.TRUE.
   TEMP(1)=295 TEMP(2)=298 TEMP(3)=300 TEMP(4)=313 TEMP(5)=333
   TEMP(6)=343 TEMP(7)=353 TEMP(8)=363 TEMP(9)=373
 $END
 $DATA
H2 molecule
C1
H     1.0    -0.02189     0.00000     0.00000
H     1.0     0.72189     0.00000     0.00000
 $END
```

```
!   Input file for GAMESS - [Mn(CO)dppe2]+ total energy
 $CONTRL SCFTYP=RHF RUNTYP=ENERGY EXETYP=RUN MAXIT=100
    ICHARG=1 ECP=READ MPLEVL=2
 $END
 $SYSTEM MEMDDI=5000 MWORDS=75 PARALL=.TRUE. $END
 $BASIS GBASIS=LANL2DZ EXTFIL=.T. NDFUNC=1 NPFUNC=1 $END
 $GUESS GUESS=HUCKEL $END
 $SCF DIRSCF=.TRUE. CONV=5.0e-6 DAMP=.T. $END
 $FORCE METHOD=SEMINUM NVIB=2 SCLFAC=0.96 VIBANL=.TRUE. $END
 $DATA
Mn(CO)dppe2
C1
Mn    25.0     7.63915     8.25871    -0.17076
P    15.0     6.80440    10.48348     0.40231
P    15.0    10.03343     8.68254     0.46829
C     6.0     7.80899    12.00670    -0.06697
C     6.0     8.41575    12.80365     0.92860
C     6.0     9.18881    13.92344     0.57182
C     6.0     9.37064    14.25496    -0.78388
C     6.0     8.77771    13.45677    -1.78008
C     6.0     8.00270    12.33682    -1.42714
C     6.0     6.09011    10.95594     2.08989
C     6.0     5.41715    12.19073     2.24304
C     6.0     4.85152    12.54799     3.47908
C     6.0     4.95272    11.67639     4.58227
C     6.0     5.62140    10.44598     4.43943
C     6.0     6.18261    10.08777     3.19684
C     6.0    10.99848     9.82003    -0.68696
C     6.0    11.57620    11.02012    -0.22346
C     6.0    12.24450    11.87684    -1.11772
C     6.0    12.33958    11.54598    -2.48175
C     6.0    11.76096    10.35003    -2.94897
C     6.0    11.09311     9.49230    -2.05749
C     6.0    10.64164     9.22840     2.17911
C     6.0    11.99512     9.04822     2.55223
C     6.0    12.45650     9.47932     3.80829
C     6.0    11.57490    10.10942     4.70993
C     6.0    10.23157    10.30581     4.34160
C     6.0     9.77060     9.86598     3.08386
C     6.0     5.22563    10.60882    -0.65777
C     6.0    10.92628     7.00022     0.27383
H     1.0     8.28047    12.56904     1.98092
H     1.0     9.64570    14.53016     1.34994
H     1.0     9.96799    15.12063    -1.05957
H     1.0     8.92200    13.69719    -2.83033
H     1.0     7.57290    11.72992    -2.21880
H     1.0     5.34222    12.88358     1.40787
H     1.0     4.33523    13.49950     3.57956
H     1.0     4.52123    11.95695     5.53969
H     1.0     5.71092     9.77276     5.28788
H     1.0     6.70066     9.13493     3.10543
```

H	1.0	11.51071	11.29539	0.82472
H	1.0	12.68419	12.79936	-0.74656
H	1.0	12.85050	12.21231	-3.17239
H	1.0	11.81724	10.08961	-4.00281
H	1.0	10.64476	8.58127	-2.44477
H	1.0	12.70675	8.59982	1.86342
H	1.0	13.49976	9.33314	4.07764
H	1.0	11.93331	10.44584	5.67969
H	1.0	9.54480	10.79879	5.02560
H	1.0	8.73462	10.03373	2.81571
H	1.0	4.71834	11.55759	-0.45158
H	1.0	5.51441	10.60044	-1.71413
H	1.0	11.25777	6.90672	-0.76625
H	1.0	11.81718	6.98247	0.90738
P	15.0	8.44675	5.93852	-0.48843
P	15.0	5.25408	7.75887	-0.54741
O	8.0	7.87916	9.25753	-2.93164
C	6.0	7.44457	4.42678	0.03607
C	6.0	6.84619	3.59186	-0.93305
C	6.0	6.10695	2.46108	-0.54091
C	6.0	5.94889	2.15606	0.82408
C	6.0	6.52941	2.99370	1.79527
C	6.0	7.26987	4.12484	1.40452
C	6.0	9.23256	5.34581	-2.11054
C	6.0	9.92018	4.10880	-2.13543
C	6.0	10.53720	3.65761	-3.31516
C	6.0	10.47460	4.43437	-4.49026
C	6.0	9.78854	5.66144	-4.47391
C	6.0	9.17572	6.11731	-3.28966
C	6.0	4.37805	6.60626	0.66776
C	6.0	3.75902	5.41269	0.24249
C	6.0	3.14358	4.55928	1.17719
C	6.0	3.14423	4.88402	2.54591
C	6.0	3.76927	6.07002	2.97799
C	6.0	4.38428	6.92451	2.04473
C	6.0	4.62751	7.15670	-2.22522
C	6.0	3.26925	7.31135	-2.58869
C	6.0	2.80543	6.85034	-3.83361
C	6.0	3.68904	6.21332	-4.72764
C	6.0	5.03906	6.04682	-4.36835
C	6.0	5.50333	6.51842	-3.12498
C	6.0	7.82093	8.83046	-1.81339
C	6.0	9.97754	5.85093	0.65043
C	6.0	4.31352	9.41607	-0.32056
H	1.0	6.96963	3.80229	-1.99186
H	1.0	5.66034	1.82250	-1.29933
H	1.0	5.38356	1.27781	1.12612
H	1.0	6.40590	2.77034	2.85201
H	1.0	7.70859	4.75473	2.17588
H	1.0	9.96301	3.48354	-1.24677
H	1.0	11.06700	2.70860	-3.31765

```
H     1.0    10.94763     4.08353    -5.40401
H     1.0     9.72549     6.26707    -5.37444
H     1.0     8.66213     7.06963    -3.30953
H     1.0     3.74910     5.14293    -0.80890
H     1.0     2.66763     3.64429     0.83320
H     1.0     2.66894     4.22232     3.26577
H     1.0     3.77553     6.33004     4.03384
H     1.0     4.84723     7.84247     2.39876
H     1.0     2.55812     7.76962    -1.90574
H     1.0     1.75890     6.97888    -4.09912
H     1.0     3.33012     5.85827    -5.69035
H     1.0     5.72990     5.55687    -5.05009
H     1.0     6.54792     6.39060    -2.86795
H     1.0    10.46594     4.87801     0.53073
H     1.0     9.65357     5.93540     1.69541
H     1.0     3.97098     9.47018     0.71924
H     1.0     3.42691     9.42236    -0.96062
 $END
 $ECP
 MN-ECP GEN     10     2
 3      ----- d potential     -----
   -10.0000000        1    357.3914469
   -60.2990287        2     64.6477389
   -10.4217834        2     16.0960833
 5      ----- s-d potential     -----
     3.0000000        0    107.4127215
    16.2591819        1    111.4958973
   276.9373928        2     46.5568346
   241.3174342        2      8.3688135
  -146.4635329        2      7.7237489
 5      ----- p-d potential     -----
     5.0000000        0     80.0415103
     5.7589756        1    105.6043646
   285.2918654        2     40.8300466
   143.4222647        2      8.0098457
   -88.7031851        2      7.3390928
 P-ECP GEN     10     2
 5      ----- d   potential     -----
   -10.0000000        1    462.1211423
   -79.4864658        2     93.6863701
   -28.3668251        2     21.2349094
    -9.8577589        2      6.3388415
    -1.0163783        2      2.0620684
 5      ----- s-d potential     -----
     3.0000000        0     78.0831823
    12.9104154        1     58.9576810
   150.0250298        2     36.0571255
    71.7083146        2     11.2464453
    23.0397012        2      2.6757561
 6      ----- p-d potential     -----
     5.0000000        0     75.1617880
```

```
     6.3446507        1     57.4544041
   198.5585104        2     47.9481748
   111.1470820        2     18.4588360
    40.3944144        2      5.9414190
     6.4483233        2      1.8487507
P-ECP
C-ECP NONE
C-ECP NONE
C-ECP NONE
C-ECP NONE
C-ECP NONE
C-ECP NONE
C-ECP NONE
C-ECP NONE
C-ECP NONE
C-ECP NONE
C-ECP NONE
C-ECP NONE
C-ECP NONE
C-ECP NONE
C-ECP NONE
C-ECP NONE
C-ECP NONE
C-ECP NONE
C-ECP NONE
C-ECP NONE
C-ECP NONE
C-ECP NONE
C-ECP NONE
C-ECP NONE
C-ECP NONE
C-ECP NONE
H-ECP NONE
H-ECP NONE
H-ECP NONE
H-ECP NONE
H-ECP NONE
H-ECP NONE
H-ECP NONE
H-ECP NONE
H-ECP NONE
H-ECP NONE
H-ECP NONE
H-ECP NONE
H-ECP NONE
H-ECP NONE
H-ECP NONE
H-ECP NONE
H-ECP NONE
H-ECP NONE
H-ECP NONE
```

```
H-ECP NONE
H-ECP NONE
H-ECP NONE
H-ECP NONE
H-ECP NONE
P-ECP
P-ECP
O-ECP NONE
C-ECP NONE
C-ECP NONE
C-ECP NONE
C-ECP NONE
C-ECP NONE
C-ECP NONE
C-ECP NONE
C-ECP NONE
C-ECP NONE
C-ECP NONE
C-ECP NONE
C-ECP NONE
C-ECP NONE
C-ECP NONE
C-ECP NONE
C-ECP NONE
C-ECP NONE
C-ECP NONE
C-ECP NONE
C-ECP NONE
C-ECP NONE
C-ECP NONE
C-ECP NONE
C-ECP NONE
C-ECP NONE
C-ECP NONE
C-ECP NONE
H-ECP NONE
H-ECP NONE
H-ECP NONE
H-ECP NONE
H-ECP NONE
H-ECP NONE
H-ECP NONE
H-ECP NONE
H-ECP NONE
H-ECP NONE
H-ECP NONE
H-ECP NONE
H-ECP NONE
H-ECP NONE
H-ECP NONE
H-ECP NONE
```

```
H-ECP NONE
H-ECP NONE
H-ECP NONE
H-ECP NONE
H-ECP NONE
H-ECP NONE
H-ECP NONE
H-ECP NONE
 $END
 $VIB
         IVIB=   0 IATOM=   0 ICOORD=   0 E=    -2251.6692921649
-9.831384019E-05 3.602828603E-06 2.466054810E-05-1.000560608E-04-5.010269339E-05
-6.886866185E-05 3.074987707E-04 3.376021209E-04 1.248616312E-05 3.131049098E-05
-7.015209532E-05 1.181574968E-04 1.266482900E-04-4.435106506E-05-2.246477482E-04
 7.999638955E-05 1.787656449E-05 1.253391555E-04 1.159115151E-04-1.305466054E-04
-9.075270098E-05 2.624877471E-04-2.039162349E-04-3.242084912E-05 8.227021643E-05
-1.553437383E-05-2.431833795E-05-1.357350951E-05-4.935395680E-05-5.581756147E-05
-1.308765761E-04 4.211833145E-05-4.689503117E-05 3.773138900E-04 2.498890210E-04
 2.812086517E-05-3.568698690E-04 5.309145366E-05-8.184232638E-05-2.293354898E-05
-5.004133648E-04 1.978012856E-04 2.293683457E-04 4.782293494E-04-5.650517653E-05
-4.387719359E-04-1.563780407E-05-1.502657545E-04 6.642312079E-05-5.396478693E-05
 2.090038791E-04-4.716224085E-04 2.934986204E-04 7.055110375E-05 3.458790964E-05
 2.728137577E-05 1.266575890E-04-3.396690857E-04 2.032680813E-05-1.344198408E-04
 1.154262872E-04 1.518334812E-04 1.149040037E-04-1.478733408E-04-2.727966734E-04
 3.701045186E-04-1.379165930E-04-4.483367569E-04 3.177874900E-04-1.972777985E-05
-8.249628686E-05-1.423262633E-04 2.259636536E-04 2.208925560E-04 1.975223991E-04
 2.647571665E-04 4.652205243E-04-1.987564101E-04 1.195645557E-04 3.634194104E-04
-1.406567421E-05 2.790691377E-06 4.403537483E-05-2.170522123E-04-1.140584172E-04
-3.825641517E-05 2.935720330E-04-3.476750544E-06-1.111878008E-04 4.093515227E-05
 1.154663756E-04-1.622883059E-04-1.783883321E-05 1.992014208E-04-1.332662183E-04
 5.063894360E-05 1.408601439E-04-2.580612632E-05 3.128880408E-06 8.143958562E-05
 3.365842146E-07-5.872744497E-05-1.788798862E-04-6.103102898E-05-1.526885701E-04
-2.146559125E-04-2.310782698E-05-1.755355238E-04 1.669545261E-04 1.698272547E-04
-7.969493704E-05 1.949347694E-04 4.574746287E-04-1.662360883E-04 8.578358707E-05
 4.027982250E-05 3.836142590E-05 1.008629993E-04-5.021986704E-05 6.774867229E-05
-2.711749946E-05-1.524649993E-05 4.921069315E-05-3.589685196E-04 1.189048973E-04
 1.237628332E-05-3.844542067E-04 1.755567871E-04 1.246318696E-04-2.908094406E-04
 8.063284706E-05 7.640765030E-05 1.132197080E-04-1.036089043E-05 3.921680515E-06
 1.246842938E-04-1.990449816E-05 1.134765786E-04 9.241741313E-05 3.573356980E-05
 1.748951260E-05 1.369393727E-04 1.956577450E-05 7.090810603E-05 1.814152243E-04
 3.107844430E-05 1.304955659E-04 5.730851369E-06-2.714415228E-05-3.640002281E-05
 4.751159887E-06-1.201055074E-04 1.997863174E-05 7.833618434E-05-5.672325866E-06
 6.425030030E-05 4.066942056E-05-1.884508787E-05 8.423186005E-05 1.135593397E-05
-4.749224045E-05 1.268409321E-05-1.381646072E-05-1.137663301E-05-8.980913551E-05
 3.043192255E-06-7.656690169E-05 2.524662534E-04-9.116491049E-05 7.017689802E-05
 3.816517994E-05-5.472637412E-05 2.392149215E-05 4.081828749E-05 9.405598307E-05
-9.279547494E-05-6.285072070E-05-2.882632912E-04 1.527604358E-04-7.126223968E-06
-2.178572033E-05-4.351471719E-06 1.882914919E-05-5.310382493E-05-8.708069192E-05
-1.789437738E-05-1.473608629E-04 1.625088565E-05-6.956375377E-05 3.612652789E-04
 1.104201100E-04 1.452188874E-04-7.529923401E-04-4.287243253E-04-2.312649709E-04
 5.378186132E-04 1.491307820E-04 2.116266895E-04-7.619183697E-05 2.668874678E-04
```

```
!   Input file for GAMESS - [Mn(CO)dppe2]+ agostic total energy
 $CONTRL SCFTYP=RHF RUNTYP=ENERGY EXETYP=RUN MPLEVL=2
    MAXIT=150 ICHARG=1 ECP=READ $END
 $SYSTEM MEMDDI=5000 MWORDS=75 PARALL=.TRUE. $END
 $BASIS GBASIS=LANL2DZ EXTFIL=.T. NDFUNC=1 NPFUNC=1 $END
 $GUESS GUESS=HUCKEL $END
 $STATPT OPTTOL=0.0001 NSTEP=100 TRMIN=0.01 $END
 $SCF DIRSCF=.TRUE. CONV=5.0e-6 DAMP=.T. $END
 $FORCE METHOD=SEMINUM VIBSIZ=0.010000 SCLFAC=0.960000 NVIB=2 $END
 $DATA
Mn(CO)dppe2
C1
Mn    25.0     6.01631     6.28789     5.69874
P    15.0     8.01900     5.20284     6.52822
P    15.0     3.96610     7.20457     4.77793
P    15.0     4.48275     5.24569     7.31666
P    15.0     7.47139     6.87365     3.80446
O     8.0     6.50326     8.73462     7.27172
C     6.0     8.53389     5.20945     8.33794
C     6.0     9.00099     6.40752     8.92414
C     6.0     9.37543     6.43610    10.27997
C     6.0     9.27948     5.27194    11.06670
C     6.0     8.80582     4.07888    10.48855
C     6.0     8.43392     4.04657     9.13158
C     6.0     8.34264     3.43273     5.96337
C     6.0     9.58723     2.80047     6.18972
C     6.0     9.82024     1.49998     5.70746
C     6.0     8.81222     0.81469     4.99763
C     6.0     7.56930     1.43584     4.77586
C     6.0     7.33970     2.73901     5.25608
C     6.0     2.99249     6.16247     3.54528
C     6.0     1.66144     6.49685     3.20369
C     6.0     0.92797     5.68514     2.32085
C     6.0     1.51791     4.53087     1.76519
C     6.0     2.84499     4.19831     2.09341
C     6.0     3.57801     5.01077     2.98091
C     6.0     3.81916     8.95877     4.11124
C     6.0     3.89696    10.05271     5.00273
C     6.0     3.79275    11.37035     4.51954
C     6.0     3.61866    11.60986     3.14263
C     6.0     3.55482    10.52295     2.25036
C     6.0     3.65609     9.20378     2.73071
C     6.0     4.52007     5.57842     9.17490
C     6.0     5.42793     6.49806     9.73422
C     6.0     5.38704     6.78678    11.11280
C     6.0     4.44166     6.15878    11.94216
C     6.0     3.53228     5.23369    11.38814
C     6.0     3.56928     4.94705    10.01299
C     6.0     4.33030     3.36433     7.21146
C     6.0     3.66755     2.76905     6.11397
C     6.0     3.58434     1.36811     6.00419
```

```
C      6.0      4.17197     0.54423     6.98315
C      6.0      4.84608     1.13205     8.07073
C      6.0      4.92731     2.53244     8.18395
C      6.0      7.02143     6.06276     2.15756
C      6.0      6.40426     6.81404     1.13291
C      6.0      6.01892     6.19540    -0.07088
C      6.0      6.23897     4.81825    -0.26487
C      6.0      6.84512     4.06198     0.75648
C      6.0      7.22938     4.67825     1.96293
C      6.0      7.92226     8.63690     3.30637
C      6.0      8.81777     8.84351     2.22933
C      6.0      9.21724    10.14346     1.87662
C      6.0      8.72974    11.25283     2.59805
C      6.0      7.84051    11.05097     3.66830
C      6.0      7.43674     9.74799     4.02229
C      6.0      6.30908     7.73755     6.63338
C      6.0      9.21457     6.14957     4.16804
C      6.0      9.46632     6.11495     5.68293
C      6.0      2.70409     5.83486     6.89141
C      6.0      2.75366     7.22978     6.25144
H      1.0      6.36785     3.19858     5.09725
H      1.0      4.61062     4.75280     3.20248
H      1.0      9.07261     7.32194     8.34007
H      1.0      9.74146     7.36221    10.71654
H      1.0      9.57188     5.29354    12.11354
H      1.0      8.72972     3.17573    11.08938
H      1.0      8.08682     3.11346     8.69559
H      1.0     10.36943     3.30844     6.74975
H      1.0     10.77993     1.02148     5.88672
H      1.0      8.99318    -0.19218     4.62961
H      1.0      6.78012     0.90984     4.24445
H      1.0      1.19642     7.39177     3.61161
H      1.0     -0.09402     5.95259     2.06415
H      1.0      0.95060     3.90565     1.08015
H      1.0      3.31301     3.32060     1.65463
H      1.0      4.04017     9.89639     6.06928
H      1.0      3.84447    12.20316     5.21669
H      1.0      3.53141    12.62798     2.77144
H      1.0      3.42257    10.69905     1.18550
H      1.0      3.58926     8.37519     2.03048
H      1.0      6.16425     6.99596     9.11667
H      1.0      6.09363     7.50022    11.52913
H      1.0      4.41078     6.38388    13.00547
H      1.0      2.79993     4.74016    12.02234
H      1.0      2.86652     4.22506     9.60229
H      1.0      3.20372     3.37906     5.34251
H      1.0      3.05441     0.92580     5.16375
H      1.0      4.10021    -0.53765     6.90361
H      1.0      5.30182     0.50358     8.83195
H      1.0      5.43330     2.96959     9.04025
H      1.0      6.24204     7.88106     1.25935
```

```
H     1.0     5.94926     4.34395    -1.19923
H     1.0     7.02827     2.99934     0.61460
H     1.0     7.69693     4.06703     2.73133
H     1.0     9.19586     7.99969     1.65568
H     1.0     9.90437    10.29019     1.04694
H     1.0     9.04023    12.25878     2.32640
H     1.0     7.45878    11.89978     4.22968
H     1.0     6.74937     9.61636     4.84839
H     1.0     9.27648     5.14134     3.74610
H     1.0     9.95751     6.77326     3.66171
H     1.0     9.51734     7.12918     6.09420
H     1.0    10.40675     5.60401     5.91655
H     1.0     2.23990     5.11369     6.21082
H     1.0     2.11949     5.84830     7.81634
H     1.0     3.10701     7.97732     6.97058
H     1.0     1.76213     7.54062     5.90377
H     1.0     5.55414     6.78851    -0.85473
 $END
 $ECP
 MN-ECP GEN     10     2
 3      ----- d potential      -----
   -10.0000000        1    357.3914469
   -60.2990287        2     64.6477389
   -10.4217834        2     16.0960833
 5      ----- s-d potential      -----
     3.0000000        0    107.4127215
    16.2591819        1    111.4958973
   276.9373928        2     46.5568346
   241.3174342        2      8.3688135
  -146.4635329        2      7.7237489
 5      ----- p-d potential      -----
     5.0000000        0     80.0415103
     5.7589756        1    105.6043646
   285.2918654        2     40.8300466
   143.4222647        2      8.0098457
   -88.7031851        2      7.3390928
 P-ECP GEN     10     2
 5      ----- d   potential      -----
   -10.0000000        1    462.1211423
   -79.4864658        2     93.6863701
   -28.3668251        2     21.2349094
    -9.8577589        2      6.3388415
    -1.0163783        2      2.0620684
 5      ----- s-d potential      -----
     3.0000000        0     78.0831823
    12.9104154        1     58.9576810
   150.0250298        2     36.0571255
    71.7083146        2     11.2464453
    23.0397012        2      2.6757561
 6      ----- p-d potential      -----
     5.0000000        0     75.1617880
```

```
     6.3446507        1     57.4544041
   198.5585104        2     47.9481748
   111.1470820        2     18.4588360
    40.3944144        2      5.9414190
     6.4483233        2      1.8487507
P-ECP
P-ECP
P-ECP
O-ECP NONE
C-ECP NONE
C-ECP NONE
C-ECP NONE
C-ECP NONE
C-ECP NONE
C-ECP NONE
C-ECP NONE
C-ECP NONE
C-ECP NONE
C-ECP NONE
C-ECP NONE
C-ECP NONE
C-ECP NONE
C-ECP NONE
C-ECP NONE
C-ECP NONE
C-ECP NONE
C-ECP NONE
C-ECP NONE
C-ECP NONE
C-ECP NONE
C-ECP NONE
C-ECP NONE
C-ECP NONE
C-ECP NONE
C-ECP NONE
C-ECP NONE
C-ECP NONE
C-ECP NONE
C-ECP NONE
C-ECP NONE
C-ECP NONE
C-ECP NONE
C-ECP NONE
C-ECP NONE
C-ECP NONE
C-ECP NONE
C-ECP NONE
C-ECP NONE
C-ECP NONE
C-ECP NONE
C-ECP NONE
```

```
C-ECP NONE
C-ECP NONE
C-ECP NONE
C-ECP NONE
C-ECP NONE
C-ECP NONE
C-ECP NONE
C-ECP NONE
C-ECP NONE
C-ECP NONE
C-ECP NONE
H-ECP NONE
H-ECP NONE
H-ECP NONE
H-ECP NONE
H-ECP NONE
H-ECP NONE
H-ECP NONE
H-ECP NONE
H-ECP NONE
H-ECP NONE
H-ECP NONE
H-ECP NONE
H-ECP NONE
H-ECP NONE
H-ECP NONE
H-ECP NONE
H-ECP NONE
H-ECP NONE
H-ECP NONE
H-ECP NONE
H-ECP NONE
H-ECP NONE
H-ECP NONE
H-ECP NONE
H-ECP NONE
H-ECP NONE
H-ECP NONE
H-ECP NONE
H-ECP NONE
H-ECP NONE
H-ECP NONE
H-ECP NONE
H-ECP NONE
H-ECP NONE
H-ECP NONE
H-ECP NONE
H-ECP NONE
H-ECP NONE
H-ECP NONE
H-ECP NONE
H-ECP NONE
```

```
H-ECP NONE
H-ECP NONE
H-ECP NONE
H-ECP NONE
H-ECP NONE
H-ECP NONE
H-ECP NONE
H-ECP NONE
 $END
```

```
!   Input file for GAMESS - [Mn(H2)(CO)dppe2]+ total energy
 $CONTRL SCFTYP=RHF RUNTYP=ENERGY EXETYP=RUN MPLEVL=2
    MAXIT=150 ICHARG=1 ECP=READ $END
 $SYSTEM MEMDDI=5000 MWORDS=50 PARALL=.TRUE. $END
 $BASIS GBASIS=LANL2DZ EXTFIL=.T. NDFUNC=1 NPFUNC=1 $END
 $GUESS GUESS=HUCKEL $END
 $SCF DIRSCF=.TRUE. CONV=5.0e-6 DAMP=.T. $END
 $STATPT OPTTOL=0.0001 NSTEP=100 TRMIN=0.01 $END
 $FORCE METHOD=SEMINUM VIBSIZ=0.010000 SCLFAC=0.960000 NVIB=2 $END
 $DATA
Mn(CO)(H2)dppe2
C1
Mn    25.0     7.67730     8.22523    -0.12511
P    15.0     6.83663    10.45490     0.43054
P    15.0    10.06420     8.69477     0.35876
C     6.0     7.81434    12.00004    -0.02869
C     6.0     8.45704    12.76586     0.96929
C     6.0     9.17441    13.92583     0.62454
C     6.0     9.26547    14.32884    -0.72140
C     6.0     8.64309    13.55812    -1.72116
C     6.0     7.92416    12.39751    -1.37986
C     6.0     6.09032    10.93832     2.11054
C     6.0     5.47288    12.20460     2.24797
C     6.0     4.86593    12.57934     3.45919
C     6.0     4.86874    11.69562     4.55705
C     6.0     5.48313    10.43646     4.43179
C     6.0     6.08638    10.06183     3.21416
C     6.0    11.05912     9.83221    -0.77533
C     6.0    11.57075    11.06415    -0.31746
C     6.0    12.31376    11.89022    -1.18137
C     6.0    12.55061    11.49776    -2.51139
C     6.0    12.02709    10.27664    -2.97837
C     6.0    11.28000     9.45228    -2.11819
C     6.0    10.64005     9.21270     2.08456
C     6.0    12.01118     9.17540     2.43234
C     6.0    12.42944     9.53383     3.72608
C     6.0    11.48466     9.94225     4.68986
C     6.0    10.12176     9.99760     4.34669
C     6.0     9.70644     9.63487     3.04989
C     6.0     5.27107    10.58247    -0.65027
C     6.0    11.00144     7.03561     0.14125
H     1.0     8.38717    12.47921     2.01520
H     1.0     9.65371    14.51239     1.40474
H     1.0     9.81252    15.23021    -0.98688
H     1.0     8.71504    13.85471    -2.76449
H     1.0     7.46361    11.81775    -2.17443
H     1.0     5.47598    12.90947     1.42001
H     1.0     4.39684    13.55611     3.54631
H     1.0     4.40213    11.98683     5.49472
H     1.0     5.49316     9.74779     5.27324
H     1.0     6.55186     9.08220     3.14768
```

H	1.0	11.40396	11.38286	0.70696
H	1.0	12.70545	12.83506	-0.81250
H	1.0	13.13198	12.13301	-3.17519
H	1.0	12.19623	9.96741	-4.00694
H	1.0	10.87809	8.52094	-2.50886
H	1.0	12.76014	8.88775	1.69797
H	1.0	13.48610	9.49909	3.97945
H	1.0	11.80980	10.21800	5.69004
H	1.0	9.38515	10.32174	5.07802
H	1.0	8.65448	9.69031	2.79720
H	1.0	4.76541	11.53268	-0.44573
H	1.0	5.57637	10.57936	-1.70180
H	1.0	11.33035	6.96520	-0.90108
H	1.0	11.89587	7.04588	0.77144
P	15.0	8.51354	5.94307	-0.56221
P	15.0	5.28721	7.72144	-0.48258
O	8.0	7.91183	9.28937	-2.88259
C	6.0	7.52694	4.44538	0.02702
C	6.0	6.84736	3.61578	-0.89193
C	6.0	6.12196	2.49801	-0.43963
C	6.0	6.05710	2.20175	0.93507
C	6.0	6.71600	3.03656	1.85747
C	6.0	7.44372	4.15268	1.40612
C	6.0	9.23311	5.33421	-2.20904
C	6.0	9.79132	4.03508	-2.27776
C	6.0	10.39128	3.57597	-3.46305
C	6.0	10.44267	4.40832	-4.59982
C	6.0	9.88975	5.69953	-4.53872
C	6.0	9.29064	6.16188	-3.34951
C	6.0	4.32183	6.64454	0.74035
C	6.0	3.82768	5.37662	0.36970
C	6.0	3.11709	4.59018	1.29594
C	6.0	2.89676	5.05564	2.60493
C	6.0	3.39871	6.31543	2.98558
C	6.0	4.10931	7.10199	2.06062
C	6.0	4.67751	7.09314	-2.15619
C	6.0	3.29497	7.09395	-2.45847
C	6.0	2.83863	6.65365	-3.71305
C	6.0	3.75749	6.20138	-4.68230
C	6.0	5.13185	6.18857	-4.38438
C	6.0	5.58691	6.63306	-3.12738
C	6.0	7.84068	8.83405	-1.78076
C	6.0	10.09607	5.84994	0.50388
C	6.0	4.34801	9.39419	-0.33860
H	1.0	6.89503	3.81985	-1.95823
H	1.0	5.61639	1.85964	-1.16031
H	1.0	5.50375	1.33293	1.28270
H	1.0	6.66727	2.82057	2.92183
H	1.0	7.94590	4.77831	2.14128
H	1.0	9.74715	3.37165	-1.41727
H	1.0	10.81444	2.57527	-3.49980

```
H     1.0    10.90583     4.05296    -5.51695
H     1.0     9.92180     6.35052    -5.40907
H     1.0     8.87666     7.16245    -3.33638
H     1.0     3.98149     4.99862    -0.63624
H     1.0     2.73790     3.61779     0.99106
H     1.0     2.34048     4.44980     3.31603
H     1.0     3.23191     6.68812     3.99363
H     1.0     4.47629     8.07404     2.37833
H     1.0     2.56722     7.41701    -1.71719
H     1.0     1.77373     6.66052    -3.93190
H     1.0     3.40419     5.86442    -5.65381
H     1.0     5.84950     5.84186    -5.12391
H     1.0     6.64939     6.62192    -2.91673
H     1.0    10.60000     4.89586     0.31441
H     1.0     9.81518     5.88015     1.56315
H     1.0     3.94833     9.47299     0.67791
H     1.0     3.50022     9.37783    -1.02964
H     1.0     7.33331     8.01452     1.61113
H     1.0     7.62802     7.30800     1.41007
 $END
 $ECP
 MN-ECP GEN     10     2
 3      ----- d potential     -----
   -10.0000000        1    357.3914469
   -60.2990287        2     64.6477389
   -10.4217834        2     16.0960833
 5      ----- s-d potential     -----
     3.0000000        0    107.4127215
    16.2591819        1    111.4958973
   276.9373928        2     46.5568346
   241.3174342        2      8.3688135
  -146.4635329        2      7.7237489
 5      ----- p-d potential     -----
     5.0000000        0     80.0415103
     5.7589756        1    105.6043646
   285.2918654        2     40.8300466
   143.4222647        2      8.0098457
   -88.7031851        2      7.3390928
 P-ECP GEN     10     2
 5      ----- d   potential     -----
   -10.0000000        1    462.1211423
   -79.4864658        2     93.6863701
   -28.3668251        2     21.2349094
    -9.8577589        2      6.3388415
    -1.0163783        2      2.0620684
 5      ----- s-d potential     -----
     3.0000000        0     78.0831823
    12.9104154        1     58.9576810
   150.0250298        2     36.0571255
    71.7083146        2     11.2464453
    23.0397012        2      2.6757561
```

```
 6      ----- p-d potential     -----
     5.0000000        0     75.1617880
     6.3446507        1     57.4544041
   198.5585104        2     47.9481748
   111.1470820        2     18.4588360
    40.3944144        2      5.9414190
     6.4483233        2      1.8487507
P-ECP
C-ECP NONE
C-ECP NONE
C-ECP NONE
C-ECP NONE
C-ECP NONE
C-ECP NONE
C-ECP NONE
C-ECP NONE
C-ECP NONE
C-ECP NONE
C-ECP NONE
C-ECP NONE
C-ECP NONE
C-ECP NONE
C-ECP NONE
C-ECP NONE
C-ECP NONE
C-ECP NONE
C-ECP NONE
C-ECP NONE
C-ECP NONE
C-ECP NONE
C-ECP NONE
C-ECP NONE
C-ECP NONE
C-ECP NONE
H-ECP NONE
H-ECP NONE
H-ECP NONE
H-ECP NONE
H-ECP NONE
H-ECP NONE
H-ECP NONE
H-ECP NONE
H-ECP NONE
H-ECP NONE
H-ECP NONE
H-ECP NONE
H-ECP NONE
H-ECP NONE
H-ECP NONE
H-ECP NONE
H-ECP NONE
```

```
H-ECP NONE
H-ECP NONE
H-ECP NONE
H-ECP NONE
H-ECP NONE
H-ECP NONE
H-ECP NONE
P-ECP
P-ECP
O-ECP NONE
C-ECP NONE
C-ECP NONE
C-ECP NONE
C-ECP NONE
C-ECP NONE
C-ECP NONE
C-ECP NONE
C-ECP NONE
C-ECP NONE
C-ECP NONE
C-ECP NONE
C-ECP NONE
C-ECP NONE
C-ECP NONE
C-ECP NONE
C-ECP NONE
C-ECP NONE
C-ECP NONE
C-ECP NONE
C-ECP NONE
C-ECP NONE
C-ECP NONE
C-ECP NONE
C-ECP NONE
C-ECP NONE
C-ECP NONE
C-ECP NONE
H-ECP NONE
H-ECP NONE
H-ECP NONE
H-ECP NONE
H-ECP NONE
H-ECP NONE
H-ECP NONE
H-ECP NONE
H-ECP NONE
H-ECP NONE
H-ECP NONE
H-ECP NONE
H-ECP NONE
H-ECP NONE
```

```
H-ECP NONE
H-ECP NONE
H-ECP NONE
H-ECP NONE
H-ECP NONE
H-ECP NONE
H-ECP NONE
H-ECP NONE
H-ECP NONE
H-ECP NONE
H-ECP NONE
H-ECP NONE
 $END
```

```
!   Input file for GAMESS - [FeHdppe2]+ total energy
 $CONTRL SCFTYP=RHF RUNTYP=ENERGY EXETYP=RUN
    MAXIT=200 ICHARG=1 ECP=READ MPLEVL=2 $END
 $SYSTEM MEMDDI=4000 MWORDS=50 PARALL=.TRUE. $END
 $BASIS GBASIS=LANL2DZ EXTFIL=.T. NDFUNC=1 NPFUNC=1 $END
 $GUESS GUESS=HUCKEL $END
 $SCF DIRSCF=.T. CONV=5.0e-6 DAMP=.T. $END
 $STATPT OPTTOL=0.0001 NSTEP=100 TRMIN=0.01 $END
 $FORCE METHOD=SEMINUM VIBSIZ=0.010000 SCLFAC=0.960000 NVIB=2 $END
 $DATA
[FeHdppe2]+
C1
Fe    26.0     7.17168     8.36120     2.15485
P    15.0     7.63169    10.03577     3.76677
P    15.0     6.74479     6.62234     3.75390
P    15.0     7.48298    10.13150     0.56603
P    15.0     6.90199     6.63269     0.54478
C     6.0     7.56996    11.76737     1.55802
C     6.0     6.94193     4.97393     1.49593
H     1.0     8.02431    12.53977     0.92891
H     1.0     6.55830     4.18026     0.84642
H     1.0     6.55350    12.08928     1.80977
H     1.0     7.98298     4.73821     1.74047
C     6.0     8.87503     9.78535     5.15714
C     6.0     5.41708     6.85150     5.07310
C     6.0    10.24656     9.68658     4.83255
C     6.0     4.05199     6.83013     4.70696
H     1.0    10.57850     9.75114     3.79854
H     1.0     3.75373     6.63591     3.67845
C     6.0     6.11872    10.48553    -0.68796
C     6.0     8.19918     6.33903    -0.78829
C     6.0     9.08120    10.26428    -0.42313
C     6.0     5.24935     6.46508    -0.34510
C     6.0     8.47746     9.67266     6.50626
C     6.0     5.76109     7.10802     6.41823
H     1.0     7.42813     9.75344     6.77672
H     1.0     6.80403     7.12393     6.72258
C     6.0     6.25138    10.10097    -2.03994
C     6.0     7.94726     6.62073    -2.14757
H     1.0     7.17547     9.64986    -2.39116
H     1.0     6.97507     6.99227    -2.46041
C     6.0     5.17118    12.65483     5.93809
C     6.0     9.02087     4.08797     6.18725
H     1.0     5.29937    13.52104     6.58246
H     1.0     8.82847     3.26699     6.87367
C     6.0     6.30054    12.00311     5.41158
C     6.0     7.94429     4.74546     5.56673
H     1.0     7.29272    12.37253     5.66211
H     1.0     6.92823     4.42663     5.78957
C     6.0     3.85903    11.29830    -1.16995
C     6.0    10.46219     5.61962    -1.38116
```

```
H     1.0     2.93994    11.76946    -0.82924
H     1.0    11.42992     5.22616    -1.07879
C     6.0    10.80594     9.39066     7.18856
C     6.0     3.39954     7.29479     7.01234
H     1.0    11.54769     9.24560     7.97003
H     1.0     2.62587     7.45763     7.75855
C     6.0     4.85137    10.40700     4.27969
C     6.0     9.50658     6.21346     4.40679
H     1.0     4.71591     9.52263     3.66077
H     1.0     9.68999     7.03274     3.71935
C     6.0     8.38819    11.52183     2.83306
C     6.0     6.09952     5.11298     2.77129
H     1.0     8.37847    12.39948     3.48781
H     1.0     6.17048     4.22113     3.40250
H     1.0     9.43063    11.28733     2.59248
H     1.0     5.04403     5.27121     2.52325
C     6.0     9.27002    11.32606    -1.33870
C     6.0     4.97831     5.36924    -1.19685
H     1.0     8.46965    12.03736    -1.53158
H     1.0     5.74679     4.62617    -1.39961
C     6.0    11.20621     9.49627     5.84253
C     6.0     3.04974     7.04665     5.67098
H     1.0    12.25963     9.43363     5.58015
H     1.0     2.00325     7.01445     5.37700
C     6.0     4.00109    10.92016    -2.51903
C     6.0    10.20389     5.89668    -2.73773
H     1.0     3.19244    11.09448    -3.22437
H     1.0    10.97056     5.71956    -3.48792
C     6.0     4.90887    11.07736    -0.25892
C     6.0     9.46885     5.84593    -0.41173
H     1.0     4.77161    11.37866     0.77773
H     1.0     9.69639     5.63926     0.63164
C     6.0     9.43955     9.47623     7.51580
C     6.0     4.75773     7.32504     7.38124
H     1.0     9.12286     9.39704     8.55301
H     1.0     5.03713     7.51107     8.41558
C     6.0     3.87674    12.18593     5.63306
C     6.0    10.34552     4.48964     5.91799
H     1.0     3.00441    12.69072     6.04093
H     1.0    11.17749     3.97907     6.39706
C     6.0     5.19974    10.31968    -2.94915
C     6.0     8.94574     6.40127    -3.11601
H     1.0     5.31871    10.02645    -3.98949
H     1.0     8.73822     6.61769    -4.16124
C     6.0     3.71907    11.05922     4.80525
C     6.0    10.58435     5.55325     5.02905
H     1.0     2.72441    10.68411     4.57718
H     1.0    11.60286     5.87230     4.82122
C     6.0    10.13014     9.35278    -0.19282
C     6.0     4.23828     7.41951    -0.11071
H     1.0     9.98747     8.53741     0.50870
```

```
H     1.0     4.43571     8.28214     0.52127
C     6.0     6.14925    10.87354     4.57462
C     6.0     8.18175     5.81446     4.67070
C     6.0    11.35621     9.49749    -0.87106
C     6.0     2.97261     7.28335    -0.71356
H     1.0    12.15776     8.78546    -0.69024
H     1.0     2.20434     8.03091    -0.53269
C     6.0    10.49353    11.46672    -2.01671
C     6.0     3.71579     5.23318    -1.80054
H     1.0    10.63049    12.28419    -2.72031
H     1.0     3.51867     4.38856    -2.45612
C     6.0    11.54150    10.55227    -1.78279
C     6.0     2.70839     6.18974    -1.55842
H     1.0    12.48825    10.66358    -2.30587
H     1.0     1.73300     6.08410    -2.02704
H     1.0     8.63123     8.02756     2.14222
 $END
 $ECP
 FE-ECP GEN     10     2
 3      ----- d potential     -----
   -10.0000000        1    392.6149787
   -63.2667518        2     71.1756979
   -10.9613338        2     17.7320281
 5      ----- s-d potential     -----
     3.0000000        0    126.0571895
    18.1729137        1    138.1264251
   339.1231164        2     54.2098858
   317.1068012        2      9.2837966
  -207.3421649        2      8.6289082
 5      ----- p-d potential     -----
     5.0000000        0     83.1759490
     5.9535930        1    106.0559938
   294.2665527        2     42.8284937
   154.4244635        2      8.7701805
   -95.3164249        2      8.0397818
 P-ECP GEN     10     2
 5      ----- d   potential     -----
   -10.0000000        1    462.1211423
   -79.4864658        2     93.6863701
   -28.3668251        2     21.2349094
    -9.8577589        2      6.3388415
    -1.0163783        2      2.0620684
 5      ----- s-d potential     -----
     3.0000000        0     78.0831823
    12.9104154        1     58.9576810
   150.0250298        2     36.0571255
    71.7083146        2     11.2464453
    23.0397012        2      2.6757561
 6      ----- p-d potential     -----
     5.0000000        0     75.1617880
     6.3446507        1     57.4544041
```

```
   198.5585104         2     47.9481748
   111.1470820         2     18.4588360
    40.3944144         2      5.9414190
     6.4483233         2      1.8487507
P-ECP
P-ECP
P-ECP
C-ECP NONE
C-ECP NONE
H-ECP NONE
H-ECP NONE
H-ECP NONE
H-ECP NONE
C-ECP NONE
C-ECP NONE
C-ECP NONE
C-ECP NONE
H-ECP NONE
H-ECP NONE
C-ECP NONE
C-ECP NONE
C-ECP NONE
C-ECP NONE
C-ECP NONE
C-ECP NONE
H-ECP NONE
H-ECP NONE
C-ECP NONE
C-ECP NONE
H-ECP NONE
H-ECP NONE
C-ECP NONE
C-ECP NONE
H-ECP NONE
H-ECP NONE
C-ECP NONE
C-ECP NONE
H-ECP NONE
H-ECP NONE
C-ECP NONE
C-ECP NONE
H-ECP NONE
H-ECP NONE
C-ECP NONE
C-ECP NONE
H-ECP NONE
H-ECP NONE
C-ECP NONE
C-ECP NONE
H-ECP NONE
H-ECP NONE
```

```
C-ECP NONE
C-ECP NONE
H-ECP NONE
H-ECP NONE
H-ECP NONE
H-ECP NONE
C-ECP NONE
C-ECP NONE
H-ECP NONE
H-ECP NONE
C-ECP NONE
C-ECP NONE
H-ECP NONE
H-ECP NONE
C-ECP NONE
C-ECP NONE
H-ECP NONE
H-ECP NONE
C-ECP NONE
C-ECP NONE
H-ECP NONE
H-ECP NONE
C-ECP NONE
C-ECP NONE
H-ECP NONE
H-ECP NONE
C-ECP NONE
C-ECP NONE
H-ECP NONE
H-ECP NONE
C-ECP NONE
C-ECP NONE
H-ECP NONE
H-ECP NONE
C-ECP NONE
C-ECP NONE
H-ECP NONE
H-ECP NONE
C-ECP NONE
C-ECP NONE
H-ECP NONE
H-ECP NONE
C-ECP NONE
C-ECP NONE
C-ECP NONE
C-ECP NONE
H-ECP NONE
H-ECP NONE
C-ECP NONE
C-ECP NONE
H-ECP NONE
```

```
H-ECP NONE
C-ECP NONE
C-ECP NONE
H-ECP NONE
H-ECP NONE
H-ECP NONE
 $END
 $VIB
         IVIB=   0 IATOM=   0 ICOORD=   0 E=    -2158.5076639139
 9.367530189E-07 9.437550664E-06 1.183524052E-05-2.217125480E-06-1.393143827E-05
 8.969250960E-06-8.914897361E-06-7.180886026E-06 1.964244714E-05-2.019309454E-05
-2.200343407E-05-2.024153763E-05 5.197725439E-06 7.665886404E-06-1.117651352E-05
 1.703342758E-07-2.779189516E-06-8.260752603E-06-1.301263341E-05-5.793965372E-06
-7.879656426E-08-9.475930443E-06 5.070088457E-06-1.026168429E-06-1.828723919E-05
 2.470810479E-06 1.248369570E-05-9.928059722E-06-2.696477066E-06 5.024477027E-06
-6.426644111E-06-5.118567863E-06 6.807462932E-06-3.537376520E-07 6.507341368E-06
-5.384008324E-06 1.146860983E-05 6.313794499E-05-5.144875788E-06-6.861339106E-08
 1.609093260E-05 7.965492240E-07-7.258652939E-06 5.607198057E-05 7.403953480E-06
-2.716029881E-06-2.019405892E-06-9.967761280E-06-7.520580946E-06 6.435296789E-06
 1.776732811E-05-9.754999360E-06 2.402099195E-05-6.219519412E-06 1.361105430E-05
 1.947946715E-05 2.023124812E-05 1.323347804E-05 5.161914971E-05 4.530455025E-05
-2.737060488E-05-4.887519050E-05 5.560611573E-05 6.176356885E-06-6.554464654E-06
-2.798234971E-06-1.557221422E-06-6.842192971E-05 3.508393779E-05 6.913730225E-07
-6.360187276E-06-3.092543740E-06 1.350057637E-05-3.178033287E-06 2.119551995E-07
-8.661829548E-06-1.968647446E-05 5.132046360E-06 1.503351376E-05-4.803463560E-05
 3.334606969E-06-9.679756975E-06 8.501365192E-06-2.136113349E-07 2.369090846E-05
 1.053571169E-05 4.595116623E-06-2.841854675E-06 1.518429612E-05-1.322717689E-05
-2.138084021E-06-4.032781320E-06 2.603076118E-05 1.055992776E-05-9.820221770E-07
 1.452556095E-05 1.844392156E-06-2.098711406E-05-3.429053548E-05 5.948755349E-06
-4.360870520E-05 7.275242073E-05 1.921168405E-05-2.360836992E-06-1.406492575E-05
 6.326531624E-06 1.937501678E-06-7.860539846E-07-2.744227335E-06 1.924266843E-06
 2.562363440E-06 9.357401527E-06 1.842806858E-05-5.178726504E-06 9.188492993E-06
 1.087387233E-05 2.068134102E-05-1.415432878E-05-1.110655980E-05 2.745606493E-06
 1.395510820E-05-1.350421068E-05 4.039167899E-05-1.211980920E-06 1.511718815E-05
-6.349355489E-06 2.246782819E-06-2.574696890E-05 3.060664588E-05 8.923605088E-06
-1.187407104E-05-7.777436417E-06 1.513645113E-05 2.842338152E-05 1.491935898E-05
 1.185943282E-05-4.385321362E-05 8.212644347E-05-1.376685131E-05-1.135452251E-05
 1.853682774E-05-9.811794797E-06 2.763798404E-05-2.571508022E-05-4.130894291E-06
 6.453411726E-06-1.146156651E-05-1.082925588E-05 1.022736960E-05-2.547500752E-06
-1.715107004E-05-8.746567960E-07 2.118476587E-06-2.421998593E-06-3.559399641E-07
-2.589649997E-06-1.793906106E-05 6.351150715E-06 4.691491550E-06-3.949823211E-06
-1.199287516E-06-4.163681903E-06-6.914141782E-06 1.240416307E-05 8.511142873E-06
 1.310993896E-07 2.650500737E-05 3.081475067E-05 2.806780017E-05 2.229011871E-05
-5.709568353E-05-1.455702722E-05-7.917870507E-06-1.064896621E-05 8.632740651E-06
 1.514773655E-06-6.023976391E-06-6.013063107E-06-5.665534713E-05-1.709697933E-05
 6.167349456E-06-7.098556822E-05 2.443575573E-05 4.344700328E-06 1.453692793E-05
-9.871117998E-06 4.743395993E-06 6.464647675E-05 1.151780614E-05-1.581963511E-05
 7.778763534E-06-1.260988429E-05 1.883039552E-05-2.110772299E-06 2.489083444E-05
-1.403676685E-05-1.039554653E-05 4.596221034E-06 2.703073718E-05-1.147501410E-05
 3.328903707E-05-2.823721974E-05-3.203150235E-05 2.411009760E-05 1.522776674E-06
-2.154038506E-05 3.233570314E-05-5.524507176E-06 5.096150297E-06-7.159167589E-06
```

```
!   Input file for GAMESS - [FeH(H2)dppe2]+ total energy
 $CONTRL SCFTYP=RHF RUNTYP=ENERGY EXETYP=RUN MPLEVL=2
    MAXIT=200 ICHARG=1 ECP=READ $END
 $SYSTEM MEMDDI=5000 MWORDS=75 PARALL=.TRUE. $END
 $BASIS GBASIS=LANL2DZ EXTFIL=.T. NDFUNC=1 NPFUNC=1 $END
 $GUESS GUESS=HUCKEL $END
 $SCF DIRSCF=.TRUE. CONV=5.0e-6 DAMP=.T. $END
 $STATPT OPTTOL=0.0001 NSTEP=100 TRMIN=0.01 $END
 $FORCE METHOD=SEMINUM VIBSIZ=0.010000 SCLFAC=0.960000 NVIB=2 $END
 $DATA
[FeH(H2)dppe2]+
C1
Fe    26.0     6.97167     8.39792     2.15327
P    15.0     7.54614    10.05383     3.76618
P    15.0     6.64272     6.67353     3.76011
P    15.0     7.35390    10.12366     0.54925
P    15.0     6.83222     6.64351     0.54574
C     6.0     7.43224    11.75571     1.53864
C     6.0     6.83850     5.00383     1.53105
H     1.0     7.85410    12.54044     0.90219
H     1.0     6.46173     4.20151     0.88973
H     1.0     6.41868    12.05642     1.82650
H     1.0     7.87203     4.76484     1.80209
C     6.0     8.86552     9.74790     5.07736
C     6.0     5.35766     6.88789     5.12295
C     6.0    10.22197     9.64709     4.69699
C     6.0     3.98417     6.88905     4.78906
H     1.0    10.51330     9.73493     3.65276
H     1.0     3.66063     6.72680     3.76263
C     6.0     6.02789    10.48040    -0.74263
C     6.0     8.23188     6.36007    -0.68614
C     6.0     8.97986    10.25492    -0.39300
C     6.0     5.27669     6.38382    -0.50292
C     6.0     8.52137     9.60631     6.43870
C     6.0     5.73567     7.10461     6.46570
H     1.0     7.48523     9.69195     6.75457
H     1.0     6.78546     7.10441     6.74542
C     6.0     6.19450    10.09710    -2.09106
C     6.0     8.06734     6.63618    -2.06000
H     1.0     7.12366     9.63826    -2.41801
H     1.0     7.11279     6.99409    -2.43652
C     6.0     5.51274    12.84594     6.14814
C     6.0     8.99841     4.11143     6.08724
H     1.0     5.77436    13.73602     6.71517
H     1.0     8.82745     3.29289     6.78220
C     6.0     6.51645    12.12801     5.47512
C     6.0     7.90265     4.78760     5.52282
H     1.0     7.54700    12.46793     5.55040
H     1.0     6.89431     4.48314     5.79481
C     6.0     3.78699    11.30822    -1.28366
C     6.0    10.53277     5.65456    -1.12847
```

```
H     1.0     2.86212    11.78432    -0.96654
H     1.0    11.48110     5.26708    -0.76337
C     6.0    10.87122     9.29365     7.02321
C     6.0     3.39033     7.29636     7.12061
H     1.0    11.64194     9.12619     7.77149
H     1.0     2.63583     7.44472     7.88914
C     6.0     4.85498    10.53670     4.68639
C     6.0     9.42735     6.22956     4.28478
H     1.0     4.58614     9.63399     4.14808
H     1.0     9.58976     7.04663     3.58961
C     6.0     8.29618    11.50808     2.78266
C     6.0     5.97585     5.16974     2.78957
H     1.0     8.33587    12.39529     3.42174
H     1.0     6.02400     4.28176     3.42847
H     1.0     9.32163    11.24704     2.50031
H     1.0     4.92672     5.34544     2.52624
C     6.0     9.18193    11.30107    -1.32399
C     6.0     5.14661     5.21233    -1.28699
H     1.0     8.37713    11.99435    -1.55903
H     1.0     5.96210     4.49457    -1.34482
C     6.0    11.21902     9.42856     5.66498
C     6.0     3.00660     7.08846     5.78138
H     1.0    12.26129     9.36715     5.36108
H     1.0     1.95332     7.07367     5.51133
C     6.0     3.96273    10.92987    -2.62907
C     6.0    10.36154     5.92608    -2.50007
H     1.0     3.17409    11.10953    -3.35540
H     1.0    11.17594     5.75047    -3.19852
C     6.0     4.81120    11.08016    -0.34577
C     6.0     9.47738     5.87812    -0.22596
H     1.0     4.64948    11.38176     0.68722
H     1.0     9.63741     5.67683     0.83076
C     6.0     9.51965     9.38033     7.40529
C     6.0     4.75694     7.30474     7.45769
H     1.0     9.24212     9.28092     8.45197
H     1.0     5.06197     7.46264     8.48937
C     6.0     4.17232    12.41216     6.09076
C     6.0    10.31409     4.49104     5.75115
H     1.0     3.39617    12.96740     6.61181
H     1.0    11.16096     3.96629     6.18674
C     6.0     5.16865    10.32265    -3.02777
C     6.0     9.12777     6.42196    -2.96087
H     1.0     5.31265    10.02769    -4.06438
H     1.0     8.98634     6.63413    -4.01795
C     6.0     3.84811    11.25267     5.36390
C     6.0    10.52446     5.55153     4.85142
H     1.0     2.82038    10.89992     5.32751
H     1.0    11.53631     5.85452     4.59285
C     6.0    10.03728     9.37060    -0.10588
C     6.0     4.21477     7.30932    -0.47990
H     1.0     9.88499     8.56838     0.60859
```

```
H     1.0     4.30044     8.23077     0.08649
C     6.0     6.19532    10.96957     4.72772
C     6.0     8.11122     5.85378     4.61600
C     6.0    11.28280     9.52277    -0.74613
C     6.0     3.03553     7.06456    -1.21190
H     1.0    12.08956     8.82824    -0.52513
H     1.0     2.22831     7.79238    -1.18859
C     6.0    10.42546    11.45141    -1.96198
C     6.0     3.97094     4.96619    -2.01620
H     1.0    10.57147    12.25709    -2.67729
H     1.0     3.88637     4.06064    -2.61205
C     6.0    11.48052    10.56130    -1.67400
C     6.0     2.90727     5.89058    -1.97580
H     1.0    12.44170    10.67766    -2.16891
H     1.0     1.99611     5.69889    -2.53717
H     1.0     8.44932     8.07448     2.15763
H     1.0     5.26921     8.36457     2.02598
H     1.0     5.42761     9.12683     2.24373
 $END
 $ECP
 FE-ECP GEN     10     2
 3      ----- d potential     -----
   -10.0000000        1    392.6149787
   -63.2667518        2     71.1756979
   -10.9613338        2     17.7320281
 5      ----- s-d potential     -----
     3.0000000        0    126.0571895
    18.1729137        1    138.1264251
   339.1231164        2     54.2098858
   317.1068012        2      9.2837966
  -207.3421649        2      8.6289082
 5      ----- p-d potential     -----
     5.0000000        0     83.1759490
     5.9535930        1    106.0559938
   294.2665527        2     42.8284937
   154.4244635        2      8.7701805
   -95.3164249        2      8.0397818
 P-ECP GEN     10     2
 5      ----- d   potential     -----
   -10.0000000        1    462.1211423
   -79.4864658        2     93.6863701
   -28.3668251        2     21.2349094
    -9.8577589        2      6.3388415
    -1.0163783        2      2.0620684
 5      ----- s-d potential     -----
     3.0000000        0     78.0831823
    12.9104154        1     58.9576810
   150.0250298        2     36.0571255
    71.7083146        2     11.2464453
    23.0397012        2      2.6757561
 6      ----- p-d potential     -----
```

```
      5.0000000        0     75.1617880
      6.3446507        1     57.4544041
    198.5585104        2     47.9481748
    111.1470820        2     18.4588360
     40.3944144        2      5.9414190
      6.4483233        2      1.8487507
P-ECP
P-ECP
P-ECP
C-ECP NONE
C-ECP NONE
H-ECP NONE
H-ECP NONE
H-ECP NONE
H-ECP NONE
C-ECP NONE
C-ECP NONE
C-ECP NONE
C-ECP NONE
H-ECP NONE
H-ECP NONE
C-ECP NONE
C-ECP NONE
C-ECP NONE
C-ECP NONE
C-ECP NONE
C-ECP NONE
H-ECP NONE
H-ECP NONE
C-ECP NONE
C-ECP NONE
H-ECP NONE
H-ECP NONE
C-ECP NONE
C-ECP NONE
H-ECP NONE
H-ECP NONE
C-ECP NONE
C-ECP NONE
H-ECP NONE
H-ECP NONE
C-ECP NONE
C-ECP NONE
H-ECP NONE
H-ECP NONE
C-ECP NONE
C-ECP NONE
H-ECP NONE
H-ECP NONE
C-ECP NONE
C-ECP NONE
```

```
H-ECP NONE
H-ECP NONE
C-ECP NONE
C-ECP NONE
H-ECP NONE
H-ECP NONE
H-ECP NONE
H-ECP NONE
C-ECP NONE
C-ECP NONE
H-ECP NONE
H-ECP NONE
C-ECP NONE
C-ECP NONE
H-ECP NONE
H-ECP NONE
C-ECP NONE
C-ECP NONE
H-ECP NONE
H-ECP NONE
C-ECP NONE
C-ECP NONE
H-ECP NONE
H-ECP NONE
C-ECP NONE
C-ECP NONE
H-ECP NONE
H-ECP NONE
C-ECP NONE
C-ECP NONE
H-ECP NONE
H-ECP NONE
C-ECP NONE
C-ECP NONE
H-ECP NONE
H-ECP NONE
C-ECP NONE
C-ECP NONE
H-ECP NONE
H-ECP NONE
C-ECP NONE
C-ECP NONE
H-ECP NONE
H-ECP NONE
C-ECP NONE
C-ECP NONE
C-ECP NONE
C-ECP NONE
H-ECP NONE
H-ECP NONE
C-ECP NONE
```

```
C-ECP NONE
H-ECP NONE
H-ECP NONE
C-ECP NONE
C-ECP NONE
H-ECP NONE
H-ECP NONE
H-ECP NONE
H-ECP NONE
H-ECP NONE
 $END
```

Bibliography

[1] Schlapbach, L.; Zuttel, A. *Nature* **2001**, *414*, 353.

[2] Satyapal, S.; Petrovic, J.; Read, C.; Thomas, G.; Ordaz, G. *Catalysis Today* **2007**, *120*, 246.

[3] Zuttel, A. *Materials Today* **2003**, 6, 24.

[4] US Department of Energy Hydrogen, Fuel Cells and Infrastructure Technologies Program Multiyear Research, Development and Demonstration Plan, **2009**, http://www1.eere.energy.gov/hydrogenandfuelcells/mypp (accessed October 31, 2012).

[5] Long, J.; Dinca, M. *Angew Chem Int Ed* **2008**, *47*, 6766.

[6] Sieverts, A.*Z Phys Chem-Stoch Ve* **1907**, *60*, 129.

[7] Blach, T. P.; Gray, E. MacA. *J. Alloys Compd.* **2007**, *446–447*, 692.

[8] Vajo, J. J.; Mertens, F.; Ahn, C. C.; Bowman Jr., R. C.; Fultz, B. *J. Phys. Chem. B* **2004**, *108*, 13977.

[9] Graetz, J.; Wegrzyn, J.; Reilly J. J. *J. Am. Chem. Soc.* **2008**, *130*, 17790.

[10] Shaw, L. L.; Wan, X.; Hu, J. Z.; Kwak, J. H.; Yang, Z. *J. Phys. Chem. C* **2010**, *114*, 8089.

[11] Bogdanović, B.; Schwickardi, M. *J. Alloys Compd.* **1997**, *253-254*, 1.

[12] Sakintuna, B.; Lamari-Darkrim, F.; Hirscher, M. *Int. J. Hydrogen Energy* **2007**, *32*, 1121.

[13] Kaye, S. S.; Long, J. R. *J. Am. Chem. Soc.* **2005**, *127*, 6506.

[14] Hino, S.; Ichikawa, T.; Tokoyoda, K.; Kojima, Y.; Fujii, H. *J. Alloys Compd.* **2007**, *446–447*, 342.

[15] Mosegaard, L.; Møller, B.; Jørgensen, J.-E.; Bŏsenberg, U.; Dornheim, M.; Hanson, J. C.; Cerenius, Y.; Walker, G.; Jakobsen, H. J.; Besenbacher, F.; Jensen, T. R. *J. Alloys Compd.* **2007**, *446–447*, 301.

[16] Alapati, S.V.; Johnson, J.K.; Sholl, D.S. *J Alloy Compd* **2007**, *446*, 23.

[17] Alapati, S.V.; Johnson, J.K.; Sholl, D.S. *J Phys Chem C* **2007**, *111*, 1584.

[18] Bowman Jr., R. C.; Fultz, B. *MRS Bulletin* **2002**, *27*, 688.

[19] Sandrock, G. *J. Alloys Compd.* **1999**, *293–295*, 877.

[20] Ozolins, V.; Majzoub, E. H.; Wolverton, C. *Phys. Review Letters* **2008**, *100*, 135501.

[21] Lemmon, E.; Huber, M.; McLinden, M. *2007 NIST Standard Reference Database 23: Reference Fluid Thermodynamics and Transport Properties—REFPROP*, Number version 8.0 in Standard Reference Data Program, National Institute of Standards and Technology, Gaithersburg, MD, USA.

[22] Zuttel, A.; Wenger, P.; Rentsch, S.; Sudan, P.; Mauron, Ph.; Emmenegger, Ch. *J. Power Sources* **2003**, *118*, 1.

[23] Li, H.-W.; Yan, Y.; Orimo, S.-I.; Zuttel, A.; Jensen, C. M. *Energies* **2011**, *4*, 185.

[24] Sousa, T.; Fernandes, V. R.; Pinto, P. J. R.; Slavkov, Y.; Bosukov, L.; Rangel, C. M. *Chem. Eng. Sci.* **2012**, *84*, 70.

[25] Vajo, J. J.; Skeith, S. L.; Mertens, F. *J. Phys. Chem. B* **2005**, *109*, 3719.

[26] Rönnebro, E.; Majzoub, E. H. *J. Phys. Chem. B* **2007**, *111*, 12045.

[27] Au, M.; Jurgensen, A. R.; Spencer, W. A.; Anton, D. L.; Pinkerton, F. E.; Hwang, S.-J.; Kim, C.; Bowman Jr., R. C. *J. Phys. Chem. C* **2008**, *112*, 18661.

[28] Hwang, S.-J.; Bowman Jr., R. C.; Reiter, J. W.; Rijssenbeek, J.; Soloveichik, G. L.; Zhao, J.-C.; Kabbour, H.; Ahn, C. C. *J. Phys. Chem. C* **2008**, *112*, 3164.

[29] Capurso, G.; Agresti, F.; Crociani, L.; Rossetto, G.; Schiavo, B.; Maddelena, A.; Russo, S. L.; Principi, G. *Int. J. Hydrogen Energy* **2012**, *37*, 10768.

[30] Au, M.; Jurgensen, A.; Zeigler, K. *J. Phys. Chem. B* **2006**, *110*, 26482.

[31] Wong, B. M.; Lacina, D.; Nielson, I. M. B.; Graetz, J.; Allendorf, M. D. *J. Phys. Chem. C Nanomater. Interfaces* **2011**, *115*, 7778.

[32] Graetz, J.; Reilly, J. J. *J. Alloys Compd.* **2006**, *424*, 262.

[33] Lacina, D.; Wegrzyn, J.; Reilly, J.; Celebi, Y.; Graetz, J. *Energy Environ. Sci.* **2010**, *3*, 1099.

[34] Bogdanovic, B.; Brand, R. A.; Marjanovic, A.; Schwikardi, M.; Tölle, J. *J. Alloys Compd.* **2000**, *302*, 36.

[35] Graetz, J.; Lee, Y.; Reilly, J. J.; Park, S.; Vogt, T. *Phys. Review B* **2005**, *71*, 184115.

[36] Sulic, M.; Cai, M.; Kumar, S. *Int. J. Hydrogen Energy* **2012**, *37*, 15187.

[37] Sandrock, G.; Gross, K.; Thomas, G.; Jensen, C.; Meeker, D.; Takara, S. *J. Alloys Compd.* **2002**, *330–332*, 696.

[38] Varin, R. A.; Parviz, R. *Int. J. Hydrogen Energy* **2012**, *37*, 9088.

[39] Fu, J.; Röntzsch, L.; Schmidt, T.; Weißgärber, T.; Kieback, B. *J. Alloys Compd.* **2012**, *525*, 73.

[40] Chen, P.; Xiong, Z.; Luo, J.; Lin, J.; Tan, K. L. *Nature* **2002**, *420*, 302.

[41] Leng, H. Y.; Ichikawa, T.; Hino, S.; Hanada, N.; Isobe, S.; Fujii, H. *J. Phys. Chem. B* **2004**, *108*, 8763.

[42] Wolf, G.; Baumann, J.; Baitalow, F.; Hoffman, F. P. *Themochim. Acta* **2000**, *343*, 19.

[43] Denney, M. C.; Pons, V.; Hebden, T. J.; Heinekey, D. M.; Goldberg, K. I. *J. Am. Chem. Soc.* **2006**, *128*, 12048.

[44] Keaton, R. J.; Blacquiere, J. M.; Baker, R. T. *J. Am. Chem. Soc.* **2007**, *129*, 1844.

[45] Davis, B. L.; Dixon, D. A.; Garner, E. B.; Gordon, J. C.; Matus, M. H.; Scott, B.; Stephens, F. H. *Angew. Chem. Int. Ed.* **2009**, *48*, 6812.

[46] Sutton, A. D.; Davis, B. L.; Bhattacharyya, K. X.; Ellis, B. D.; Gordon, J. C.; Power, P. P. *Chem. Commun.* **2010**, *46*, 148.

[47] Sutton, A. D.; Burrell, A. K.; Dixon, D. A.; Garner III, E. B.; Gordon, J. C.; Nakagawa, T.; Ott, K. C.; Robinson, J. P.; Vasiliu, M. *Science* **2011**, *331*, 1426.

[48] Ibikunle, A.; Goudy, A. J.; Yang, H. *J. Alloys Compd.* **2009**, *475*, 110.

[49] Mao, J.; Guo, Z.; Yu, X.; Liu, H. *J. Phys. Chem. C* **2011**, *115*, 9283.

[50] Hirscher, M.; Panella, B. *Scripta Mater.* **2007**, *56*, 809.

[51] Stadie, N. P.; Purewal, J. J.; Ahn, C. C.; Fultz, B. *Langmuir* **2010**, *26*, 15481.

[52] Purewal, J. J.; Keith, J. B.; Ahn, C. C.; Fultz, B.; Brown, C. M.; Tyagi, M. *Phys. Rev. B* **2009**, *79*, 054305.

[53] Im, J. S.; Park S.-J.; Lee, Y.-S. *Int. J. Hydrogen Energy* **2009**, *34*, 1423.

[54] Gogotsi, Y.; Portet, C.; Osswald, S.; Simmons, J. M.; Yildirim, T.; Laudisio, G.; Fischer, J. E. *Int. J. Hydrogen Energy* **2009**, *34*, 6314.

[55] Kojima, Y.; Kawai, Y.; Koiwai, A.; Suzuki, N.; Haga, T.; Hioki, T.; Tange, K. *J. Alloys Compd.* **2006**, *421*, 204.

[56] Dillon, A. C.; Heben, M. J. *Appl. Phys. A* **2001**, *72*, 133.

[57] Myers, A. L. *AICHE Journal* **2004**, *48*, 145.

[58] Simpson, L. *HSCoE Final Report*, US Department of Energy Office of Energy Efficiency and Renewable Energy Fuel Cell Technologies Program, Hydrogen Sorption Center of Excellence **2010**, http://www1.eere.energy.gov/hydrogenandfuelcells/pdfs/hydrogen_sorption_coe_final_report.pdf (accessed October 31, 2012).

[59] Anderson, R. J.; McNicholas, T. P.; Kleinhammes, A.; Wang, A.; Liu, J.; Wu, Y. *J. Am. Chem. Soc.* **2010**, *132*, 8618.

[60] Stadie, N. P.; Vajo, J. J.; Cumberland, R. W.; Wilson, A. A.; Ahn, C. C.; Fultz, B. *Langmuir* **2012**, *28*, 10057.

[61] Benard, P.; Chahine, R. *Scripta Mater.* **2007**, *56*, 803.

[62] Nishihara, H.; Hou, P.-X.; Li, L.-X.; Ito, M.; Uchiyama, M.; Kaburagi, T.; Ikura, A.; Katamura, J.; Kawarada, T.; Mizuuchi, K.; Kyotani, T. *J. Phys. Chem. C* **2009**, *113*, 3189.

[63] Liu, C.; Fan, Y. Y.; Cong, H. T.; Cheng, H. M.; Dresselhaus, M. S. *Science*, **1999**, *286*, 1127.

[64] Darkrim, F. L.; Malbrunot, P.; Tartaglia, G. P. *Int. J. Hydrogen Energy* **2002**, *27*, 193.

[65] Tibbetts, G. G.; Meisner, G. P.; Olk, C. H. *Carbon* **2001**, *39*, 2291.

[66] Kabbour, H.; Baumann, T. F.; Satcher Jr., J. H.; Saulnier, A.; Ahn, C. C. *Chem. Mater.* **2006**, *18*, 6085.

[67] Gutowska, A.; Li, L.; Shin, Y.; Wang, C. M.; Li, X. S.; Linehan, J. C.; Smith, R. S.; Kay, B. D.; Schmid, B.; Shaw, W.; Gutowski, M.; Autrey, T. *Ang. Chem. Int. Ed.* **2005**, *44*, 3578.

[68] Wang, P.-J.; Fang, Z.-Z.; Ma, L.-P.; Kang, X-D.; Wang, P. *Int. J. Hydrogen Energy* **2008**, *33*, 5611.

[69] Gross, A. F.; Vajo, J. J.; Van Atta, S. L.; Olson, G. L. *J. Phys. Chem. C* **2008**, *112*, 5651.

[70] Yildirim, T.; Ciraci, S. *Phys Rev Letters* **2005**,*94*, 175501.

[71] Campesi, R.; Cuevas, F.; Gadiou, R.; Leroy, E.; Hirscher, M.; Vix-Guterl, C. *Carbon* **2008**, *46*, 206.

[72] Li, Y.W.; Yang, R.T. *J Phys Chem C* **2007**, *111*, 11086.

[73] Lueking, A. D.; Yang, R. T. *Appl. Catal., A* **2004**, *265*, 259.

[74] Mitchell, P. C. H.; Ramirez-Cuesta, A. J.; Parker, S. F.; Tomkinson, J.; Thompsett, D. *J. Phys. Chem. B* **2003**, *107*, 6838.

[75] Chung, T. C. M.; Jeong, Y.; Chen, Q.; Kleinhammes, A.; Wu, Y. *J. Am. Chem. Soc.* **2008**, *130*, 6668.

[76] Zhou, Z.; Gao, X.; Yan, J.; Song, D. *Carbon* **2006**, *44*, 939.

[77] Kang, K. Y.; Lee, B. I.; Lee, J. S. *Carbon* **2009**, *47*, 1171.

[78] Collins, D. J.; Zhou, H.-C. *J. Mater. Chem.* **2007**, *17*, 3154.

[79] Pan, L.; Sander, M. B.; Huang, X.; Li, J.; Smith, M.; Bittner, E.; Bockrath, B.; Johnson, J. K. *J. Am. Chem. Soc.* **2004**, *126*, 1308.

[80] Liu, Y.; Kabbour, H.; Brown, C.; Neumann, D.; Ahn, C. *Langmuir* **2008**, *24*, 4772.

[81] Kaye, S. S.; Dailly, A.; Yaghi, O. M.; Long, J. R. *J. Am. Chem. Soc.* **2007**, *129*, 14176.

[82] Dietzel, P. D. C.; Georgiev, P. A.; Eckert, J.; Blom, R.; Strässle, T.; Unruh, T. *Chem. Commun.* **2010**, *46*, 4962.

[83] FitzGerald, S.A.; Hopkins, J.; Burkholder, B.; Friedman, M.; Rowsell, J.L.C. *Phys. Review B* **2010**, *81*, 104305.

[84] Kong, L.; Román-Pérez, G.; Soler, J.M.; Langreth, D.C *Phys. Rev. Letters* **2009**, *103* 096103.

[85] Hoang, T. K. A.; Morris, L.; Rawson, J. M.; Trudeau, M. L.; Antonelli, D. M. *Chem. Mater.* **2012**, *24*, 1629.

[86] Simmons, J.M.; Yildirim, T.; Hamaed, A.; Antonelli, D.M.; Webb, M.I.; Walsby, C.J. *Chem. Eur. J.* **2012**, *18*, 4170.

[87] Kubas, G.J.; Ryan, R.R.; Swanson, B.I.; Vergamin, P.J.; Wasserman, H.J. *J. Am. Chem. Soc.* **1984**, *106*, 451.

[88] Kubas, G.J. *Chem. Rev.* **2007**, *107*, 4152.

[89] Li, J.; Ziegler, T. *Organometallics* **1996**, *15*, 3844.

[90] Heinekey, D. M.; Oldham Jr., W. J. *Chem. Rev.* **1993**, *93*, 913.

[91] Hanwell, M. D.; Curtis, D. E.; Lonie, D. C.; Vandermeersch, T.; Zurek, E.; Hutchison, G. R. *J. Cheminformatics* **2012**, *4*, 17.

[92] Kubas, G. J. *J. Organomet. Chem.* **2001**, *635*, 37.

[93] Dapprich, S.; Frenking, G. *Angew. Chem. Int. Ed.* **1995**, *34*, 354.

[94] Grundler, P. V.; Yazyev, O. V.; Aebischer, N.; Helm, L.; Laurenczy, G.; Merbach, A. E. *Inorg. Chim. Acta* **2006**, *359*, 1795.

[95] Gonzalez, A.A.; Hoff, C.D. *Inorg. Chem.* **1989**, *28*, 4295.

[96] Bautista, M. T.; Cappellani, E. P.; Drouin, S. D.; Morris, R. H.; Schweitzer, C. T.; Sella, A.; Zubkowski, J. *J. Am. Chem. Soc.* **1991**, *113*, 4876.

[97] Cappellani, E. P; Drouin, S. D.; Jia, G.; Maltby, P. A.; Morris, R. H.; Schweitzer, C. T. *J. Am. Chem. Soc.* **1994**, *116*, 3375.

[98] Brookhart, M.; Green, M. L. H.; Parkin, G. *Proc. Natl. Acad. Sci.* **2007**, *104*, 6908.

[99] Wasserman, H. J.; Kubas, G. J.; Ryan, R. R. *J. Am. Chem. Soc.* **1984**, *108*, 2294.

[100] King, W. A.; Scott, B. L.; Eckert, J.; Kubas, G. J. *Inorg. Chem.* **1999**, *38*, 1069.

[101] de los Ríos, I.; Tenorio, M. J.; Padilla, J.; Puerta, M. C.; Valerga, P. *Organometallics* **1996**, *15*, 4565.

[102] Kubas, G. J. *Chem. Comm.* **1980**, 61.

[103] Cappellani, E. P.; Maltby, P. A.; Morris, R. H.; Schweitzer, C. T.; Steele, M. R. *Inorg. Chem.* **1989**, *28*, 4437.

[104] Chin, B.; Lough, A. J.; Morris, R. H.; Schweitzer, C.; D'Agostino, C. *Inorg. Chem.* **1994**, *33*, 6278.

[105] Heinekey, D. M.; Voges, M. H.; Barnhart, D. M. *J. Am. Chem. Soc.* **1996**, *118*, 10792.

[106] Bianchini, C.; Peruzzini, M.; Zanobini, F. *J. Organomet. Chem.* **1988**, *354*, C19.

[107] Franke, O.; Wiesler, B. E.; Lehnert, N.; Peters, G.; Burger, P. *Z. Anorg. Allg. Chem.* **2006**, *632*, 1247.

[108] Bender, B. R.; Kubas, G. J.; Jones, L. H.; Swanson, B. I.; Eckert, J.; Capps, K. B.; Hoff, C. D. *J. Am. Chem. Soc.* **1997**, *119*, 9179.

[109] Upmacis, R. K.; Poliakoff, M.; Turner, J. J. *J. Am. Chem. Soc.* **1986**, *108*, 3645.

[110] Eckert, J.; Blank, H.; Bautista, M. T.; Morris, R. H. *Inorg. Chem.* **1990**, *29*, 747.

[111] Eckert, J.; Kubas, G. J. *J. Chem. Phys.* **1993**, *97*, 2378.

[112] Heinekey, D. M.; Lledós, A.; Lluch, J. M. *Chem. Soc. Rev.* **2004**, *33*, 175.

[113] Jessop, P. G.; Morris, R. H. *Coord. Chem. Rev.* **1992**, *121*, 155.

[114] Tomàs, J.; Lledós, A.; Jean, Y. *Organometallics* **1998**, *17*, 190.

[115] King, W. A.; Luo, X.-L.; Scott, B. L.; Kubas, G. J.; Zilm, K. W. *J. Am. Chem. Soc.* **1996**, *118*, 6782.

[116] Crabtree, R. H.; Lavin, M. J. *J. Chem. Soc., Chem. Commun.* **1985**, 1661.

[117] Hamilton, D. G.; Crabtree, R. H. *J. Am. Chem. Soc.* **1988**, *110*, 4126.

[118] Bautista, M. T.; Earl, K. A.; Maltby, P. A.; Morris, R. H.; Schweitzer, C. T.; Sella, A. *J. Am. Chem. Soc.* **1988**, *110*, 7031.

[119] Morris, R. H.; Schlaf, M. *Inorg. Chem.* **1994**, *33*, 1725.

[120] Kubas, G. J.; Unkefer, C. J.; Swanson, B.I.; Fukushima, E. *J. Am. Chem. Soc.* **1986**, *108*, 7000.

[121] Maltby, P. A.; Schlaf, M.; Steinbeck, M.; Lough, A. J.; Morris, R. H.; Klooster, W. T.; Koetzle, T. F.; Srivastava, R. C. *J. Am. Chem. Soc.* **1996**, *118*, 5396.

[122] Luther, T. A.; Heinekey, D. M. *Inorg. Chem.* **1998**, *37*, 127.

[123] Gonzalez, A.A.; Zhang, K.; Nolan, S.P.; de la Vega, R.L.; Mukerjee, S.L.; Hoff, C.D.; Kubas, G.J. *Organometallics* **1988**, *7*, 2429.

[124] Kubas, G.J.; Burns, C.J.; Khalsa, G.R.K.; Van Der Sluys, L.S.; Kiss, G.; Hoff, C.D. *Organometallics* **1992**, *11*, 3390.

[125] Crabtree, R.H.; Lavin, M.; Bonneviot, L. *J. Am. Chem. Soc.* **1986**, *108*, 4032.

[126] Zhao, Y.; Kim, Y.; Dillon, A.C.; Heben, M.J.; Zhang, S.B. *Phys. Rev. Letters* **2005**, *94*, 155504.

[127] Sun, Q.; Wang, Q.; Jena, P.; Kawazee, Y. *J. Am. Chem. Soc.* **2005**, *127*, 14582.

[128] Lee, H.; Choi, W.I.; Nguyen, M.C.; Cha, M.H.; Moon, E.; Ihm, J. *Phys. Rev. B* **2007**, *76*, 195110.

[129] Durgen, E.; Ciraci, S.; Zhou, W.; Yildirim, T. *Phys. Rev. Letters* **2006**, *97*, 226102.

[130] Hoang, T.K.A.; Morris, L.; Rawson, J.M.; Trudeau, M.L.; Antonelli, D.M. *Chem. Mater.* **2012**, *24*, 1629.

[131] Reger, D.L.; Little, C.A.; Lamba, J.J.S.; Brown, K.J. *Inorg. Synth.* **2004**, *34*, 5.

[132] Reimann, R.H.; Singleton, E.; *Organometallic Chem.* **1972**, *38*, 113.

[133] Purewal, J.; Hwang S-J; Bowman, Jr., R.C.; Ronnebro, E.; Fultz, B.; Ahn, C. *J. Phys. Chem. C* **2008**, *112*, 8481.

[134] Schmidt, M.W.; Baldridge, K.K.; Boatz, J.A.; Elbert, S.T.; Gordon, M.S.; Jensen, J.H.; Koseki, S.; Matsunaga, N.; Nguyen, K.A.; Su, S.; WIndus, T.L.; Dupuis, M.; Montgomery, J.A. *J. Comp. Chem.* **1993**, *14*, 1347.

[135] Becke, A.D. *J. Chem. Phys.* **1993**, *98*, 5648.

[136] Lee, C.; Yang, W.; Parr, R.G. *Phys. Rev. B.* **1988**, *37*, 785.

[137] Dunning, Jr., T.H.; Hay, P.J. *Methods of Electronic Structure Theory*. H.F. Schaefer III, editor. Plenum Press: New York, 1977; Vol. 2.

[138] Hay, P.J.; Wadt, W.R. *J. Chem. Phys.* **1985**, *82*, 270.

[139] Hay, P.J.; Wadt, W.R. *J. Chem. Phys.* **1985** *82*, 299.

[140] Hay, P.J.; Wadt, W.R. *J. Chem. Phys.* **1985** *82*, 284.

[141] Grimme, S. *J. Chem. Phys.* **2003**, *118*, 9095.

[142] Tomàs, J.; Lledós, A.; Jean, Y. *Organometallics* **1998**, *17*, 190.

[143] NIST Computational Chemistry Comparison and Benchmark Database. D. Russell III, editor. NIST Standard Reference Database Number 101, Release 15b, August 2011. http://cccbdb.nist.gov/.

[144] Murray, L.J.; Dincă, M.; Long, J.R. *Chem. Soc. Rev.* **2009**, *38*, 1294.

[145] Ozolins, V.; Majzoub, E.H.; Wolverton, C. *J. Am. Chem. Soc.* **2009**, *131*, 230.

[146] Morris, R.H. *Inorg. Chem.* **1992**, *31*, 1471.

[147] Maseras, F.; Duran, M.; Lledós, A.; Bertrán, J. *J. Am. Chem. Soc.* **1991**, *113*, 2879.

[148] Jean, Y.; Eisenstein, O.; Volatron, F.; Maouche, B.; Sefta, F. *J. Am. Chem. Soc.* **1986**, *108*, 6587.

[149] Ricci, J.S.; Koetzle, T.F.; Bautista, M.T.; Hofstede, T.M.; Morris, R.H.; Sawyer, J.F. *J. Am. Chem. Soc.* **1989**, *111*, 8823.

[150] Albinati, A.; Klooster, W.T.; Koetzle, T.F.; Fortin, J.B.; Ricci, J.S.; Eckert, J.; Fong, T.P.; Lough, A.J.; Morris, R.H.; Golombek, A.P. *Inorg. Chim. Acta* **1997**, *259*, 351.

[151] Farrar, D.H.; Maltby, P.A.; Morris, R.H. *Acta Cryst.* **1992**, *C48*, 28.

[152] Morris, R.H.; Sawyer, J.F.; Shiralian, M.; Zubkowski, J.D. *J. Am. Chem. Soc.* **1985**, *107*, 5581.

[153] Hills, A.; Hughes, D.L.; Jimenez-Tenorio, M.; Leigh, G.J. *J. Organometallic Chem.* **1990**, *391*, C41.

[154] Blaha, P. In *Journal of Physics: Conference Series*, Proceedings of the International Conference on the Applications of the Mössbauer Effect, **2010**, *217*, 012009.

[155] Grills, D. C.; van Eldik, R.; Muckerman, J. T.; Fujita, E. *J. Am. Chem. Soc.* **2006**, *128*, 15728.

[156] Barclay, J.E.; Leigh, J.G.; Houlton, A.; Silver, J. *J. Chem. Soc. Dalton Trans.* **1988**, *11*, 2865.

[157] Bancroft, G. M.; Libbey, E. T. *J. Chem. Soc. Dalton, Trans.* **1973**, 2103.

[158] Bianchini, C.; Meli, A.; Peruzzini, M.; Frediani, P.; Bohanna, C.; Esteruelas, M.A.; Oro, L.A. *Organometallics* **1992**, *11*, 138.

[159] Bianchini, C.; Meli, A.; Peruzzini, M.; Vizza, F.; Zanobini, F.; Frediani, P. *Organometallics* **1989**, *8*, 2080.

[160] Spijkerman, J. J.; Snediker, D. K.; Ruegg, F. C.; DeVoe, J. R. *NBS Misc. Publ. 260-13, Standard Reference Materials: Mossbauer Spectroscopy Standard for the Chemical Shift of Iron Compounds* **1967**, 11.

[161] Grellier, M.; Vendier, L.; Sabo-Etienne, S. *Angew. Chem. Int. Ed* **2007**, *46*, 2613.

[162] Grellier, M.; Vendier, L.; Chaudret, B.; Albinati, A.; Rizzato, S.; Mason, S.; Sabo-Etienne, S. *J. Am. Chem. Soc.* **2005**, *127*, 17592.

[163] Chen, S.; Rousseau, R.; Raugei, S.; Dupuis, M.; DuBois, D. L.; Bullock, R. M. *Organometallics* **2011**, *30* 6108.

[164] Harvey, J. N.; Poli, R. *Dalton Trans.* **2003**, 4100.

[165] Mock, M. T.; Potter, R. G.; O'Hagan, M. J.; Camaioni D. M.; Dougherty, W. M.; Kassel, W. S.; Dubois, D. L. *Inorg. Chem.* **2011**, *50*, 11914.

[166] Perthuisot, C.; Fan, M.; Jones, W. D. *Organometallics* **1992**, *11*, 3622.

[167] Salt, J. E.; Girolami, G. S.; Wilkinson, G.; Motevalli, M.; Thornton-Pett, M.; Hursthouse, M. B. *J. Chem. Soc. Dalton Trans.* **1985**, 685.

[168] Dapprich, S.; Frenking, G. *Organometallics* **1996**, *15*, 4547.

[169] Feller, D. *J. Comp. Chem.* **1996**, *17*, 1571.

[170] Schuchardt, K. L.; Didier, B. T.; Elsethagan, T.; Sun, L.; Gurumoorthi, V.; Chase, J.; Li, J.; Windus, T. L. *J. Chem. Inf. Model.* **2007**, *47*, 1045.